THE TRANSPORT OF MANUFACTURED NANOPARTICLES WITHIN THE HYPORHEIC ZONE

By

ADAM PETER HITCHMAN

A thesis submitted to
The University of Birmingham
for the degree of
DOCTOR OF PHILOSOPHY

The School of Geography,
Earth and Environmental
Sciences
College of Life Sciences
University of Birmingham
June 2011

Abstract

The field of nanotechnology has seen much growth in recent years as nanoparticles have found usage in many applications. This has led to increases in nanoparticle production and as such it is ever more likely that these nanoparticles will find their way into the aquatic environment.

In this work, sterically stabilised polyvinyl pyrrolidone (PVP) 7 nm gold nanoparticles (NPs) were synthesised and characterised as prepared by their surface plasmon resonance (SPR), size, aggregation, morphology and surface charge. They were then exposed to changes in environmentally relevant conditions (pH, ionic strength, Ca concentration and fulvic acid presence) and the results quantified. These sterically stabilised NPs showed no aggregation with changes in pH or inorganic ions, even under high (0.1 M) Ca concentrations. In addition, the presence of fulvic acid resulted in no observable and significant changes in SPR, size, aggregation or surface chemistry, suggesting limited interaction between the PVP stabilised nanoparticles and fulvic acid. Due to the lack of aggregation and interaction, these NPs are expected to be highly mobile and potentially bioavailable in the environment.

The second half of this investigation focused upon how these NPs were transported within a recirculating flume with both a plane bed structure and with a bedform present. This showed that the nanoparticles moved freely between the stream and the bed and appear to be under the influence of water flow rather than simply diffusion.

Acknowledgements

I would like to thank my supervisors Jamie Lead, Greg Sambrook Smith and Mark Sterling for their support and guidance throughout the course of this project, without their help none of this work would have been able to take place. I would also like to thank Mike Vanderstam for his assistance with the flume experiments and Steve Baker for his patience and help with the temperamental ICP-MS. The initial efforts of Yon Ju-Nam to help identify a suitable nanoparticle for the project and her guidance with the synthesis are extremely appreciated. The help of Ruth Merrifield regarding the AFM and Mohammed Baalousha with the FlFFF was invaluable. Lastly the entertainment provided by Paula Cole made everyday a unique experience. I would like to thank NERC for funding throughout my work and additionally I would like to thank Pete and Liz for their support throughout and a big thank you to Alix for everything.

For Wens and Morv

'Water is the most expressive element in nature. It responds to every mood from tranquillity to turbulence' – Walter Phillips

'Publish and be damned' – Sir Arthur Wellesley, 1st Duke of Wellington

'As a rule, men worry more about what they cannot see than what they can'

– Gaius Julius Caesar

Contents

1.0 Introduction 13

1.1 Thesis Statement 13
1.2 Objectives 14
1.3 Contributions 15

2.0 Literature review 16

2.1 Introduction 16
2.2 Nanoparticle structures 18
2.2.1 Carbon based nanoparticles 18
2.2.1.1 Fullerenes 18
2.2.1.2 Carbon nanotubes 19
2.2.2 Inorganic nanoparticles 20
2.2.2.1 Quantum dots 20
2.2.2.2 Metal oxide nanoparticles 21
2.2.2.3 Metal nanoparticles 24
2.2.2.3.1 Stabilisation 25
2.2.2.4 Zero valent nanoparticles 31
2.2.3 Gold Nanoparticles 31
2.2.3.1 Introduction 31
2.2.3.2 Polyvinylpyyrolidone stabilised gold nanoparticles 34
2.3 Ecotoxicological impacts 36
2.3.1 Carbon based nanoparticles 36
2.3.1.1 Fullerenes 36
2.3.1.2 Carbon nanotubes 38
2.3.2 Inorganic nanoparticles 40
2.3.2.1 Quantum dots 40
2.3.2.2 Metal oxide nanoparticles 40
2.3.2.3 Metal nanoparticles 42
2.3.2.4 Zero valent iron nanoparticles 43
2.3.2.5 Gold Nanoparticles 43
2.3.3 Nanoparticles in the environment 45
2.4 Rivers 50
2.4.1 Overview 50
2.4.2 Hyporheic flow 53
4.3.3 Implications 62

3.0 Methodology 64

3.1 Introduction 64
3.2 Chemicals used 64
3.3 Synthesis 65
3.4 Characterisation 66
3.4.1 Dynamic light scattering 67
3.4.2 Surface plasmon resonance measurements 70
3.4.3 Transition electron microscopy 73
3.4.4 Zeta Potential 74
3.4.5 Ultrafiltration 78
3.4.6 Atomic Force Microscopy 78
3.5 Inductively Coupled Plasma Mass Spectrometry (ICP-MS) 82
3.6 Field flow fractionation 84
3.7 Experimental procedures 88
3.7.1 Sample preparation and handling 88
3.8 Flume Experiment 89
3.8.1 Introduction 89
3.8.2 Flume design and construction 90

3.8.3 Flume Experimental Procedure *91*
3.8.4 Sampling *92*

4.0 Study of the effects of environmentally relevant conditions upon various sizes of PVP stabilised gold nanoparticles 95

4.1 INTRODUCTION 95
4.2 SYNTHESIS AND CHARACTERISATION OF GOLD NANOPARTICLES 99
4.3 ENVIRONMENTALLY RELEVANT CONDITIONS 99
4.3.1 Sample preparation *99*
4.3.2 NP_1 ..... *99*
4.3.2.1 'As prepared' 99
4.3.2.2 Characterisation results 102
4.3.2.3 Transmission electron microscopy 104
4.3.3 NP_2 ..... *110*
4.3.3.1 Dynamic light scattering 110
4.3.3.2 Surface plasmon resonance 112
4.3.3.2 Zeta potential 115
4.3.4 NP_3 ..... *116*
4.3.4.1 Dynamic light scattering 116
4.3.4.2 Atomic force microscopy 116
4.3.4.2.1 Introduction 116
4.3.4.2.2 Methodology 117
4.3.4.2.3 Contact mode 117
4.3.4.2.3.1 Gold nanoparticles in water 117
4.3.4.2.3.2 Gold nanoparticles in 10^{-3} M $NaNO_3$ 119
4.3.4.2.3.3 Gold nanoparticles in 10^{-3} M $NaNO_3$ and 10 mg L^{-1} fulvic acid 121
4.3.4.2.3.4 Discussion of contact mode AFM samples 122
4.3.4.2.4.3 Gold nanoparticles in 10^{-3}M $NaNO_3$ and 10 mg L^{-1} SRFA 126
4.3.4.2.3.4 Discussion of non contact mode AFM results 128
4.3.4.2.5 Liquid Cell 128
4.3.4.2.6 PVP analysis 129
4.3.4.2.7 Summary and discussion of all AFM modes 130
4.3.5 NP_4 ..... *131*
4.3.5.1 Flow field flow fractionation 131
4.4 CONCLUSIONS 136

5.0 Fate and behaviour of gold nanoparticles in a recirculating flume. 139

5.1 INTRODUCTION 139
5.2 FLUME DESIGN 140
5.2.1 Flume *140*
5.2.2 Flume bed *147*
5.2.3 Flume water *149*
5.3 FLUME CHARACTERISTICS 149
5.3.1 Introduction *149*
5.3.2 Hydraulic parameters *152*
5.3.3 Velocity profiles *155*
5.4 NANOPARTICLES IN FLUME 160
5.4.1 Nanoparticle introduction *160*
5.4.2 Attachment of nanoparticles *161*
5.4.3 Flume experiment overview *163*
5.4.4 Plane bed (no bedform present) *164*
5.4.4.1 Results and discussion 164
5.4.5 Bedform present *169*
5.4.5.1 Results and discussion 169
5.6 CONCLUSIONS 183

6.0 Conclusions 185

6.1 SUMMARY 185
6.2 FUTURE WORK 188

List of Tables and Figures

Figure 2.1 The three main polymorphs of TiO_2, rutile, anatase and brookite, after (Xu et al., 2010) 23
Figure 2.2 Synthetic route for PNIPAM-AuNPs by the 'grafting from' technique. Here pre-formed AuNPs are modified into macro-RAFT (Reversible addition – fragmentation chain transfer) agents and this step is then followed by RAFT polymerisation, after (Shan and Tenhu, 2007). 27
Figure 2.3 One pot reaction dissolving RAFT-PNIPAM and $HAuCl_4$ in THF to give PNIPAM-AuNPs from the covalent ''grafting to'' technique, after (Shan and Tenhu, 2007). 29
Figure 2.4 Crystal planes within lattice as determined by Miller Indices, these show the direction of approach to the crystal structure and the fact that the stabilising agent binds preferably to one plane over others promotes growth in these other planes. 30
Table 2.1 Toxic effects of carbon containing fullerenes, adapted from (Klaine et al, 2008).. 37
Table 2.2 Toxic effects of CNTs, after (Klaine et al, 2008). 39
Table 2.3 Toxic effects of metal oxide NPs, adapted from (Klaine et al, 2008). 41
Table 2.4 Cytotoxicity data for gold NPs, adapted from (Murphy et al., 2009). 44
Figure 2.5 The flow of a) AgNPs b) TiO_2 NPs and c) CNT from consumer products to the different environmental compartments and Waste Incineration Plants and Sewage Treatment Plants in a high level emission scenario, flows are in tons/year, after (Mueller and Nowack, 2008) 46
Table 2.5 Predicted environmental concentrations of Nano-Ag, Nano-TiO_2 and CNT, redrawn from (Mueller and Nowack, 2008). 47
Figure 2.6 a) Hydrological and b) geomorphological view of a river, after (United States Geological Survey, 2007). 51
Figure 2.7 Uniform and non-uniform flow, after (University Corporation for Atmospheric Research, 2011) 52
Figure 2.8 The hyporheic zone as it relates to a natural river system, after (Smith, 2005) 53
Figure 2.9 Flow conditions around objects in a flow field, a) Over bed and within bed, b) Flow across circular cylinders, λ = bedform wavelength, redrawn from (Thibodeaux and Boyle, 1987). 56
Figure 2.10 Pumping exchange in bed with uneven bed surface streamlines within the bed due to periodic pressure variations along an uneven bed surface, after (Worman, 2002). 56
Figure 2.11 Longitudinal section of stream and sand bed, after (Packman et al., 2000a) U is mean stream velocity, d is the stream depth d_b is the depth of the bed d' is the total volume of water in the flume and M is the extent of solute penetration.. 57
Figure 3.1 The synthesis proceeds as the PVP acts as a reducing agent. This process can be understood by taking into account two main reactions: 1) The direct abstraction of hydrogen atoms from the polymer by the metal ion; 2) The reduction of the metal precursor by the PVP radicals formed in 1 or during the metal accelerated degradation of PVP, after (Hoppe et al., 2006) 65
Fig. 3.2 Malvern Zetasizer as used throughout DLS experiments 67
Fig 3.3 Samples for DLS analysis. 70

Fig 3.4 Hewlett-Packard 8452A spectrometer and sample. 73
Figure 3.5 Energy Barrier (Malvern, 2001)..... 76
Figure 3.6 Diagram showing the electric double layer and the slipping plane. The potential at the boundary of this layer is the zeta Potential (Malvern, 2001)..... 76
Figure 3.7 Instrumental components of ICP-MS, after (Thomas, 2007). 83
Fig. 3.8 FFF separation (A) Ribbon like FFF channel, sandwiched between channel walls this is usually 75–260 µm in thickness. (B) Different distributions of two particles, X and Y, across the parabolic flow path, and the mean elevations above the accumulation wall ℓ_y and ℓ_x (C)Symmetrical Flow FFF and (D) Thermal FFF, where the separation is driven by a cross flow and temperature gradient respectively, after (Giddings, 1993). 85
Fig 3.9 Gold nanoparticles samples under differing environmentally relevant conditions..... 88
Figure 3.10 The 3 m x 0.15 m test section of the larger flume..... 90
Fig 3.11 Final configuration showing the sampling points (1-12 and NB 1&2) throughout the bed and free flow within the channel of the recirculating benchtop flume where water samples were taken both with (top) and without a bedform (bottom). The recirculation system is shown alongside the bottom configuration. The blue arrows show the direction of flow. 93
Figure 4.1 Showing Van der Waals attractive force (V_A) and the electrostatic repulsion (V_R) and the total potential energy as a function of distance, after (Washington, 2011)..... 96
Figure 4.2 The effect of Suwannee river humic acid (SRHA) on charge stabilised gold NPs. Here partial substitution of the small citrate anions by the SRHA occurs and when the pH of the solution is decreased protonation occurs and the electrostatic stability is lost and aggregation occurs, though the SRHA does offer some steric stabilisation and retards further aggregation, after (Diegoli et al., 2008). 97
Figure 4.3 The polymerisation of vinylpyrrolidone, after (Haaf et al., 1985)..... 98
Figure 4.4 a) TEM image of manufactured gold nanoparticles in water with b) histogram. c) Distribution by volume taken from DLS analysis and d) UV-Vis spectrum showing the absorbance of several aliquots of the nanoparticles taken at different times throughout the synthesis. 103
Figure 4.5 TEM images of gold nanoparticles in water (a) and in 10^{-3} M $NaNO_3$ (b). Histograms show the NP size as determined by a manual count from the TEM images, not all images shown..... 105
Figure 4.6 TEM images of gold NPs in a) water, b, c) in 0.1M $NaNO_3$ and d) in 0.1M $NaNO_3$ and fulvic acid..... 106
Figure 4.7 TEM images of gold NPs in A) water and B) 10^{-3} M $NaNO_3$..... 107
Figure 4.8a TEM images of Gold NPs in (A, C) water and (B, D) 10^{-3} M $NaNO_3$ (right)... 108
Figure 4.8b TEM image of Gold NPs in 10 mg L^{-1} SRFA. 109
Table 4.1 Average particle diameter under different conditions as determined by DLS, plasmon band peak as determined by UV/Vis and zeta potential..... 110
Figure 4.9a The wavelength of the maximum of the Plasmon band for citrate stabilised gold NPs at across a pH range and in SRHA, after (Diegoli et al., 2008)..... 113
Figure 4.9b The wavelength of the maximum of the plasmon band for three sub batches of AuNPs under different environmentally relevant conditions. Indicating no change across conditions. 114
Table 4.2 DLS Data for Batch NP_3 used in AFM analyses..... 116
Figure 4.10 Contact mode AFM images of the AuNPs used in water alone..... 118
Figure 4.11Distribution of the gold NPs in water using contact mode..... 118
Figure 4.11Contact mode AFM images of the AuNPs used in 10^{-3} M $NaNO_3$..... 119
Figure 4.12 Size distribution of the AuNPs used in 10^{-3} M $NaNO_3$..... 120

Figure 4.13 Contact mode AFM images of the AuNPs used in 10^{-3} M $NaNO_3$ and 10 mg L^{-1} SRFA. 121
Figure 4.14 Size distribution of AuNPs in SRFA. 122
Figure 4.15 Non contact mode AFM images of the gold AuNPs used throughout in water alone. 123
Figure 4.16 Non contact mode AFM images of the AuNPs used in water illustrating that some of the shapes shown have moved away from a purely spherical arrangement. 124
Figure 4.17 Histogram of AuNPs used in water alone imaged using non contact mode AFM 125
4.3.4.2.4.2 Gold nanoparticles in 10^{-3} M $NaNO_3$ 125
Figure 4.18 Non contact mode AFM images of the AuNPs used in 10^{-3} M $NaNO_3$. 125
Figure 4.19 Distribution of AuNPs in 10^{-3} M $NaNO_3$. 126
Figure 4.20 Non contact AFM images of the AuNPs used in 10^{-3} M $NaNO_3$ and fulvic acid solution. 127
Figure 4.21 Size distribution of the AuNPs used in 10^{-3} M $NaNO_3$ and fulvic acid solution. 127
Figure 4.22Liquid cell AFM images of a) AuNPs in 10^{-3} M $NaNO_3$ and b) AuNPs in SRFA. 129
Table 4.3 Mean diameter of gold AuNPs and PVP samples obtained using contact and non contact mode AFM. 130
Figure 4.23 Non contact mode images of the AuNPs used in a) Water, b) 10^{-3} M $NaNO_3$ and c) 10 mg L^{-1} SRFA. From the images it is apparent that no change has occurred in the spherical shape of the particles, confirming what has been noted when using the other experimental techniques within this chapter. 131
Figure 4.24 FFF Fractograms showing nanoparticle size in water (a and b) and 0.1 M $NaNO_3$ (c) at pH 5.5. 133
Figure 4.25 Fractogram showing the size of the AuNPs used here in 10^{-3} M $NaNO_3$ at pH 8.5. 134
Figure 4.26 Fractograms showing the AuNPs used in SRFA at pH 5.5 (a) and 8.5 (b). 135
Table 4.4 Diameters obtained using FFF compared to DLS values obtained for the same batch. 136
Table 4.5 Summary table of results for the four NP batches. 137
Figure 5.1 Initial flume experimental section showing sampling points and 5 depths (based on the plastic sphere diameter) that experiments were to take place at as well as showing the face centred cubic configuration of the plastic spheres used to simulate the gravel river bed. 141
Table 5.1 The concentration of AuNPs in the pilot study using the large flume as determined by ICP-MS. 142
Figure 5.2 TEM image of debris left on the one surviving grid after pilot study in the larger flume, no NPs are detectable. 142
Figure 5.3 Side and plan view of the benchtop flume used after moving away from the larger flume, also a photograph of the flume from the inlet end. The blue arrows show the direction of water within the flume channel. In the plan view the location of the small weir used to stabilise flow from the inlet to the channel is shown. 143
Figure 5.4 Photographs of the test section toward inlet showing the bed of plastic spheres as well as the metallic bedform used in some of the experiments. The blue arrows indicate the direction of water flow. 144
Figure 5.5 Cross section of the benchtop flume from within the tank showing the test channel with plastic spheres facing toward the inlet i.e. water flows toward the viewer. 145

Figure 5.6 A cross section within the tank perpendicular to the channel showing the depth of the tank. 145
Figure 5.7a The test bed section made from 19 mm nylon 66 plastic spheres, above the plastic spheres is the steel block coated with Red Oxide Primer used as a bedform, for experiments considering just the plane bed this was removed. 148
Figure 5.7b Similar to the view shown earlier in Fig 3.11 the side view of plastic sphere test bed section added to the benchtop flume, with the bedform present experiment on top and the plane bed without bedform on the bottom. Orange dots show sampling points across both experiments, whilst the blue dots indicate samples taken only with a plane bed. The dashed lines show the positions where velocity readings were taken, sites 1, 2, 3 and 4, with A, B and C being located in the same position as 1,2 and 3 respectively. 149
Figure 5.8 Sampling head of typical acoustic Doppler velocimeter showing remote sampling volume which extends below the sampling head, (www.sontek.com). 150
Figure 5.9 Combined Pitot static tube, the outer holes measure the static pressure whilst the inner tube measures the combined pressure, attached to a manometer the differential head *H*, is available to measure and velocity calculated, after (Hamill, 2001). 151
Table 5.2 Hydraulic parameters for the four different depths that were trialled for the NP experiments conducted using the benchtop flume. 155
Figure 5.10 Velocity profiles plotting measurement depth (d_m) against the Velocity/(Discharge/A) at four different depths of flow and associated Froude number for the benchtop flume. 156
Table 5.3 Local depths at the four velocity measuring positions for the four velocity profile experiments. (Depths are in mm). 157
Figure 5.11 Velocity profile from initial larger flume at a depth of three plastic sphere diameters, 57mm. Inlet indicates the channel opening, whilst A, B and C are arbitrary measuring points moving downstream respectively. 158
Figure 5.12 Velocity profile s in the benchtop flume at depth 3D with the bedform present a) shows the velocity across the channel at the position furthest upstream b) Shows the velocity profile across the channel at position B c) The velocity profile across the channel at the position furthest downstream. 159
Table 5.4 ICP-MS determined gold concentrations showing the initial and final concentrations of NPs within the beaker indicating that no significant deposition of the particles occurred. 162
Table 5.5 Experimental labels and bed configurations. Also shown is the average difference found in AuNPs concentration found in the stream bed and stream flow, these values are non directional and simply show the magnitude of difference and not whether the bed or stream flow has a higher concentration. 163
Figure 5.13 Contour maps showing concentration distribution throughout the bed and free flow. F1 Top left) 2 minutes. Top Right) 25 minutes. Bottom Left) 50 minutes. Bottom right) 75 minutes. 165
Figure 5.14 Contour maps showing concentration distribution throughout the bed and free flow. F2 Top left) 2 minutes. Top Right) 25 minutes. Bottom Left) 50 minutes. Bottom right) 75 minutes. 167
Figure 5.15 Contour maps showing concentration distribution throughout the bed and free flow. F3 Top left) 2 minutes. Top Right) 25 minutes. Bottom Left) 50 minutes. Bottom right) 75 minutes. The white spot in the model reflects the fact that since the bedform is solid the concentration at this point must be zero. 169

Figure 5.16 Contour maps showing concentration distribution throughout the bed and free flow. F4 Top left) 2 minutes. Top Right) 25 minutes. Bottom Left) 50 minutes. Bottom right) 75 minutes. 171
Figure 5.17 The red dots show the upstream (left) and downstream (right) sampling points referred to in Figures 5.16 and 5.17 173
Figure 5.18 Normalised concentrations of AuNPs in the a) free flow and two points within the bed and b) average values in the free flow and upstream and downstream sections of the bed for the experiment F1..... 175
This possible flux of NPs toward the bed over time however is not seen in the data for F2, where the opposite, in fact, is seen as the free flow concentration seems to build over time. From this it might seem likely that the concentrations of NPs is rapidly moving between the bed and the stream flow and these snapshots have picked up different stages of that dynamic behaviour. 175
Figure 5.19 Normalised concentrations of AuNPs in the A) free flow and two points within the bed and B) average values in the free flow and upstream and downstream sections of the bed for the experiment F2..... 176
Figure 5.20 Normalised concentrations of AuNPs in the a) free flow and two points within the bed and b) average values in the free flow and upstream and downstream sections of the bed for the experiment F3 (inset shows zoomed section on the values after 50 and 75 minutes). 178
Figure 5.21 Normalised concentrations of AuNPs in the a) free flow and two points within the bed and b) average values in the free flow and upstream and downstream sections of the bed for the experiment F4..... 179
Figure 5.22 Average concentrations in the free flow, and upstream and downstream sections of the bed for plane bed experiments. 182
Figure 5.23 Average concentrations in the free flow, and upstream and downstream sections of the bed for bedform experiments. 182
Figure 5.24 Average concentrations in the free flow, and upstream and downstream sections of the bed for plane bed and bedform experiments..... 183

1.0 Introduction

1.1 Thesis Statement

One of the major advances in current nanoscale science is the manufacture and use of nanoparticles in a wide range of disciplines, these nanoparticles (NPs) are smaller than 100 nm and exhibit novel properties compared to bulk molecules of the same material due to the combination of quantum and Newtonian scales (Liu, 2006).

Due to the rise in production in order to meet increasing industrial demands and the subsequent waste and loss from this process, NPs will find their way into all sectors of the environment: aquatic, atmospheric and soil (Wiesner et al., 2006). In the aquatic environment the fate and behaviour of these NPs will be governed by their interaction with natural organic matter (NOM), their behaviour under the varying chemical conditions that are found in surface waters and hydrodynamic factors within rivers.

The hyporheic zone is located at the interface between ground and surface water, exchange between the two is common and is dependent upon local and reach scale stream properties (Krause et al., 2009). Of significant ecological importance (Boulton et al., 2007), the hyporheic zone has the potential to act as a sink for contaminants due to exchange mechanisms (Packman et al., 2004).

As such the issue of whether or not 'changes in bed structure and how this influences surface-subsurface exchange will have an effect upon the transport of manufactured nanoparticles in the hyporheic zone' is an important question in forming a full picture of the

fate and behaviour of NPs, which have the potential to act as contaminants within the aquatic environment.

1.2 Objectives

To understand fully the transport of NPs in the natural environment a number of key issues need to be addressed, which provide the objectives for this research:

- The behaviour of monodispere charge stabilised NPs under different water chemistries needs to be fully characterised as aggregation or disaggregation at different pH may result in very different transportation dynamics within the aquatic environment (Baalousha et al., 2006). This will also allow the comparison of the behaviour of these NPs under varying environmental conditions to that of other NPs which has been previously reported (Baalousha et al., 2008; Diegoli et al., 2008; Yang et al., 2009).

- The effects of changes in the flow paths of water within the bed and in the exchange of water between the free flow of the stream and the bed upon NP transport, brought about by pressure variations at the bed surface, need to be characterised fully.

- This exchange is known to be influenced by the presence of bedforms (Packman et al., 2004) and hence a further objective is to undertake a comprehensive analysis of NP movement within a simulated gravel river bed, both with and without a bedform will be required.

- The work Boncagni (2009) will need to be developed to provide a quantification of NP movement within the river bed, in addition to determining the mass transfer of NPs from the free flow of the stream to the pore water. This foundation provided by Boncagni's work will be further expanded upon by using sterically stabilised NPs that may be less susceptible to aggregation and perhaps exhibit differing environmental fates and behaviours.

It is hoped that with this information known it will be possible to provide a clearer picture of NP fate and behaviour within an aquatic system and that this work will form the basis of future study in this area.

1.3 Contributions

Previous work in the field has focused upon the effect of NOM upon charge stabilised NPs (Baalousha et al., 2008; Diegoli et al., 2008; Yang et al., 2009), here similar studies were performed on sterically stabilised gold NPs in order to achieve a full assessment of the potential effects that NOM and different environmental conditions may have upon NPs and how this may have consequences regarding transportation.

Regarding contaminant transport with the hyporheic zone, previous investigations have focused on the exchange of contaminants between the surface and subsurface (De Smedt, 2007; Packman et al., 2000b; Ren and Packman, 2004a; Ren and Packman, 2004b; Ren and Packman, 2005), whilst recently this has been extended to include some NPs (Boncagni et al., 2009), here we analyse the effect of flow into and through the subsurface as it pertains to the distribution of NPs within the bed.

2.0 Literature review

2.1 Introduction

It has been said that the twenty first century is in many ways the 'century of nanotechnology' (Pachon and Rothenberg, 2008). The scope of opportunity associated with the unique properties displayed by these materials upon transition from the macro to the nanoscale has fuelled many branches of research into the potential application of these properties (Hoppe et al., 2006; Shan and Tenhu, 2007).

The field of nanoscience bridges the gap between the molecular state and bulk materials (Chen and Mao, 2007; Klaine et al., 2008; Murdock et al., 2008) and involves the study of materials with at least one dimension in the 1-100 nm range. The backbone of this field and the building block for many emerging nanotechnologies are nanoparticles (NPs) which can be defined as having all three dimensions in the 1-100 nm range. The large specific surface area leads to quantum size effects which can give the nanoparticle (NP) very different physical properties in comparison to the bulk material (Li et al., 2006).

These NPs can be categorised into several broadly defined areas, carbon based materials such as fullerenes and carbon nanotubes and inorganic NPs including metal oxides, metals and quantum dots (Biswas and Wu, 2005; Ju-Nam and Lead, 2008). Synthesis of NPs is achieved by a direct chemical synthesis i.e. a 'bottom up' approach, or the application of grinding or milling etc. – i.e. a 'top down' approach (Klaine et al., 2008). Within this a myriad of different techniques and materials are used, resulting in numerous morphologies, surface properties and sizes. This is caused by the ratio of surface to near surface atoms increasing as the size of the nanoparticle decreases (Li et al., 2006) as the larger specific

surface area leads to greater surface density, reactivity and energy due to surface atoms tending to have more incomplete bonds. This gives these surface atoms a tendency to adsorb and react with other atoms or molecules in order to achieve stabilisation (Service, 1998) and thus a significant surface energy. This surface energy is such a factor that if the NP surface is not protected by a particular molecule, sometimes called a capping agent e.g. a polymer or small ion, interactions between the particles will occur at a high rate, reducing the surface energy and resulting in aggregation and the loss of their unique properties. This also gives the potential for other changes such as phase transformation (Christian et al., 2008).

With many potential applications production of NPs is likely to increase as successful commercial uses are developed. In addition to the many benefits to society (Scown et al., 2010), there will also be a corresponding increase in the probable NP release into the environment and in such sufficient quantities as to be significant (Klaine et al., 2008; Scown et al., 2010). In an effort to understand the potential environmental impacts of these NPs there has thus far been a significant amount of research into the toxicological and eco-toxicological effects of NPs, giving some interesting and often uncertain results. Much of which seems to indicate that different NPs behave in many different manners and that there is not one universal answer. In essence, they must be looked at on a case by case basis as charge stabilised NPs behave differently from sterically stabilised NPs, metal oxide NPs will have different properties to metal NPs and so on.

This chapter will give an overview of the various types of NPs that are being synthesised at the moment and detail any potential toxicological effects that they may possess and their likely pathways within the environment. In the latter half of the chapter the importance of rivers to the environment will be discussed as well as how changes in the river bed structure

can affect the exchange and flow of water into and through the hyporheic zone and how this relates to NP fate and behaviour once their likely release to the environment has occurred.

2.2 Nanoparticle structures

2.2.1 Carbon based nanoparticles

2.2.1.1 Fullerenes

One NP that attracted early attention is the family of fullerenes, which due to their potential for wide spread use and thus environmental exposure are of interest to environmental and health scientists around the world. Fullerenes have a spherical cage structure and their discovery in the mid 1980s (Kroto et al., 1985) led to the award of the Nobel prize to Harold Kroto, Richard Smalley and Robert Curl in 1996. This subsequently led to the discovery of other carbon based NPs including carbon nanotubes and graphene. The particles are composed of carbon when unfunctionalised and take the form of a hollow sphere or a tube, similar to graphite, they may contain pentagonal or heptagonal rings in addition to hexagonal rings which allows a three dimensional structure (Aitken et al., 2006; Khlobystov et al., 2005)

Produced by the evaporation of graphite electrodes brought upon by the heat at the contact point of the electrodes as a charge is passed across them (Ju-Nam and Lead, 2008; Klaine et al., 2008). This evaporation of the carbon results in the formation of soot which contains ~ 13% C_{60} and is then separated by liquid chromatography (Ju-Nam and Lead, 2008). With C_{60} having a limited solubility in organic solvents coupled with the fact that it is almost insoluble in water, there was a restriction on the potential methods by which it could be used. This was until it was discovered that stable C_{60} clusters could be suspended in water with the resulting NPs being hydrophilic and charged (Brant et al., 2006; Brant et al., 2005b). There are two widely used techniques to obtain these suspensions (Chen and Elimelech, 2006); the

first are methods based upon solvent exchange principles, where fullerenes are suspended in an organic solvent and then mixed with water after which the organic solvent is then removed from the mixture (Dhawan et al., 2006). The second set of methods involve the direct dispersion of the C_{60} molecules into water and then prolonged mixing (Dhawan et al., 2006). These second methods generally result in more polydisperse solution of colloidal fullerenes. This second method is particularly interesting as it could be indicative of early stage transport scenarios in the natural environment (Dhawan et al., 2006). Fullerenes can also be deliberately functionalised in an endohedral (inside the cage) or exohedral (outside the cage) in order to give additional properties and uses (Bidell et al., 1998; Gimenez-Lopez et al., 2010).

2.2.1.2 Carbon nanotubes

Initially reported by Iijima in 1991 (Iijima, 1991), carbon nanotubes (CNT) are a particular form of fullerene. Similar in structure to C_{60} they differ in that they are elongated to form tubes with a diameter of 1-2 nm for the single walled variety (Aitken et al., 2006). Production can be achieved with very large aspect ratios and lengths of 1 mm are possible (Aitken et al., 2006).

Single-walled carbon nanotubes (SWCNTs) are made up of a single layer of carbon atoms arranged in tubular fashion. These SWCNTs can be combined as multiple concentric tubes to give multi-wall carbon nanotubes (MWCNTs) with diameters of around 20 nm (Aitken et al., 2006). These MWCNTs often contain defects unlike the SWCNTs which can have an important impact upon their properties as these stem from the graphite structure (Service, 1998).

These carbon nanotubes are synthesised under specific conditions (which control shape and size variability) from graphite using evaporation from an electrode - as in fullerene synthesis - or laser ablation. An alternative is chemical vapour deposition using a carbon containing gas (Klaine et al., 2008). For all of these synthetic methods general conditions of a catalytic metal and an inert atmosphere of 600-1200°C are required (Nikolaev et al., 1999). Due to their geometry and hydrophobic surface, carbon nanotubes have a predisposition toward agglomeration, folding into bundle like forms and requiring suspension in organic solvents or debundling (Wick et al., 2007).

Nanotubes have many unique and interesting qualities. Such as a tensile strength that makes them 100 times stronger than steel whilst being only one sixth it's weight (Maynard et al., 2004). They also have a high electrical conductivity, large specific surface area and interesting electronic properties, such as the ability to switch between conductor and semi conductor based upon the formation or removal of defects within the graphite structure (Service, 1998), which are industrially useful. This range of properties gives an indication of the fact that their use and thus potential for environmental exposure is only likely to increase (Maynard et al., 2004).

2.2.2 Inorganic nanoparticles

2.2.2.1 Quantum dots

Semi conductor quantum dots (QDs) have attracted a lot of attention due to their potential for applications in molecular biology, medicine and information technology (Chen, 2008). They consist of a reactive core which governs the optical properties of the particle and is made of metals or semi conductors (Klaine et al., 2008), such as cadmium selenide (CdSe), cadmium telluride (CdTe) and zinc selenide (Klaine et al., 2008). In most cases, the nanocrystallite

core is covered with high band gap inorganic materials such as silica, which enhance photoluminescence by preventing oxidation (Dabbousi et al., 1997). Synthesis is mainly based on wet chemical colloidal procedures (Ju-Nam and Lead, 2008), such as high temperature solution phase synthesis where reaction conditions govern size and surfactants in solution form an organic cap, stabilising the NP.

2.2.2.2 Metal oxide nanoparticles

Recent years have seen the use of metal oxide NPs in a large number of applications across food, material, chemical and biological sciences (Aitken et al., 2006). Zinc oxide (ZnO) has seen commercial usage in cosmetics and sunscreens (Starowicz and Stypula, 2008) as has titanium dioxide (TiO_2) in addition to its use in solar cells, paints and coatings (Klaine et al., 2008). Whilst cerium oxide (CeO_2) is an additive in diesel fuels alongside other applications such as gas sensors, UV filters, solar cells and the photocatalytic oxidation of water (Gu and Soucek, 2007). The synthetic procedures for these metal oxide NPs all proceed via different means and even within type there is not one universal 'correct' synthetic procedure, examples of which are given below.

ZnO is a wide band-gap semi conductor, with a band gap energy of 3.36 eV and a high dielectric constant (Ju-Nam and Lead, 2008), as such this material has seen much research and already is used in commercial applications, including sunscreens where the ZnO NPs block broad UV-A and UV-B rays (Ju-Nam and Lead, 2008). The microstructure and chemical properties of ZnO NPs depend on the manner of synthesis. Various techniques have been developed over time, including, high temperature hydrothermal synthesis (Music et al., 2005), laser heating (Wu et al., 2000) and high temperature decomposition (Kanade et al., 2006). Due to high energy consumption, alternatives to these methods were needed,

which include solution based routes, using lower reaction temperatures and giving the option of large scale production (Hung and Whang, 2003). Electrochemical studies have also been shown to successfully yield ZnO NPs using cyclic voltammetry and chronoampperometry techniques to polarise a zinc metal precursor in a LiCl/ethanol solution, before the addition of varying quantities of water gives ZnO NPs of various (5-20 nm) sizes depending on water volume, (Starowicz and Stypula, 2008).

TiO_2 is another semiconductor with a large band gap of 3.2 eV. With extensive photocatalytic properties TiO_2 has seen use in the degradation process and complete mineralisation of certain organic pollutants and has seen widespread use in water and air purification components (Xia et al., 2007). The tendency for TiO_2 to aggregate has meant that despite its large specific surface area, commercial applications initially developed fairly slowly (Ju-Nam and Lead, 2008) and is now very widely used.

Comprising of three main polymorphs, anatase, rutile and brookite, TiO_2 shows differing properties based on the three differing structures, of which rutile is the most thermodynamically stable (Arami et al., 2007) (Figure 2.1 illustrates these main polymorphs).

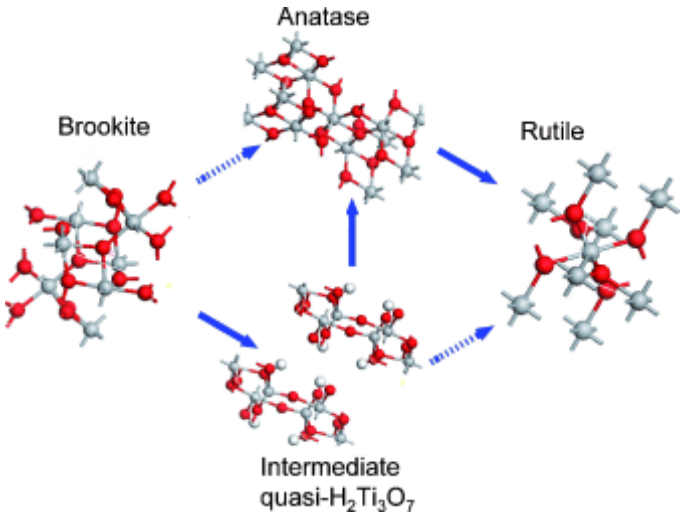

Figure 2.1 The three main polymorphs of TiO_2, rutile, anatase and brookite, after (Xu et al., 2010).

Most syntheses are based upon the hydrothermal method where TiO_2 bulk particles are added to high ionic strength NaOH solutions, and then treated at high temperatures in an autoclave for varying amounts of time (Kasuga et al., 1999), whilst sonochemical formation of rutile 20 nm TiO_2 particles has been shown to be possible using the same initial dissolution of bulk TiO_2 in highly concentrated NaOH as in the hydrothermal method before being irradiated in an ultrasonic bath (Arami et al., 2007).

Many advances regarding the use of NPs have taken advantage of ceria NPs significant size dependent physical properties. Ceria has potential applications in areas such as uv-blockers, (Tsunekawa et al., 2000), silicon wafer buffer layers (Tashiro et al., 2002), gas sensors (Garzon et al., 2000), high refractive index materials (Mogensen et al., 2000) and luminescent

materials (Yu et al., 2001). These uses alongside those mentioned in the introductory paragraph above show h the great potential for use that ceria has. With the physical properties of ceria being so size dependent it is without surprise that numerous procedures for ceria nanoparticle synthesis have been developed. CeO_2 NPs in the size range 3-12 nm have been prepared by mixing equal volumes of $Ce(NO_3)_3$ and hexamethlenetetramine solutions at room temperature (Zhang et al., 2002a). Whilst hydrothermal (Hirano and Inagaki, 2000) and sol gel (Makishima et al., 1986), processes have also been used. Mono disperse ceria NPs have been synthesised by decomposing cerium-oleate complexes in hydrocarbon solvents at high temperatures with the use of various solvents providing excellent size selection (5-20 nm) (Gu and Soucek, 2007).

2.2.2.3 Metal nanoparticles

In particular among the varying groups of nanotechnology, metallic NPs (gold, silver, copper and iron) have garnered increasing interest due to the optical, catalytic, chemical and electronic properties that they possess. These properties have led to applications in fields such as optical imaging in the life sciences, nanodevices and nanomachines, catalysts and optical sensors (Kemal et al., 2008).

The physical characteristics of metal NPs such as their shape, size and distribution play an important role in determining the properties of the molecules and because of this many attempts have been made in order to control size and shape during the synthesis (Kemal et al., 2008). Examples of this include nanorods and nanowires of silver and gold with controllable diameters and aspect ratios can be synthesised from soft templates such as cetyltrimethylammonium bromide (Wiley et al., 2005). Also the seeded growth of palladium nanocrystals, which could have many important applications in the field of catalysis as

palladium is a key industrial catalyst - invaluable to many processes including, hydrogenation, low temp reduction of CO_2 in automobiles and petroleum cracking (Lim et al., 2009). The preparation of colloidal monodisperse ZnSe nanospheres by aerosol spray pyrolysis assisted by ultrasonic nebulisation of these important semi-conductors is another example of shape and size controlled synthesis (Kim and Koo, 2009) these NPs may have application as UV emitting materials and in Light Emitting Diodes (LEDs) due to their wide band gap.

Nanolithiographic techniques have led to various complex nanostructures being created via a number of etching techniques such as dip pen lithography and micro contact printing (Yun et al., 2005). The fabrication of specifically designed versatile nanocomponents is of interest as these could well form the building blocks of sophisticated nano- and micro machines. This has been achieved on a few levels by combining solution based methods and nanolithography techniques. This has led to nanoscale gears, wheels and dumbbells as well as the letter 'A', showing the extent to which they can be manipulated (Yun et al., 2005). This is done by selective etching of single crystalline Au nanoplates synthesised via solution (Yun et al., 2005).

2.2.2.3.1 Stabilisation

Particle growth in regard to metallic NPs revolves around the stabilisation of the kinetically and thermodynamically unstable NPs (Kemal et al., 2008; Pachon and Rothenberg, 2008). One important factor in controlling the morphologies of the NPs is the particular reaction environment in which they are synthesised (Kemal et al., 2008). This reaction environment falls into two main categories; the first being where stacking faults in the face centred cubic structure of these metals direct particle morphologies (Germain et al., 2003), whilst the

second is the use of stabilising agents which are chemically or physically adsorbed at the particle surface (Pachon and Rothenberg, 2008). Due to their small size NPs have a low energy barrier toward aggregation (Petosa et al., 2010) and as such it becomes thermodynamically favourable without the presence of stabilising agents for aggregation to occur in the aqueous phase. This can play a crucial role in the control of the size and shape of nanocrystals (Hoppe et al., 2006).

There are two main types of NP stabilisation via protecting agents. The first of these is electrostatic stabilisation where anions and cations from the starting reagents remain in solution and associate with the NPs. This results in an electrical double layer around the NPs giving a Coulombic repulsion preventing aggregation. This interaction can be traditionally described by Derjaguin, Landau, Verwey and Overbeek (DLVO) theory, where the colloidal stability is described by the total interaction energy experienced by a nanoparticle when it approaches another particle. This can be evaluated as the sum of the van der Waals and electrical double layer interactions (Petosa et al., 2010). The use of electrostatic stabilisation methods can later lead to aggregation in the environment as humic substances break down this double layer (Baalousha et al., 2008), which is an important consideration in regard to potential environmental behaviour (See later). More details on DVLO theory are given in the next chapter (Section 3.4.4). The second is steric stabilisation where thermodynamically favourable aggregation is prevented by the sorption of large molecules (e.g. polymers) onto the NP surface which prevent the NPs from coming into contact with one another (Pachon and Rothenberg, 2008). One example of such is the polymer poly(vinyl pyrollidone) PVP which is used as a capping agent in many gold and silver syntheses. It has shown size and shape selectivity via its ability to interact differentially with different gold planes (e.g. 111, 100 and 110) (Kemal et al., 2008) (Figure 2.4). This coupled with its ability to act as a

reducing agent make it a simple and effective agent for nanoparticle synthesis that is taken advantage of within this study.

The advantages of using polymers as stabilisers are not just the increase in long term stability gained but the control of solubility combined with the ability to tailor more bespoke qualities (Shan and Tenhu, 2007). With steric stabilisation, there are two ways in which the polymer is bound to the particle surface: 1) direct covalent attachment via functional groups on the polymer and 2) physisorption.

Different procedures can be used in order to covalently attach the polymer to the nanoparticle surface; the covalent 'grafting from' technique and, the contrasting, covalent 'grafting to' technique. The grafting from technique involves polymer chains growing from small initiators that are preanchored to the particle surface (Zhao et al., 2005).

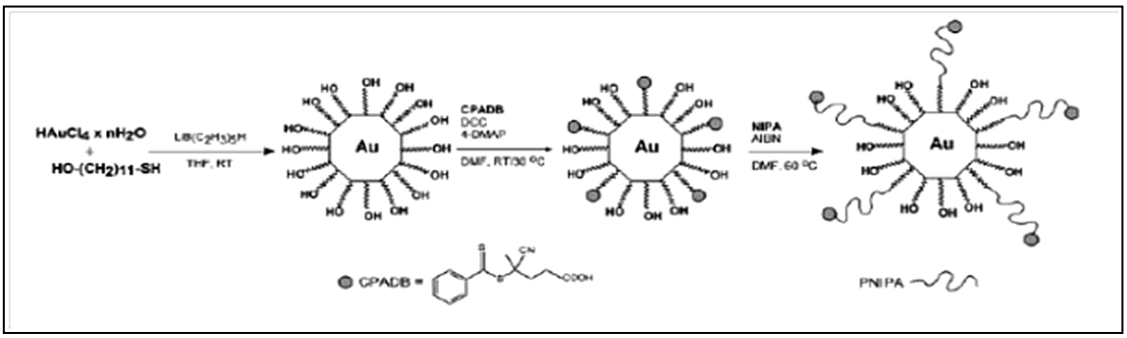

Figure 2.2 Synthetic route for PNIPAM-AuNPs by the 'grafting from' technique. Here pre-formed AuNPs are modified into macro-RAFT (Reversible addition – fragmentation chain transfer) agents and this step is then followed by RAFT polymerisation, after (Shan and Tenhu, 2007).

Initiators are usually anchored to the particle surface via one of three roots: modification of preformed NPs where the protective ligands contain active functional groups such as the synthesis of 11-mercapto-1-undecanol protected AuNPs which are subsequently modified into macro-RAFT agents containing dithiobenzoate end groups via esterification. Poly(*N*-isopropylacrylamide) (PNIPAM) brushes are then grafted from the AuNPs using a RAFT polymerisation (Figure 2.2) (Shan and Tenhu, 2007). Secondly stoichiometric exchange between new initiator ligands and older ligands already bound to the NPs and thirdly via direct attachment.

These methods allow polymer brushes to form with a high graft density obtained due to the lack of interference from fully formed polymer chains, however the 'grafting to' technique does away with the need for more complicated multi step synthesis and purifications that are required with the 'grafting from' process, whilst maintaining a higher surface graft density for nanocores (Corbierre et al., 2004). Much of this work centres on sulphur containing polymers due to their functionality, such as the use of RAFT-PNIPAMs synthesised through RAFT polymerisation containing a dithioester end group in a one pot synthesis with $HAuCl_4$ in THF, using $LiB(C2H_5)_3H$ as reductant (Figure 2.3) (Shan and Tenhu, 2007). Polymers which are water soluble have the ability to coordinate with metal particles and as a result of this most syntheses of metallic NPs take place under aqueous conditions in the presence of a water soluble polymer (Ah et al., 2005; Dong et al., 2006).

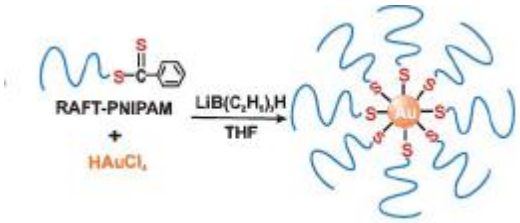

Figure 2.3 One pot reaction dissolving RAFT-PNIPAM and $HAuCl_4$ in THF to give PNIPAM-AuNPs from the covalent ''grafting to'' technique, after (Shan and Tenhu, 2007).

There are however a few problems in regard to the physisorption of polymers onto NPs for stabilisation. This stems from the fact that the polymers are not specifically adsorbed on to the surface as is the case in the covalent manner, through one end of the polymer or the other, but are instead 'wrapped ' around the nanoparticle cores via weak bonds through heteroatoms that act as ligands (Pachon and Rothenberg, 2008) and provide steric and/or electrostatic stabilisation through this process (Hussain et al., 2005; Shan and Tenhu, 2007). Compared to the covalent methods NPs prepared in this method show less long term stability and therefore require a higher concentration of protective agent (Shan 2007). Interestingly this lower level of protection has seen the formation of several differently shaped NPs that would have required detailed synthesis and preparation in order to form via a covalent method (Shan 2007).

Though despite the amount of time and effort placed into it and the technological importance of it, there was no early standard method for the synthesis of metal nanostructures with controllable and readily defined morphologies (Wiley et al., 2005). More understanding of the particle growth systems was needed and this involved molecular dynamics based studies. These are able to calculate surface and interaction energies in addition to the binding energy

of metals and the surrounding stabilising agents at a molecular level (Kemal et al., 2008). An example of this was on an dioctyl sodium sulfosuccinate (AOT) stabilised silver NP system, with a nanoplate based structure. Interaction energies at the different Ag crystal surfaces between the silver and the AOT, were 460.1, 323.4 and 249.9 kcal mol^{-1} for the crystal lattice planes (which are illustrated in Figure 2.4) Ag (111), Ag (110) and Ag (100) respectively (Kemal et al., 2008).

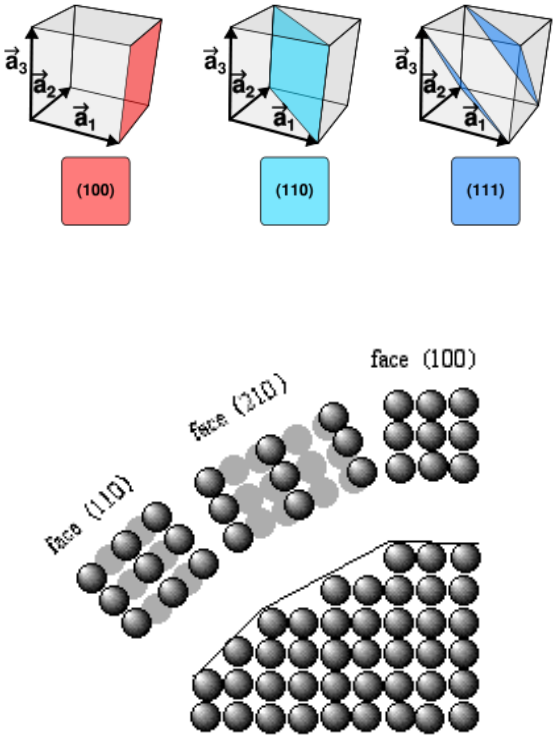

Figure 2.4 Crystal planes within lattice as determined by Miller Indices, these show the direction of approach to the crystal structure and the fact that the stabilising agent binds preferably to one plane over others promotes growth in these other planes.

The strong interaction in the Ag (111) planes restrict growth here and this causes faster growth in the other directions leading toward the nanoplate structure (Kemal et al., 2008). Kemal (2008) and colleagues also reported that close control of temperature during synthesis

has a governing relationship upon shape and so it seems that with the understanding and modelling of these binding energies that the synthesis of controlled size and shape is going to become increasingly possible (Kemal et al., 2008).

2.2.2.4 Zero valent nanoparticles

Zero valent iron NPs have shown much potential in the remediation of environmental systems with the ability of these NPs to dechlorinate chlorinated organic contaminants and capacity to immobilise heavy metals that are commonly found in groundwater (Phenrat et al., 2007; Sun et al., 2006; Wang and Zhang, 1997). These iron NPs typically consist of a core shell structure with a zero valent core surrounded by a Fe(II) or Fe(III) oxide shell formed from the oxidation of the zero valent core (Li et al., 2006). With its zero valent core these iron NPs are excellent electron donors and coupled with their reactivity in water this provides the basis for their versatility in remediation matters (Li et al., 2006).

Synthesis of these NPs has been successfully shown using both, the top down approach, with successful synthetic procedures including, vacuum sputtering (Kuhn et al., 2002), the reduction of goethite and hematite particles at elevated temperatures, and the decomposition of pentacarbonyl iron in organic solvents (Karlsson et al., 2005), amongst others (Li et al., 2006). While bottom up approaches include the reduction of Fe(III) or Fe(II) to Fe^0 with sodium borohydride (Zhang, 2003).

2.2.3 Gold Nanoparticles

2.2.3.1 Introduction

Generally gold can be considered to be an inert and stable material when considered as large particles but on the nanoscale it has received much attention due to its catalytic electronic and

optical properties (Burns et al., 2006; Li et al., 2006; Medina-Ramirez et al., 2009; Sun and Xia, 2003). NPs with a size of less than 10 nm have shown an ability to be used in medical sciences as molecular delivery carriers based on their attraction toward functionalised species such as amino and nucleic acids (Li et al., 2006), and when functionalised with oligonucleotides can act as control for protein expression in cells (Rosi et al., 2006). Displaying very intense colours when dispersed in water due to surface plasmon resonance (SPR) (the collective oscillation of conductance band electrons in response to the application of an electromagnetic field see section 3.4.2), gold NPs have intriguing optical (Liz-Marzán, 2004), electronic (Kamat, 2002) and catalytic (Mallick et al., 2005) properties attracting interest in sensing and other related fields (Hoppe et al., 2006).

Metallic NPs have emerged as intense colorimetric reporters in medicine and tracing due in large part to their extinction coefficients which are several orders of magnitude higher than those of the incumbent organic dyes used in these processes (Labande and Astruc, 2000; Xia and Halas, 2005). Gold and silver NPs have been found ideally suited for use in sensing once coupled with a surface bound receptor molecule, such as crown ether potassium ion and EDTA for a variety of generic metal ions (Kim et al., 2001), due to a detectable change in the plasmon absorption band (see section 3.4.2) of gold NPs which occurs upon aggregation, alongside other colour changes, brought on by changes in inter-particle distance (Obare et al., 2002). This is unique in gold and silver systems due to the densities of free electrons being in the proper range for their NPs to have surface plasmon peaks in the visible range (Xia and Halas, 2005). Again using the optical properties of the gold NPs sensitivity toward lithium ions and their detection has been developed and is of interest to the medical and industrial fields due to the importance of understanding lithium ion transport in biomedical environments and batteries (Keck et al., 1999; Meyer, 1998). This sensitivity is provided by

coating 4nm gold NPs with a 1,10-phenanthroline ligand (Obare et al., 2002) which selectively binds with lithium ions, this then causes the NPs to aggregate resulting in a red shift in the plasmon band corresponding with the presence of lithium ions (Obare et al., 2002).

Another potential advantage of gold NPs is that it may become possible to negate some of the environmental effects of organic solvents used in industry by using gold NPs as replacements for these solvents where appropriate (Hoppe et al., 2006; Raveendran et al., 2003; Wang et al., 2003)

Surface enhanced Raman scattering (SERS) is an important spectroscopic tool (Xu et al., 2000) used to enhance the signal obtained during Raman spectroscopy giving the potential to detect single molecules. Raman scattering occurs when photons interact with the electron cloud of a molecule, this causes an excitation within the molecular energy states and upon relaxation a photon is emitted at a different wavelength. This signal is enhanced via surface enhancement for a large number of different molecules when they are adsorbed to curved noble metal surfaces with the enhancement factor being between factors of 10^3 and 10^6 in comparison to the flat substrate, but research has shown that in the presence of gold and silver single molecular colloids this enhancement factor rises to as much 10-15 orders of magnitude larger with the upper end of the scale being dependent upon additional factors such as chemisorption which are used to further enhance the mechanism (Shipway et al., 2000; Xu et al., 2000). This stems from an enhanced electromagnetic field as a consequence of surface plasmon resonance as well as the appearance of new electronic states that are established by the adsorption. So the potential is there to achieve an even greater enhancement.

With many of these properties dependent upon size, controllable synthesis is a priority and as such many such procedures are in existence, generally following the chemical reduction of a metal salt precursor (Bajpai et al., 2007). With a tendency toward aggregation as is the case with other metal NPs (section 2.2.2.3) stabilisation is again of key importance. One commonly used electrostatic stabilising agent is sodium citrate. The choice of stabilising agent is an important one as this can govern long term stability within the environment (Diegoli et al., 2008) in addition to factors such as toxicity (Ju-Nam and Lead, 2008).

A wide range of polymers have been used for the synthesis of gold NPs alone, and include both charged and uncharged species, such as, poly(*N*-vinyl pyrrolidone) (Hoppe et al., 2006), poly(vinyl pyridine), PEG (Ishii et al., 2004), poly(vinyl alcohol) (Khanna et al., 2005; Sakamoto et al., 2006), and numerous others (Shan 2007). A few of these have shown the ability to behave not just as a protective capping agent but as a reducing agent in their own right and so provide for a simpler and potentially greener synthesis.

2.2.3.2 Polyvinylpyyrolidone stabilised gold nanoparticles

The protective capabilities from aggregation of a stabilising agent can be rated using a value which is defined as the weight, in grams, of gold in a red gold sol, which is protected by 1g of the protecting agent against flocculation by 1% sodium chloride (Hirai and Yakura, 2001). PVP is a commonly used protective agent with a relatively high protective value of 50.0 (Hirai and Yakura, 2001). This compares with values of 5.0, 1.3, 0.07 and 0.04 for poly(vinyl alcohol), poly(acrylamide), poly(acrylic acid) and poly(ethyleneimine), respectively. Thus it can be seen that the protecting power of PVP is much greater than

other synthetic homopolymers (Hirai and Yakura, 2001). Due to its solubility in water and other polar solvents alongside its non-toxic nature it has seen frequent use with good overall results in size and shape selectivity (Kan et al., 2006; Zhou et al., 2006b). The polymer has proven to be a successful protecting agent in the polyol process (which uses a polyol – alcohol with multiple hydroxyl groups - as a reducing agent to reduce metal salts to metal particles (Liu et al., 2004)) where it has been shown to prevent the agglomeration silver and gold NPs and other metallic NPs (Sun and Xia, 2002). In regard to the physisorption of PVP in particular onto a metallic core, part of the PVP adsorbs directly on to the metal creating a first inner shell, while the remaining PVP is dissolved into suspension, creating a second outer protective shell (Pachon, 2008). Offering a compromise between the covalent and physisorption based steric stabilisation detailed in the previous chapter.

With regard to the structure of the NPs and the binding of the PVP to the gold and how this effects shape, Kemal (2008) show that PVP preferentially binds with gold at the Au (111) plane (0.0197 eV) over the Au (100) (-0.0425 eV) and Au (110) (-0.0531eV), inhibiting growth in this direction. This led to the formation of nanorod like structures, in addition, by using different variations of temperatures and cooling during the reaction process it was found that spherical particles were formed as well as worm like structures (Kemal et al., 2008), due the growth mechanism being interrupted and then altered. This shows again how changes in the reaction environment can influence the size and structure of NPs.

Recently, due to the versatility of PVP and its utility in varying nanoparticle syntheses research has expanded on the role of PVP from simply being a protective agent to functioning as both protective agent and reducing agent in order to streamline synthesis in the case of gold and silver NPs (Hoppe et al., 2006). Prior to this there had been some mention of the

potential ability of PVP to act as a reducing agent alone (Deivaraj et al., 2005) by the direct abstraction of hydrogen atoms from the polymer by the metal ion or the reduction of the metal by organic macroradicals formed by degrading the PVP (Hoppe et al., 2006). This combination allows a simple and controllable synthesis, with the size of the NPs produced dependent upon the ratio of PVP to salt precursor used (section 3.2), whilst yielding NP dispersions that are stable even several months after synthesis (Hoppe et al., 2006).

2.3 Ecotoxicological impacts

2.3.1 Carbon based nanoparticles

2.3.1.1 Fullerenes

The release of C_{60} into the environment is seen as a long term hazard to human health and may also have ecological effects (Porter et al., 2007). Fullerenes are of particular interest to the toxicological community, as C_{60} molecules have a diameter of around 0.7 nm which is sufficiently small for the molecules to enter into cells via passive diffusion in ion channels and to be able to diffuse through the nuclear membrane (Smith et al., 2007). This size range is significantly smaller that the sizes under consideration in this project but is indicative of the need to model the pathways to potential exposure of NPs in general though it should be noted that fullerenes exist as aggregates in water. Invertebrate studies have shown that a 50% mortality level could not be reached with an environmentally relevant concentration. This suggests that acute toxicity is unlikely to occur though significant sub lethal effects were identified, including reduced reproductive activity, suggesting that population level effects may be seen (Oberdorster et al., 2006a).

Author	Material	Toxicity
(Oberdorster, 2004)	Filtered C_{60} suspended in THF and stirred overnight	Significant lipid peroxidation found in Largemouth bass exposed to 0.5 mg L^{-1}
(Lovern and Klaper, 2006)	Filtered C_{60} suspended in THF and stirred overnight	Lethal concentration (LC_{50}) for *Daphnia Magna* was 460 µg L^{-1}
(Lovern and Klaper, 2006)	C_{60} water suspension	Lethal concentration (LC_{50}) for Daphnia Magna was 7.9 mg L^{-1}
(Oberdorster et al., 2006b)	C_{60} water suspension stirred for two months	Exposure to 2.5 mg L^{-1} delayed molting and reduced offspring production
(Zhu et al., 2006)	C_{60} suspension in water stirred for two weeks	Exposure over 8 days resulted in just under 50% mortality in *Daphnia Magna at 35 mg* L^{-1}
(Zhu et al., 2006)	C_{60} prepared with THF	Exposure over 8 days resulted in just under 100% mortality in *Daphnia Magna* at 1 and 2 ppm
(Gimbert et al., 2006)	C_{60} prepared with benzene, THF and acetone	Zebra fish suffered delayed embryo development, decreased survival and hatching rates and pericardial edema over 96 hours at 1.5 mg L^{-1}
(Gimbert et al., 2006)	Fullerol: $C_{60}(OH)_{16\text{-}18}$ prepared with benzene, THF and acetone	No effects upon zebra fish
(Brausch et al., 2011)	C_{60} stirred for two months and used to prepare reconstituted moderately hard water	Affected *Daphnia Magna* vertical migration and influenced their swimming velocity
(van der Ploeg et al., 2011)	C_{60} dissolved in aqueous soil extract	Dose dependant reduced cocoon production and higher juvenile mortality in earthworms

Table 2.1 Toxic effects of carbon containing fullerenes, adapted from (Klaine et al, 2008).

There is a concern that the true toxicity of fullerenes is difficult to assess due to the nature of their synthesis, the solvents that are used to disperse the fullerenes are themselves highly toxic. Whilst the dispersion method can often lead to aggregation during toxicological tests resulting in different ecotoxicological effects (Smith et al., 2007). However this can be managed by the careful selection of solvent and use of controls. It has been suggested that some toxicity may stem from the solvents used (Oberdorster et al., 2006a).

2.3.1.2 Carbon nanotubes

Having aspect ratios of over 100, with lengths of several µm and diameters of 0.1 – 1.5 nm for SWCNTs and 2 – 50 nm for MWCNTS (Nel et al., 2006), carbon nanotubes have similar structures to asbestos, suggesting that they may share a toxicity (Ju-Nam and Lead, 2008). This has been shown in a number of studies with a dose of 0.5 mg of SWCNTs causing 56 % mortality in mice over a seven day period (Handy et al., 2008), with macrophage granulomas forming beneath the bronchial epithelium, though the high dose of the particles caused by the application of a non-physiologic exposure route (intratracheal instillation), coupled with second order effects from metal impurities could lead toward an artificially high toxicity (Nel et al., 2006).

Author	Material	Toxicity
(Zhu et al., 2006)	MWCNTs	Dose dependant growth inhibition of Stylonchia mytilus at concentrations of 0.1 - 200 mg L^{-1}. Co-localisation of CNTs within the mitochondria was observed
(Roberts et al., 2007)	Lysophophatidylcholine coated SWCNTs	100% mortality observed in 20 mg L^{-1} doses to Daphnia magna
(Gimbert et al., 2007)	SWCNTs dispersed in SDS	Oxidative stress linked effect and dose dependant rise in ventilation rate, gill pathologies and mucus excretion for rainbow trout over 10 days at doses of 0.1 - 0.5 mg L^{-1}
(Gulson and Wong, 2006)	SWCNTs raw	Hatching delays for zebra fish embryos at concentrations over 120 mg L^{-1}
(Gulson and Wong, 2006)	Double walled CNTs	Hatching delays for zebra fish embryos at concentrations over 240 mg L^{-1}
(Gulson and Wong, 2006)	Carbon black	No hatching delays observed in zebra fish embryos up to 240 mg L^{-1}
(Yuan et al., 2011)	SWCNTs	Increased generation of ROS, induced changes of protoplast morphology and leaves changing from green to yellow
(Srivastava et al., 2011)	MWCNTs	Oxidative stress and apoptosis in human lung cancer cells

Table 2.2 Toxic effects of CNTs, after (Klaine et al, 2008).

Questions also surround the actual risk posed by airborne CNTs as producing CNT aerosols appears to be difficult (Ju-Nam and Lead, 2008), though the release from a commercial product such as car tyres is always possible (Nel et al., 2006). CNTs have also been shown to act as respiratory toxicants in rainbow trout with CNTs precipitating in the gills and also appearing in the gut (Smith et al., 2007)

2.3.2 Inorganic nanoparticles

2.3.2.1 Quantum dots

Toxicity of quantum dots may stem from the leaching of heavy metals from colloids (Ju-Nam and Lead, 2008), or from the theoretical ability of the quantum dots to transfer energy to oxygen atoms leading to the formation of reactive oxygen species, leading to cell inflammation and death, lipid peroxidation and cell death has been shown (Choi et al., 2008). Oxidative stress within the gills and DNA damage has been reported in freshwater mussels (Ju-Nam and Lead, 2008).

2.3.2.2 Metal oxide nanoparticles

Metal oxide particles appear to be relatively non toxic, with a few exceptions, such as cadmium oxide in rats (Handy et al., 2008). TiO_2 NPs have been shown to be relatively non toxic to fish, with no effects found in zebra fish found at up to 1000 µg L^{-1} (Scown et al., 2010), and an LC_{50} in fathead minnow of in excess of 500 mg L^{-1} (Hall et al., 2009). Though a study by Federici (2007) found epithelial injury to the gill and intestine at similar concentrations to those above, with an increase in the content of liver and spleen TiO_2, though these level were close to the limits of detection (Scown et al., 2010). Though there is some evidence of oxidative stress in aquatic systems brought upon by the production of reactive oxygen species in the presence of light (Hirano et al., 2005).

Author	Material	Toxicity
(Lovern et al., 2007)	TiO_2 suspended in THF	10 mg L^{-1} caused 100% mortality in *Daphnia magna*
(Lovern et al., 2007)	TiO_2 sonicated	No mortality greater than 9% for *Daphnia magna*
(Federici et al., 2007)	TiO_2 sonicated	Oxidative and respiratory stress
(Hund-Rinke and Simon, 2006)	TiO_2 sonicated	EC_{50} of 44 mg L^{-1} for mainly anatase 25 nm NPs in algae
(Adams et al., 2006)	TiO_2 prepared with THF	No effect upon *Daphnia magna* at 2 mg L^{-1}
(Franklin et al., 2007)	ZnO	No difference in comparison to dissolved zinc for which an effective concentration of 60 µg L^{-1} was determined
(Manzo et al., 2011)	ZnO	Higher toxic effect in insoluble form towards different terrestrial organisms with respect to similar amounts of ionic zinc
(Gustafsson et al., 2011)	TiO_2	Innate immune activation and long term lymphocyte response in Dark Agouti rat

Table 2.3 Toxic effects of metal oxide NPs, adapted from (Klaine et al, 2008).

Ceria NPs have shown little toxicity in humans (Ju-Nam and Lead, 2008) or fish (Scown et al., 2010), though there may be some toxicity toward *e. coli* where the NPs can become absorbed onto the outer membrane (Ju-Nam and Lead, 2008). ZnO NPs appear to have a low toxicity at relevant concentrations (Zhou et al., 2006a) though some toxicity has been shown at higher concentrations and toward *daphnia magna* (Heinlaan et al., 2008) though there is evidence that given their high solubility, free metal ions were toxic toward lung cell and free algae at environmentally relevant concentrations (Ju-Nam and Lead, 2008).

2.3.2.3 Metal nanoparticles

Silver NPs have shown significant antibacterial properties and are used as coatings for many medical types of equipment, including catheters, infusion systems and medical textiles (Bosetti et al., 2002). The exposure of silver NPs toward zebra fish embryos has induced dose dependant increases in mortality and cause hatching delays, deformations, slow blood flow and induced cardiac arrhythmia (Scown et al., 2010). Differing from carbon nanotubes, silver NPs have been shown to be transported through chorion pore channels by Brownian diffusion (Scown et al., 2010) showing that NPs may be able to reach the foetus. The mechanism of the antibacterial activity that silver NPs display may result in the long term release of silver ions (Ag^+) by the oxidation of the zero valent metallic silver in Ag^0 in contact with water (Kumar et al., 2005). Ag^+ can block DNA transcription as well as inhibiting the enzymes for P, S and N cycles of nitrifying bacteria (Ratte, 1999). One study found that silver ions were 300 times more toxic toward zebra fish, than the associated silver NPs, though Griffitt (2009) has shown that a different response is found between silver NP exposed and silver ion exposed fish suggesting that silver NP toxicity is not solely driven by the release of silver ions (Griffitt et al., 2009).

Copper NPs can cause gill damage and this was put down toward the NPs rather than copper ions released due to dissolution as the NPs produced a greater hypertrophy of epithelial cells and differing gene expression within the gills that the soluble copper (Griffitt et al., 2007). Aluminium NPs have also been shown to inhibit gill function at high doses (Scown et al., 2010).

2.3.2.4 Zero valent iron nanoparticles

Though the fact that iron is present throughout the environment, acts as a limiting nutrient and has even been considered to stimulate algae growth in order to slow down CO_2 driven climate change (The Royal Society, 2009), means that it is not considered to be an environmental risk. The fact remains that zero valent iron is one of few examples (Ju-Nam and Lead, 2008) of a field based study on NP impact that has shown an unfavourable impact (Zhang, 2003) with these NPs shown to reduce oxygen levels in groundwater and significantly alter pH. This shows that full studies on NP impact are required for whichever environmental area may be at risk for a particular NP.

2.3.2.5 Gold Nanoparticles

In the case of gold NPs there is evidence that they possess little toxicity (Zharov et al., 2006). In particular toxicity has not been seen toward red blood cells or *E. Coli* (Goodman et al., 2004), human leukaemia cells (Connor et al., 2005) or in mice (Lasagna-Reeves et al., 2010). Straight forward synthesis coupled with the ability to readily receive functionalised ligands does mean though that they are ideally suited to use in biomedical applications (Goodman et al., 2004), and due to increasingly varied use toxicity may become a factor that will require consideration. Intracellular uptake of bare gold NPs can cause significant biological response in ECV-304 cells, such as the disorganisation of the cytoskeleton, whereas when polymer coated gold NPs (polycaprolactone) are introduced they still make their way to the cell membrane though they have much less influence upon the cytoskeleton and cytotoxicity is reduced even at very high concentration (Mao et al., 2007).

Summary of cytotoxicity data for gold nanoparticles					
Author	Size (nm)	Shape	Surface group	Cell line	Result
(Shukla et al., 2005)	3.5±0.7	Sphere	lysine, poly-lysine	Mouse macrophage cells	85% cell viability after being exposed to 100µM gold NPs for 72 h
(Connor et al., 2005)	4,12,18	Sphere	citrate, cysteine, glucose, CTAB	human leukaemia	no toxicity at micromolar ranges used
(Goodman et al., 2004)	2	Sphere	quatemary ammonium, carboxylic acid	mammalian red blood cells, *E-Coli*	Cationic NPs much more toxic than anionic NPs
(Niidome et al., 2006)	65 ± 5, 11 ± 1	Rod	CTAB, PEG	HeLa cells	80% cell death with 0.05 mM CTAB NPs, 10% cell death with 0.05 mM PEG NPs
(Huff et al., 2007)		Rod	CTAB	human tumour KB cells	NPs rapidly taken into cells and formed aggregates, but cells remained healthy
(Patra et al., 2007)	33	Sphere	CTAB, citrate	baby hamster kidney cells, human liver cardnoma cells, human carnoma lung cells	toxic to lung cells, non toxic to rest
(Takahashi et al., 2006)	65, 11	Rod	Phosphatidylcholine	HeLa cells	much less toxic than CTAB coated NPs
(Khan et al., 2007)	18	Sphere	Citrate	HeLa cells	Internalised into cells but no cytotoxicity or gene expression
(Lasagna-Reeves et al., 2010)	12.5		Naked	Mice	No evidence of toxicity 40 - 400 µg/kg/day
(Chen et al., 2009)	3 – 100	Sphere	Citrate	Mice	NPs in range 7 - 38 nm 8000 µg/g/week induced severe sickness in the mice

Table 2.4 Cytotoxicity data for gold NPs, adapted from (Murphy et al., 2009).

Table 2.4 shows that when functionalised with various surface groups gold NPs generally show very little toxicity, though in a few cases (often when coated with Cetyl trimethylammonium bromide (CTAB)) certain levels of toxicity were to be found, unfunctionalised spherical gold NPs have been shown to be non toxic in concentrations of up to 100 µM gold atoms (Murphy et al., 2009).

2.3.3 Nanoparticles in the environment

Inevitably the life cycles of nanomaterial based products will mean that at some point they will become discharged into the air, water or soils of the planet (Wiesner et al., 2006). Once this release into the environment has occurred, a major factor in determining the potential impact that they may have, alongside the potential toxicity of the particular NPs, is the extent of transportation that they will undergo (Biswas and Wu, 2005; Daughton, 2004).

In many products NPs are embedded within a surface or applied as a coating (Marini et al., 2007). Due to this there is a potential for metal ions rather than complete NPs to be released upon disposal or through use, and as such this needs to be considered as well (Blaser et al., 2008). This is the case of NPs such as silver and copper which have relatively high solubility and may not be seen with less soluble metals such as gold. Blaser (2008) and Mueller and Nowack (2008) have both made attempts to identify the pathways for exposure that may occur from the industrial usage of some NPs and likely dosages that may be met. The flow paths that were determined for silver NPs, titanium oxide and CNTs are shown with amounts in Figure 2.5.

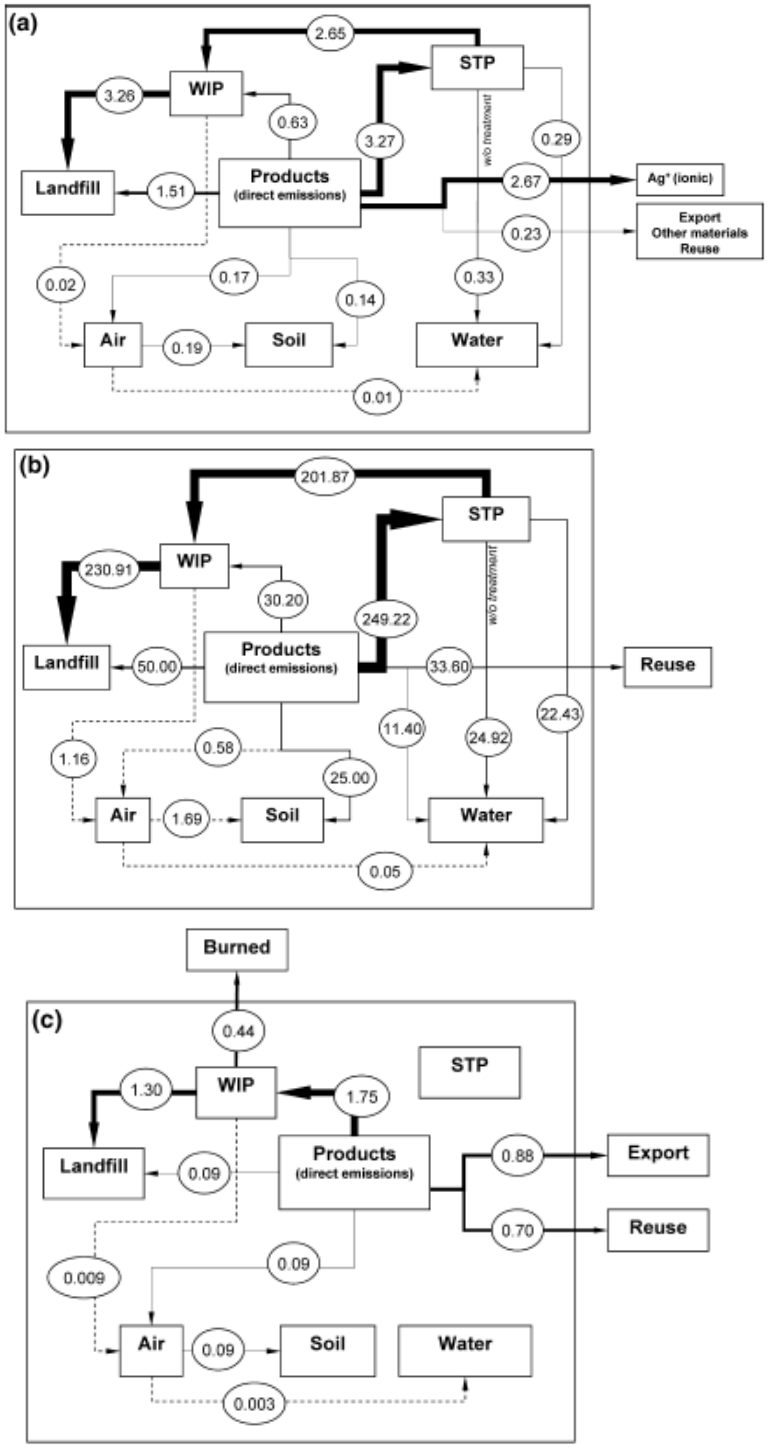

Figure 2.5 The flow of a) AgNPs b) TiO_2 NPs and c) CNT from consumer products to the different environmental compartments and Waste Incineration Plants and Sewage Treatment Plants in a high level emission scenario, flows are in tons/year, after (Mueller and Nowack, 2008).

As is clear from Figure 2.5 with regard to AgNPs and TiO_2 both Mueller and Blaser's models assume that wastewater treatment facilities would result in the removal of 90% of the NPs

from water. However sludge from sewage treatment plants is often used in agricultural processes and as such provides a pathway back into the environment for the NPs (Mueller and Nowack, 2008). NP silver and titania were much less likely to end up in the air. Whilst CNTs were found to be almost exclusively in air and soil and even then at very low concentrations as they are expected to be released into the environment only at very low concentrations for now due to the high cost associated with their purchase, this is expected to change as their cost decreases and subsequent use increases. For both silver and titania the main sink was the landfill site via the sewage treatment works and waste incineration plant (Mueller and Nowack, 2008). The predicted environmental concentrations of the three NPs are shown in table 2.5. At these level only TiO_2 is high enough to warrant any potential risk toward aquatic life and more data is required (Mueller and Nowack, 2008).

Predicted Environmental Concentration (PEC) of Nano-Ag, Nano-TiO_2 and CNT in Air, Water and Soil

		nano-Ag		nano-TiO_2		CNT	
	unit	Realistic	High	Realistic	High	Realistic	High
air	$\mu g\ m^{-3}$	1.7×10^{-3}	4.4×10^{-3}	1.5×10^{-3}	4.2×10^{-2}	1.5×10^{-3}	2.3×10^{-3}
water	$\mu g\ L^{-1}$	0.03	0.08	0.7	16	0.0005	0.0008
soil	$\mu g\ kg^{-1}$	0.02	0.1	0.4	4.8	0.01	0.02

Table 2.5 Predicted environmental concentrations of Nano-Ag, Nano-TiO_2 and CNT, redrawn from (Mueller and Nowack, 2008).

Nanomaterial mobility within aquifers and sand filters has been shown to differ depending upon the material, with some showing high degrees of mobility whilst others show a very limited tendency toward transportation (Wiesner et al., 2006) indicating that there is no

universal ‘NPs will do this’ answer but instead each NPs behaviour is affected by charge, size and water chemistry of the environmental media, as detailed below.

When in the environment, the NPs will be exposed to numerous other particles and this may have an effect on their tendency toward aggregation or to attach to surfaces which becomes an important consideration when discussing the potential transport of NPs within the environment. The small size of NPs might be expected to make them highly mobile within porous media (Wiesner et al., 2006), and this must be taken into consideration with the fact that the NPs diffuse readily and will subsequently undergo a lot of collisions with surfaces within the media. These collisions of small NPs with collectors, such as soil particles are as a result of diffusion, interception and sedimentation (Christian et al., 2008). The efficiency of these collisions is the ratio of NPs that attach to the collector surface compared to the total number of collisions. Attachment is, in part, reliant upon electrostatic interactions between the particles and the porous media, if electrostatic repulsive forces dominate then attachment of the NP to the collector is inhibited where as opposite charges upon NP and collector lead to enhanced attachment (Christian et al., 2008).

Other important factors include water chemistry, size distribution and the flow velocity of the water as they will all impact upon the extent of attachment. Due to this it becomes important to take into account the nature of the surface chemistry of the particle when considering transportation rather than merely the size as attachment to surfaces within the porous media is just as important. Almost all minerals within soils and sediments as a result of their crystallographic properties or due to the sorption of electrolytes such as humic acid onto the surface exhibit a negative charge (Petosa et al., 2010). This being so, the charge of the NP is one factor of importance, as are the other factors determining NP stability, and their charge,

these include pH, which can alter the chemistry of the functional groups stabilising particular NPs, as well as the ionic strength of the water, which can have a similar affect. Groundwaters usually have ionic strengths of > 10^{-4}M (Wiesner et al., 2006) and as such the influence of this upon NPs being investigated in transportation studies is a critical factor as it becomes vitally important when considering whether attachment will or will not occur. It is important to consider how the water chemistry of the water in which NPs may be moving will affect the surface chemistry of the NPs which could potentially lead to aggregation and/or attachment within a porous media, or in the case of some NPs which possess uncharged surfaces whether there will in fact be any change at all. These factors and the effects they may have make up the first half of the work presented here as without this understanding it is impossible to fully assess how they will behave within the aquatic environment. In addition to transportation kinetics the physiochemical properties of NPs will also determine their toxicity toward living organisms (Xie et al., 2008).

Under aqueous conditions there are a number of components that have the potential to interact with NPs and have an effect upon their transport. Found throughout aquatic systems, natural organic matter (NOM) is known to form nanoscale coatings on macroscopic surfaces (Baalousha et al., 2008) and is known to provide stabilisation to some NPs as it provides a steric barrier (Chen and Elimelech, 2007). With a much higher concentration in aquatic media than manufactured NPs, NOM has the potential to be a controlling influence upon NP transport (Lead and Wilkinson, 2006). This adsorption of NOM on NP surfaces may enhance the transport pathways of NPs in streams, soils and porous media (Klaine et al., 2008). Due to this, it is important when analysing the fate and behaviour of particular NPs in aquatic systems that the interactions between NPs, humic substances, pH and various salts (such as $NaNO_3$ and $Ca(NO_3)_2$ are taken into account as this may have a dramatic effect on the surface

properties of the NPs. One other important factor in the ultimate fate and behaviour of NPs are the flow characteristics of the aquatic system that the NPs are in. There are a number of factors that control flow and it is important to understand how river systems work and how they may affect NP transport.

2.4 Rivers

2.4.1 Overview

Complex natural systems, rivers are important sculptors of the natural landscape (Rosgen, 1994). A river system's hydrology and material movement are fundamental to the creation and maintenance of different ecosystems (Naiman et al., 2002) as they act as conduits for the movement of water, solute and sediment from the land to the oceans. Since time immemorial rivers have helped shape the growth of civilisation by sustaining life through the provision of drinking water, facilitating trade by providing a means of transportation, enabled industry and innovation by providing power and allowed self sufficiency as fisheries and the rich agricultural lands provided by river bottom lands have allowed generations to feed themselves (United States Geological Survey, 2007).

Rivers act to integrate processes across a diverse range of environments and scales. The flow regime of a river is dependent upon a number of factors, including the climate, topography, geology, land cover and river size (United States Geological Survey, 2007). These hydrological factors combined with, sediment load, nutrient assimilation and ecology show how the river network is integral to the surrounding landscape (United States Geological Survey, 2007). The size of river catchment areas can vary in size greatly from a few square kilometres to thousands. As the river travels from its headwaters to the ocean the physical, chemical and biological make up can change significantly and are intrinsically linked. Small

scale physical processes can impact upon reach scale ecological habitats (United States Geological Survey, 2007).

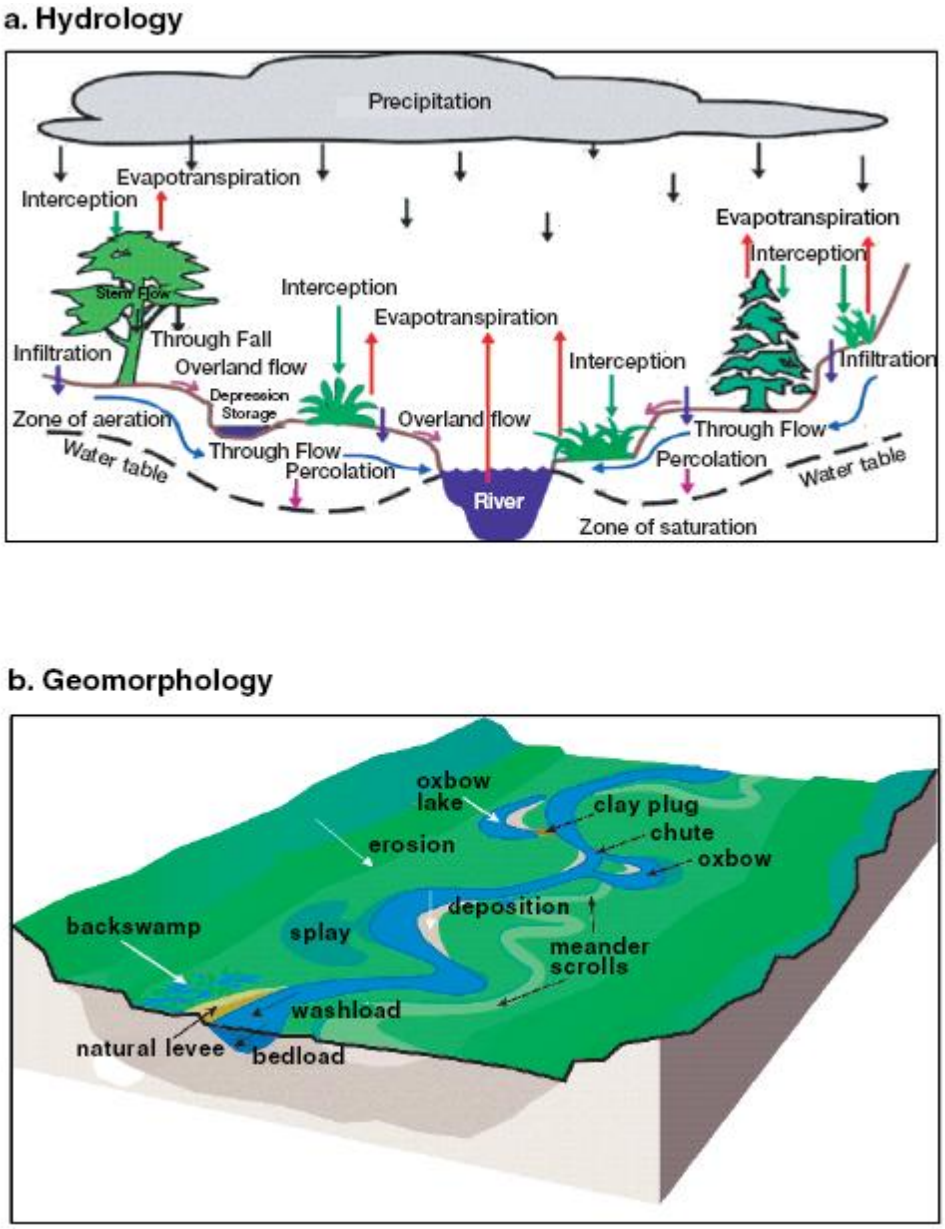

Figure 2.6 a) Hydrological and b) geomorphological view of a river, after (United States Geological Survey, 2007).

One important role that rivers play is in the transportation of sediment. This flux occurs in a number of ways, either as bed load where sediment is carried by fluid drag along the river

bed or suspended within the steam by turbulence with the finest suspended sediment known as washload (United States Geological Survey, 2007) (See Figure 2.6b). This sediment transportation and subsequent deposition provides new habitats for wetland species and can be greatly impacted by the damming of rivers (United States Geological Survey, 2007).

The flow of water within the surface channel is influenced the topography of the streambed, among other factors such as channel size and the gradient of the river. For a uniform flow to occur; all conditions must be the same at all cross sections of the river. For most natural streams, non-uniform flow is prevalent due to variations in width, depth and bed slope (Hamill, 2001).

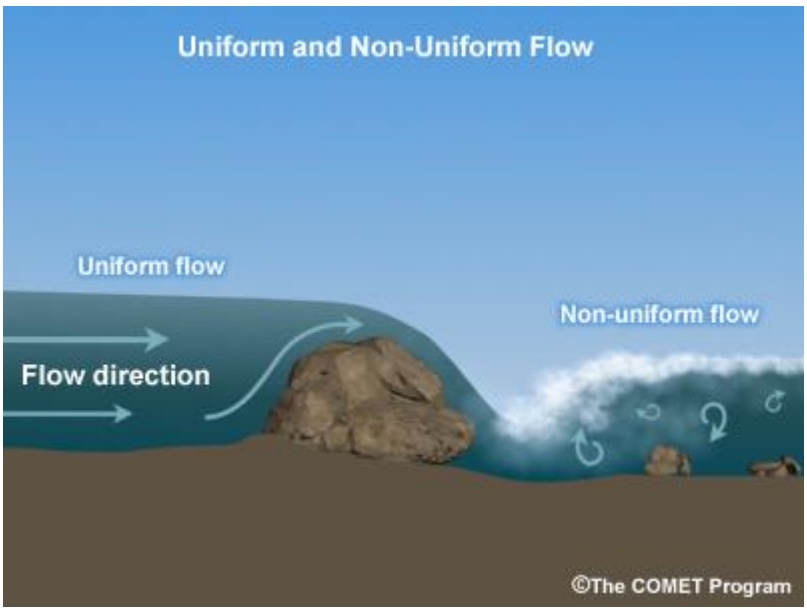

Figure 2.7 Uniform and non-uniform flow, after (University Corporation for Atmospheric Research, 2011).

Flow in the surface channel is linked with flow within the bed by pressure variations and turbulence upon the bed surface; this is discussed in the next section. With uniform flow turbulence is determined by the bed roughness, where, as in non-uniform flow the bed

geometry can also have an effect. Determining whether flow within a channel is turbulent or laminar is done by calculating the Reynolds number (section 5.3.2), generally for a river it will be turbulent (Hamill, 2001) and as such that is the case in the recirculating flume experiments conducted in this work and illustrated later. The flow of water in the channel and over the bed can have an effect on flow conditions within the bed in an area known as the hyporheic zone which is where a significant portion of this investigation is centred as we consider the fate and behaviour of NPs when influenced by this flow into and out of the hyporheic zone.

2.4.2 Hyporheic flow

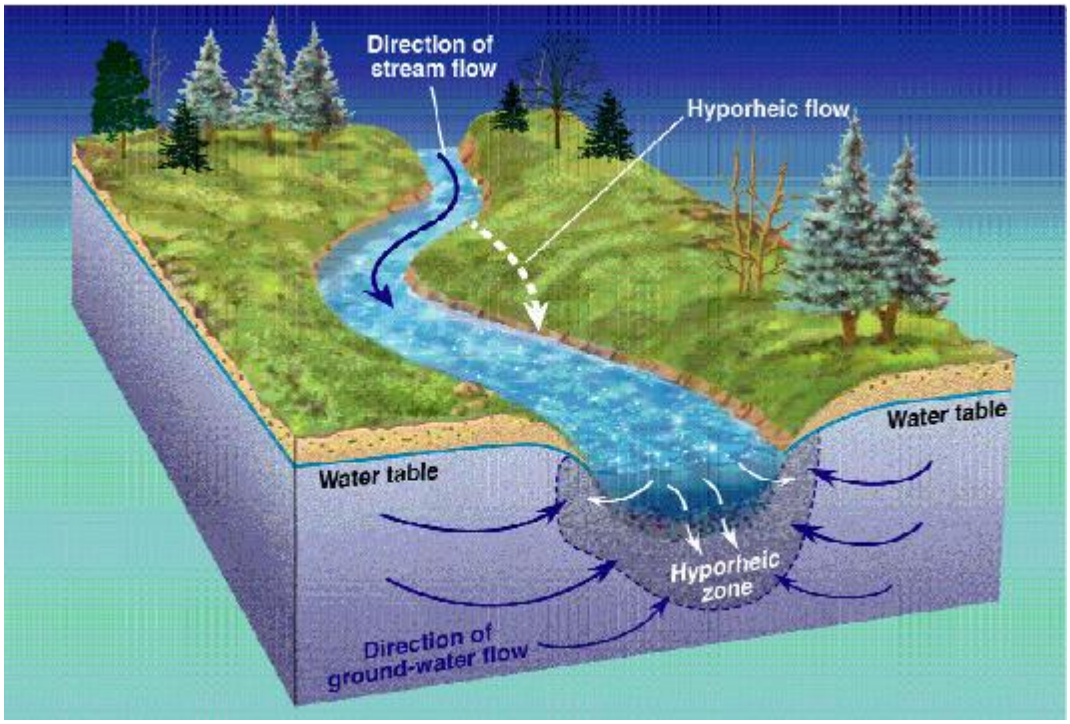

Figure 2.8 The hyporheic zone as it relates to a natural river system, after (Smith, 2005)

The bed of a river can have an important role in governing the transport of contaminants within an aquatic system (Elliott and Brooks, 1997) as the exchange of water between the bed and the surface flow of the river can be a controlling factor in the fate of many contaminants. The flow interactions between the surface and subsurface can influence the mass transfer of many important substances, both dissolved and suspended, between the stream and the hyporheic zone (Packman et al., 2004), which is defined as a porous area at the interface of the stream water and the subsurface water which results in exchange of water between the two different media (Winter et al., 1998) (Figures 2.8 and 2.9).

The exchange taking place at this interface governs the deposition of contaminants into the bed where they may be stored for some time before being released back into the surface flow (Elliott and Brooks, 1997). Investigations in this area have been driven by the desire to understand the process of contaminant transfer as well as the important factors that pore water fluxes play in the geochemistry of marine and freshwater sediments (Packman et al., 2004) and which control the transport of biologically important substances including nitrogen and carbon (Ren and Packman, 2004a). Due to the recent growth of NP production and the likely subsequent release of these particles into the environment, the nature of the effects of these exchange processes upon NPs is something that is of interest (Boncagni et al., 2009) and is investigated within this work.

There are several factors which might affect the exchange of water from the hyporheic zone into the stream flow. On a larger scale, hyporheic exchange is influenced by valley width, depth to bedrock and the composition of the aquifer (Hannah et al., 2009). On the local scale, flow irregularities on the bed surface, such as those caused by bedforms, result in spatial variations in the pressure at the bed surface. These differences in pressure result in advective

subsurface flow paths into and out of the bed which would result in mass transfer in a process known as ‘pumping’ (Elliott and Brooks, 1997; Packman et al., 2004), or from the turbulent coupling of stream and pore water flows (Packman et al., 2004).

For rivers with granular surfaces the flow of water and natural sediment transport processes usually results in the formation of bedforms, such as ripples, dunes and bars (Thibodeaux and Boyle, 1987). The wavelength of ripples is determined by the grain size of the sediment while the depth of water controls the wavelength of dunes (Fourriere 2010). Bedforms are ubiquitous topographical features within natural rivers, with dunes in sandy river beds and cluster formations in gravel river beds formed by the movement of bed material within the flow and its deposition. Exchange between the surface flow and the subsurface has been shown to occur due to bedform induced advection or to the turbulent coupling of stream and pore water flows (Chen and Chiew, 2004; De Smedt, 2007; Nikora and Goring, 2000; Nikora et al., 2001; Shimizu et al., 1990; Suekane et al., 2003; Thibodeaux and Boyle, 1987). Studies have also been conducted on a combination of these effects and results indicate that they can also work simultaneously (Packman et al., 2004). Thibodeaux and Boyle (1987) showed that the presence of bedforms induced a localised advective pumping mechanism.

This exchange process is driven by the pressure variations at the bed surface, with the protrusion of the bedforms into the streamflow causing a variation in the dynamic head at the bed surface, (Packman and Salehin, 2003), resulting in a high pressure area forming upstream of the bedform, and a low pressure area forming in the lee of the bedform (Packman et al., 2004; Thibodeaux and Boyle, 1987). Water is forced down by this high pressure and flows within the bed toward the low pressure area (Figure 2.9) (Thibodeaux and Boyle, 1987).

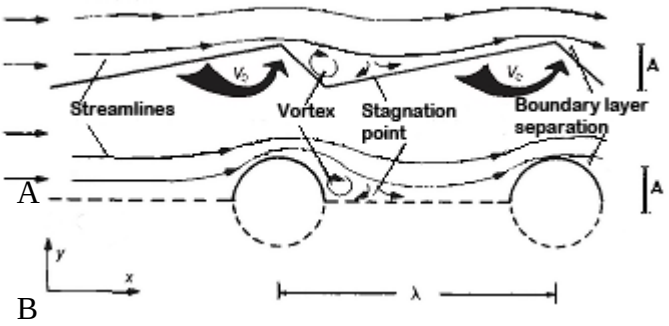

Figure 2.9 Flow conditions around objects in a flow field, a) Over bed and within bed, b) Flow across circular cylinders, λ = bedform wavelength, redrawn from (Thibodeaux and Boyle, 1987).

Within this work the effect of bedforms on NP transport is considered as well as how this may differ when compared to a simple bed with no bedform.

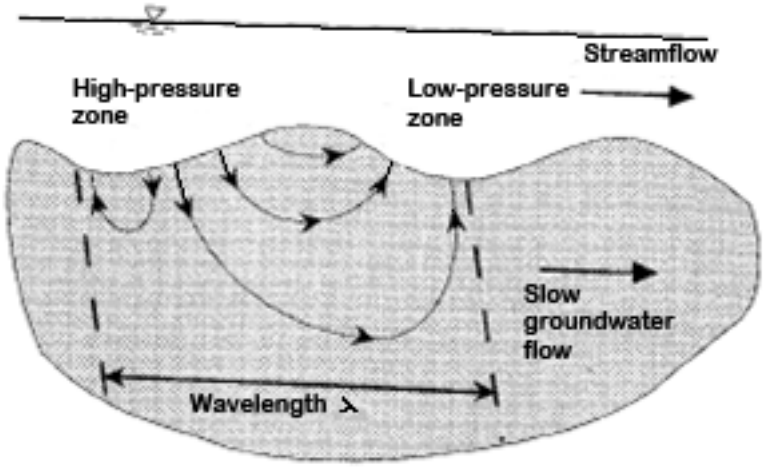

Figure 2.10 Pumping exchange in bed with uneven bed surface streamlines within the bed due to periodic pressure variations along an uneven bed surface, after (Worman, 2002).

Elliott and Brooks (1997) found that dynamic pressure variations across bed forms, which control flow into and out of the streambed, could be approximated by:

$$h_d = h_m \sin(kx) \tag{2.1}$$

Where h_d, is the dynamic head at the bed surface, h_m, is half the amplitude of head variation, k is the wavenumber of the variation, ($k=2\pi/\lambda$, where λ is the wavelength of the bedform, see Figure 2.9, 2.10 and 2.11) (Elliott and Brooks, 1997).

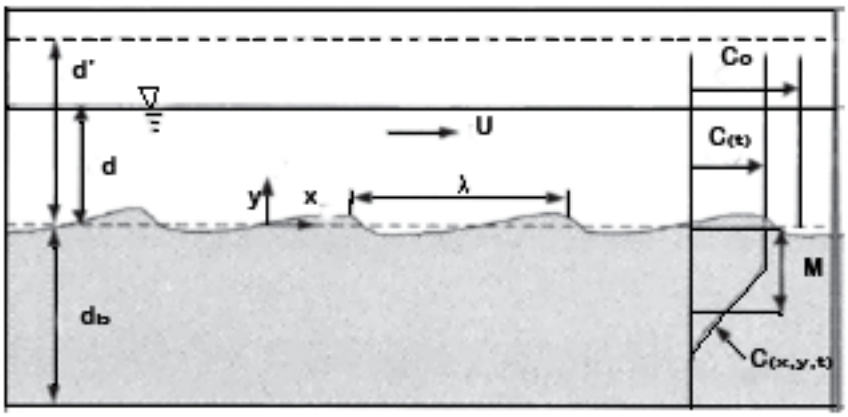

Figure 2.11 Longitudinal section of stream and sand bed, after (Packman et al., 2000a) U is mean stream velocity, d is the stream depth d_b is the depth of the bed d' is the total volume of water in the flume and M is the extent of solute penetration..

h_m is found via the relationship:

$$h_m = 0.28\frac{U^2}{2g}\begin{cases}\left(\dfrac{H/d}{0.34}\right)^{3/8} & H/d \le 0.34 \\ \left(\dfrac{H/d}{0.34}\right)^{3/2} & H/d \ge 0.34\end{cases} \tag{2.2}$$

U is the mean stream velocity, though it is not clear if this is the depth averaged parameter or a cross sectional averaged one, g is the acceleration due to gravity, H is the bedform height whilst d is the stream depth. This represents the head difference on the bed surface produced by the drag of bedforms (Packman et al., 2000b).

The head distribution at the subsurface can be determined and from this the velocity of water within the bed can be found using Darcy's law, assuming laminar flow. This describes the steady flow of water through a permeable bed:

$$Q=k\,h\,A \tag{2.3}$$

Q is the flow rate (m^3day^{-1}), k is the hydraulic conductivity of the material ($m\ day^{-1}$), h is the hydraulic gradient (which is a fraction determined by the change in height of the water table over a given distance, though the water table will not be represented within the experiments undertaken later), and A is the cross sectional area of flow (m^2) (Hamill, 2001). The law is a mathematical proof of several observed properties of flowing groundwater, this includes the flow of water from high pressure toward low pressure areas, the greater the difference in pressure the faster the discharge and that this rate will be effected by the material (Hamill, 2001). In this case the maximum velocity within the bed, u_m, occurs at the surface and is given by:

$$u_m=k\,H\,h_m \tanh\,(kd_b) \tag{2.4}$$

k is the hydraulic conductivity of the bed sediments and d_b the depth of the sediment bed. This induced velocity decreases with depth away from the bed surface (Packman et al., 2004).

One manner in which to illustrate the extent of exchange within the bed is the dimensionless penetration equivalent to the fraction of the bed exchanged as used by Packman et al (2004), to show the transport of NaCl between the stream and subsurface, see Figure 2.7.

$$\frac{C}{C_0} = \frac{d'}{M\theta + d'} \tag{2.5}$$

Where C_0 is the initial in stream concentration (for transfer to the bed, the tracer is well mixed within the stream but not present in the bed, so $C_0 = 1$ and $C_{bed} = 0$ at $t = 0$), d' is the effective stream depth (volume per unit bed area) and M is the average depth of solute penetration, θ is the porosity of the stream bed sediments (Packman et al., 2000a). The flume used in the current work (see section 5.2) ensures that d' reflects the total volume of water within the flume whilst M has a maximum value of d_b (Packman et al., 2004).

Without the driving force in the shape of the bedforms, migration of soluble materials is also known to occur (Shimizu et al., 1990), most likely due to the turbulent interactions between the stream and pore water flows (Packman et al., 2004). This induces a non Darcy flow within the stream bed that decreases with distance from the bed surface (Packman et al., 2004). This decay of pore water velocities is expressed by the equation;

$$U_{pw}(y) = U_d + (U_s - U_d)e^{-\alpha y} \tag{2.6}$$

In this case U_{pw} is the steady bulk pore water velocity, U_s is the slip velocity at the bed surface, U_d is the Darcy velocity deep in the bed. α is a constant reflecting the decay of turbulence away from the surface and y is the depth measured downward from the surface (Packman et al., 2004; Shimizu et al., 1990).

With the mass transfer of solutes between the surface and subsurface occurring for both flat gravel beds (Shimizu et al., 1990) which as mentioned above is theorised as being due to a turbulent interaction between the stream and pore water flows resulting in diffusion (Packman et al., 2004). As well as with data from flume experiments fitting both a diffusion

and advective pumping model there is currently no conclusive answer as to which method is the most important (Packman et al., 2004). In the case of bedform induced advective pumping, the size of the bedform was not a major factor in the magnitude of flux in the bed whereas the presence of a bedform did have a significant impact of the magnitude of the flux (Packman et al., 2004). In this work the affect that these two variations may have upon NPs has been considered.

The local water table level also needs to be considered as an important factor when discussing exchange. As local groundwater dynamics are known to have an important role when considering long term catchment area wide exchange (Cardenas and Wilson, 2006). Whilst short term residence exchange is controlled by bed morphology which acts in addition to the groundwater based dynamics (Hannah et al., 2009). The work conducted here being within a recirculating flume could make no attempt to assess the importance of the water table on NP transport as the immediate focus was on short term residency times.

Thus far the ability to link the physical transport processes with biogeochemical processes occurring within the bed is somewhat limited. Certain models have been developed in order to aid the assessment of residence times of contaminants in the hyporheic zone, a common one being the Transient Storage Model which has seen a number of enhancements since its development (Kazezyilmaz-Alhan, 2008).

Transient storage models have been developed in order to give a representation of the effects that the storage of contaminants in both river banks and the hyporheic zone, has on the downstream transport of solutes and suspended materials. Transient storage occurs when water and the chemicals dissolved or suspended within it become temporarily isolated from

the main channel in stagnant water zones such as pools and deep sided channels (De Smedt, 2007), in addition to hyporheic exchange. Due to this exchange the shape of solute concentration profiles are skewed due to the resultant longer residence times (De Smedt, 2007).

Empirical accounts of the effects of dead zones and hyporheic exchange have been achieved by the transient storage model, presented by Bancala and Walters (1983), consisting of a physical transport sub-model combined with a kinetic sub-model, where the physical sub-model represents conservative solutes in the channel under advective and dispersive processes, whilst the kinetic model looks at reactive solutes and takes into account chemical reactions alongside advection and dispersion (Bencala and Walters, 1983; Kazezyilmaz-Alhan, 2008). This model, however, did not take into account the effects of longitudinal advection within the storage zone, which has been shown to have an effect upon residence time (Packman et al., 2004).

More recent models proposed by Worman (2002), De Smedt (2007) and Kazezyilmaz-Ahlan (2007), have built upon this premise and take into account the diffusion of the solute within the channel meaning that advection is possible at all points of the wetted perimeter within the channel (De Smedt, 2007; Kazezyilmaz-Alhan, 2008; Worman, 2002). This has resulted in models that can provide a fairly accurate empirical account of the concentrations of contaminants that can be expected downstream of a point source in a river.

The physiochemical processes that cause the removal of particles from pore water such as filtration and straining (Bradford et al., 2002), are defined using models that rely on clearly defined pore spaces. These are simulated using sediment which is clean and homogenous (Elimelech et al., 2000), this is important to consider when discussing models as in natural

systems sediment beds are likely to be covered with NOM and biofilms (Costerton, 1995) which have been shown in addition to stream velocity, exchange processes and particle size to have an effect upon particle deposition in the hyporheic zone (Arnon et al., 2010).

4.3.3 Implications

In order to accurately assess what is physically happening to the contaminant within the bed rather than just achieving a bulk value further, more detailed work on quantifying the flow on both sides of the interface must be undertaken. This is due to the fact, that as stated above, both diffusive and advective models can give accurate representations, in order to differentiate between the two, advanced measurement methods such as particle-image velocimetry (PIV) and laser-induced fluorescence (LIF) could be used to shed more light onto the physical processes now that the bulk transport issues seem to be accurately represented (Packman et al., 2004).

Recent work using PIV has been used to investigate induced flow within a permeable bed, this found that the mean flow within the pore sites was strongly dependent on the bedform location, which validates the theory that the flow is controlled by the topographical induced pressure gradient (Blois et al., 2010). In addition, it was found that jets with different vectors and strengths, driven by local pressure gradients contributed to the overall characterisation of the flow and that these formed three discrete flow regions: 1) upstream of the bedform, flow moving downward into the bed deflects downstream with a horizontal flow acceleration (Blois et al., 2010) 2) beneath the bedform, flow is horizontal and forms a complex pattern due to the interaction of multiple jets, and 3) downstream an initial angular vector back toward the surface in the downstream direction remains significant before vertically upward flow tendencies begin to dominate (Blois et al., 2010). It will be interesting to see how NPs,

with the different physical properties that they possess when compared to the same material at the bulk state, may behave in this area as they may behave differently to the contaminants and solutes that have been investigated so far, mainly salts (Packman et al., 2004) or dissolved metals, (Ren and Packman, 2004b). The ability to combine the results of studies into nanoparticle transport with results garnered from PIV and LIF studies into pore flows is an exciting prospect for both nanoparticle science and the hydrological sciences.

Initial studies regarding nanoparticle exchange in regard to TiO_2 NPs (Boncagni et al., 2009), have indicated that due to the aggregation characteristics of TiO_2 and the enabling of the aggregation process by the flow of the water at differing pH, there is significant sedimentation of the NPs which appears to dominate the exchange process (Boncagni et al., 2009). Studies on iron NPs in saturated porous media have indicated that without the presence of a protecting agent, such as a polymer, they are almost immobile whilst when stabilised, in this case with guar gum, the iron NPs showed considerable transport (Tiraferri and Sethi, 2009).

Aggregation is therefore to be seen as an important factor when determining the behaviour of the NPs and when investigating the manufactured gold NPs used in the experimental work undertaken, their aggregation behaviour under differing conditions need to be established as this will have great relevance on the results gained from exchange experiments. This means that it is important to have a full understanding on the potential aggregation behaviour under a variety of environmental conditions for the NPs that are to be used in this investigation.

3.0 Methodology

3.1 Introduction

The analysis of NP fate and behaviour within the hyporheic zone required a two pronged approach. Prior to this was the important step of the identification of a suitable NP upon which the investigation could be centred. Once this was decided, these NPs had to be analysed for their behaviour in the potential aquatic environment to which they may become exposed to. In order to achieve this, a number of experiments were carried out and the details of which are given within this chapter and in Chapter 4. The second approach toward the consideration of NP behaviour in the hyporheic zone and how the effects of flow and exchange may influence NP transport required the use of a recirculating flume and a simulated gravel river bed. This approach is covered later in this chapter as well as in greater detail in Chapter 5.

3.2 Chemicals used

The chemicals and solvents used throughout were purchased from Aldrich and are considered to meet the purity standards set by the American Chemical Society. Stock solutions of the $NaNO_3$ and $Ca(NO_3)_2$ were prepared and these were used to prepare samples at the environmentally relevant conditions that were used throughout whilst HNO_3 and NaOH were used to control the pH. Ultra high purity water (maximum resistivity of 18.2 $M\Omega cm^{-1}$) was used in all experiments. Suwannee River fulvic acid (SRFA) was purchased from the International Humic Substances Society (IHSS) and aqueous solutions were prepared by the dilution of the solid form to a stock solution of 20 mg L^{-1}, and left for 24 hours for complete

dissolution. SRFA is a well characterised reference material (e.g. Lead et al., 2000 and references therein).

3.3 Synthesis

The NPs used had to meet several criteria throughout the programme of work. These included ease of detection, low polydispersity and ideally long term stability. Rapid aggregation occurring within the flume experiments would have significantly complicated data interpretation. To this end poly(*N*-vinyl-2-pyrrolidone) supported gold nanoparticles were synthesised using the procedure reported by Hoppe and colleagues (Hoppe et al., 2006) with a few modifications. This method uses poly(*N*-vinyl-2-pyrrolidone) as both protecting and reducing agent in the reaction (Figure 3.1).

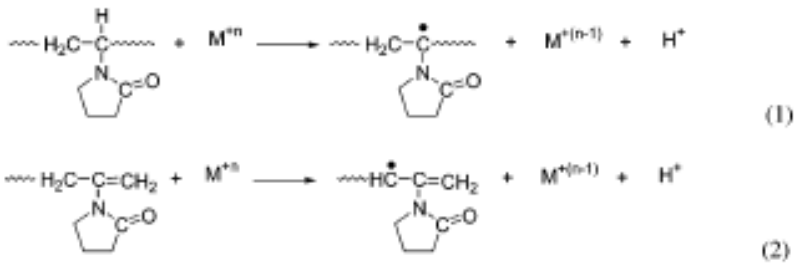

Figure 3.1 The synthesis proceeds as the PVP acts as a reducing agent. This process can be understood by taking into account two main reactions: 1) The direct abstraction of hydrogen atoms from the polymer by the metal ion; 2) The reduction of the metal precursor by the PVP radicals formed in 1 or during the metal accelerated degradation of PVP, after (Hoppe et al., 2006).

A solution of 26 mM PVP10 (average molar mass of 10 000) was prepared in ultra high purity (UHP) water by dissolving 54 g of PVP10 in 180 ml of UHP water. To this a 1mM

solution of potassium tetrachloroaurate was added, this consisted of 75 mg potassium tetrachloroaurate dissolved in 20 ml of UHP water. This was shaken at room temperature until complete homogenisation. The solution was then vigorously stirred and heated at 70°C for 3 hours, which produced a deep red solution. After 3 hours the stirring and heating were stopped and the solution left until it had returned to room temperature. Extractions using acetone were then carried out using a ratio of acetone : solution of 3:1 for the purification of the nanoparticle colloidal solution (Chou and Lai, 2004). Three of these acetone extractions were completed with the excess acetone being removed via pipette. 2 ml aliquots were taken throughout the synthesis and used for UV-Vis analysis.

Several batches (denoted NP_1, NP_2, NP_3 and NP_4) were made which were all similar: highly monodisperse with mean sizes approximately 7 nm and a standard deviation of ~ ± 1nm; no significant differences in surface plasmon resonance data or charge; no aggregation as prepared. Each NP batch was characterised under a range of similar conditions using a range of different methods

3.4 Characterisation

Physio-chemical characterisation of the NPs used in this study is key to identifying any changes that may occur in the NPs due to exposure to the relevant environmental conditions used here. Initial characterisation was performed on the 'as prepared' NPs and subsequently under different relevant experimental conditions. The NPs were characterised using dynamic light scattering (DLS), transition electron microscopy (TEM) and zeta potentiometry. Size, shape and polydispersity of NPs as well as aggregates, surface properties and dissolution all need to be considered as these properties can all be effected by solution conditions and are

considered to be among the key parameters when analysing the behaviour of NPs (Montes-Burgos et al., 2010). In addition to size, surface charge can also affect the stability of NPs and need to be considered as poorly characterised NPs have the potential to mislead the investigation from the very beginning (Montes-Burgos et al., 2010)

3.4.1 Dynamic light scattering

Fig. 3.2 Malvern Zetasizer as used throughout DLS experiments

This method determines the particle size by the scattering of light caused by the Brownian motion of the particles in concentrated suspensions using an autocorrelation function (Tanguchi et al., 2009). The instrument used causes light to be back scattered at an angle of 173° to the detector. Time dependent fluctuations in the scattering intensity are used to determine the translational diffusion coefficient (D) and from this the hydrodynamic diameter (Malvern, 2009). The rate of these intensity fluctuations is dependent upon the particle size. These fluctuations are then analysed by a digital correlator in order to obtain an autocorrelation function for the sample. The second order autocorrelation curve is generated from the intensity trace using the equation:

$$g^2(q;\tau) = \frac{[\mathrm{I}(t)\mathrm{I}(t+\tau)]}{[\mathrm{I}(t0]^2} \tag{3.1}$$

Where $g^2(q;\tau)$ is the second order autocorrelation function at a particular wave vector, q. Whilst τ is the delay time and I the intensity (Berne and Pecora, 2003). As the delay time increases then the correlation between scattered intensities decays exponentially and the Sigert equation relates the second order auto correlation function to the first order autocorrelation function $g^1(q;\tau)$:

$$g^2(q;\tau) = 1 + \beta[g^1(q;\tau)]^2 \tag{3.2}$$

β is a correction factor depending upon laser alignment. Where a monodisperse sample is present the next step is to treat the first order autocorrelation function as a single exponential decay (Berne and Pecora, 2003):

$$g^1(q;\tau) = \exp(-\Gamma\tau) \tag{3.3}$$

Where Γ is the decay rate and D_t is the translational coefficient which can be derived from the equation:

$$\Gamma = q^2 D_t \tag{3.4}$$

This translational coefficient can yield the hydrodynamic diameter of a spherical particle through the Stokes-Einstein equation:

$$D_t = \frac{k_B T}{6\pi\eta r} \tag{3.5}$$

Where k_B is the Boltzmann constant, T the absolute temperature, η is the viscosity of water and r is the hydrodynamic radius. Where the system contains polydisperse particles to any degree then the first order autocorrelation function is a sum of the exponential decays of all of the sizes present:

$$g^1(q;\tau) = \sum_{i=1}^{n} G_i(\Gamma_i)\exp(-\Gamma_i\tau) = \int G(\Gamma)\exp(-\Gamma\tau)d\Gamma \tag{3.6}$$

From here the cumulant method is used to extract more information regarding the system:

$$g^1(q;\tau) = \exp\left(-\bar{\Gamma}\right)\left(1 + \frac{\mu_2}{2!}\tau^2 - \frac{\mu_3}{3!}\tau^3 + \ldots\right) \tag{3.7}$$

Here $\bar{\Gamma}$ is the average decay rate and $\mu_2/\bar{\Gamma}^2$ is the second order polydispersity index. If the sample is highly polydisperse then a third order polydispersity index may be required. The cumulant method then allows the determination of the z-average (D_z):

$$\bar{\Gamma} = q^2 D_z \tag{3.8}$$

Due to the use of PVP in the synthesis process and the fact that despite the purification process there may be a small amount of excess PVP present in the samples that the acetone extraction process failed to remove and because of the large size relative to that of the gold NPs it is necessary to consider not just the z-average given by the Zetasizer, which is sensitive to and weighted in favour of larger particles due to their increased intensity, but instead to consider the number average which is based upon the number of particles at a certain size (Malvern, 2009) and reveals the dominant species to have the smaller size expected of these gold NPs (Gebhardt et al., 2006). Most analyses involving light scattering require dilution of the sample due to need to ensure singly scattered photons to prevent interference (Tanguchi et al., 2009) as was the case here.

In this case dynamic light scattering measurements were undertaken at room temperature using a Malvern Instruments NANO ZetaSizer.

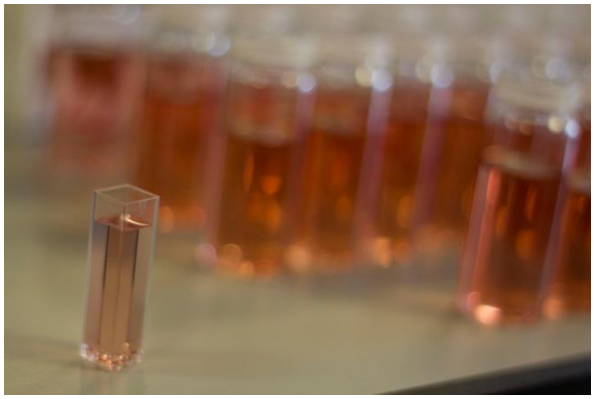

Fig 3.3 Samples for DLS analysis.

2ml of the gold NPs solution was diluted with 18ml of ultra high purity water. Diameters recorded were the average of three readings taken on each sample. DLS measurements were also repeated seven days later and compared to determine particle stability.

3.4.2 Surface plasmon resonance measurements

The optical properties of metallic NPs are heavily influenced by the structure and size of the particles. Bulk Au has a yellowish 'gold' colour in reflected light whilst thin Au films can appear blue, this colour gradually shifts toward orange as size decreases below 3 nm via a deep red colour that is characteristic of gold NPs, (Liz-Marzán, 2004). This colour change is due to the surface plasmon resonance (SPR) (Kreibig and Vollmer, 1996) where the conduction band electrons are polarised in respect to the heavier ionic core by the alternating electromagnetic field given off by incoming light (Link and Ei-Sayed, 2003; Liz-Marzán, 2004; Noguez, 2007)

The intense surface plasmon band shows absorption in the UV-visible region for metallic nanoparticles larger than 2 nm (Moores and Goettmann, 2006). All metals are known to show this band though gold, silver and copper as well as the alkali metals give very intense surface plasmon bands in the visible region due to the presence of free electrons (Liz-Marzán, 2004) . This SPR is attributed to the collective oscillation of conduction electrons induced by an electromagnetic field (Sun and Xia, 2003). The SPR is responsible for the very intense colours displayed by metallic NPs. As stated above, in a classical sense the electric field of incoming light induces a polarisation of the electrons against the heavier ionic core of the nanoparticle (Link and Ei-Sayed, 2003). A restoring force in the form of a net charge difference felt only at the NP surface is present. This creates a dipolar oscillation of all the electrons of the same phase and when this oscillation is the same frequency as that of the electric field a strong absorption is felt. This is what causes the strong colouration and UV-Vis signal (Link and Ei-Sayed, 2003). The phenomenon is felt most strongly in the noble metals due to the 'freedom' of the conduction band electrons in the metals of this group. The oscillation wavelength of the SPR of NPs is different from that of the bulk material (Sun and Xia, 2003) and is dependent upon factors such as size, shape and aggregation of the NPs (Sun and Xia, 2003), as well as by the nature and dielectric constant of the surrounding media. Any interaction between the stabilising ligands and the NPs which may alter the electron density of the nanoparticles may also have an effect (Moores and Goettmann, 2006).

The optical properties of small spherical metallic spheres that account for the SPR formed part of the theoretical work undertaken by Gustav Mie (Mie, 1908). This initially solved Maxwell's equation for the interaction of electromagnetic light with small spheres that had the same properties as the bulk metal (Link and Ei-Sayed, 2003). With boundary conditions, these calculations gave multiple oscillations for the extinction and scattering cross section as

a function of the radius (Link and Ei-Sayed, 2003). This method had a power behind it as it separated the problem into two distinct areas, the electromagnetic side, which is completely solvable and the material, which requires the determination of the dielectric constant ε(ω, R). The fact that this value requires the radius (R) allows the inclusion of all cluster effects at this stage (Moores and Goettmann, 2006). For particles larger than 20 nm Mie's theory holds true as size increases until the bulk material no longer displays a SPR. With particles smaller than 20 nm only the dipole oscillations are of significance and the theory is reduced to the expression:

$$\sigma_{ext} = \frac{9V\varepsilon_m^{3/2}}{c} \cdot \frac{\varepsilon_2}{[\varepsilon_1 + 2\varepsilon_m]^2 + \varepsilon_2{}^2} \tag{3.9}$$

Here V is the particle volume, ω is the angular frequency of the exciting light and c is the speed of light and ε_m and ε are the dielectric functions for the surrounding media and metal respectively.

The equation (3.9) highlights the importance that the dielectric constant of the surrounding media lays in determining the position of the maximum of the plasmon band and its intensity. Changing media to one with a distinctly different refractive index results in a clearly different plasmon behaviour for the NP (Moores and Goettmann, 2006). These effects can range from severe shifts seen when transferring NPs from water to a transparent oxide matrix (Goettmann et al., 2005) to the subtle shifts presented when gradually increasing the size of a silica shell surrounding NPs. This results in changes in the local dielectric constant and gives an initial red shift of the SPR followed by a blue shift as the thicker shell diminishes the dielectric constant (LizMarzan et al., 1996).

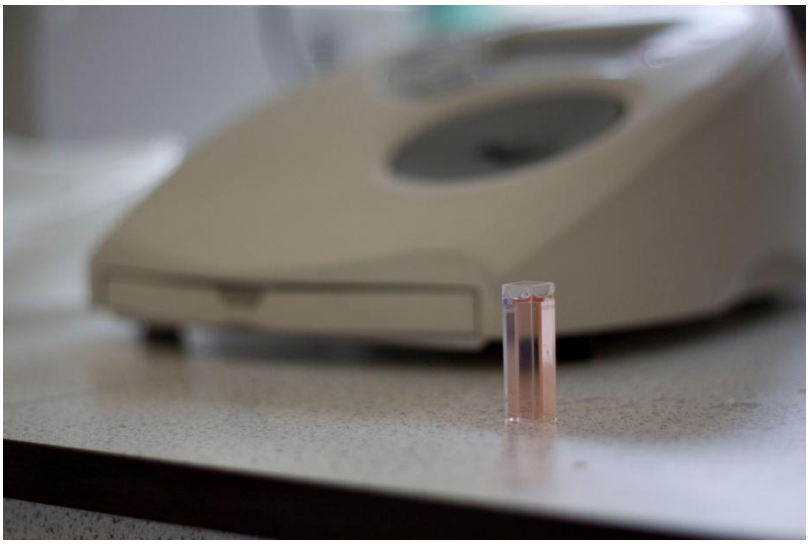

Fig 3.4 Hewlett-Packard 8452A spectrometer and sample.

UV-visible spectra were measured with a Hewlett-Packard 8452A spectrometer. The samples, 2ml of which were diluted with 18 ml of UHP water, were placed in a 1cm x 1cm x 3cm quartz cuvette and spectra were recorded at 25°C and at a wavelength of 520 nm.

3.4.3 Transition electron microscopy

The early roots of electron microscopy lie in de Broglie's discovery that every particle exhibits wave like properties in addition to physical particle properties (de Broglie, 1936). This discovery coupled with the knowledge that magnetic fields can affect electrons in the same way that a glass lens can effect photons (Busch, 1926), led to the subsequent development of the first electron microscope in 1931 by Ernst Ruska (Knoll and Ruska, 1932). This was a microscope based on the use of electrons rather than photons allowing the use of higher magnifications and resolutions than were possible with optical microscopy.

In transition electron microscopy (TEM) a thin sample specimen is illuminated with electrons of uniform intensity (Williams and Carter, 1996). As the electron beam passes through a thin

sample layer, the electrons are either scattered by the nuclei of the atoms in the sample or the electrons in the outer shells (Williams and Carter, 1996), though some may remain unaffected and pass through without any interaction with the sample. This non-uniform distribution of the electrons contains the structural and chemical properties of the sample (Williams and Carter, 1996) and an image is formed.

In the case of the NPs under consideration in these experiments TEM can provide the morphology, size distribution and crystallinity of the gold NP core (Medina-Ramirez et al., 2009). This is required in order to fully characterise them and analyse any effects that different environmental factors may have upon them. In these experiments, TEM analysis was performed using a Tecnai 20 instrument operating at 200kV. Samples were prepared via placing a drop of a dispersion of the PVP coated gold nanoparticles onto carbon coated copper grids and excess solution was removed by filter paper (Baalousha et al., 2005). In order to prevent the increases in salt concentrations which may lead to substantial aggregation (Domingos et al., 2009) the grids were rinsed with UHP water prior to drying as we have done with other NPs (Diegoli et al., 2008). It is acknowledged that some changes in the Suwannee river fulvic acid (SRFA) structure may occur due to ultra high vacuum drying but is of little concern given the focus of this work which is on the structure of the NPs.

3.4.4 Zeta Potential

Upon coming into contact with an aqueous solution the surface charge of a solid causes a rearrangement of local free ions in the solution which gives a region of non zero charge near to the interface between the solid and the liquid. A thin layer of immobile counter ions next to the solid are known as the Stern layer, mobile counter ions outside of the compact layer form the diffuse layer (Sze et al., 2003). The zeta potential reflects the charge at the interface

between the compact and diffuse layer slipping plane and is a measure of surface charge of a particle as affected by the composition of the surrounding medium. Zeta potential is related to electrostatic repulsion and a high positive or negative value of zeta potential can be indicative of stability for charge stabilised nanoparticles (Borm et al., 2006).

This zeta potential is exhibited by colloidal dispersions and can be used to evaluate and estimate long term stability. Colloidal stability can be explained by DLVO theory and the fact that particle stability in solution is dependent upon its total potential energy function (V_T) (Derjaguin and Landau, 1945). Several contributing factors apply:

$$V_T = V_A + V_R + V_S \tag{3.10}$$

V_S is the marginal energy contribution made by the solvent, of more importance is the balance between the attractive and repulsive factors V_A and V_R respectively as they are of higher value and operate over greater distances.

$$V_A = \frac{-A}{(12.\pi.D^2)} \tag{3.11}$$

Where A is the Hamaker constant and D is the particle separation.

$$V_R = 2.\pi.\varepsilon.a.\zeta^2 \exp(-\kappa.D) \tag{3.12}$$

Where a is the particle radius, π is the solvent permeability, κ is a function of the ionic composition and ζ is the zeta potential, (Delgado et al., 2005). The sum of these attractive and repulsive forces that exist between the particles as they approach each other under Brownian motion governs the stability of the colloidal system, (Delgado et al., 2005). Where an energy barrier exists that prevents two particles from adhering to one another. If the particles collide with sufficient energy this barrier can be overcome and permanent aggregation occur (Figure 3.5) (Delgado et al., 2005).

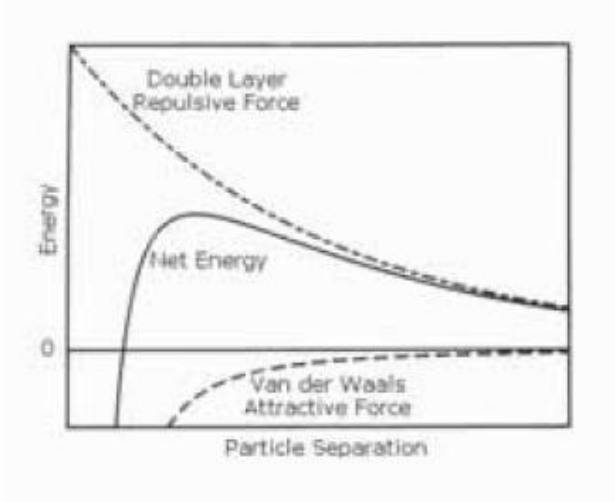

Figure 3.5 Energy Barrier (Malvern, 2001)

These forces manifest themselves in the electrical double layer surrounding the particle which is split into two parts; an inner Stern layer where counterions are strongly bound and the diffuse region where ions are less firmly attached. This diffuse layer features a boundary where inside ions and particles are stable such that when the particle moves ions within the boundary move with it. Ions outside of this boundary stay where they are within the solvent. The potential at this boundary is the zeta potential (Figure 3.6) (Ross and Morrison, 1988; Shaw, 1992).

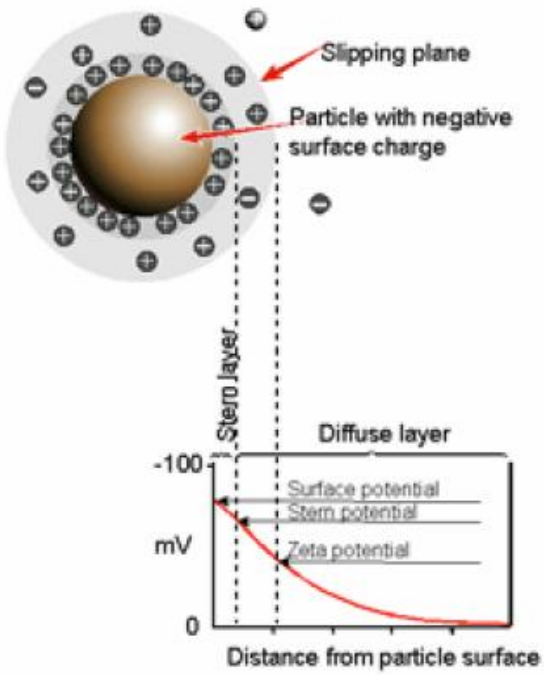

Figure 3.6 Diagram showing the electric double layer and the slipping plane. The potential at the boundary of this layer is the zeta Potential (Malvern, 2001).

This charge possessed by some particles is measured via an electrical field applied across an electrolyte. Here charged particles are attracted toward anode and cathode based upon their charge. This force is opposed by viscous forces within the solvent and upon equilibrating a constant velocity is obtained. The velocity is dependent upon the strength of the electrical field, the viscosity of the media and the zeta potential and is known as the electrophoretic mobility, related to the zeta potential via the Henry equation:

$$U_E = \frac{2\,\varepsilon\, z\, F(\kappa a)}{3\eta} \tag{3.13}$$

Where U_E is the electrophoretic mobility, η is the viscosity, ε is the dielectric constant, *z* is the Zeta potential and f(κa) Henry's function.

In this study zeta potential measurements were performed using a Malvern Instruments Zetasizer. Measurements were performed at 25°C and repeated four times per sample. Samples were assessed using a low volume zeta cell which was washed with UHP water in between each sample (3 x 10ml). This system utilises an electrophoretic light scattering technique, where upon the application of a charged field across the cell, charged particles will move to the electrode with the opposite polarity to the charge that they display. When a laser is shone through these particles as they undergo electrophoresis the light will be shifted to a different frequency, from this the electrophoretic mobility and subsequently the zeta potential can be calculated, (Jiang et al., 2009).

3.4.5 Ultrafiltration

Dissolution studies were conducted using ultrafiltration which involved the use of 1 kDa 63.5 mm regenerated cellulose membranes (Cole Palmer, UK) in a 8200 stirred cell (Millipore, UK).

3.4.6 Atomic Force Microscopy

Scanning probe microscopy (SPM) (alongside TEM) revolutionised our ability to characterise small particles and understand some of the interactions that they undertake (Turner et al., 2007). Allowing the imaging of samples with sub nanometre resolution in three directions and under differing conditions, in ambient air or submerged, SPM techniques all originate from the scanning tunnelling microscope (Binnig and Rohrer, 1982; Turner et al., 2007).

The main principle surrounding these techniques is that of a probe scanning across a sample surface, with the probe's position relative to the sample recorded and held constant via a feedback loop (Sitterberg et al., 2010). For the scanning tunnelling microscope the process requires the sample to have a conductive surface as the method employs the detection of electrons along the surface (Binnig and Rohrer, 1982). Most environmental samples do not possess sufficient surface conductivity or the required rigidity to be directly examined via scanning tunnelling microscopy (Sitterberg et al., 2010).

A solution to this problem is atomic force microscopy (AFM), first designed and built in 1986 (Binnig et al., 1986). AFM allows non-conductive samples to be imaged (Turner et al., 2007) as well as avoiding the complex sample preparation that is often required in other techniques such as SEM and TEM (Alessandrini and Facci, 2005) as samples can be investigated in air and liquid at varying temperatures (Turner et al., 2007). The ability to

image non conductive samples is achieved by using the deflection of a fine leaf spring, the AFM cantilever, for feedback along the z-axis (Binnig et al., 1986). This arrangement avoids the need for the conductance and rigidity of the sample to be considered, (Sitterberg et al., 2010). During the imaging process a sharp probe tip located on the underside of a flexible cantilever raster scans over a sample surface (Turner et al., 2007). As the cantilever and tip scan across the surface the cantilever bends and twists due to the forces between the tip and the sample, this deflection (z_t) is proportional to the force applied as derived from Hooke's law (Meyer, 1992):

$$F = c_B z_t \tag{3.14}$$

Where c_B is the spring constant, which for a beam with constant cross section is given by:

$$C_B = 3\,E\,I\,/\,l^3 \tag{3.15}$$

Where E is the Young's modulus, l is the length and i the moment of inertia. The moment of inertia of a regular beam with width b and thickness t is given by the equation (Meyer, 1992):

$$i = b\,d^3/\,12 \tag{3.16}$$

This deflection is usually monitored by the reflections of a laser beam back onto a position sensitive photodiode detector which allows the degree of bending to be determined by the change in the position of the laser spot (Sitterberg et al., 2010) which is measured by taking into account the difference in intensity between the lower and upper halves of the detector divided by the total intensity (Meyer, 1992):

$$\frac{\Delta I}{I} = \frac{I_A - I_B}{I_A - I_B} = \frac{6\Delta z_t}{l}\frac{1}{\delta} \tag{3.17}$$

Where I is the intensity, l the length of the lever and δ the beam divergence of the reflected beam. This angle can be determined by the focal length f_l and aperture F of the lens:

$$\delta = f_l / F \tag{3.18}$$

This information regarding the defection is then relayed back into a feedback loop that controls the z- position of the AFM tip (Turner et al., 2007) and the force applied accordingly. The three-dimensional motion of the AFM tip relative to the sample is controlled using piezoelectric crystals (Sitterberg et al., 2010; Turner et al., 2007) up to an accuracy of 1 nm (Sitterberg et al., 2010). The geometry of the apex of the tip represents one of the key factors that determines the resolution, with the highest resolutions achieved by the use of tips that end in single atom (Sitterberg et al., 2010). Though the final resolution is dependent on a number of factors, which include long range forces within the atom, in general the harder and flatter the sample the higher the achievable resolution (Alessandrini and Facci, 2005). The surface can be imaged non-destructively as the spring constant of the cantilever is around ten times lower than the interatomic spring constant of the sample and the force applied is well below the force that would result in atoms shifting in their sites, whilst still maintaining cantilever deflections (Kasas et al., 1997).

Three principle modes are employed in AFM imaging, these are, contact mode, intermittent mode (often known as 'tapping' mode), and non-contact mode (Alessandrini and Facci, 2005). For these studies contact and non contact mode were utilised in an effort to get the most complete picture possible.

In contact mode the cantilever tip is in constant gentle contact with the surface of the sample (Binnig et al., 1986) as the cantilever deflection is kept constant by the feedback loop as the surface is scanned. Images are then formed from the changes in the piezo – vertical position

that is required in order to maintain the same cantilever deflection (Alessandrini and Facci, 2005). This mode enables the highest resolution and is the method of choice for rigid and flat samples. One advantage of contact mode is the ability to determine the lateral force applied onto the tip from different chemical functionalities distributed on the surface. This is detected from the torsion that they may apply on to the cantilever and detected by lateral segments of the photo diode (Alessandrini and Facci, 2005). One disadvantage of contact mode is the potential for dragging forces to form from the movement of the tip over the surface, this problem becomes increasingly evident where the sample is loosely bound to the substrate and therefore easily dislodged (Alessandrini and Facci, 2005).

In non contact mode the tip has no contact with the surface and the cantilever is oscillated at or close to its resonant frequency at a distance of 1-10 nm above the sample surface (Kasas et al., 1997). The image is formed from the induced changes in the amplitude, phase and frequency of the lever by long range attractive forces in the sample (Kasas et al., 1997) and the required force to keep that distance constant (Turner et al., 2007). The forces used are generally around 3 orders of magnitude less than in contact mode and as such allow the imaging of even the softest sample (Kasas et al., 1997).

With the ability to accurately control the tip and subsequently accurately determine NP size and the fact that the process is quicker and requires a simpler sample preparation technique than electron microscopy (Sitterberg et al., 2010), AFM is shown to be a suitable technique for an examination of NP characteristics after exposure to the different environmentally relevant conditions used in this work (Sitterberg et al., 2010).

AFM experiments were conducted using a XE 100 AFM (Park Systems, Korea), operating in both Contact and Non Contact modes, as well as under liquid cell conditions. Data was

recorded using XEP Software (Park Systems, Korea). Non Contact mode silicon AFM cantilevers PPP-NCHR (Nanosensors, Switzerland), spring constant 42 N/m were used for Non Contact mode and Liquid cell conditions. For Liquid cell conditions a combination of Non Contact mode tip operating in Contact mode lead to the best results. Contact mode AFM cantilevers PPP-CONT (Nanosensors, Switzerland) spring constant 0.2 N/m were used in contact mode. Samples were prepared following an adsorption method (Lead et al., 1999). This was the same for all three of the methods used and involved a freshly sliced mica slide held vertically in the sample solution for 30 minutes, this was then removed and washed in UHP water and dried in an enclosed vial overnight to prevent contamination from airborne particles (Lead et al., 1999).

3.5 Inductively Coupled Plasma Mass Spectrometry (ICP-MS)

Most work in the analysis of monodispere colloids from suspension usually involves separation via filtration with subsequent imaging using AFM or TEM (Degueldre et al., 2006). However, given the low concentration of the nanoparticles in the flume due to the large amount of water required and the possible presence of contaminants, imaging the samples does not give a reliable method for determining the concentrations within the pore space. Degueldre et al (2006) reported the use of ICP-MS in single particle mode to determine gold colloid concentrations and found that concentrations as low as 1 particle per ml were detectable. ICP-MS has also been used for ultra low level analysis of gold in rock samples (Pitcairn et al., 2006).

ICP-MS is composed of five distinct segments: sample injection, the inductively coupled plasma, interfacing, mass separation and the detection phase (Figure 3.7)(Ha et al., 2011). The liquid sample is taken up into the nebuliser using a peristaltic pump. In the nebuliser the

liquid is converted into an aerosol with the addition of argon gas. In the spray chamber the smaller aerosol droplets are separated from the larger droplets and then injected into a plasma torch (Thomas, 2007). The plasma is formed from the interaction of an intense electromagnetic field with a flow of Argon gas through concentric quartz tube (the torch). This electromagnetic field ionises the gas which when seeded with electrons from a high voltage spark forms a high temperature (10 000 K) plasma at the open end of the quartz tube (Thomas, 2007). The plasma is then used to create ions from the sample which then enter the mass spectrometer via the interface – two metallic cones with small apertures which allow the ions to pass through to the ion optics (a series of electrostatic lenses) which focuses the ions toward the mass spectrometer (Thomas, 2007). In the mass spectrometer the ions are separated based on their mass to charge ratio and sent through to the detector where the ions are converted into an electrical signal which is then converted into an analyte concentration value based on calibration standards (Thomas, 2007).

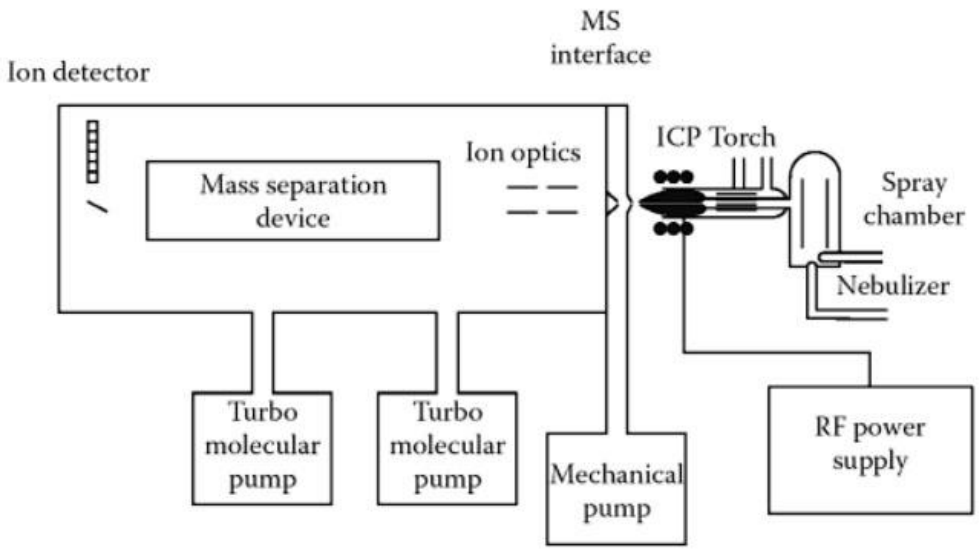

Figure 3.7 Instrumental components of ICP-MS, after (Thomas, 2007).

Most ICP-MS detection systems can be tuned to detect one element selectively. This allows detection in a working range of 9 orders of magnitude (Scheffer et al., 2008) allowing the

analysis of samples from ppt levels up to several hundred ppm depending on the system and calibration (Thomas, 2007).

Thus the use of ICP-MS to detect the presence and concentration of gold nanoparticles in the flume samples is a highly sensitive and precise technique, giving a quantitative analysis of any gold sampled from the pore spaces (Scheffer et al., 2008). The analyses were conducted using an Agilent 7500ce with an Octopole Reaction System. The ICP-MS was used to analyse samples taken from the flume pore spaces as described in section 3.8.4 and in Chapter 5. This enabled the determination of gold ion concentration within the flume and flume bed giving confirmation of the presence and the relative concentration of the manufactured gold NPs at the various sampling points used. Before the analysis could proceed though, the samples taken from the flume are filtered at 0.45 µm using a Millipore Ultrafiltration System. This step is in order to remove any potential causes of blockage during sample introduction; the filters used have been soaked in nitric acid for 24 hours previously in order to remove any possible contaminants. These samples are then acidified to pH 2 using nitric acid (HNO_3) for preservation.

3.6 Field flow fractionation

Field flow fractionation is a family of separation techniques based upon the elution of a sample through a narrow channel in the presence of a field acting perpendicular to that flow (Giddings, 1993). Separation occurs as particles are retained differentially within the field based upon their physical properties (Giddings, 1993), which affect their diffusion coefficients within in parabolic laminar field, that is a result of the liquid carrier pumped through the narrow channel (Kanzer et al., 2010). Once separated the components are eluted to a detector and can then be analysed further if so desired (Giddings, 1993). The distance at

which the particles amass above the accumulation wall is known as the equilibrium height and is dependent upon the magnitude of the field applied perpendicular to the main flow and the Brownian motion of the particles (Kanzer et al., 2010).

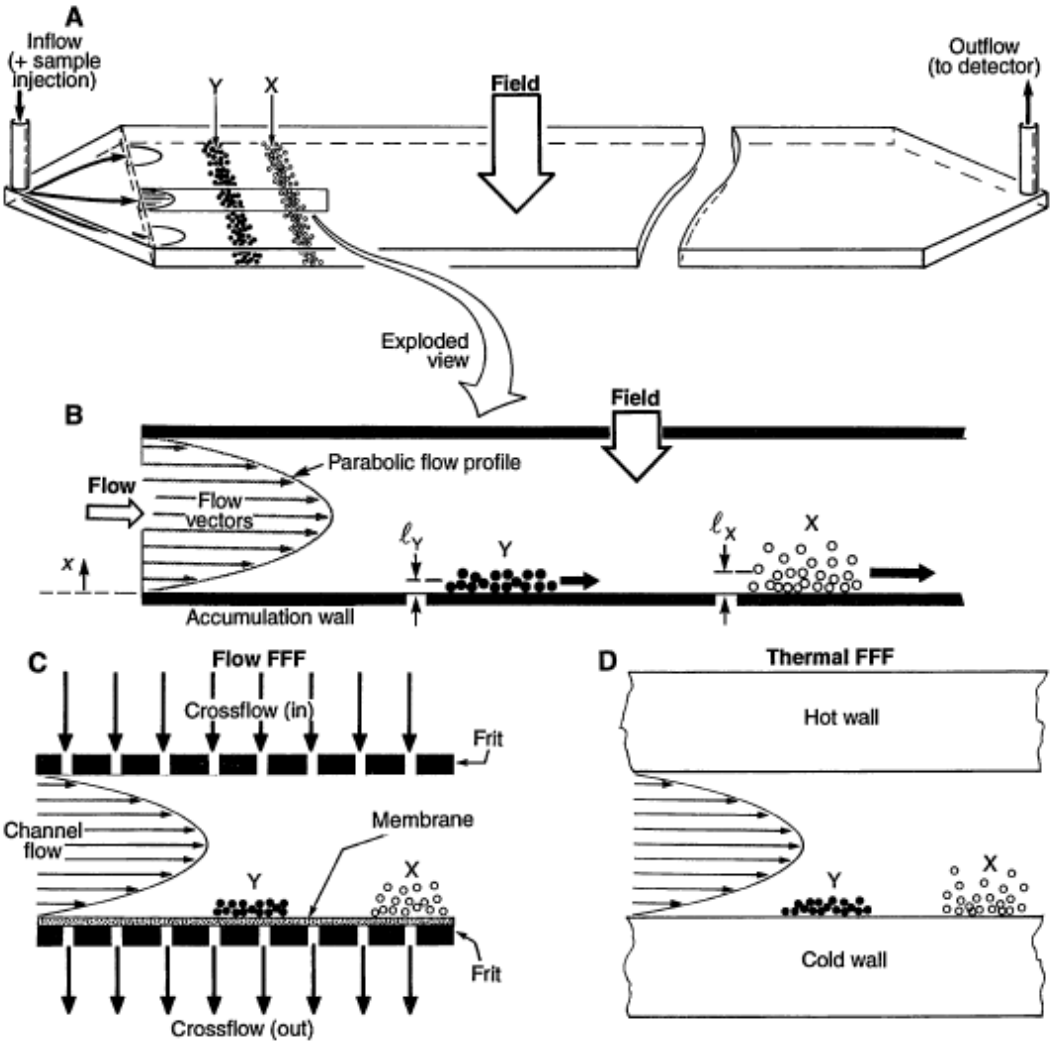

Fig. 3.8 FFF separation (A) Ribbon like FFF channel, sandwiched between channel walls this is usually 75–260 µm in thickness. (B) Different distributions of two particles, X and Y, across the parabolic flow path, and the mean elevations above the accumulation wall ℓ_y and ℓ_x (C)Symmetrical Flow FFF and (D) Thermal FFF, where the separation is driven by a cross flow and temperature gradient respectively, after (Giddings, 1993).

Smaller particles with higher diffusion constants find themselves at a greater distance from the accumulation wall whilst the larger particles are situated closer to the wall. This results in the elution of the smaller particles at a faster rate (Kanzer et al., 2010).

The system used for these experiments was that of flow-field flow fractionation which is capable of separating particles as small as 1 nm in size (Ratanathanawongs, 1993). In flow FFF, the field acts perpendicularly to the channel flow (Figure 3.8B) as separate cross flow stream addition flow stream. Working together, the channel stream drives particles toward the outlet, as the cross flow pushes particles toward the accumulation wall, as illustrated above in the text and Fig. 3.8 (Giddings, 1993).

Flow FFF is the one FFF technique that separates solely based on particle size, in particular the mass diffusion coefficient (Schimpf, 2000). There is an exact relationship between the retention time and the size of the particle based upon a Brownian mode of retention and full dilution within the carrier liquid (Schimpf, 2000). The retention time (*R*) is given by:

$$R = \frac{t^0}{t_r} \tag{3.19}$$

Based upon the analyste's retention time (t_r) and the void time within the channel (t^0). Where:

$$t^0 = \frac{V^0}{F} \tag{3.20}$$

With V^0 being the channel void volume and *F* the volumetric flow rate. *R* is related to the retention parameter (λ):

$$R = 6\lambda\left[coth\left(\frac{1}{2\lambda}\right) - 2\lambda\right] \tag{3.21}$$

The mean elevation of the sample ℓ is expressed in non dimensional form as:

$$\lambda = \frac{\ell}{w} \tag{3.22}$$

With w being the channel thickness and λ the retention parameter. This parameter is then related to the force acting upon the analyte from the external field by:

$$\lambda = \frac{kT}{F_w} \tag{3.23}$$

With k the Boltzmann constant, T the absolute temperature and F_w the force.

This can then be related to the Stokes Diameter of the particle:

$$\lambda = \frac{kTV^0}{3\pi\eta V_c w^2 d_{St}} \tag{3.24}$$

Where η is the viscosity, V_c the volumetric rate of cross flow and d_{St} the Stoke's diameter.

$$d_{St} = \frac{kTV^0}{3\pi\eta V_c w^2 \lambda} \tag{3.25}$$

As separation is based on size alone, the results are easily interpreted with residence time, t_r approximately proportional to diameter. Size selectivity, $S_d = |d \log t_r / d \log d$, for this technique is equal to 1, meaning changes of even a few percent can be detected (Giddings, 1993).

Flow Field-flow fractionation experiments were performed using a Asymmetrical flow field flow fractionator (FlFFF) (AF2000 Mid Temperature, *Postnova Analytics*, Germany). The accumulation wall was 1 kDa regenerated cellulose membrane. The channel was rectangular in shape and had dimensions of 35 cm x 6 cm x 4 cm. A high pressure liquid chromatography (HPLC) pump (515 HPLC Isocratic Pump, Waters, USA) was used to deliver the cross flow whilst the channel flow was regulated with a separate pump (PN1121 Double Piston Pump, Postnova Analytics, Germany). The eluent was 0.01M NaCl and was degassed before delivery (PN7505 Vacuum Degasser, Postnova Analytics, Germany). Channel flow was set at 1 ml min^{-1} and cross flow at 0.5 ml min^{-1} to obtain separation between the void and sample peaks. Two online UV-Vis detectors were used to achieve particle detection with one set at 525 nm and the second at 254 nm were used to monitor the

attenuation of gold nanoparticles. Data acquisition was via a Campbell CR23X data logger using Loggernet software (v 3.3.1, Campbell scientific, Loughborough, UK). Channel volume was determined for the various conditions investigated using 30 and 60 nm polyacrylamide beads PAA (Duke Scientific Corporation, USA). The diffusion gradients were calculated using the theory outlined earlier in the section and converted to size using the Stokes relationship. 1 ml of sample was injected per run and allowed to equilibrate for 5 minutes and then fractionated, with at least three independent replicates were analysed per sample and the data averaged.

3.7 Experimental procedures

3.7.1 Sample preparation and handling

Fig 3.9 Gold nanoparticles samples under differing environmentally relevant conditions.

2 ml aliquots of the purified gold NP solution (275 mg L^{-1}) were placed in 30 ml sample vials. These were then diluted with stock solutions of the salts and fulvic acid to give samples with 3 differing pHs 5.5, 7.0 and 8.5, with and without fulvic acid at 10 mg L^{-1} and at 0.1M and 10^{-4}M of sodium nitrate and calcium nitrate, giving a final gold concentration of

~ 27.5 mg L^{-1}. The pH was adjusted by the addition of NaOH and HNO_3 to values of 5.5, 7.0 and 8.5 ± 0.25 as appropriate. No buffers were included, to preclude any changes in the particle behaviour which initial results suggested were likely. However, pH was monitored and altered as required in order to ensure a steady state value had been reached prior to analysis. This range of water chemistries was chosen to provide broad similarity with the conditions that may be found in natural waters (Liu et al., 2007a). An Orion 3 Star Benchtop pH metre from the Thermo Electron Corporation with a pHC4000-8 combined pH electrode from the Radiometer Analytical Company was used for pH measurement. The pH was routinely checked and altered where necessary to ensure a constant pH value. The samples were analysed for size, shape and charge at the different environmentally relevant conditions using the techniques and procedures described in section 2.3. The results were then compared to an initial characterisation performed after synthesis in order to quantify the degree of any changes that may have occurred.

3.8 Flume Experiment

3.8.1 Introduction

Due to the importance of the interface between streams and groundwater increasing as further details about its role in regulating transport of contaminants and nutrients are published (Ren and Packman, 2004b). Further studies on hyporheic exchange and the factors that control it have been undertaken. Various factors can affect the stream – subsurface exchange and these include, riffles, obstacles, bed forms (Elliott and Brooks, 1997; Thibodeaux and Boyle, 1987) and temperature (Hannah et al., 2009). With this increasing understanding of hyporheic flow paths and reactions the processes governing contaminant transport in this area will become more transparent and open to investigation (Ren and Packman, 2004b). Due to the obvious difficulties in conducting controlled contaminant transport experiments under real world

conditions, experiments to date have been conducted using the controlled environment allowed by recirculating flumes (Packman et al., 2000a; Packman et al., 2000b; Ren and Packman, 2002; Ren and Packman, 2004b) and this allows full control of both surface and subsurface conditions and provides a closed system for the NPs in this particular case without the possibility of loss to outside factors (Packman et al., 2004)

3.8.2 Flume design and construction

Preliminary experiments were undertaken in a 3 m x 0.15 m test section positioned in a larger flume with a length of 19 m, however the volume of water required in order to achieve stable flow resulted in the need for a very large amount of nanoparticles in order to achieve detectable levels which proved to be impracticable due to the cost that this would have resulted because of the high cost of the gold salt precursor. These preliminary experiments are discussed in more detail in Chapter 5.

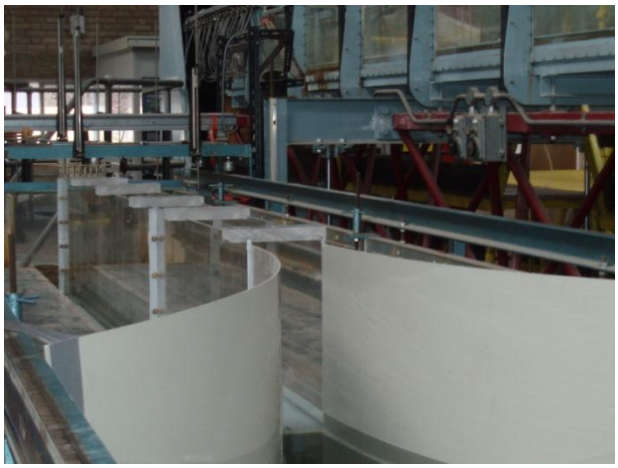

Figure 3.10 The 3 m x 0.15 m test section of the larger flume.

Due to this the experiment was moved to a smaller bench top flume with a test section of 0.5m in length with a width of 0.25 m and a maximum depth of 0.16 m. Though this is small for open channel flume studies (Packman et al., 2004) the induced exchange flux is not

known to be very sensitive to small flume channels (Packman et al., 2004) and so provides a suitable alternative. The NP added to the flume are easily recirculated through the flume via a return pipe and pump taking the water from the holding tank to the start of the flume channel.

In order to simulate the presence of a gravel river bed, whilst maintaining the necessary order that is required to fully analyse the role that bed forms are contributing to the transport and to compare with data generated by computer modelling (Hardy et al., 1999), plastic balls (nylon 66) with a diameter of 19mm (Precision Plastic Ball Company, UK) are arranged in a face centred cubic lattice across the length and width of the flume. This bed consists of 3 layers which allows access for sampling whilst still maintaining enough depth for the effects of hyporheic exchange to be observed. In order to fully investigate the exchange fluxes in the second set of flume experiments a bed form was placed one third of the way along the test section. This bed form was in the form of a metal block with a height of 19 mm and breadth of 60 mm.

3.8.3 Flume Experimental Procedure

For the benchtop flume experiments, the flume was filled with reverse osmosis purified water (125 L) and experiments were conducted at a depth of 3 D (D is the diameter of the plastic balls used in the river bed, 19 mm) so flow was controlled via the flume discharge and the use of an adjustable gate at the downstream end of the flume channel in order to fine tune this depth. This was done by selectively opening and closing the gate causing the water to back up or flow faster in the channel, much like the affect of dam (Figure 3.11). Details of why

this depth was chosen and a full profiling of the flow within the channel are given in Chapter 5.

The flume was left running for one hour before each experiment so that the flow could fully stabilise. The gold NPs were added under steady state thermodynamic conditions and poured slowly from the containment vessel into the downstream well of the flume (Figure 3.11). This allowed the concentration to be evenly distributed throughout the flume water volume as quickly as possible (Ren and Packman, 2004b). The experiments were of 1.5 hrs to 2 hrs in duration.

3.8.4 Sampling

Samples were taken manually from various several sampling points within the bed; a number of sampling arrangements were used with the final arrangement shown in Figure 3.11.

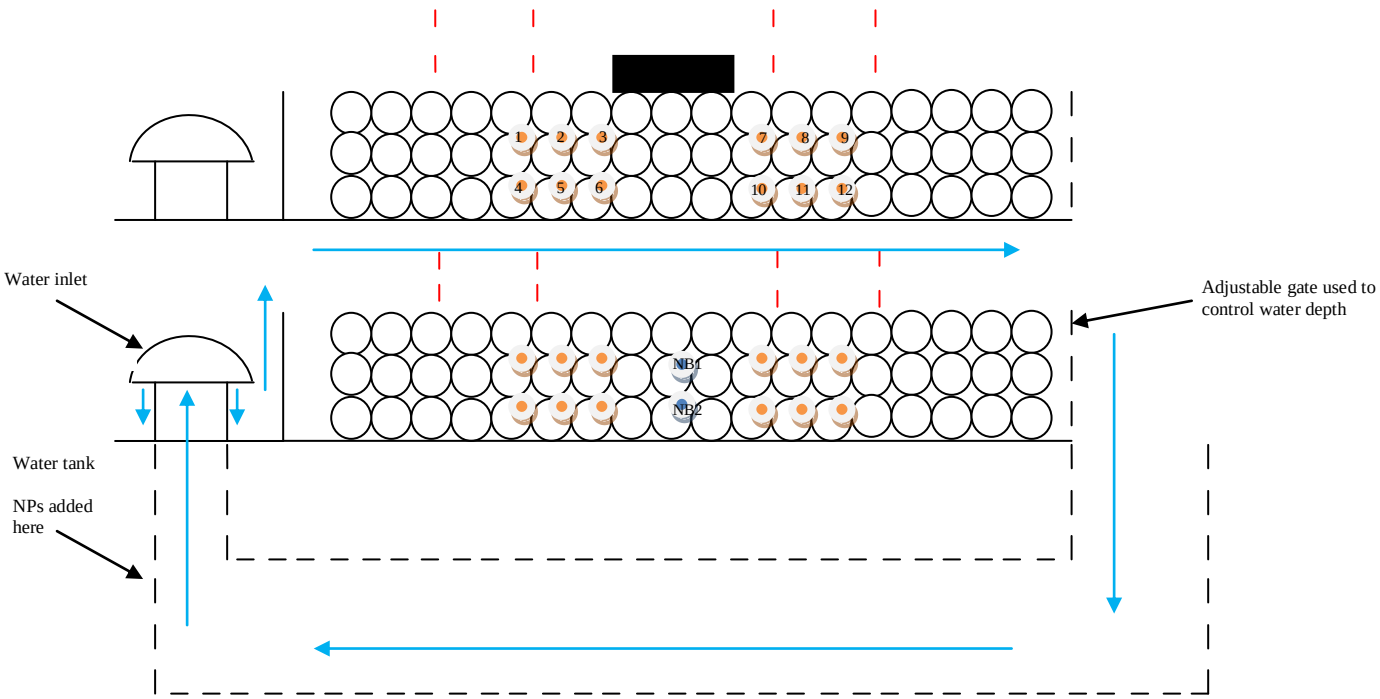

Fig 3.11 Final configuration showing the sampling points (1-12 and NB 1&2) throughout the bed and free flow within the channel of the recirculating benchtop flume where water samples were taken both with (top) and without a bedform (bottom). The recirculation system is shown alongside the bottom configuration. The blue arrows show the direction of flow.

One sample in the free flow was taken to prior to the introduction of NPs to the flume and then samples were taken at these locations every 25 minutes for 75 minutes. Samples were also taken at points 1 and 4 every 5 minutes for 90 minutes to provide an overview of stream subsurface exchange in the first experiment conducted with the bedform but this was later altered due to time constraints and is discussed in detail in Chapter 5. Initial samples were taken as soon as possible after the introduction of the NPs into the recirculating flume and are labelled within this work as occurring at 2 minutes. The aqueous samples were taken using 50 ml syringes and needle in order to take samples from within the bed. Mica slides and TEM grids were attached during a pilot study to the plastic spheres at locations 4 and 9 using

plumbers mate putty as this was found to be the adhesive that would fix them securely throughout the experiments whilst also allowing removal without damaging the slides but this proved to only offer a modicum of success and was not continued during the main experiments. This flume experimental work including the reasoning behind ceasing the TEM grid attachment is discussed in more detail in Chapter 5. Samples were then analysed for gold concentration using ICP-MS.

4.0 Study of the effects of environmentally relevant conditions upon various sizes of PVP stabilised gold nanoparticles

4.1 Introduction

NPs have been shown to be potentially toxic to environmental biota (Klaine et al., 2008) and so an understanding of exposure is vital to quantify environmental risk. This exposure will be controlled by NP chemistry and transport which is dominated by the environmental milieu in which NPs are present. A number of different factors can have an effect upon NPs fate and behaviour in aquatic systems. These include the ionic strength, pH and the presence of natural organic matter (NOM) (Baalousha et al., 2008; Brant et al., 2005a; Diegoli et al., 2008; Gao et al., 2009; Hyung et al., 2007; Liu et al., 2007b; Lu and Su, 2007; Schierz and Zanker, 2009). Previous studies have been performed on carbon based NPs (Hyung et al., 2007; Liu et al., 2007b; Lu and Su, 2007; Schierz and Zanker, 2009) and inorganic NPs (Baalousha et al., 2008; Diegoli et al., 2008) which are generally unmodified (Baalousha et al., 2008) or deliberately charge stabilised (Diegoli et al., 2008). The impact of pH and ionic strength on bare or charge stabilised NPs is generally to increase aggregation dependent on point of zero charge, as expected from a Derjaguin, Landau, Verwey and Overbeek (DLVO) theory (Chen and Elimelech, 2006). Where a diffuse electrostatic double layer (EDL) surrounds colloidal particles and the balance between the attractive Van der Waals force and electrostatic repulsion determines the colloidal stability (Derjaguin and Landau, 1945). This relationship is illustrated in Figure 4.1, pH, ionic strength and electrolyte valence all influence the magnitude and thickness of the EDL and thus affect stability, (Jiang et al., 2009).

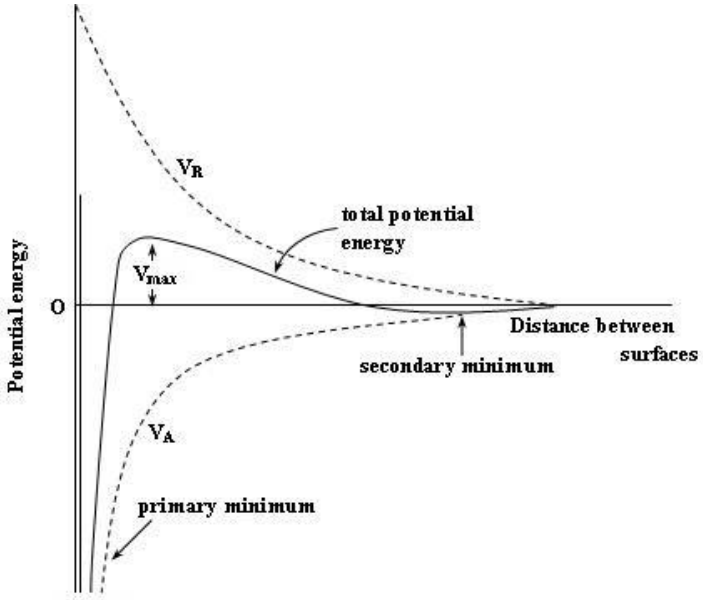

Figure 4.1 Showing Van der Waals attractive force (V_A) and the electrostatic repulsion (V_R) and the total potential energy as a function of distance, after (Washington, 2011).

The influence of NOM such as Suwannee River fulvic acid (SRFA) upon NPs is more complex with humic substances (HS) shown to generally stabilise NPs (Figure 4.2) (Diegoli et al., 2008; Hyung et al., 2007; Liu et al., 2007b; Schierz and Zanker, 2009) and cause disaggregation of existing NP aggregates (Brant et al., 2005a; Fabrega et al., 2009a). Such interactions have been shown to modify short term biological interactions, both reducing toxicity (Fabrega et al., 2009a; Fabrega et al., 2009b; Li et al., 2008) and increasing toxicity (Klaine, 2009), while non-humic NOM may destabilise NPs (Buffle et al., 1998). With the number of ways NOM can effect NP properties it is therefore of importance in any study to investigate how NOM will affect a particular NP.

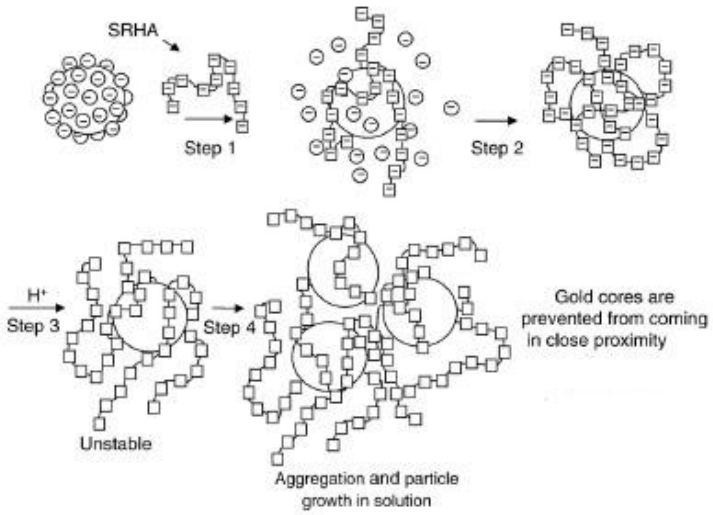

Figure 4.2 The effect of Suwannee river humic acid (SRHA) on charge stabilised gold NPs. Here partial substitution of the small citrate anions by the SRHA occurs and when the pH of the solution is decreased protonation occurs and the electrostatic stability is lost and aggregation occurs, though the SRHA does offer some steric stabilisation and retards further aggregation, after (Diegoli et al., 2008).

Sterically stabilised NPs, such as the ones used in this work, have been shown to be unaffected by changes in environmental conditions (El Badawy et al., 2010) and also to undergo aggregation under certain environmental conditions and for different polymer species, (Chen and Elimelech, 2006). These NPs typically consist of a small metallic centre stabilised by polymers or macro molecules, such as polyvinylpyrrolidone (PVP) (Figure 4.3), which does not protonate and deprotonate with environmentally relevant pH changes and remains unaffected by shifts in ionic strength and ion composition, (Csempesz and Csaki, 2000), though when using Poly(4-vinylpyridine) in place of Poly(4-vinylpyrrolidone) as a stabilising agent the polymer chain is affected by pH as it is expanded by electrostatic forces at low pH (Li et al., 2007), so care needs to be taken when using the PVP acronym in order to avoid confusion.

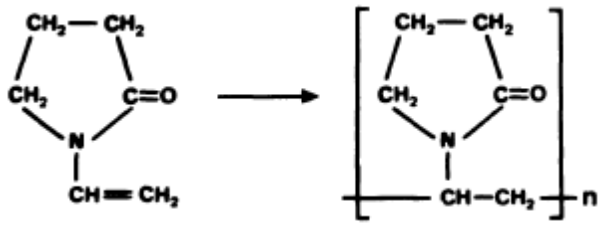

Figure 4.3 The polymerisation of vinylpyrrolidone, after (Haaf et al., 1985).

Sterically stabilised metallic NPs are likely to become more prevalent in the environment as nanotechnology develops, for instance due to their use in nanomedicine applications (Davies et al., 2005), sensing (Shipway et al., 2000) and catalysis (Mallick et al., 2005). The aim of this section is to investigate the impact on aggregation, size and surface chemistry of relevant environmental conditions on 7 nm PVP stabilised gold NPs in order to assess whether these behave in the same manner as other sterically stabilised NPs or if in this instance changes in some of the physical properties occur. A range of environmentally relevant conditions were chosen to provide broad similarity with conditions that may be found in natural waters. These include a pH range of 5.5-8.5, sodium nitrate and calcium nitrate salts at environmentally relevant concentrations of 0.1 and 10^{-3}M, and natural organic matter in the form of SRFA at a concentration of 10 mg L^{-1}.

These conditions and their effects were analysed using a variety of techniques on 4 batches of gold NPs, which were synthesised as described in section **3.2** of the previous chapter. The results for these batches are presented and discussed over the rest of this chapter. The nature of the synthesis and the time taken to comprehensively analyse the samples and subsequent results meant that it was necessary to study several distinct batches of NPs (labelled herein NP_1, NP_2, NP_3 and NP_4). These batches may have slight variations in size and as such size comparisons have been kept within batch in general.

4.2 Synthesis and characterisation of gold nanoparticles

After the initial NP synthesis using a method described in detail in the previous chapter (section **3.2)** and reported elsewhere (Hoppe et al., 2006) the NPs were characterised using UV/Vis spectrometry, DLS, zeta potentiometry and TEM, using procedures described in sections **3.3.1, 3.3.2, 3.3.3** and **3.3.4** in order to characterise their 'as prepared' state providing a baseline for comparison.

4.3 Environmentally relevant conditions

4.3.1 Sample preparation

To test how the NPs behaved when exposed to the range of environmentally relevant conditions used the samples were prepared as described in section 3.7.1.

4.3.2 NP_1

4.3.2.1 'As prepared'

'As prepared' suspensions of the gold NPs were characterised by size, surface charge and solubility. Four analytical methods were used to conduct this characterisation and a brief overview of each method is given here to build upon the details given in chapter 2. The first of which is based upon the interaction between electrons and the sample and is the most commonly used method of NP characterisation (Giersig and Mulvaney, 1993; Hasan et al., 2002), transmission electron microscopy (TEM). When the electrons hit the sample a number of signals are given off, including, secondary electrons (SE), x-rays, elastically scattered and in-elastically scattered electrons (Williams and Carter, 1996). TEM analysis utilises the transmitted or forward scattered electrons yielding an electron micrograph of variable contrast depending on the sample electron density of the NPs - a combination of sample thickness and atomic number of sample components. These micrographs can give

accurate size distributions and their relative dispersity via manual or automatic counting (Ju-Nam and Lead, 2008).

The second method of characterisation centres on the surface plasmon resonance (SPR), a strong and wide band observed via UV-visible absorption for metallic NPs greater than 2 nm in size (Moores and Goettmann, 2006). As mentioned in the previous chapter the strength, position and size of the SPB is different from that of the bulk material and dependent upon a number of factors, which include; dielectric constant of the surrounding media, electronic interactions between stabilising ligands and the nanoparticle which can alter the electron density within the nanoparticle as well as the size and shape of the nanoparticle (Moores and Goettmann, 2006; Sun and Xia, 2003). Gold has a characteristic surface plasmon peak located at between *ca*. 550 nm (Medina-Ramirez et al., 2009) and *ca.* 520 nm (Sun and Xia, 2003), previous studies involving PVP stabilised gold nanoparticles have reported a plasmon band centred at *ca.* 525 nm (Kim et al., 2010). In a thin film of gold, for example, the SPR is located at ~480 nm, while an aqueous dispersion of 13 nm spherical gold it can be found at ~520 nm (Zhang et al., 2002b).

With the position of the SPR dependent upon electron density the presence and actions of a ligand shell can be an important factor in SPR behaviour. These ligands can interact electronically with the core metal atoms and partially reduce or oxidise the NPs (Moores and Goettmann, 2006). The effects of ligand electron donation and back donation from the metal centre are known to result in shifts of NP plasmon bands (Moores et al., 2004). In the case of the NPs used here this is an important topic as any changes made to the stabilising ligand could manifest themselves as shifts in the SPR.

Size changes also affect the position of the SPR with experimental results giving evidence of a blue shift when NP size is decreased. This is reversed however for alkali metal NPs, as electrons spilling from the cationic framework cause the charge to become located outside the metal surface and give a less energetic SPR (Moores and Goettmann, 2006). Thus changes in SPR can be used to identify changes in the physical properties of the gold NPs used in this study upon their exposure to the various environmental conditions considered here.

The stability of the colloidal system can be estimated from the extent of the zeta potential value, which was the third method used in the characterisation (see Chapter 3). If all the particles constituting the system possess a large positive or negative zeta potential then they will tend to repel each other and the propensity toward aggregation will be greatly reduced. Conversely, particles displaying low zeta potential values will have no preventative forces stopping aggregation, unless steric stabilising factors are present. Zeta values of +30 or -30 mV are usually considered to be the dividing line between stable and unstable colloidal suspensions where charge stabilisation is required.

The solution pH is one of the most important factors that can have an effect upon zeta potential and is of critical importance when analysing the zeta potential value as switching from acidic to basic conditions can result in particle charge changing from positive to negative respectively, due to this there will be a point on a pH vs. zeta potential curve passing through zero, this point of zero charge and the pH values either side of it represent values at which colloidal stability could be decreased. The zeta potential of the sterically stabilised NPs used in this study are likely to be unaffected by pH changes but nevertheless it remains important to fully consider all possibilities. Another subtle reason for zeta potential being less useful as a characterisation tool in this case is the soft polymer coating that does not

resent a clearly defined slipping plane (see Chapter 3). The fourth and final technique used in the characterisation was that of dynamic light scattering and Figure 4.4 shows the TEM, DLS and SPR data for this initial characterisation.

4.3.2.2 Characterisation results

As expected strong absorbance is seen in the ~520 nm (gold) region which is increasing over the synthesis timescale (Figure 4.4d) (Hoppe et al., 2006) as the NPs are developing, culminating in a strong absorbance at this point after purification. The TEM determined diameter is 7.2 ± 1.7 nm (n=164) which is in good agreement with the DLS data, which gave a diameter of 8.5 nm ± 1.1 this size range achieved is again as expected from previous work (Hoppe et al., 2006).

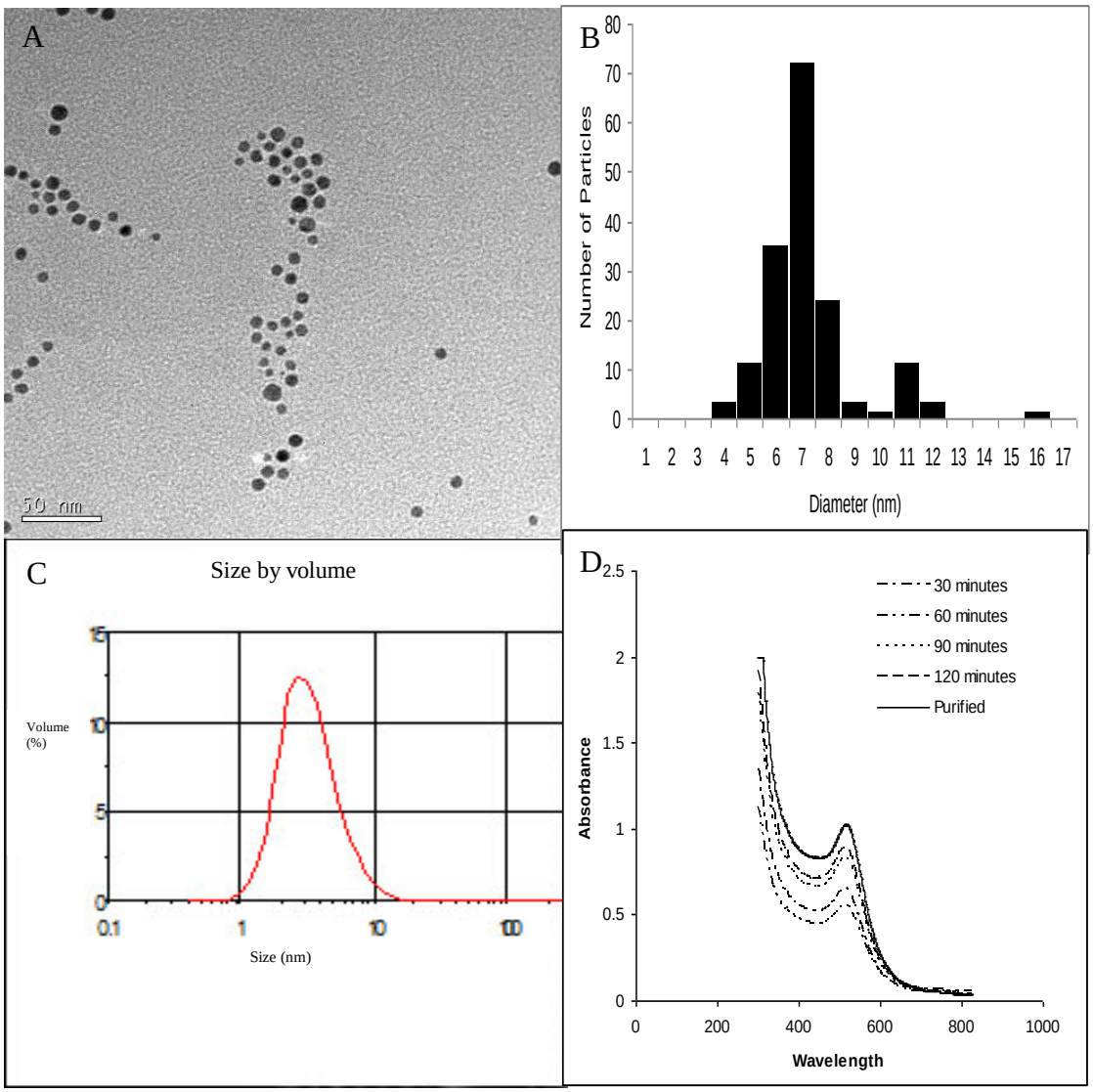

Figure 4.4 a) TEM image of manufactured gold nanoparticles in water with b) histogram. c) Distribution by volume taken from DLS analysis and d) UV-Vis spectrum showing the absorbance of several aliquots of the nanoparticles taken at different times throughout the synthesis.

Taken together the data showed that the gold NPs were small, uniform in size and had a spherical shape (length to breadth ratio 0.97 ± 0.02) which is readily visible in Figure 4.4 a. These NPs are also stable and show no obvious signs of aggregation though there does seem to be a tendency for these particles to appear in groups an indication that although full aggregation does not occur there may be some interaction between the NPs.Tthis stability is expected and the NPs are known to remain relatively stable for several months (Hoppe et al.,

2006). The zeta potential of the synthesised gold NPs was -5.2 mV ± 0.7 confirming the absence of significant charge on the particles and the steric nature of the stabilisation. Finally analysis of gold concentrations after ultra-filtration showed that > ~ 1% of the NPs passed through the ultra-filtration membrane. This was taken as a measure of dissolution, i.e. the NPs were largely insoluble, although there may be a residue from the initial synthesis and given the small size it is possible that some passed through the ultra-filter.

4.3.2.3 Transmission electron microscopy

Initial analysis of the NPs when exposed to the various environmental conditions considered focused on changes to size and shape that may be visible using the TEM. Firstly the effect of the salt was considered and Figure 4.5 shows the NPs in water and in 10^{-3} M $NaNO_3$. As can be seen from the images and the accompanying histogram there is no significant difference in the diameter noted as the conditions change, 7.6 ± 0.7 nm and 7.7 ± 0.5 nm, *(p=0.65)*. Here and throughout the statistical difference between the various conditions was determined by the use of one way ANOVA due to the comparison of more than one set of data at one time. For this technique a p value of < 0.05 indicates a significant difference at 95% confidence levels. A visual inspection also clearly shows that there is no change in the spherical shape of the NPs and indeed this was the case when analysed for length to breadth ratio which is dealt with at the end of this section.

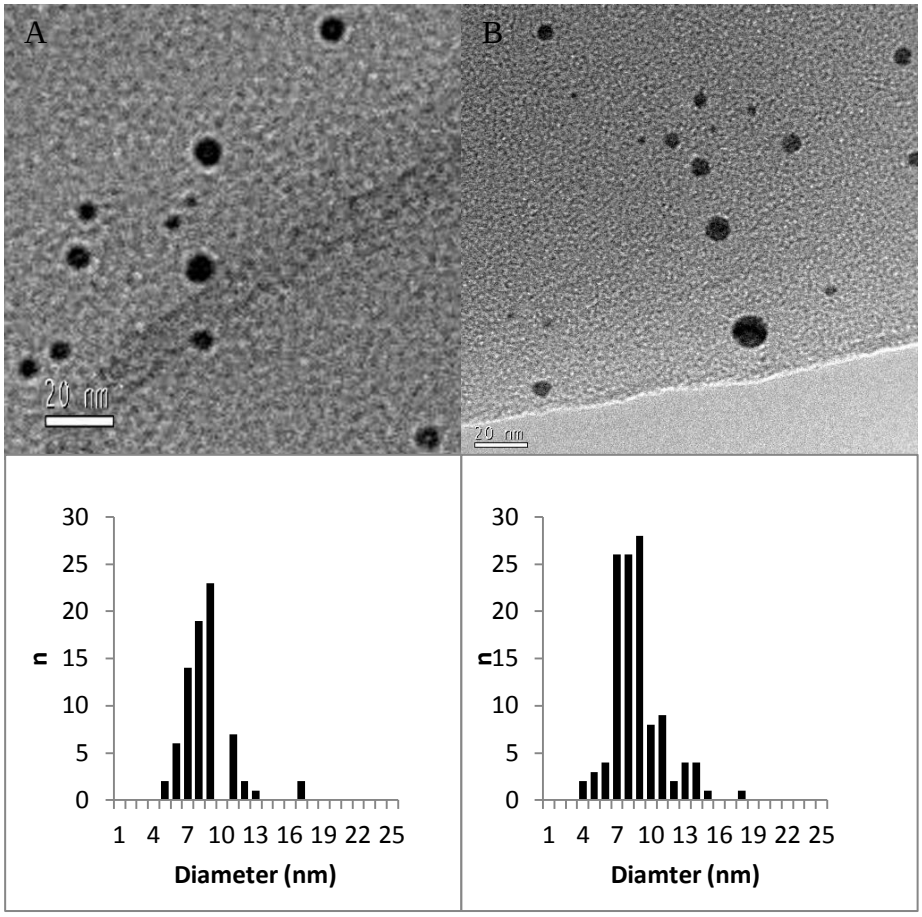

Figure 4.5 TEM images of gold nanoparticles in water (a) and in 10^{-3} M $NaNO_3$ (b). Histograms show the NP size as determined by a manual count from the TEM images, not all images shown.

The images in Figure 4.6 further show these findings as again no significant size change is shown as we move from the water solution to the SRFA containing solution where the average NP diameter was 7.7 nm ± 0.3 (*p = 0.74).*

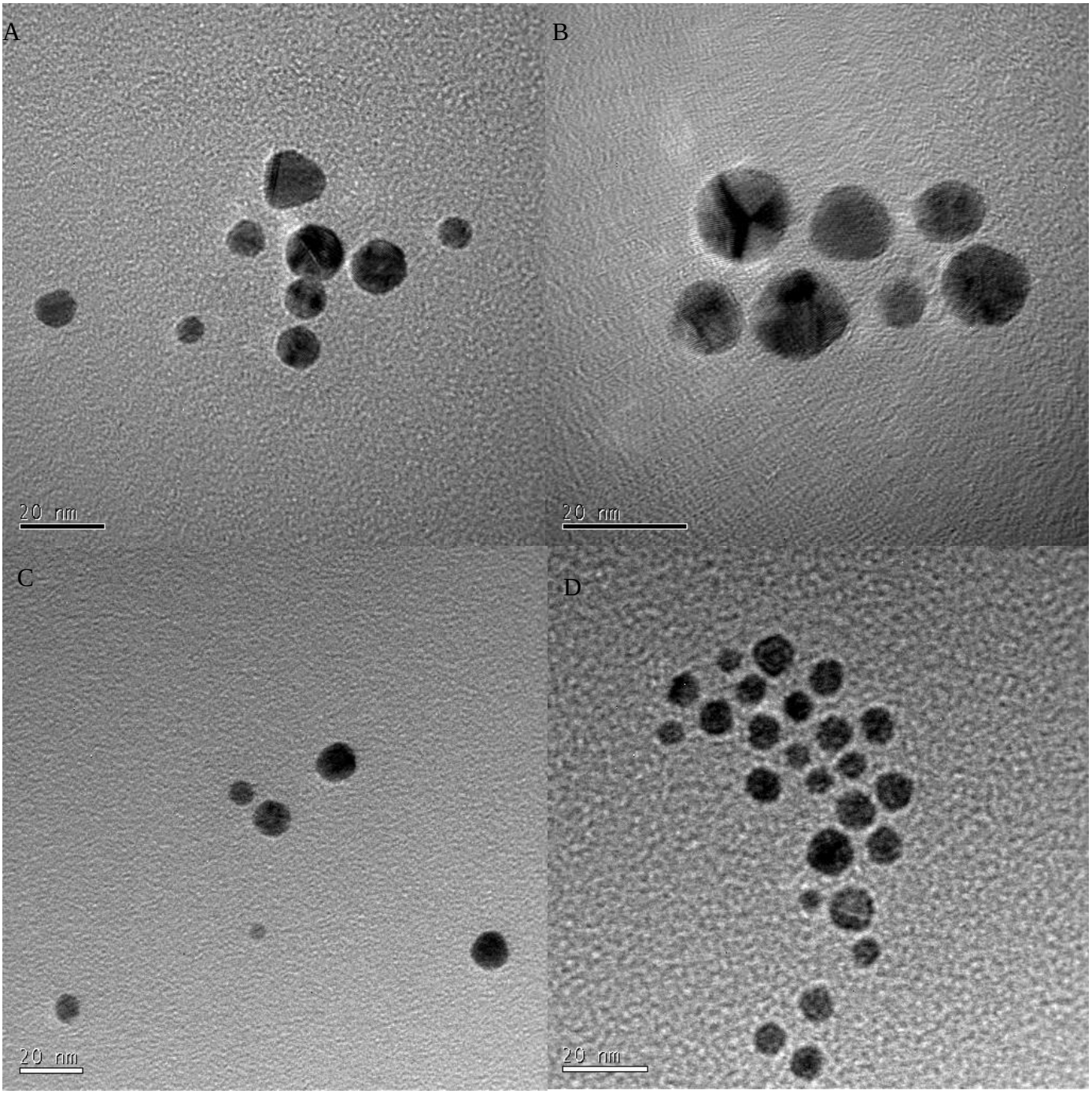

Figure 4.6 TEM images of gold NPs in a) water, b, c) in 0.1M $NaNO_3$ and d) in 0.1M $NaNO_3$ and fulvic acid.

When taken together the change in size from 7.5 nm in water to 7.7 nm and 7.7 nm in the salt and SRFA respectively is shown to be insignificant ($p = 0.88$). The images in Figures 4.7 and 4.8 show the lack of change in the size and shape of the NPs at a lower salt concentration.

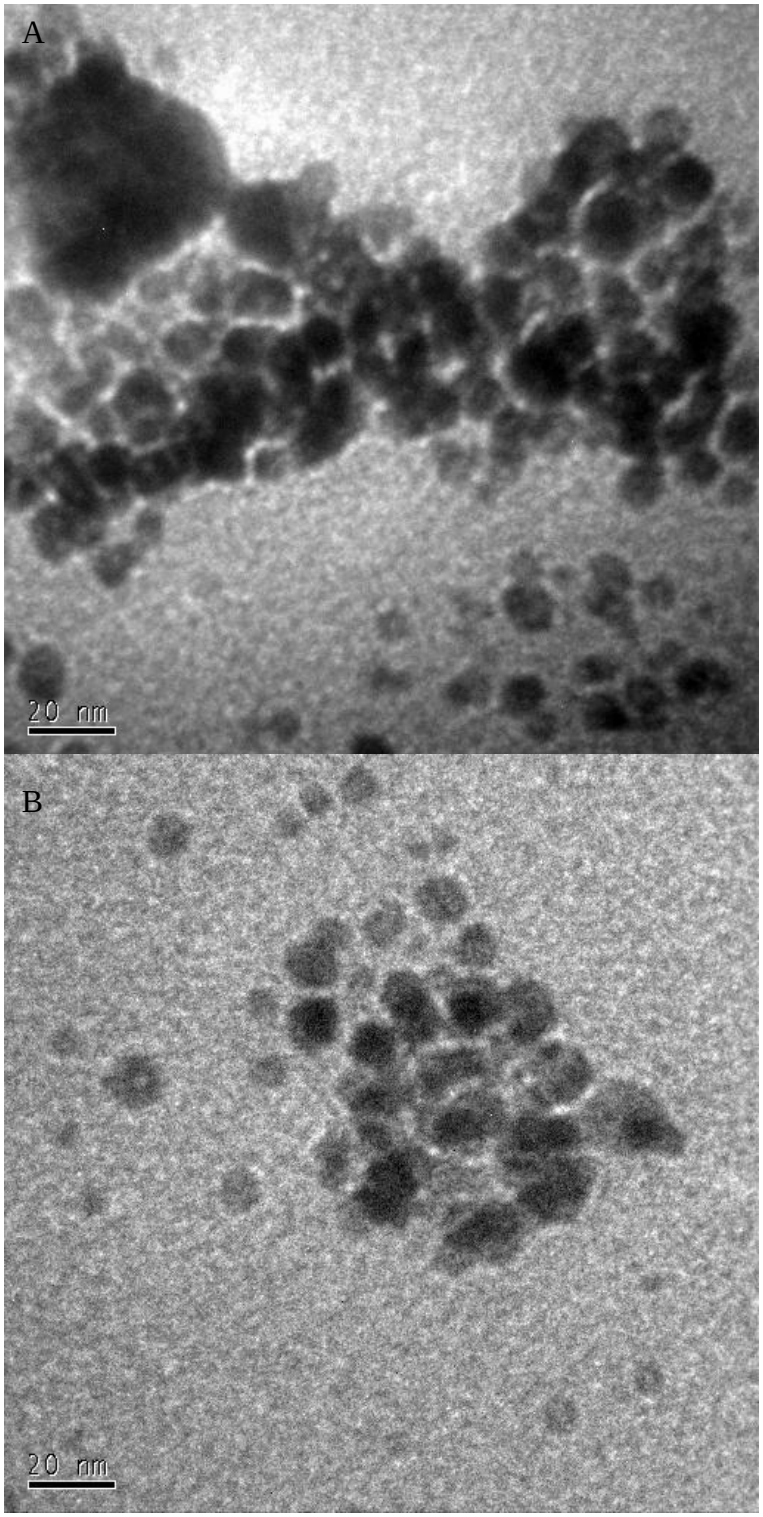

Figure 4.7 TEM images of gold NPs in A) water and B) 10^{-3} M $NaNO_3$.

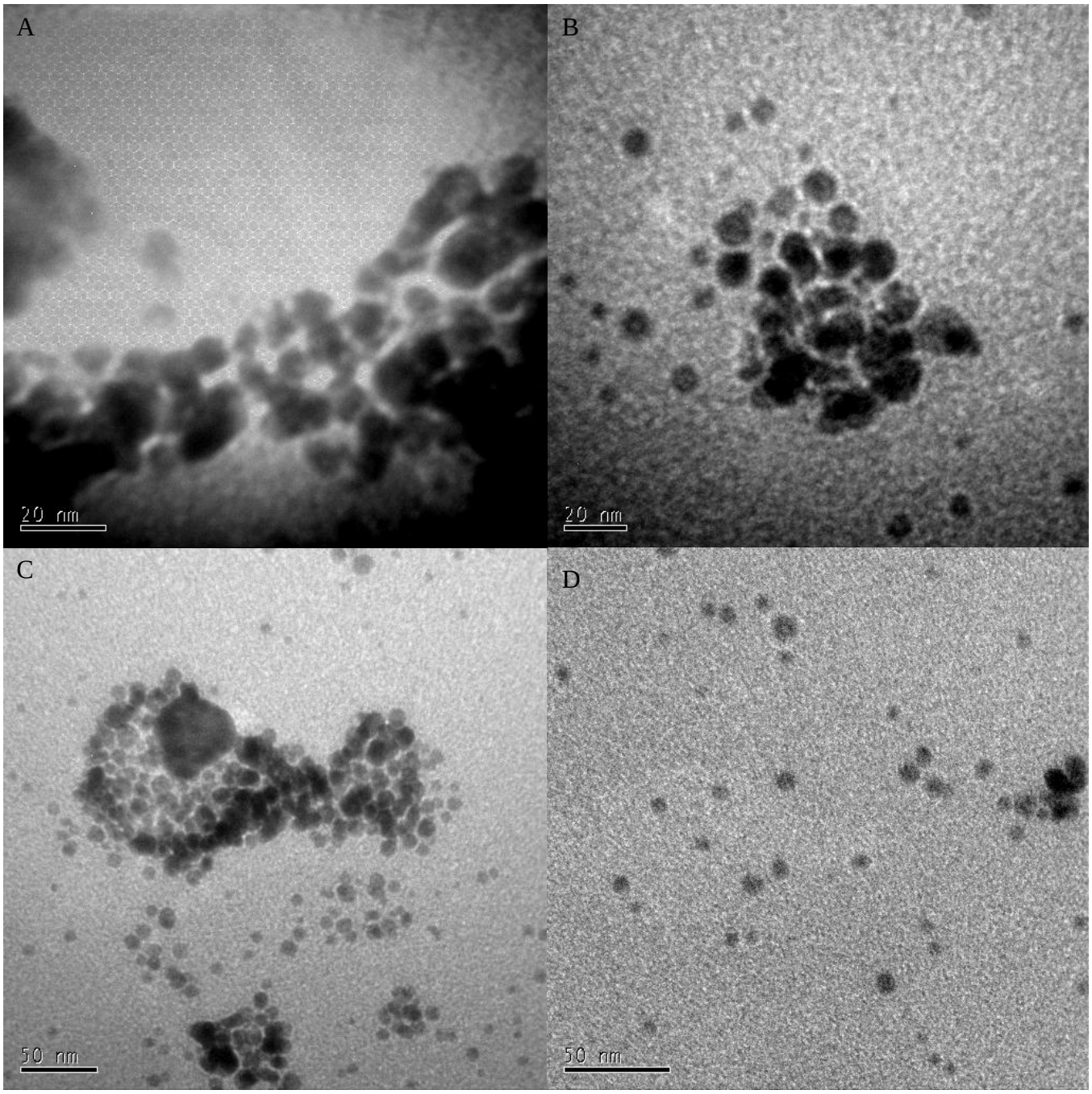

Figure 4.8a TEM images of Gold NPs in (A, C) water and (B, D) 10^{-3} M $NaNO_3$ (right).

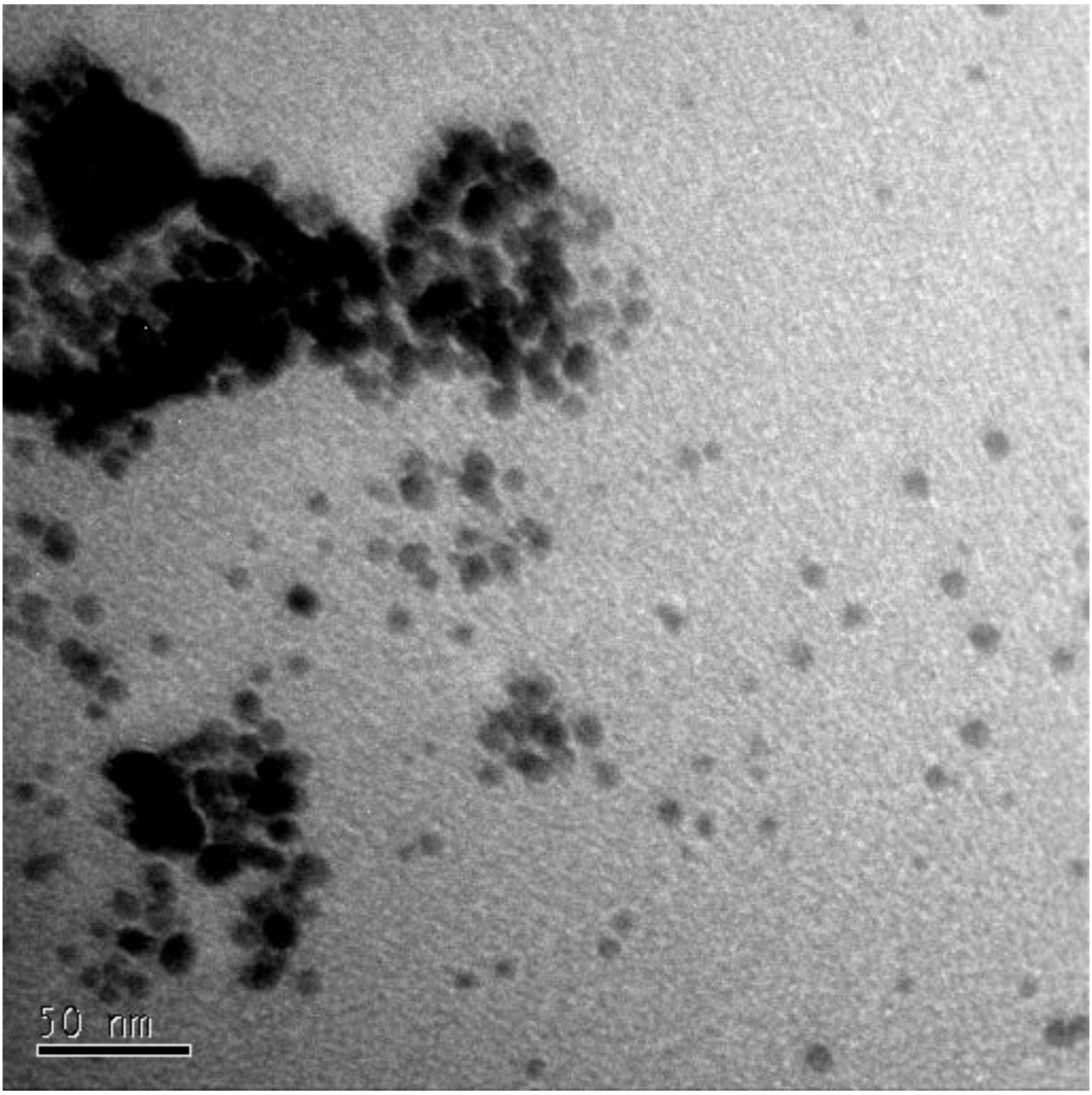

Figure 4.8b TEM image of Gold NPs in 10 mg L^{-1} SRFA.

From these TEM images it can be seen that the size of the NPs remains unaffected by the changes in pH, ionic strength and the introduction of SRFA, some of the images reveal the presence of some larger NPs though these particles are not present in a substantial amount. The presence of a handful of larger particles is put down to a small variation in conditions during the synthesis such as how long the particular solution took to come up to the reaction temperature of 75 ºC with the possibility of a small degree of aggregation. The shape of the

NPs remains spherical throughout the analysis with length to breadth ratios (where 1.00 would be perfectly spherical) of 0.98 nm ± 0.02, 0.95 nm ± 0.01 and 0.99 nm ± 0.03 for the gold NPs in water alone, 0.1 M $NaNO_3$ and with 10 mg L^{-1} SRFA respectively ($p = 0.71$). Aside from this it is important to note that the PVP stabilising agent is not visible in the micrographs and that further analysis must be performed to fully understand the effects, if any, which changes in water chemistry, will have upon this particular type of NP.

4.3.3 NP_2

4.3.3.1 Dynamic light scattering

The second batch of NPs have been comprehensively analysed for changes in size and surface properties with Table 4.1 showing the DLS measured sizes with changes in ionic strength, pH and the introduction of SRFA. The addition of $NaNO_3$ salt and increase to a maximum of 0.1M resulted in no aggregation with no significant change in the measured diameter, as the values obtained indicate (6.9 nm ± 0.1 and 6.7 nm ± 0.2, at 0.1 and 10^{-3}M, respectively, $p= 3.27$). The results are based upon 3 replicates of each sample.

Sample	Diameter Mean (nm)	RSD ±	Plasmon Band Maximum Mean (nm)	RSD ±	Zeta Potential (mv)	RSD ±
Gold NPs in pure water	6.59	0.45	518.67	1.15	-4.20	1.16
Gold NPs in 0.1 M $NaNO_3$	6.92	0.11	514.89	3.23	-2.46	1.94
Gold NPs in 10^{-3}M $NaNO_3$	6.66	0.23	517.44	0.25	-4.35	1.26
Gold NPs in 0.1M $Ca_2(NO_3)_2$	6.95	0.40	515.50	3.46	-2.16	0.68
Gold NPs in 10^{-3}M $Ca_2(NO_3)_2$	6.86	0.27	514.33	1.69	-4.55	2.60
Gold NPs in fulvic Acid	6.86	0.11	515.52	2.16	-3.25	2.01
Gold NPs pH 5.5	6.81	0.17	515.92	1.97	-3.32	1.89
Gold NPs pH 7.0	6.83	0.20	515.65	2.23	-3.28	1.90
Gold NPs pH 8.5	6.87	0.09	515.52	2.03	-3.38	1.97

Table 4.1 Average particle diameter under different conditions as determined by DLS, plasmon band peak as determined by UV/Vis and zeta potential.

A significant amount of previous work (Brant et al., 2005a; Burns et al., 2006; Chen and Elimelech, 2006), has shown that a substantial change in particle size can be observed for some NPs when ionic strength is varied, which often stems from significant aggregation as the surface charge is changed. This occurs as the increase in cation concentration changes the surface charge of the particle so that at high ionic strengths the counterion association is so pronounced that the effective charge on the NPs is close to zero (Kallay and Zalac, 2002), thus removing a barrier toward aggregation (Brant et al., 2005b) for charge stabilised NPS. From DLVO theory it is known that an electrical diffuse layer surrounds a particle and for an ionic strength of 10^{-2} mol dm $^{-3}$ this diffuse layer extends ~ 6 nm (Kallay and Zalac, 2002). This means that for the smallest of NPs that an overlap of the diffuse layer and the core of NPs can occur, Kallaly and Zalac (2002) and as such they used Bronsted theory (Bronsted, 1922) in order to model the aggregation kinetics and thermodynamics of very small NPs under differing salt and pH conditions. Others, however, have shown how DLVO theory can be applied to larger NPs such as fullerenes and accurately predict kinetics (Chen and Elimelech, 2006). The effect of water chemistry upon this electrical diffuse layer is what can drive aggregation and is of importance when considering charge stabilised NPs. Though given the steric stabilisation mechanism of the PVP used here and the low zeta potential (Table 4.1) displayed by the NPs, charge shielding by ionic strength does not play a significant role in the stabilisation of these NPs and clearly no effect of salt upon aggregation was observed as was to be expected.

Similarly solution pH affects certain charge stabilised NPs stability and aggregation as at lower pH protonation of anionic stabilising agents can occur (Diegoli et al., 2008) whilst very low pH values < 2 can increase stability of some NPs where a charge on the particle is increased (Baalousha et al., 2008). This level of diverse and opposite effects show how

important it is to consider charge on particles as this is the critical factor in defining how they will react to changes in pH. For the NPs used in this study changes in the pH and in the concentrations of both salt resulted in no aggregation and very little variation between the NPs diameters observed at the three pH ranges tested (Table 4.1). For instance, values of 6.9 ± 1.2, 6.8 ± 1.2 and 6.9 ± 1.2 were recorded for pH values of 5.5, 7.0 and 8.5 respectively and showed no significant difference ($p=0.67$). This highlights one of the differences between charge and steric stabilisation as studies based on charge stabilised manufactured NPs (Diegoli et al., 2008) have found aggregation to occur as pH was changed and altered the point of zero charge of the particles.

4.3.3.2 Surface plasmon resonance

As stated earlier, with the position of the SPR being dependent upon electron density the presence and actions of a ligand shell can be an important factor in SPR behaviour. These ligands can interact electronically with the core metal atoms and partially reduce or oxidise the NPs, (Moores and Goettmann, 2006). The effects of ligand electron donation and back donation from the metal centre are known to result in shifts of NP plasmon bands, (Moores et al., 2004). In the case of the NPs used here this is an important topic as any changes made to the stabilising ligand could manifest themselves as shifts in the SPR.

Size changes which have not been seen here would also affect the position of the SPR with experimental results giving evidence of a blue shift when NP size is decreased. This is reversed however for alkali metal NPs, as electrons spilling from the cationic framework cause the charge to become located outside the metal surface and give a less energetic SPR, (Moores and Goettmann, 2006). Thus changes in SPR can be used to identify changes in the

physical properties of the gold NPs used in this study upon their exposure to the various environmental conditions considered here. For this work the lack of change in the SPR is further evidence that the NPs are uneffected by the changes in solution conditions.

Changes in the plasmon resonance, which have been identified for charge stabilised gold NPs (Figure 4.9a shows the shift in the plasmon band maxima for citrate stabilised gold NPs) (Diegoli et al., 2008), were not present in the sterically stabilised gold NPs used here with no statistically significant variation observed in the plasmon band maxima for 3 distinct different sub batches (NP_{2a}, NP_{2b} and NP_{2c}) of gold NPs (Figure. 4.9b) that were used to further investigate this area, (*p=0.08, 0.11 and 0.89*) or across batch NP_2 as illustrated in table 4.1. Figure 4.9b shows the Plasmon band maxima for 3 batches of NPs when exposed to the range of environmental conditions used throughout and shows visually the lack of significant change across the entire range.

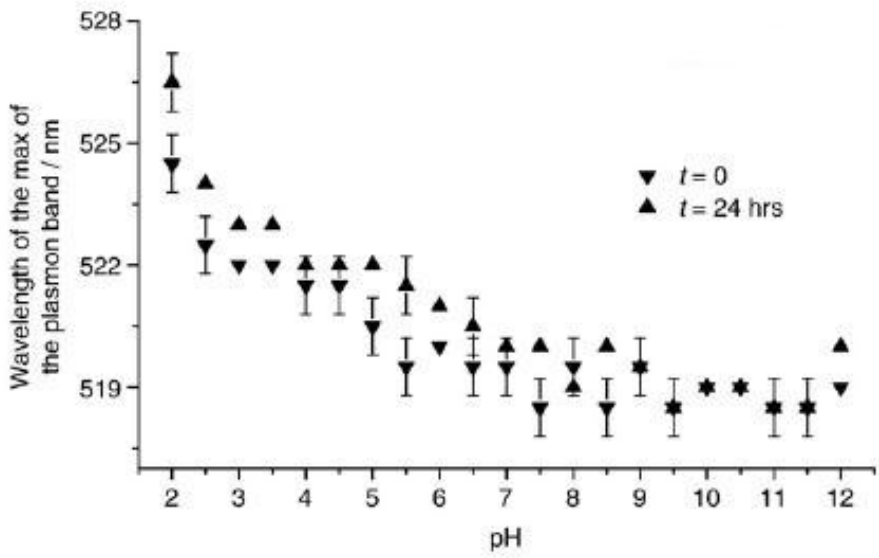

Figure 4.9a The wavelength of the maximum of the Plasmon band for citrate stabilised gold NPs at across a pH range and in SRHA, after (Diegoli et al., 2008).

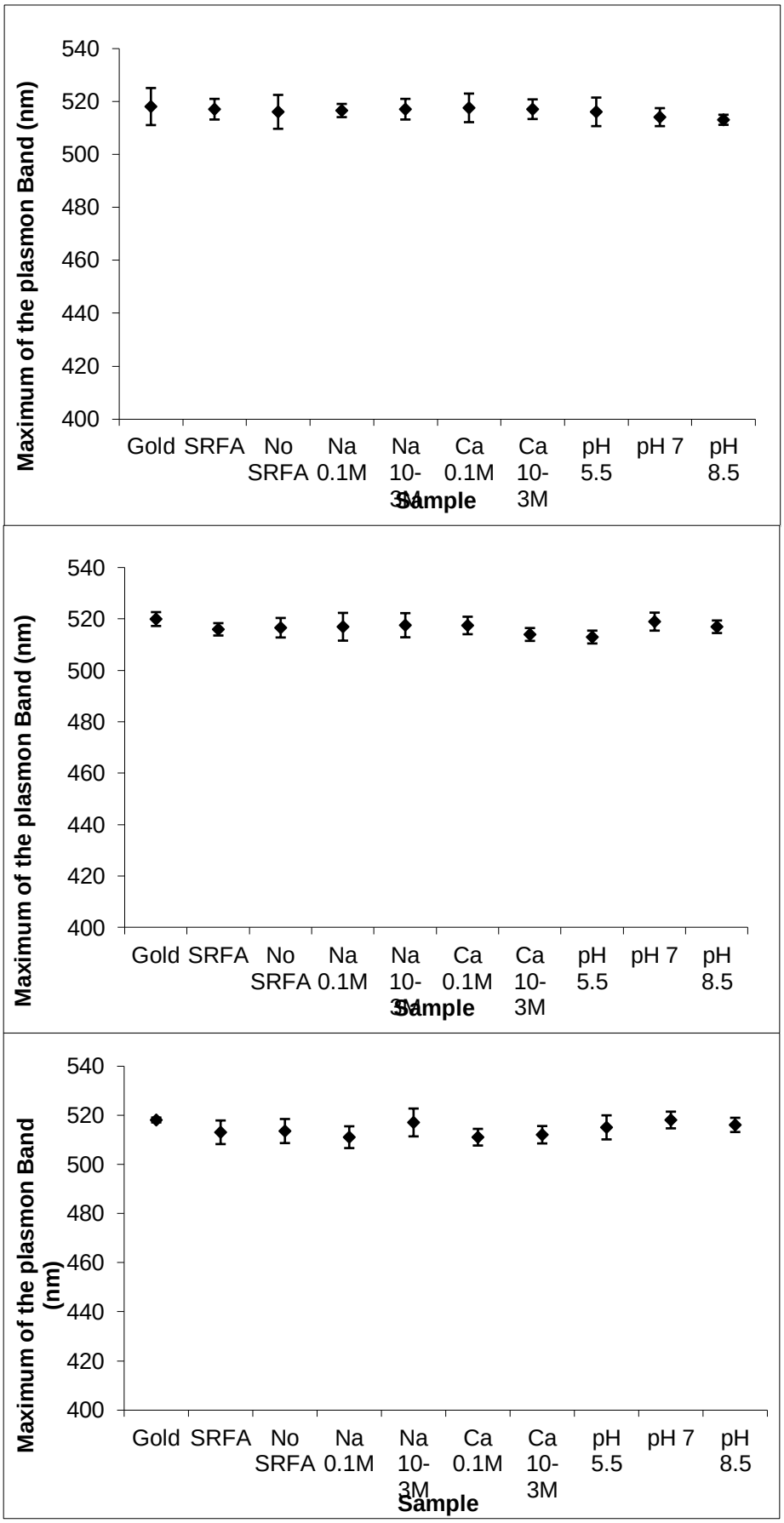

Figure 4.9b The wavelength of the maximum of the plasmon band for three sub batches of AuNPs under different environmentally relevant conditions. Indicating no change across conditions.

This data showing the lack of change in position of the SPR maxima appears to confirm the absence of interaction between the NPs and the HS and salts present in this analysis and correlates well with the results shown previously as well as with the results obtained by AFM and shown later in this chapter in section 4.3.4.2 and as seen previously for silver PVP stabilised NPs (El Badawy et al., 2010).

4.3.3.2 Zeta potential

As mentioned earlier in the chapter the gold NP zeta potential is of critical importance when considering the effects of changes in ionic strength and pH. Data for zeta potential is shown in Table 4.1 and as can be expected due to the steric nature of the stabilising agent, PVP, and the results indicated previously in this chapter, there is only a very low initial charge, nor does the charge change significantly *($p=0.08$)* as the ionic strength and pH are manipulated, though as expected as the ionic strength is increased the zeta potential decreases slightly. This lack of interaction with the environmental media gives a strong indication that aggregation will not occur due to changes in these factors and agrees with data showing no aggregation. This further emphasises the stability of these particular NPs, where the steric stabilisation process is unaffected by changes in the electrical properties of the surrounding media due to their own lack of charge. This is an especially important point when considering transport of these particular NPs within aquatic systems as these are the type of conditions that the NPs may become exposed to and thus their stability and lack of aggregation may enhance their long range transportation potential, (Wiesner et al., 2006).

4.3.4 NP_3

4.3.4.1 Dynamic light scattering

Sample	Diameter (nm)	
	Mean	±
Gold NPs in pure water	8.55	0.91
Gold NPs in 10^{-3} M $NaNO_3$	9.61	1.64
Gold NPs in 10^{-3} M $NaNO_3$ and fulvic acid	8.91	1.61

Table 4.2 DLS Data for Batch NP_3 used in AFM analyses.

Table 4.2 shows the diameters determined via DLS for the third batch of NPs which were used in the atomic force microscopy experiments undertaken, as can be seen from the DLS analysis shown here, there was again no significant change *(p=0.96)* in the mean diameters of the NPs over the reduced range of conditions that were used for the AFM. This data provides a guide as to what size should be expected from the AFM work and again shows the lack of change undergone by the NPs used here.

4.3.4.2 Atomic force microscopy

4.3.4.2.1 Introduction

The previous sections have shown the effects of different salts, pH and fulvic acid on the gold NPs, here a selection of these samples are examined in closer detail using AFM. A reduced range of conditions were used for these analyses due to the fact that it was not feasible to analyse the NPs under the entire range of conditions. This was in part because of difficulties in imaging the NPs, which had a tendency to wash off the mica slides very readily. In combination with other difficulties with the AFM system which meant the software often had to be reset, using up valuable time allotted to the imaging. Though not all the samples and

conditions could be imaged it is felt that the three sets of conditions used, NPs in pure water, NPs in 10^{-3} M $NaNO_3$ and NPs in 10^{-3} M $NaNO_3$ and SRFA, all at pH 7.0, do give a useful representation of potential changes in size and shape which may occur and a sufficient overview of the range of conditions used throughout. These analyses feature the use of AFM in contact and non contact mode. In addition to the analyses undertaken on the gold NPs the effects of the salts and SRFA on PVP alone prepared in the same manner as the gold NPs was also undertaken in order to see fully any effects and whether they were simply an artefact of the stabilising agent rather than a property of the nanoparticle.

4.3.4.2.2 Methodology

Samples of gold NPs in UHP water, 10^{-3}M $NaNO_3$ and 10^{-3} M $NaNO_3$ with 10 mg L^{-1} SRFA were prepared as described in section 3.7. These were then sampled and prepared on mica slides for AFM analysis using the technique described in section 3.4.3. These slides were then viewed using contact and non contact mode AFM (section 3.4.2). The particles were counted visually using XE Image Processing Program software (PSIA, Silicon Valley, USA), the vertical distance from the peak to the slide surface was taken as the particle diameter due to the reduction in resolution for horizontal measurements.

4.3.4.2.3 Contact mode

4.3.4.2.3.1 Gold nanoparticles in water

Firstly the NPs were imaged using contact mode where the average particle diameter of the gold NPs in UHP water is 9.5 ± 1.1 nm (*n=217*). Unfortunately some of the AFM images are of poor quality and so only a small number are presented here (a further selection is shown in Appendix 1). This poor quality of image may stem from a PVP layer on the mica slide interfering with the tip or simply be down to user inexperience, quite possibly a combination

of both is likely. Figure 4.10 shows the AFM images and the spherical shape of the NPs can be seen.

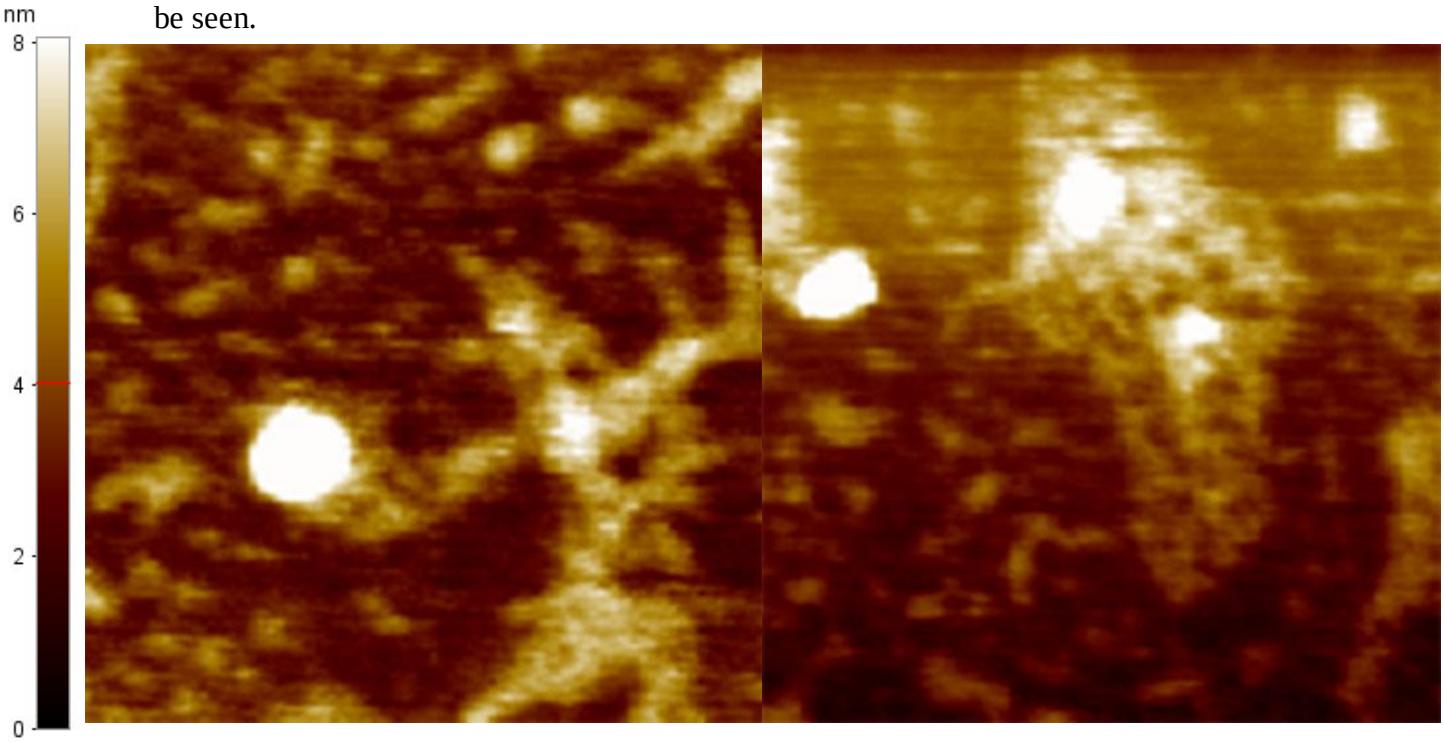

Figure 4.10 Contact mode AFM images of the AuNPs used in water alone.

Figure 4.11 shows the distribution of gold NPs in water as imaged in contact mode, from this histogram it can be seen that a few larger particles are showing and leading to a positively skewed distribution of the sample around the expected size for these gold NPs is present.

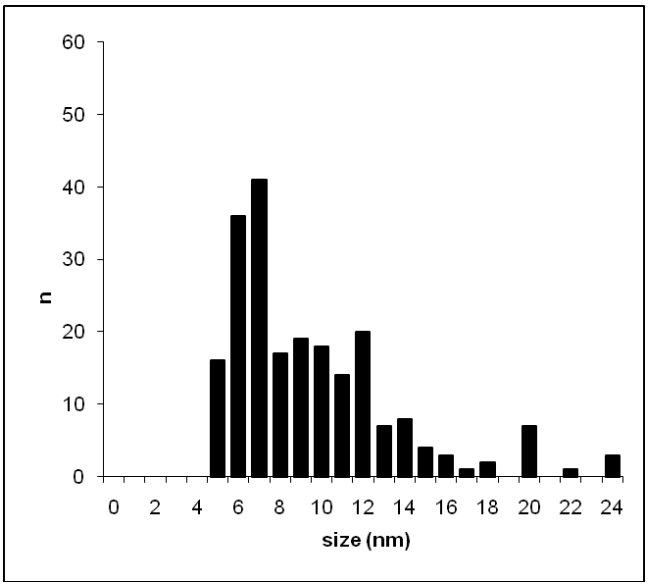

Figure 4.11Distribution of the gold NPs in water using contact mode.

4.3.4.2.3.2 Gold nanoparticles in 10^{-3} M $NaNO_3$

With the NPs in a 10^{-3} M $NaNO_3$ solution the average diameter of the gold NPs using contact mode AFM was 9.0 ± 1.0 nm (*n=136*). Figure 4.11 shows the shape of the NPs from contact mode AFM and again there is no change from the spherical state of the as prepared NPs, though in a few cases there is some slippage of the AFM tip resulting in a squaring of the particle image.

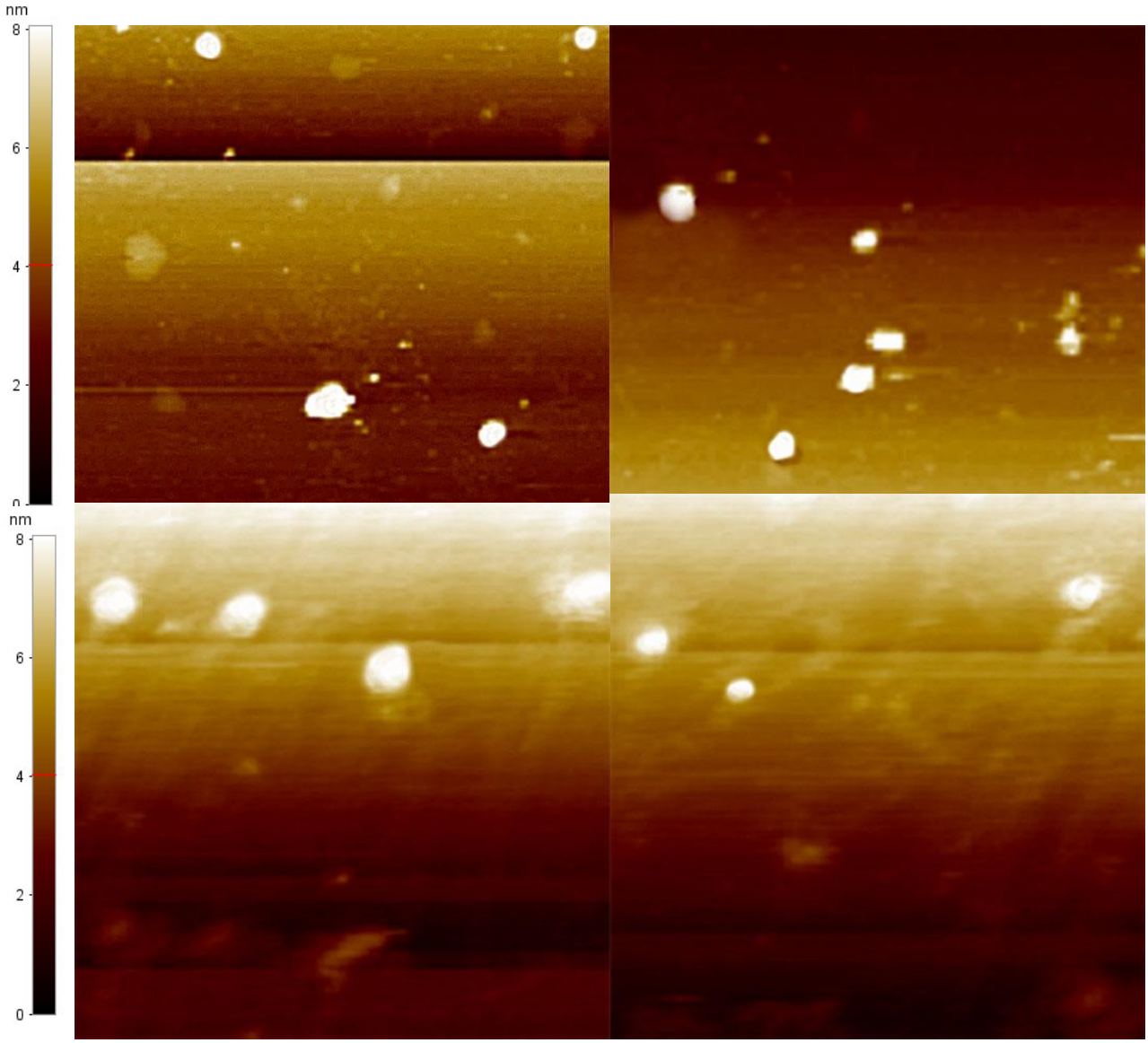

Figure 4.11Contact mode AFM images of the AuNPs used in 10^{-3} M $NaNO_3$.

Figure 4.12 shows the bimodial size distribution of the gold NPs in 10^{-3} M $NaNO_3$ centred on a large peak at 7 nm and the considerable number (5th highest peak) of NPs at 12 nm making it clear from the histogram where the 9.0 nm average diameters stem from. These larger particles are similar to what was seen for this AFM mode and NPs when in water alone though and so should not be taken as a sign that the introduction of salt has resulted in larger NPs forming though of course slight changes in size due to his introduction cannot be ruled out.

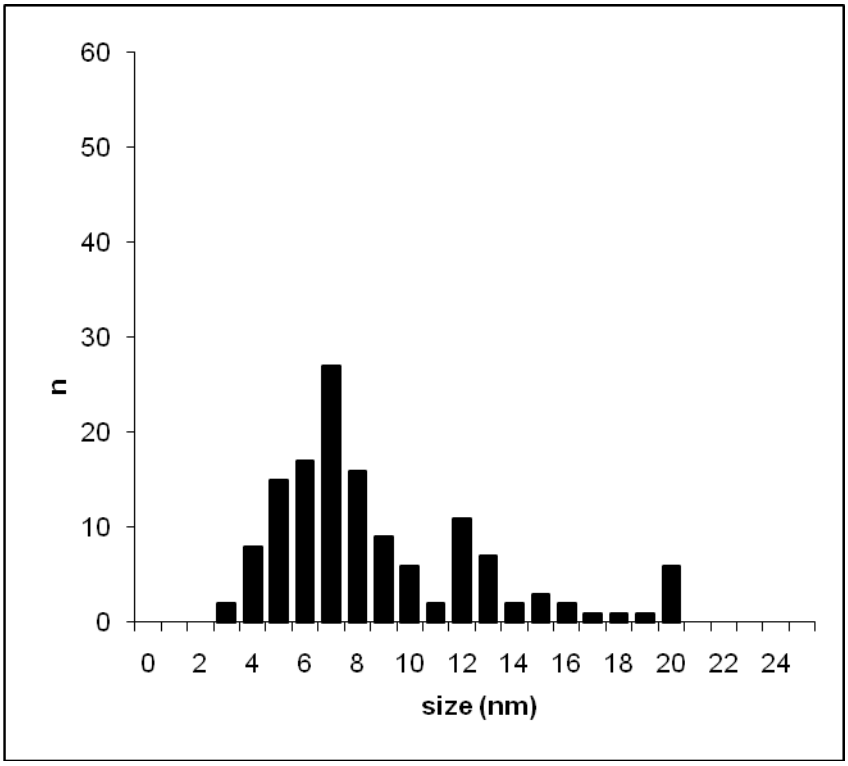

Figure 4.12 Size distribution of the AuNPs used in 10^{-3} M $NaNO_3$.

4.3.4.2.3.3 Gold nanoparticles in 10^{-3} M $NaNO_3$ and 10 mg L^{-1} fulvic acid

With the presence of fulvic acid in the solution the diameter obtained from contact AFM was 8.2 ± 1.3 nm (*n=288*) (Figure 4.20) and the shape of the NPs was in line with the spherical shape seen throughout the non contact mode assessment as well as the TEM analysis. This is again further indication that no visible or significant change has occurred upon the addition of SRFA (*p = 0.06)*.

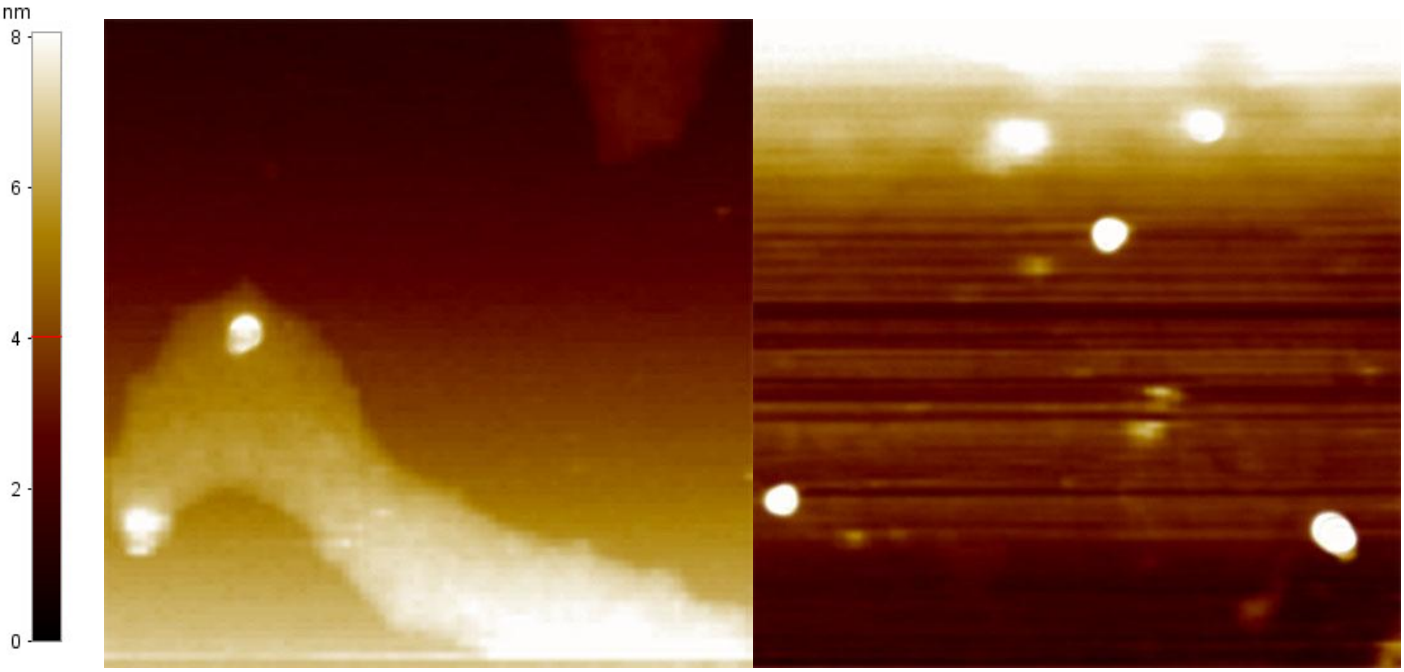

Figure 4.13 Contact mode AFM images of the AuNPs used in 10^{-3} M $NaNO_3$ and 10 mg L^{-1} SRFA.

As was the case for the AFM imaging of AuNPs + salts a positively skewed distribution was found for the NPs when in the SRFA, due to a small number of larger particles (14 – 24 nm) present throughout the images which has been noted for all the conditions when using the contact mode AFM (Figure 4.14). These large particles could possibly be due to two or more NPs becoming fixed to the mica slide within close proximity to one another.

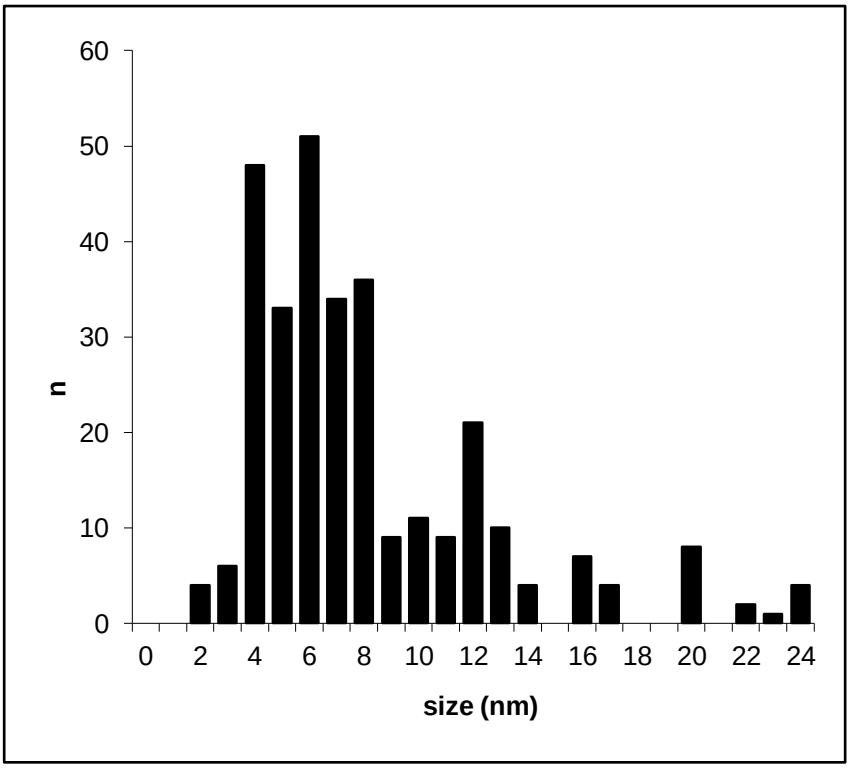

Figure 4.14 Size distribution of AuNPs in SRFA.

4.3.4.2.3.4 Discussion of contact mode AFM samples

For the contact mode AFM it was found that there was no significant difference between the diameters recorded of 9.5 ± 1.1, 9.0 ± 1.0 and 8.2 ± 1.3 nm (*p=0.06*) for pure water, 10^{-3} M $NaNO_3$ and SRFA respectively. The small number of larger particles (whether gold NPs or not is impossible to say) which have been present in all of the conditions considered in this section have contributed to the higher ranges seen in these cases. This notwithstanding the lack of change across the various environmental conditions, which has been noted in the previous sections across a wide range of techniques, is again notable and further evidence of the stability of the particles and the lack of interaction with the environmental media that they have been exposed to in these instances.

4.3.4.2.4 Non contact mode

4.3.4.2.4.1 Gold nanoparticles in water

In non contact mode the average size of the gold NPs in UHP water was found to be 8.4 ± 0.3 nm (*n=57*). Figure 4.15 shows the spherical shape of the NPs in water and serves as a further characterisation of the NPs and an important baseline for comparison to the other conditions considered.

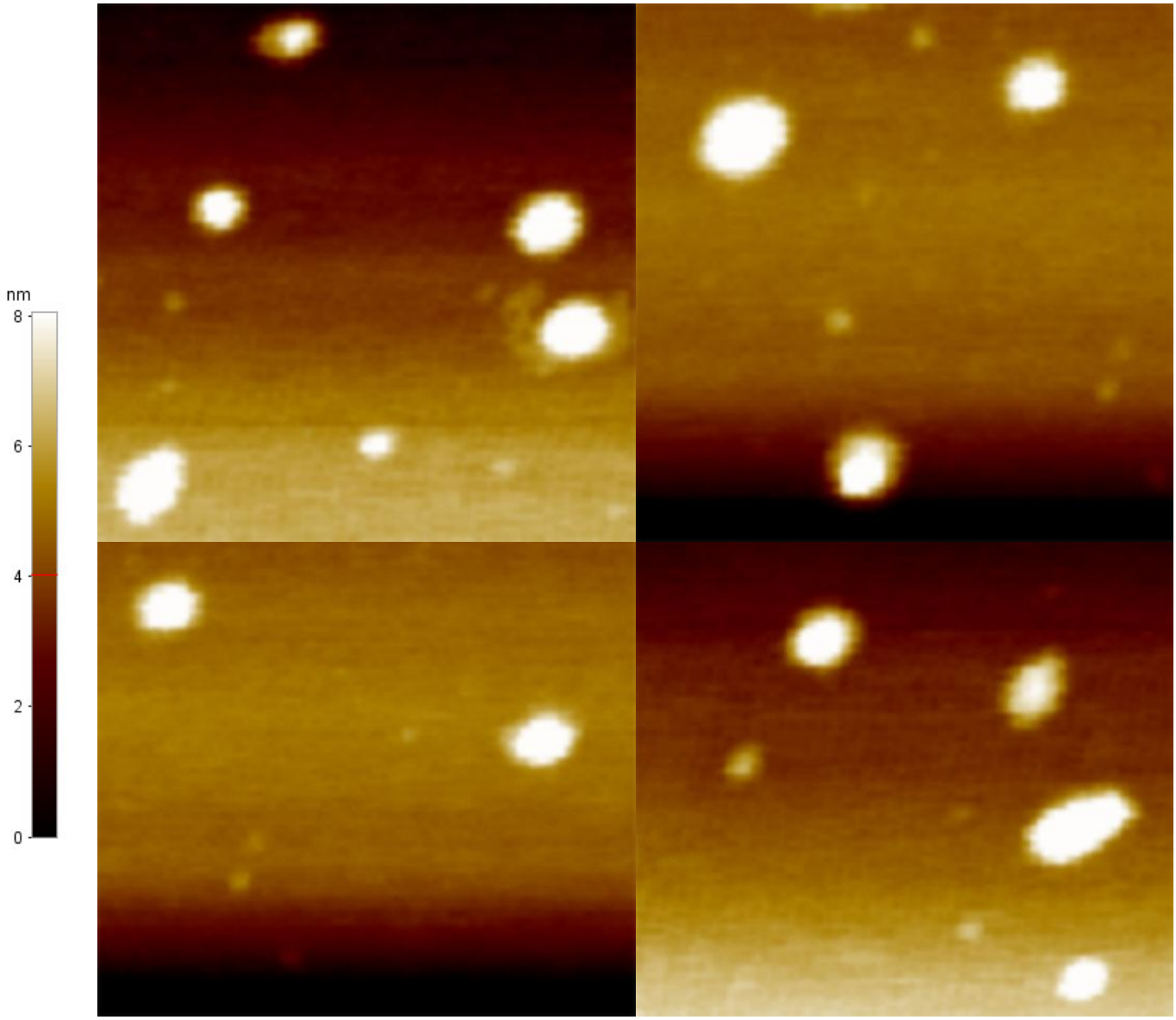

Figure 4.15 Non contact mode AFM images of the gold AuNPs used throughout in water alone.

Figure 4.16 shows some particles that have deviated from a purely spherical shape (from the TEM the particles had length to breadth ratios of ~ 0.99) which may have occurred during the synthesis, though these are only a small minority of particles within the sample. Part of this deviation may well in fact be due to the AFM probe slipping as it approaches and moves away from the particles.

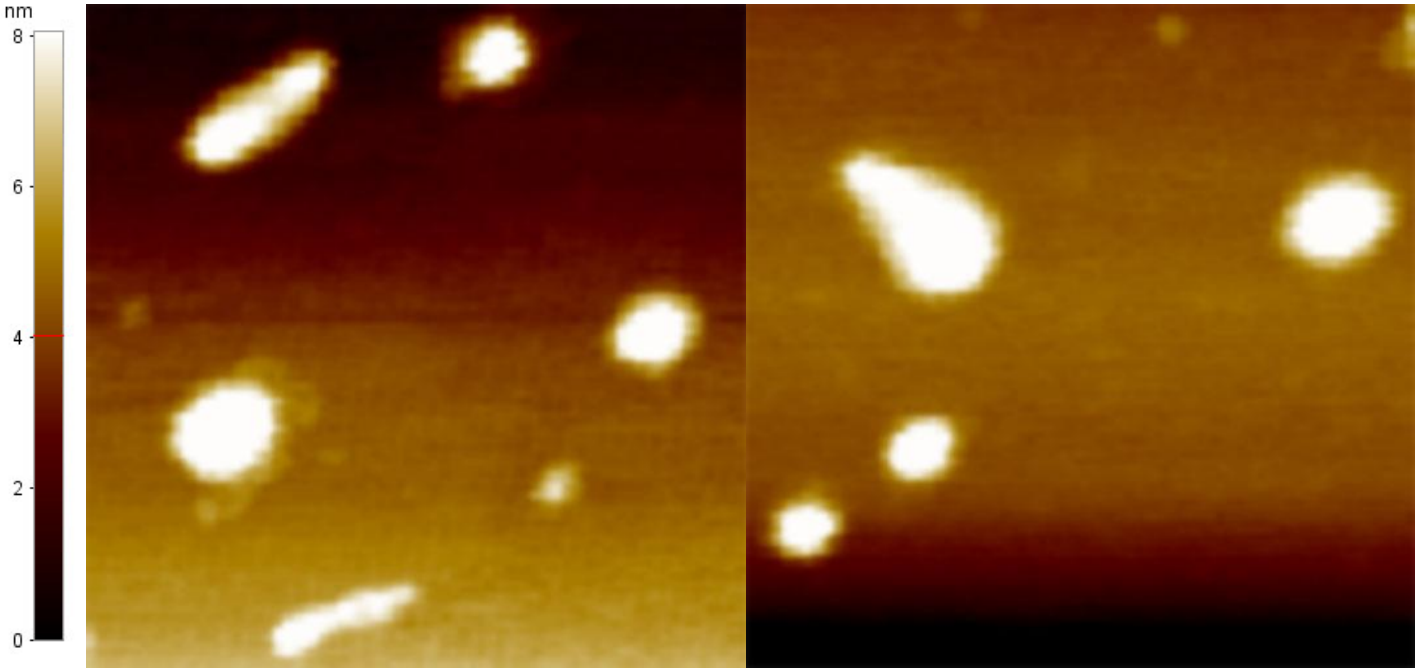

Figure 4.16 Non contact mode AFM images of the AuNPs used in water illustrating that some of the shapes shown have moved away from a purely spherical arrangement.

The distribution of the particles counted is shown in the histogram (Figure 4.17). The histogram shows a normal distribution centred on NPs with a diameter of 8 and 9 nm (*n= 57*), there were fewer particles counted in the non-contact mode AFM analysis than the contact mode possibly due to the mica slides for non-contact mode being prepared with a slightly lower concentration of NPs making them harder to find.

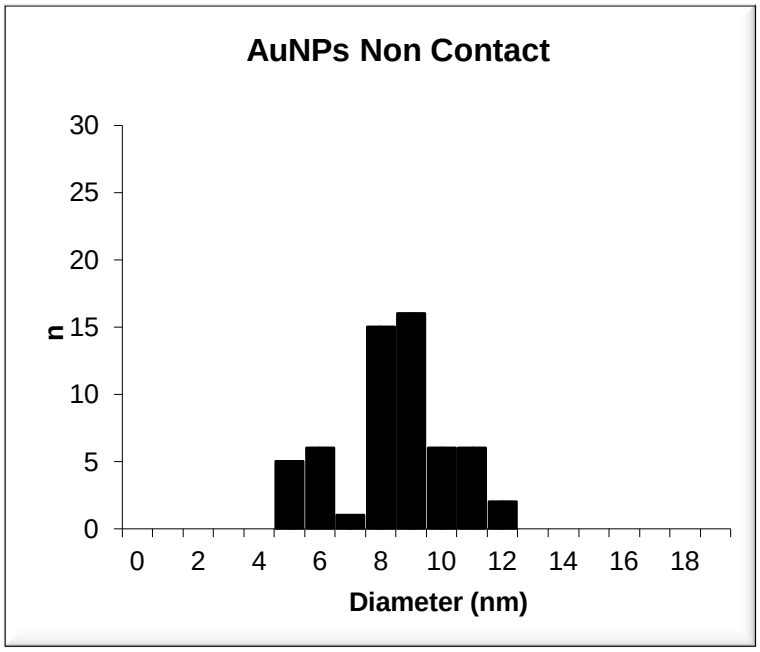

Figure 4.17 Histogram of AuNPs used in water alone imaged using non contact mode AFM

4.3.4.2.4.2 Gold nanoparticles in 10^{-3} M $NaNO_3$

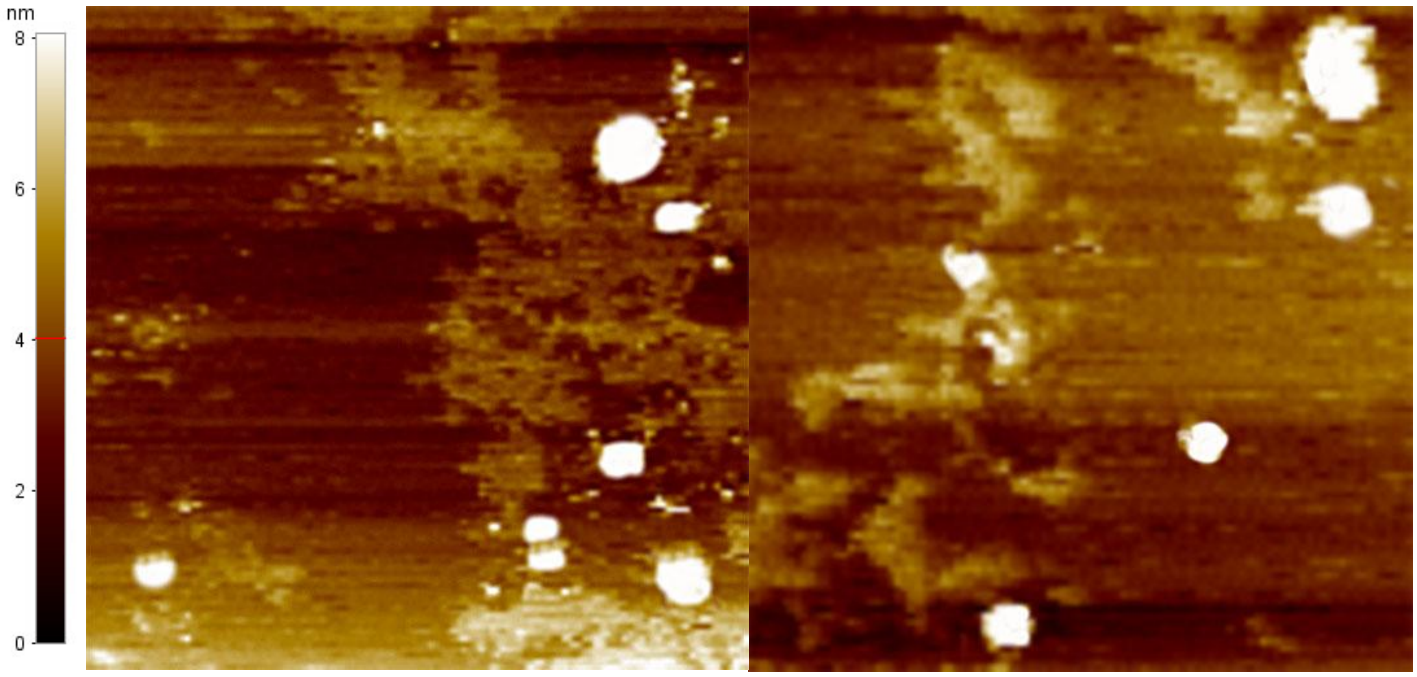

Figure 4.18 Non contact mode AFM images of the AuNPs used in 10^{-3} M $NaNO_3$.

The average size of the AuNPs in 10^{-3} M $NaNO_3$ was 8.3 ± 0.8 nm (*n=86*). The broad outline of spherical NPs can be seen in the images which show that the particles have not undergone any significant change in shape upon their exposure to 10^{-3} M $NaNO_3$. The distribution of the particles is shown in the histogram Figure 4.19 which again shows a similar positively skewed distribution as that seen when using contact mode.

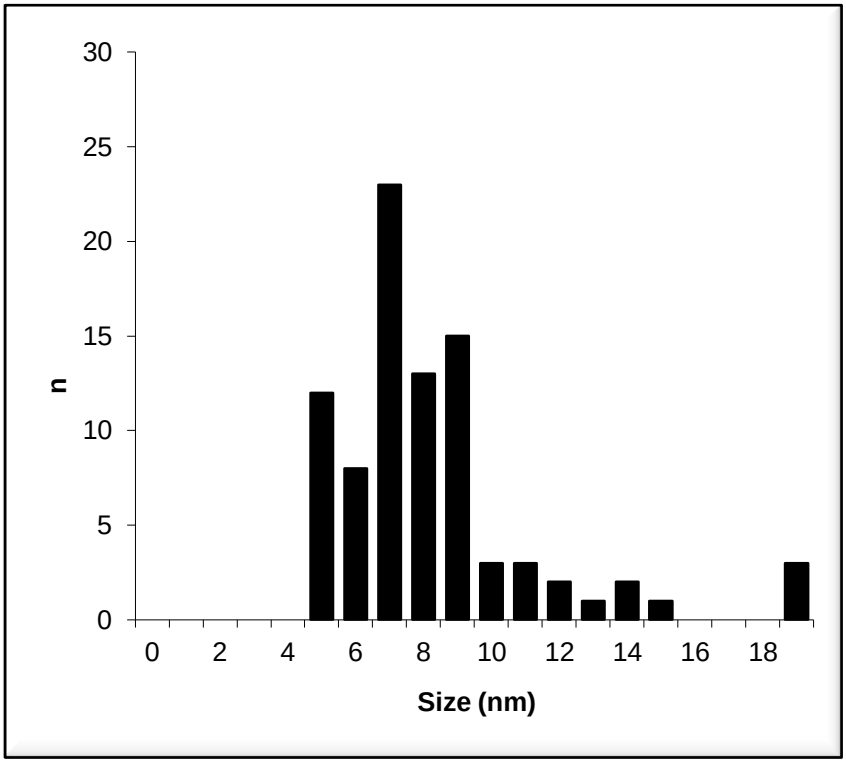

Figure 4.19 Distribution of AuNPs in 10^{-3} M $NaNO_3$.

4.3.4.2.4.3 Gold nanoparticles in 10^{-3}M $NaNO_3$ and 10 mg L^{-1} SRFA

When SRFA was also present in the system the size of the gold NPs was 8.0 ± 1.3 nm (*n=93*). The shape of the particles is illustrated by the images presented in Figure 4.20. Again it can be seen though that shape and size have not changed significantly with the introduction of the SRFA. The histogram in Figure 4.21 shows again a normal distribution of

the NPs though this time with a slightly broader range which is reflected in the larger error value reported for these results.

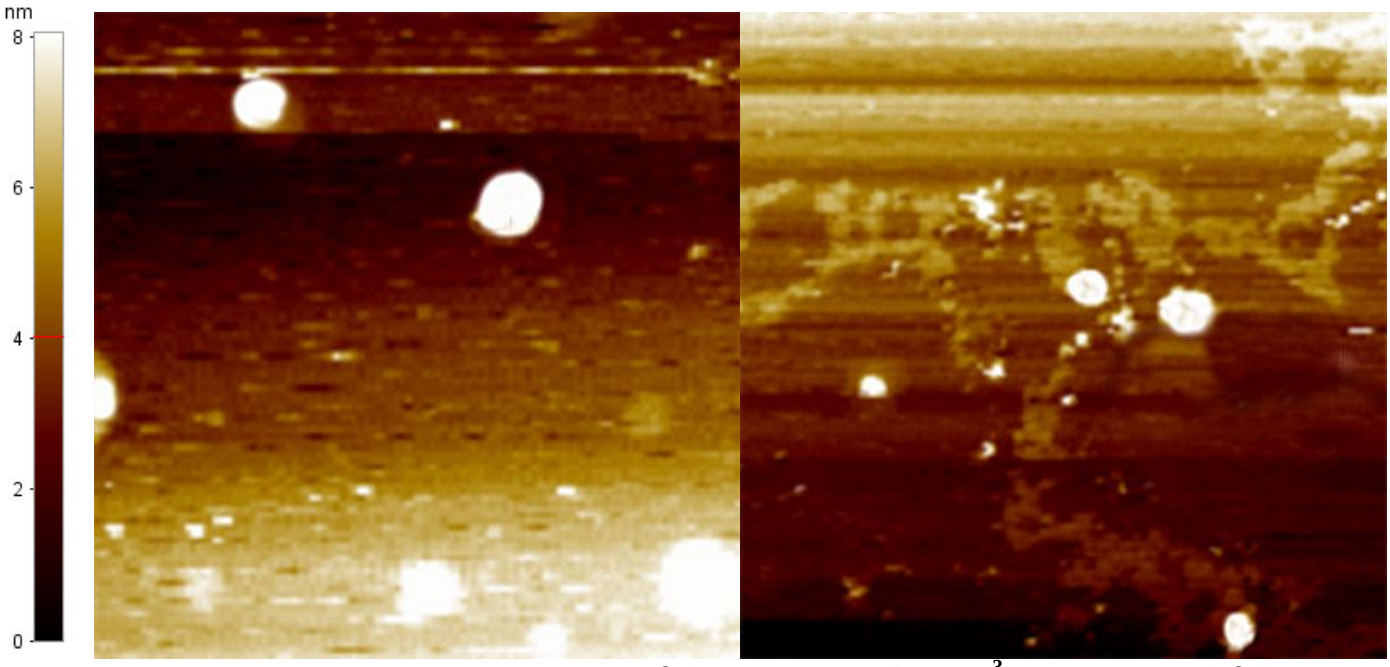

Figure 4.20 Non contact AFM images of the AuNPs used in 10^{-3} M $NaNO_3$ and fulvic acid solution.

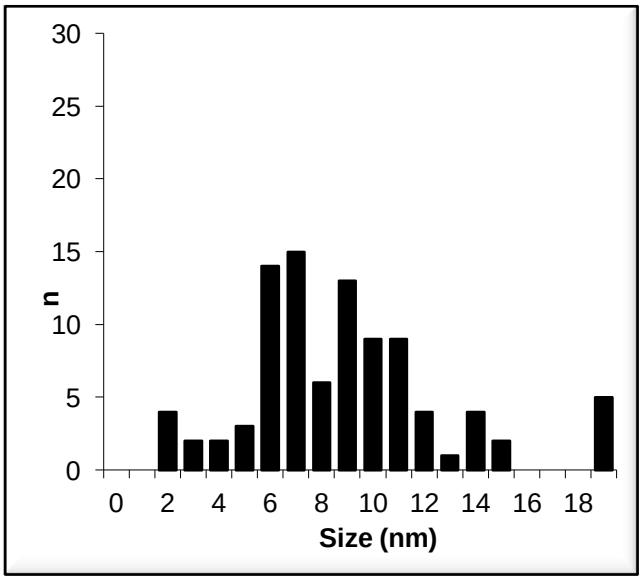

Figure 4.21 Size distribution of the AuNPs used in 10^{-3} M $NaNO_3$ and fulvic acid solution.

4.3.4.2.3.4 Discussion of non contact mode AFM results

When looking at the non contact mode AFM statistical analysis of the effects of the three different sets of environmental conditions show that there is no significant change in the diameter as the conditions change with values of 8.4 ± 0.3, 8.3 ± 0.8 and 8.1 ± 1.5 nm ($p=0.84$) for the AuNPs in water alone, 10^{-3}M $NaNO_3$ and SRFA. From the images it is also possible to note that the shape of the NPs has remained spherical throughout. This is consistent with what has been previously observed in the earlier sections within this chapter and also with what would be expected given the nature of sterically stabilised NPs and in particular the gold NPs used here.

4.3.4.2.5 Liquid Cell

Liquid cell AFM analysis which involves the dispersion of the AuNPs onto a mica slide which is covered with the salt or SRFA solutions as appropriate was undertaken to give a picture of the nanoparticle behaviour in as close to a natural environment as is realistically achievable. However, it became difficult to locate the NPs using this technique as they were liable to float away from the surface. This behaviour was very pronounced for the NPs in water alone with no added salt, to the extent that it became impossible to image them. When the salt was present it was possible to image the NPs and images of the NPs in $NaNO_3$ and SRFA were made. This was only a limited success though as the particle count for these two conditions was very low. Where successfully located the NPs showed no significant difference than to those identified with the techniques discussed earlier in this chapter. The small number of images meant that a significant count was not possible but from the few images available and of which a number are shown in Figure 4.23 sizes of 6.9 ± 1.0 nm for the 10^{-3} M $NaNO_3$ solution and 6.4 ± 0.6 nm for the SRFA solution were found.

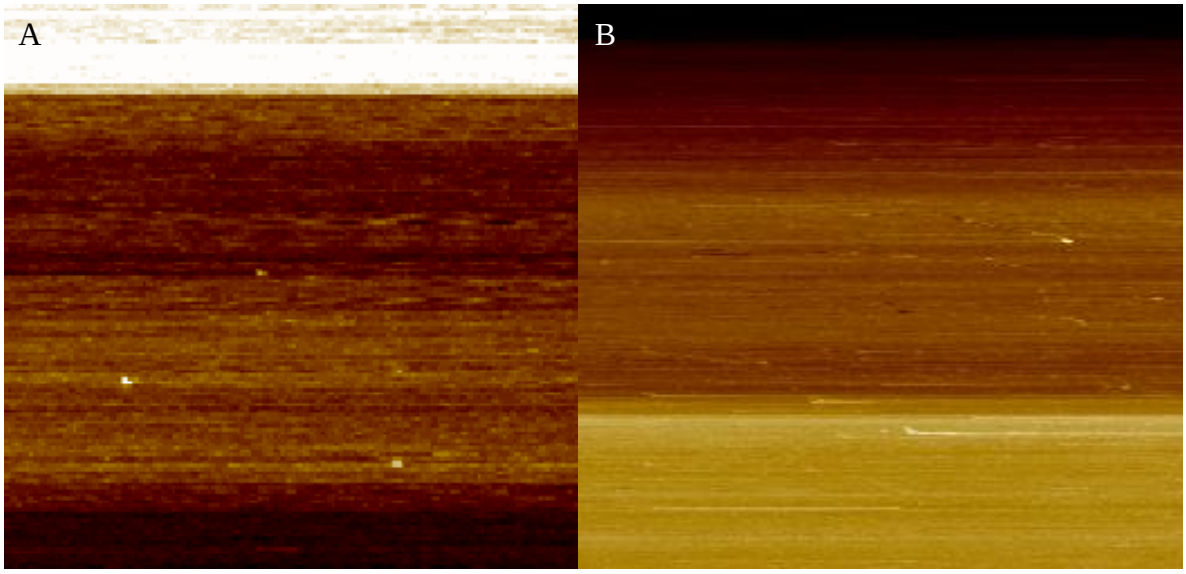

Figure 4.22Liquid cell AFM images of a) AuNPs in 10^{-3} M $NaNO_3$ and b) AuNPs in SRFA.

4.3.4.2.6 PVP analysis

As a number of smaller particles had been showing up in the AFM images PVP solutions were prepared in the same manner as the nanoparticle synthesis save for the addition of the gold source (potassium chloroaurate(III)). This was in order to try and differentiate between the images of PVP particles and the PVP coated NPs. The average sizes calculated for the pure PVP particles are shown in Table 4.3 and can be seen to be considerably lower than the average values calculated for gold NPs and as such every effort was made when counting to ensure that only NPs were counted in the previous sections. This meant that the small number of PVP only particles present, due to the removal of most at the extraction stage, were unlikely to significantly affect the results, though some cross over would appear to be likely at the edges of both ranges.

4.3.4.2.7 Summary and discussion of all AFM modes

Sample	Diameter	
Non Contact mode	Mean (nm)	±
Gold NPs in H_2O	8.4	0.3
Gold NPs in 10^{-3} M $NaNO_3$	8.3	0.8
Gold NPs in 10^{-3} M $NaNO_3$ and SRFA	8.1	1.5
PVP in H_2O	2.5	0.3
PVP in 10^{-3} M $NaNO_3$	2.9	0.6
PVP in 10^{-3} M $NaNO_3$ and SRFA	4.6	3.5
Contact mode		
Gold NPs in H_2O	9.5	1.1
Gold NPs in 10^{-3} M $NaNO_3$	9.0	1.4
Gold NPs + 0.001M Na + FA	8.2	1.3
PVP in H_2O	4.3	1.1
PVP in 10^{-3} M $NaNO_3$	2.6	1.3
PVP in 10^{-3} M $NaNO_3$ and SRFA	3.1	1.5

Table 4.3 Mean diameter of gold AuNPs and PVP samples obtained using contact and non contact mode AFM.

As can be seen from the results in the contact and non contact mode AFM section and is summarised in Table 4.3 and Figure 4.23 the introduction of salts and the presence of fulvic acid has not affected the size or spherical shape of the gold NPs in a significant manner. This is the same pattern that has been seen using all of the techniques mentioned in this chapter and confirms the fact that these NPs are stable under a variety of differing conditions. One last set of experiments was done to assert this fact with the NPs being analysed using cross flow field fractionation.

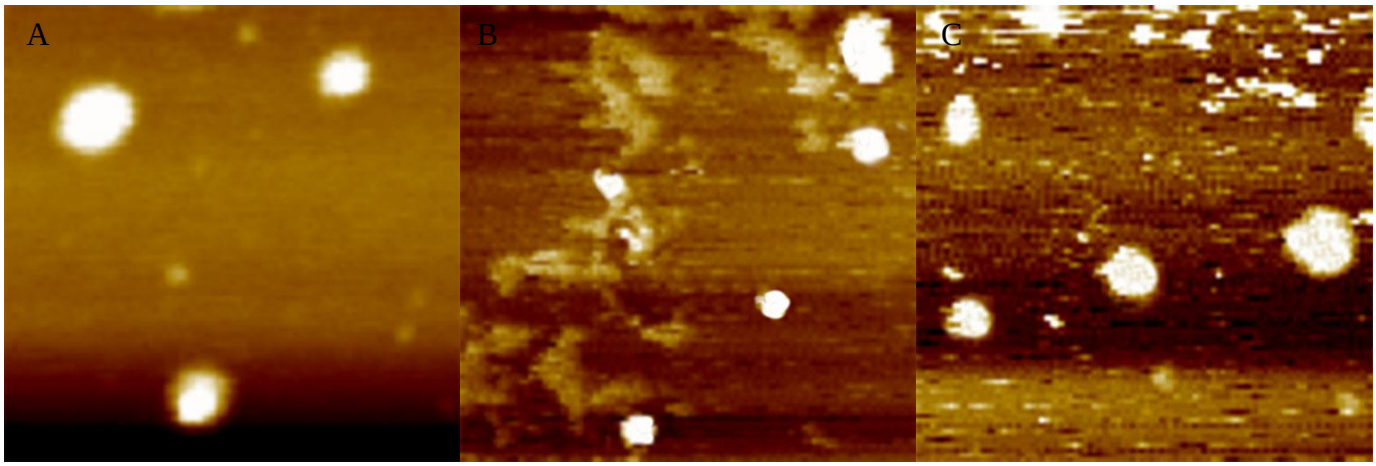

Figure 4.23 Non contact mode images of the AuNPs used in a) Water, b) 10^{-3} M $NaNO_3$ and c) 10 mg L^{-1} SRFA. From the images it is apparent that no change has occurred in the spherical shape of the particles, confirming what has been noted when using the other experimental techniques within this chapter.

4.3.5 NP_4

4.3.5.1 Flow field flow fractionation

Throughout this chapter it has been shown that the exposure of the gold NPs used to different pH, ionic strengths and SRFA has resulted in no change in their size, shape or surface properties. The lack of any significant change in size was confirmed by the use of field flow fractionation on a separate batch of AuNPs in water, 10^{-3} M $NaNO_3$ and 10^{-3} M $NaNO_3$ with fulvic acid at pH 5.5 and 8.5 (Figures. 4.24 – 4.26). No significant change is shown as diameters of 9.4 ± 0.1, 9.6 ± 0.1 and 9.6 ± 0.2 *(p=1.65)* were recorded respectively, these fractograms also show the positive skew that was present throughout the AFM size distributions and further illustrates the presence of some larger particles. This was a different batch of NPs and these results were consistent with the corresponding DLS data shown (Table 4.4). The gold NP recovery for the procedure used for this analysis was ~70%.

Figure 4.24 confirms the initial size of the NPs when in water alone whilst also showing no change upon the addition of the salt. This lack of change in NP size has been seen throughout this entire chapter and was previously expected due to the steric stabilisation of the PVP.

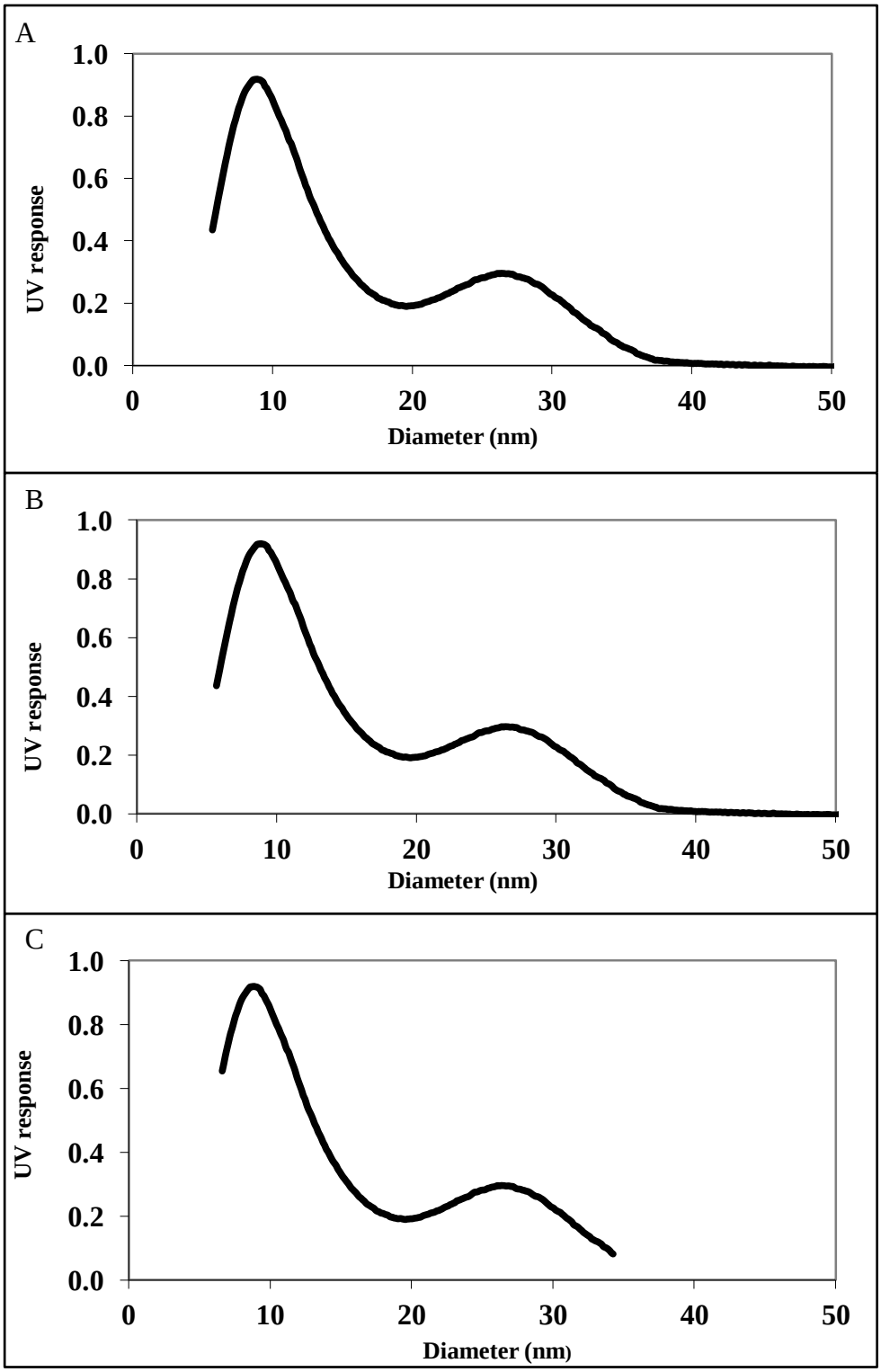

Figure 4.24 FFF Fractograms showing nanoparticle size in water (a and b) and 0.1 M $NaNO_3$ (c) at pH 5.5.

With an increase in pH from 5.5 to 8.5 there was also no change in the size of the NPs (Figure 4.25). Here the pH has been increased and no change in size is noted from the

fractogram. This remains consistent with what has been seen throughout this chapter and is as to be expected with the use of a steric stabilising agent as is the case with the PVP used here.

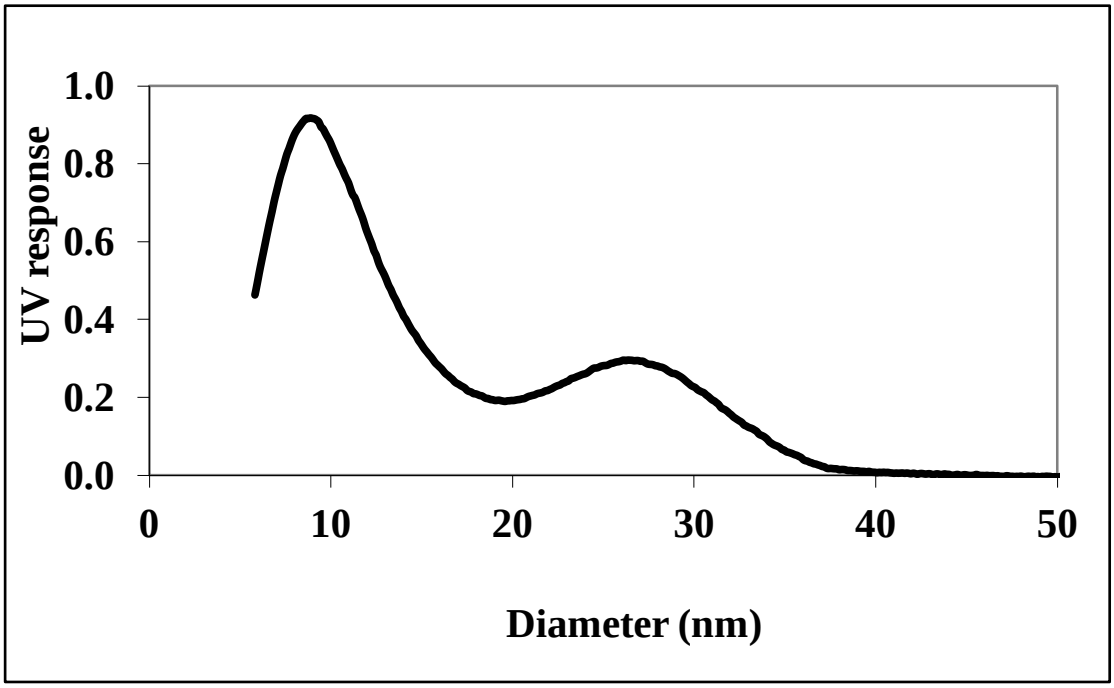

Figure 4.25 Fractogram showing the size of the AuNPs used here in 10^{-3} M $NaNO_3$ at pH 8.5.

The introduction of SRFA is of particular interest due to its abundance in natural waters and, as has been the case throughout this chapter, the fractogram shown here illustrates how again the introduction of SRFA to the system has had no effect upon the size of the NPs, at either pH value that was used for this FFF analysis (Figure 4.26).

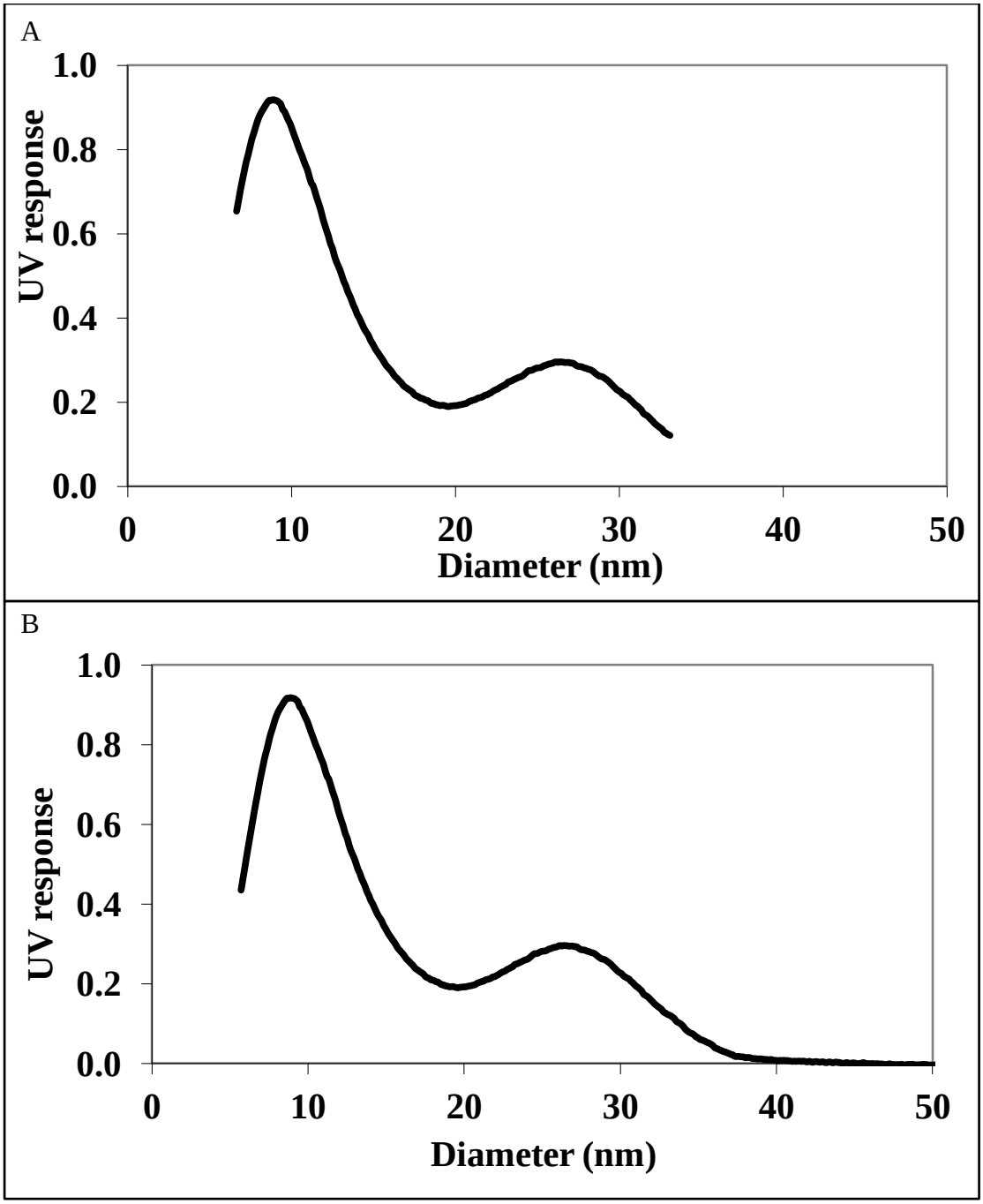

Figure 4.26 Fractograms showing the AuNPs used in SRFA at pH 5.5 (a) and 8.5 (b).

Sample	FFF		DLS
	Diameter (nm)		
	a	*b*	
Gold NPs in water	9.4 ± 0.1	9.1 ± 0.7	9.3 ± 0.6
Gold NPs in 0.1 M $NaNO_3$ at pH 5.5	9.6 ± 0.1	9.7 ± 0.2	9.9 ± 0.3
Gold NPs in0.1 M $NaNO_3$ at pH 5.5 and 10 mg L^{-1} SRFA	9.6 ± 0.2	9.7 ± 0.2	9.5 ± 0.3
Gold NPs in 0.1 M $NaNO_3$ at pH 8.5	9.9 ± 0.3	10.1 ± 0.8	9.2 ± 1.3
Gold NPs in 0.1 M $NaNO_3$ at pH 8.5 and 10 mg L^{-1} SRFA	9.6 ± 0.1	9.7 ± 0.1	10.0 ± 1.1

Table 4.4 Diameters obtained using FFF compared to DLS values obtained for the same batch.

Table 4.4 gives an overview of the data collected in this section and as can be seen this work using the FFF has confirmed what has been noted throughout the chapter and was predicted to be likely. That is that changes in pH, ionic strength and the introduction of SRFA have resulted in no change to the AuNPs size, this coupled with the other results in this chapter surrounding shape and surface properties allows valuable conclusions to be made about how these NPs may behave in natural waters.

4.4 Conclusions

The results shown in this chapter indicate that changes in water chemistry such as ionic strength, pH and the presence of NOM do not change the structure, shape, surface charge or chemistry of the manufactured gold NPs that have been used for this study. This can be seen from the summary table (Table 4.5). One thing of note form this here though is the fact that batch to batch size variation is significant $(p=1.86 \times 10^{-10})$ and as such this should be taken into account when comparing one technique with another.

NP_1 TEM	
Sample	Mean (nm)
Gold NPs	7.55 ± 0.68
Gold NPs + 0.001M Na	7.73 ± 0.52
Gold NPs + 0.001M Na + FA	7.69 ± 0.56
NP_2 DLS	Diameter
Sample	Mean (nm)
Gold NPs in pure water	6.59 ± 0.45
Gold NPs in 0.1 M $NaNO_3$	6.92 ± 0.11
Gold NPs in 10^{-3}M $NaNO_3$	6.66 ± 0.23
Gold NPs in 0.1M $Ca_2(NO_3)_2$	6.95 ± 0.4
Gold NPs in 10^{-3}M $Ca_2(NO_3)_2$	6.86 ± 0.27
Gold NPs in fulvic Acid	6.86 ± 0.11
Gold NPs pH 5.5	6.81 ± 0.17
Gold NPs pH 7.0	6.83 ± 0.2
Gold NPs pH 8.5	6.87 ± 0.09
NP_3 AFM	
Sample	Diameter
Non Contact mode	Mean (nm)
Gold NPs in H_2O	8.4 ± 0.3
Gold NPs in 10^{-3} M $NaNO_3$	8.3 ± 0.8
Gold NPs in 10^{-3} M $NaNO_3$ and SRFA	8.1 ± 1.5
Contact mode	
Gold NPs in H_2O	9.5 ± 1.1
Gold NPs in 10^{-3} M $NaNO_3$	9 ± 1.4
Gold NPs + 0.001M Na + FA	8.2 ± 1.3

NP_4 FFF		
	Diameter (nm)	
Sample	*a*	*b*
Gold NPs in water	9.4 ± 0.1	9.1 ± 0.7
Gold NPs in 0.1 M $NaNO_3$ at pH 5.5	9.6 ± 0.1	9.7 ± 0.2
Gold NPs in0.1 M $NaNO_3$ at pH 5.5 and 10 mg L^{-1} SRFA	9.6 ± 0.2	9.7 ± 0.2
Gold NPs in 0.1 M $NaNO_3$ at pH 8.5	9.9 ± 0.3	10.1 ± 0.8
Gold NPs in 0.1 M $NaNO_3$ at pH 8.5 and 10 mg L^{-1} SRFA	9.6 ± 0.1	9.7 ± 0.1

Table 4.5 Summary table of results for the four NP batches.

This knowledge of how these NPs respond to variations in environmental conditions, such as those considered here, is important when considering the fate and behaviour of such species as aggregation and sedimentation is a barrier toward long range transportation and can effect residence times within surface waters and groundwater as well as their bioavailability, toxicity and transportation within porous media (Kretzschmar and Schafer, 2005; Lead and Wilkinson, 2006). With this knowledge and their potential environmental behaviour confirmed it is now possible to consider the effects of flow within a simulated river system upon the NPs, how they are likely to be effected by the exchange of water between the surface free flow and the sub surface bed flow and the effects that this will have upon their long term transportation and ultimate environmental fate.

5.0 Fate and behaviour of gold nanoparticles in a recirculating flume.

5.1 Introduction

As discussed in Chapter 4 the NPs used in this study did not aggregate significantly which removes a likely cause of sedimentation and an environmental sink. As a result they will have a propensity toward relatively longer range transport within the aquatic environment than charge stabilised NPs making them ideal tracers for NP transport. It is therefore important to consider the effects that exchange in water flow between the stream free flow (i.e. water above the bed) and the river bed may have upon NP transportation and in particular whether the flow of water into the bed may provide another avenue towards a possible sink for the NPs in river systems. This chapter will assess the movement of NPs within the bed and any overall mass transfer of NPs from the free flow of the stream to the bed.

The exchange of water between the stream and the hyporheic zone beneath influences the transfer of a number of dissolved and suspended materials which are of ecological, environmental and geochemical importance. For example, the flux of carbon and nutrients between the streambed and stream are important for the maintenance of healthy stream ecosystems (Packman et al., 2004). The potential introduction of NPs into streams and the differing behaviour that such materials have displayed in contrast to their bulk counterparts (Wiesner et al., 2006) emphasises the need to consider these nanoparticles in such a situation. Recent studies showing that stable NPs deposit within a streambed at a slower rate than less stable NPs whilst both were readily released into the stream with increases in flow velocity (Boncagni et al., 2009) will need to be expanded upon. This will allow us to see if their behaviour differs from the solutes and tracers previously investigated and discussed in

Chapter 2, where it is seen that both turbulence and advective pumping may affect the mass transfer of solutes.

Based on the information discussed in Chapter 2 and to explore NP exchange pathways between the stream free flow and river bed pore water flow in a controlled manner and in order to achieve a level of comparability, a set of controlled experiments were conducted in a recirculating flume using two distinct bed formations. The first used a bedform to explore the influence of pressure variations and to investigate how localised advective pumping may influence the NP transport. The second simpler design featured a plane bed to identify how turbulence in the absence of any pressure variations caused by a bedform may impact NP transport. In addition to providing an insight into the mechanics of transportation these experiments provide high quality data which will be of significant benefit in calibrating numerical models. Expanding on the information presented in Chapter 3, the next section will detail the design and evolution of the flume experiments that have been conducted.

5.2 Flume design

5.2.1 Flume

The experimental work was conducted using two open channel flumes: a large flume (26 m long x 2 m wide flume – see Figure. 5.1) and a small benchtop flume (0.68 m long x 0.25 m wide). After a series of significant preliminary investigations over the course of 12 months it was discovered that the large flume was impractical for the current work due to the large volume of NPs required in order to correctly seed the flow and the subsequent costs of analysing a large number of samples. For example, the volume of water required for the flume (~2000L), was much larger than the realistic volume of nanoparticles that could be added, which was approximately 150 – 250 ml of ~ 250 ppm solution due to constraints

surrounding the amount that could be synthesised at one time. This resulted in a dilution of the nanoparticles such that they were barely detectable in the samples taken via the ICP-MS technique employed and at such a low concentration that any differences were within the margin of error. An attempt was also made in this case to attach 6 TEM grids to a number of spheres to see if any NPs would attach at these sites. Unfortunately only one TEM grid remained attached at the end of this pilot study and no NPs were present upon it (Figure 5.2).

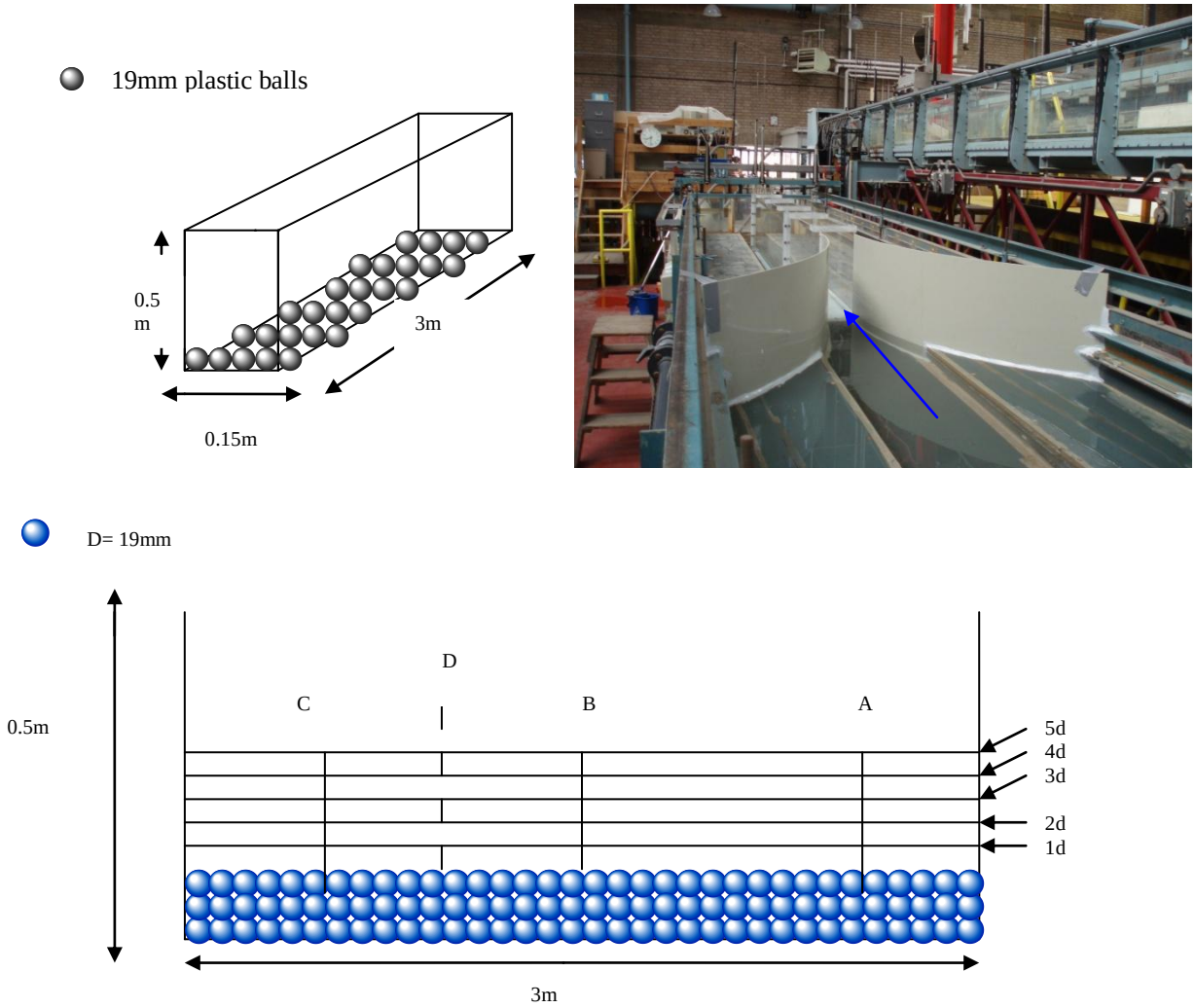

Figure 5.1 Initial flume experimental section showing sampling points and 5 depths (based on the plastic sphere diameter) that experiments were to take place at as well as showing the face centred cubic configuration of the plastic spheres used to simulate the gravel river bed.

Sample	CONCENTRATION (ppb) Au / 197
1	1.49
2	6.78
3	3.78
4	7.22
5	7.43
6	4.29
7	9.04
8	9.39
9	12.66
10	8.89
11	9.63

Table 5.1 The concentration of AuNPs in the pilot study using the large flume as determined by ICP-MS.

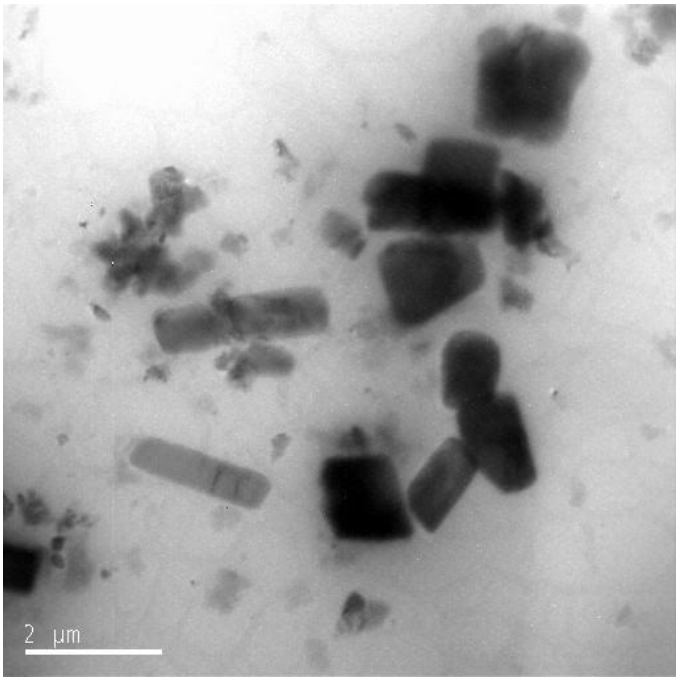

Figure 5.2 TEM image of debris left on the one surviving grid after pilot study in the larger flume, no NPs are detectable.

This posed a significant challenge as due to the expense of the gold salt used it was impossible to synthesis and add a larger amount and it is not possible to run the flume with

less than ~ 2000 L of water due to its size. This resulted in very low concentrations of AuNPs being detected (Table 5.1), which was felt to be at too low a level to accurately assess NP transport between the pore spaces. In order to address this issue experiments were moved to a much smaller bench top flume (Figures 5.3, 5.4, 5.5 and 5.6). This flume was able to function using only 125 L of water which ensured that manageable volumes of nanoparticles (same volume and concentration as indicated above) were detectable.

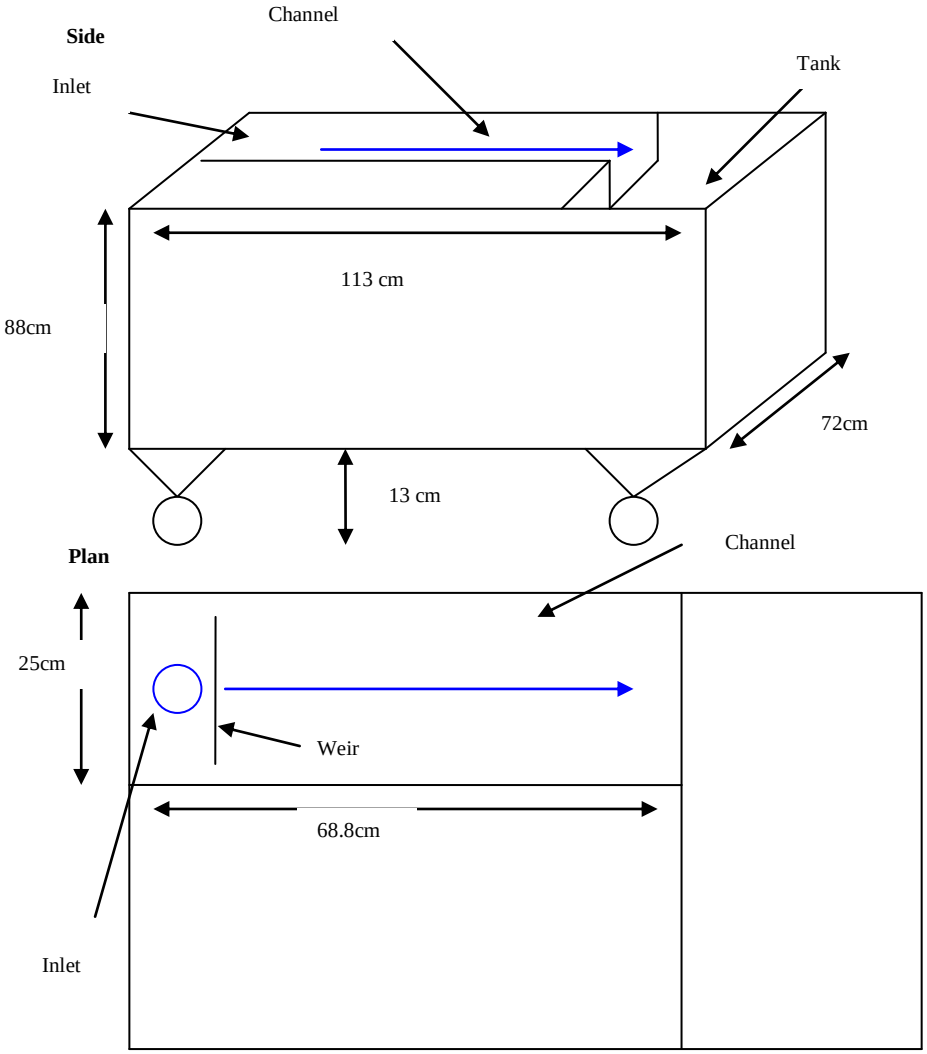

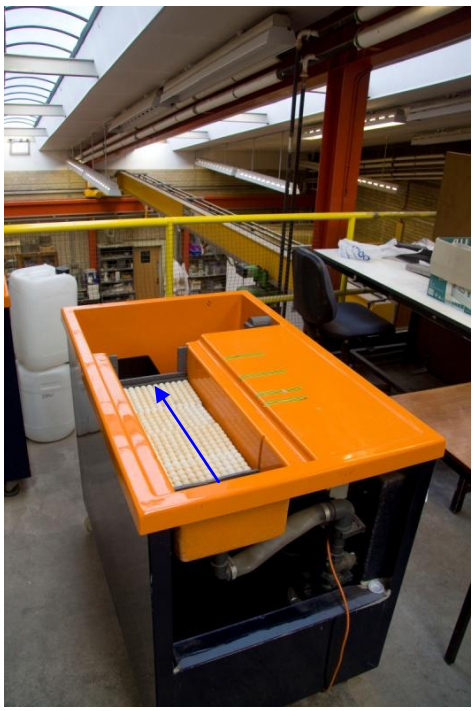

Figure 5.3 Side and plan view of the benchtop flume used after moving away from the larger flume, also a photograph of the flume from the inlet end. The blue arrows show the direction of water within the flume channel. In the plan view the location of the small weir used to stabilise flow from the inlet to the channel is shown.

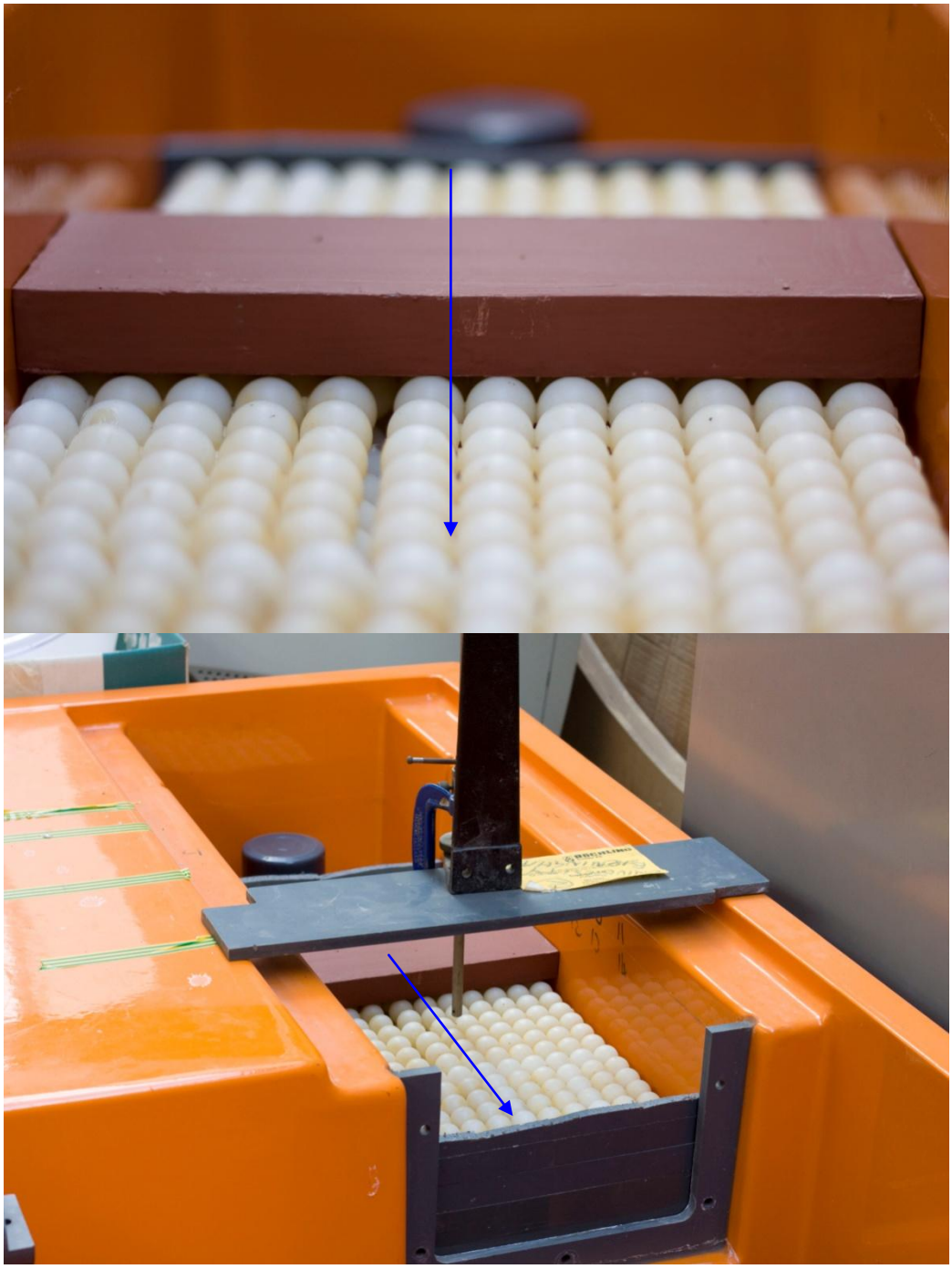

Figure 5.4 Photographs of the test section toward inlet showing the bed of plastic spheres as well as the metallic bedform used in some of the experiments. The blue arrows indicate the direction of water flow.

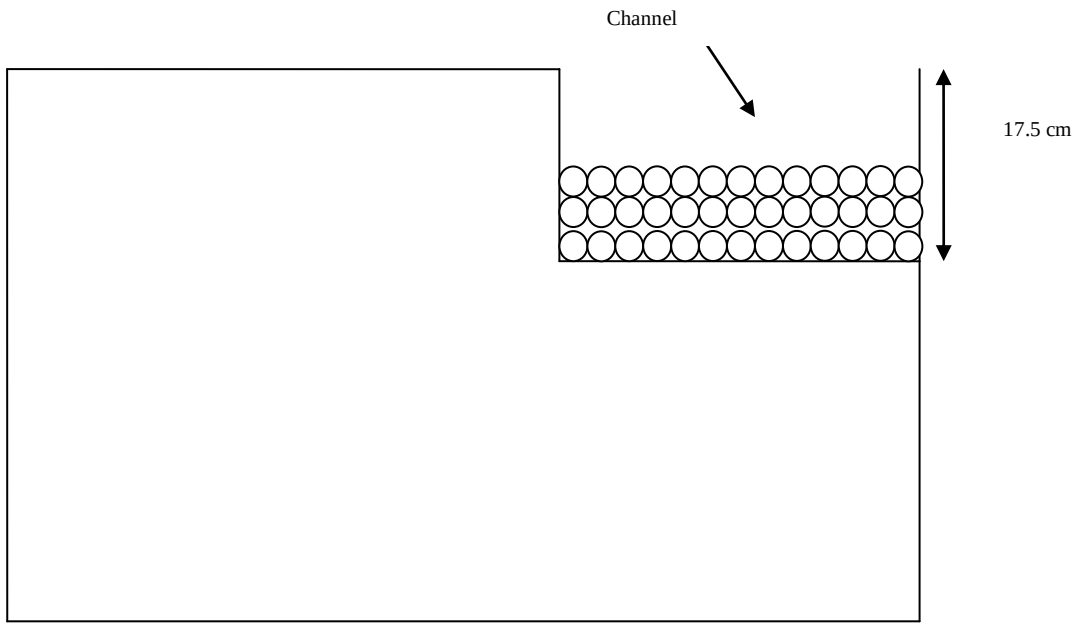

Figure 5.5 Cross section of the benchtop flume from within the tank showing the test channel with plastic spheres facing toward the inlet i.e. water flows toward the viewer.

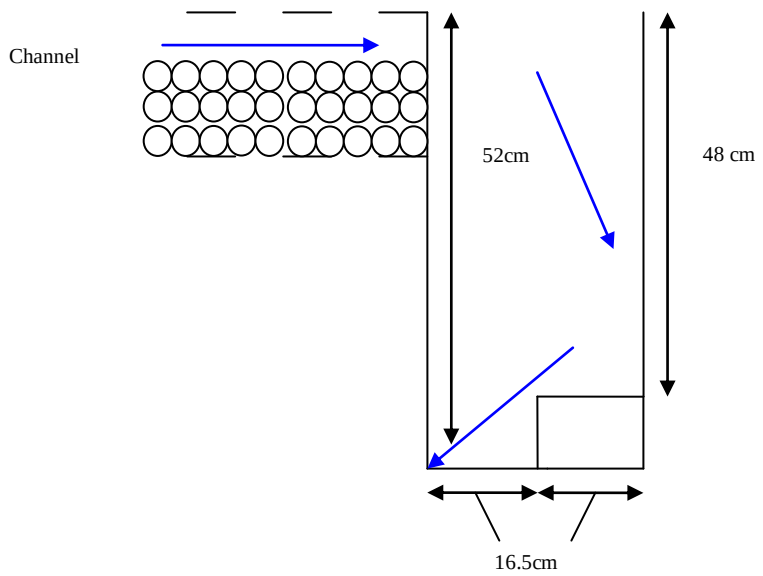

Figure 5.6 A cross section within the tank perpendicular to the channel showing the depth of the tank.

Initially the large flume had allowed a range of depths and discharges that would allow a large range of comparison. Unfortunately however the reduction in the size of the flume

meant that varying the depths of flow was no longer an option without reducing the rate of flow within the channel excessively. This reduction in the rate of flow at higher depths meant that experiments were only conducted at a depth equal to three times the diameter of the plastic spheres used to create the experimental river bed, i.e. the depth of flow was 57 mm above the plastic sphere bed giving a ratio of bed particle diameter to depth of 0.33 which is within into the range of that found in natural rivers throughout the world (Aguirre-Pe, 1990). This was due to the fact that the Froude number, which is used to define the type of flow within a channel with 0.23 indicating sub critical flow as is found in the majority of natural rivers, see section 5.3.2, best matched that being used in a related study on pore water flow (Blois et al, 2010) whilst remaining practicable for sampling, at a depth of 0.08m when sampling was attempted in the plastic sphere bed there were instances of the water overflowing the sides of the channel resulting in significant disruption to the flow as well as loss of NPs and water.

However, the main drawback in moving to the smaller flume is that due to the short channel length the flow does not have a chance to develop. This means that velocity and turbulence characteristics of the flume are heavily influenced by the conditions at the start of the flume. This is a valid concern, but in this case it is felt that since a perfect simulation of a natural river is not the main aim of this project and that this setup allows an understanding of the exchange processes taking place and how they will affect the NPs fate and behaviour, then the current simulation can be considered sufficient.

5.2.2 Flume bed

The bed of a natural river is heterogeneous. However, in order to be able to attempt to understand exchange and model flow patterns and nanoparticle transport pathways within the bed a more structured bed configuration is required as this will remove the effects of bed variability in the form of different hydraulic conductivities and thus isolate the impacts of turbulence and pressure variations. To achieve this, a bed was constructed using plastic spheres (Nylon 66) with a diameter of 19 mm (The Precision Plastic Ball Company Ltd, West Yorkshire). These plastic spheres were arranged in a face centred cubic array with a height of three spheres and a width of 13 spheres and were held in place using a small amount of adhesive (Evo Stik Serious Glue, Bostik, Leicester) applied to one sphere and then stuck together. This process was repeated until multiple lines of 13 spheres had been created which were then fixed together to form layers, these layers were then also affixed together using the same glue to form the larger bed (shown in Figure 5.7a with the bedform present and 5.7b without the bedform). For the experiments with a bedform a steel block with the dimensions 57 mm x 19 mm was used, this block was coated with Red Oxide Primer (Fortress, UK) to prevent corrosion. A block was used rather than a small section made from the plastic spheres in order to fully exaggerate the effect of the bedform.

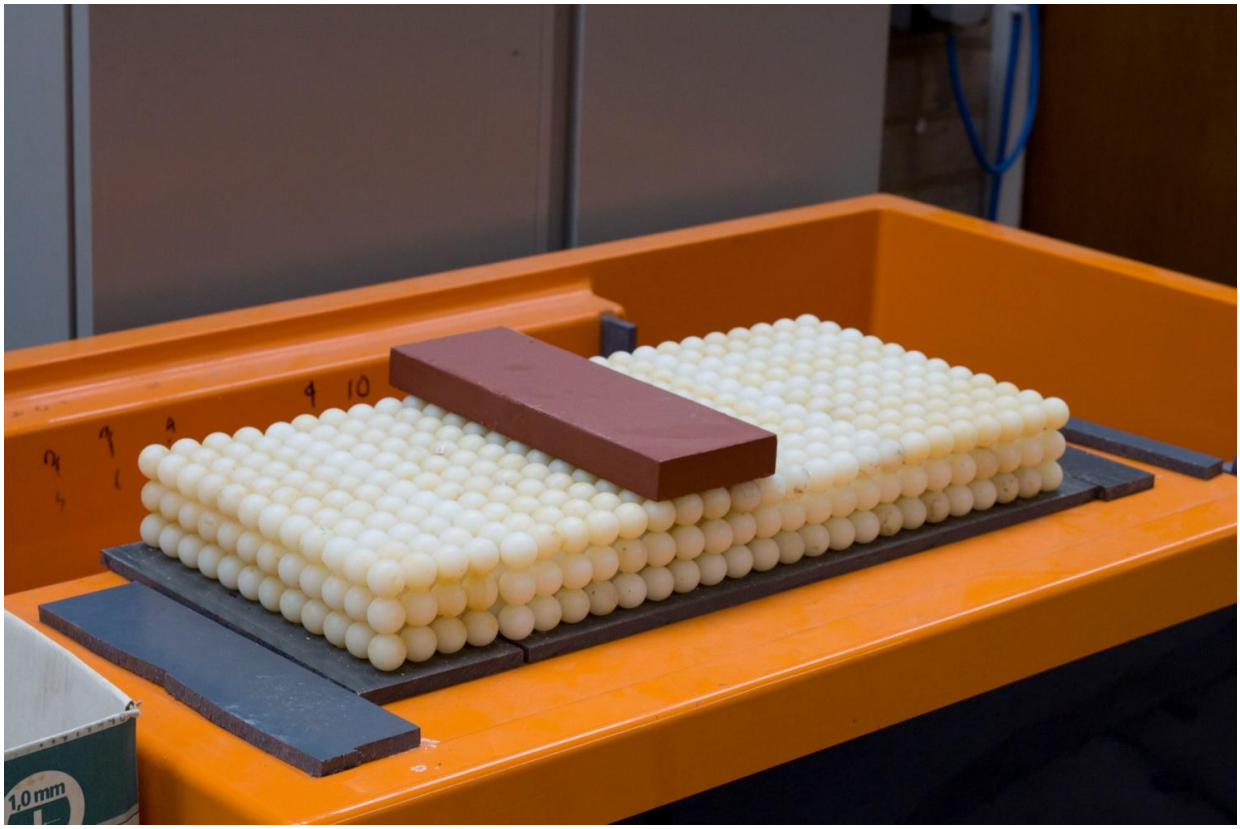

Figure 5.7a The test bed section made from 19 mm nylon 66 plastic spheres, above the plastic spheres is the steel block coated with Red Oxide Primer used as a bedform, for experiments considering just the plane bed this was removed.

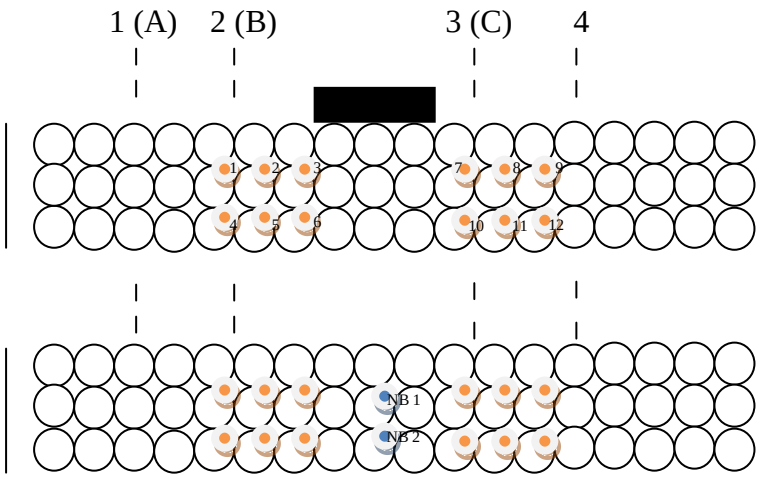

Figure 5.7b Similar to the view shown earlier in Fig 3.11 the side view of plastic sphere test bed section added to the benchtop flume, with the bedform present experiment on top and the plane bed without bedform on the bottom. Orange dots show sampling points across both experiments, whilst the blue dots indicate samples taken only with a plane bed. The dashed lines show the positions where velocity readings were taken, sites 1, 2, 3 and 4, with A, B and C being located in the same position as 1,2 and 3 respectively.

5.2.3 Flume water

The water used in the flume was reverse osmosis water from a MidiRO system (Elga Process Water, UK) and was added to the flume immediately prior to the experiments taking place so as to be as free of contamination as possible. The flow was allowed to stabilise within the channel for 1 hour prior to the addition of the nanoparticles.

5.3 Flume characteristics

5.3.1 Introduction

To characterise the flow of water in the channel above the bed, velocity readings were taken at 4 locations moving from an upstream location to downstream as indicated in Figure 5.7b. These readings were made using a simple Pitot-static tube which was connected to an

inclined manometer, enabling the local streamwise point velocity to be calculated. An additional device, an acoustic Doppler velocimeter (Vectrino, Nortek, USA) was trialled in the flume but there were two problems associated with its use: firstly, the reverse osmosis water used proved to be too clean and there was insufficient 'dirt' particles in the water present in the flow to provide the required feedback needed to generate a reading and secondly, the relatively shallow depths of flow used ensured that the measurement head of the velocimeter (Figure 5.8) could not be submerged at the lower depths resulting in no valid reading.

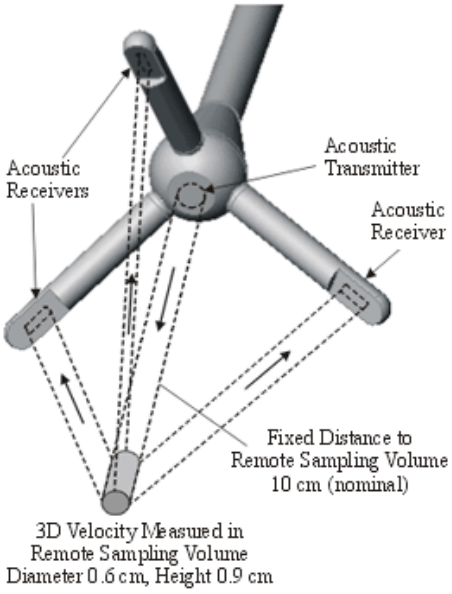

Figure 5.8 Sampling head of typical acoustic Doppler velocimeter showing remote sampling volume which extends below the sampling head, (www.sontek.com).

Due to this it was decided that a Pitot-static tube would be used throughout the experiments in order to provide detailed data relating to the local, streamwise velocity (V). The Pitot-static tube is easily moved across a cross sectional area of flow, A, and from this the discharge, Q, can be obtained.

$$Q=AV \tag{5.1}$$

The Pitot-static tube effectively measures the velocity head, $V^2/2g$, of the flow by converting the energy of the flow into the equivalent static head of liquid (Hamill, 2006). The probe takes the form of a metal tube bent at a right angle and can come in various sizes depending on the job at hand, as such relative dimensions are given here (Figure 5.9).

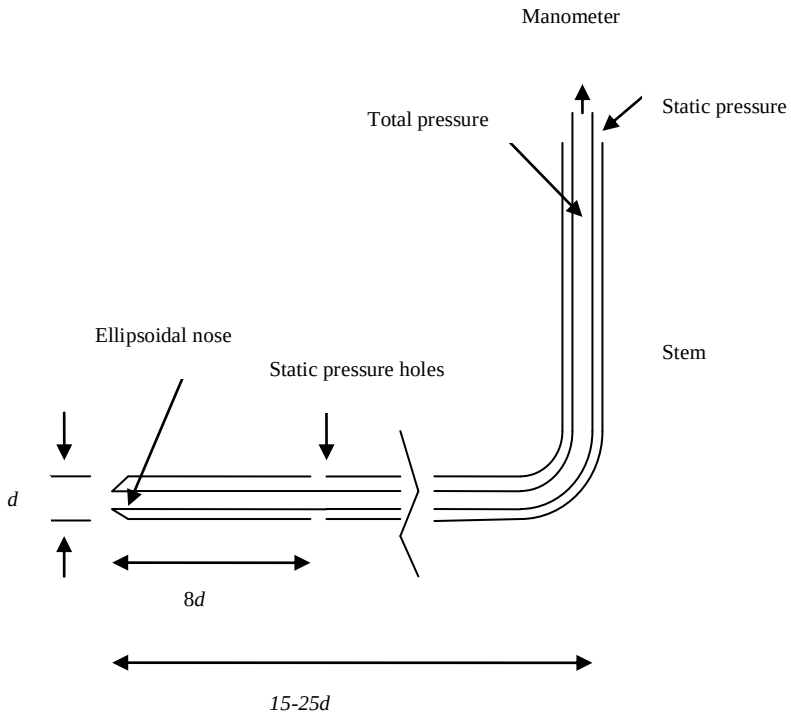

Figure 5.9 Combined Pitot static tube, the outer holes measure the static pressure whilst the inner tube measures the combined pressure, attached to a manometer the differential head *H*, is available to measure and velocity calculated, after (Hamill, 2001).

The holes located on the outside of the Pitot tube measure the static pressure of the water. In front of the ellipsoidal nose of the Pitot-static tube, water collides with the device and is brought to a stop, the stagnation point. This causes a rise in pressure within the Pitot-static tube so the liquid inside the piezometer attached rises correspondingly and sits a distance *H*,

above that of the static tube. The velocity of the flow is proportional to $H^{1/2}$,so by measuring this head difference V can be calculated (Hamill, 2001).

$$V= C(2gH)^{1/2} \tag{5.2}$$

Where C is a coefficient most often equal to 0.98 or 0.99 depending upon design, in this work a value of 0.99 was used. One drawback of this system is the lack of sensitivity which unfortunately makes it difficult to measure very low velocities. A velocity of 0.5 ms^{-1} gives an H value of only 13 mm, and indeed this far exceeds the velocity values encountered here. In an attempt to counter this problem an inclined manometer compromising two glass tubes set at an angle 45 degrees to the horizontal was connected to the Pitot-static tube by clear plastic tubes, the use of this manometer ensured that a small rise in H resulted in a relatively large movement, thus increasing the sensitivity to which the velocity could be measured. The level of uncertainty for the velocity measuremtns when using the Pitot tube can therefore be shown as the percentage error, via the equation:

$$100\frac{\Delta V}{V} = 50\frac{\Delta \ell}{\ell} \tag{5.3}$$

Where ΔV represents the change in velocity, V is the local velocity prior to the change, $\Delta \ell$ represents the movement of water along the inclined manometer and ℓ is the reading on the inclined manometer corresponding to the static tube. In the current work, $\Delta \ell$, can be measured to ± 1 mm which results in a corresponding error in the velocity of ~ 5%, which is considered reasonable for the current work.

5.3.2 Hydraulic parameters

When attempting to understand open channel flow and how this may then affect flow within and into the bed it is important to know the hydraulic parameters of the system. The wetted perimeter, P, and the hydraulic radius, R, are two of the most used variables in terms of open

channel hydraulics (Hamill, 2001). The wetted perimeter is the length of contact of the sides and base of a cross sectional area of the channel in contact with the water. The hydraulic radius is described as:

$$R = A/P \tag{5.4}$$

Where, A is the cross sectional area of flow and P the wetted perimeter. The hydraulic mean depth, $D_{M,}$ is another important factor in open channel flow, though in the uniform rectangular flume channel used in these experiments it finds itself equal to the normal depth, D_N, as it is defined as:

$$D_M = A/B_S \tag{5.5}$$

where B_S is the surface width of the water in the channel. One very important parameter used when discussing hydraulics and open channel flow associated with the hydraulic mean depth is the Froude number (F). This is a dimensionless parameter that gives an indication about the nature of flow within a channel (Hamill, 2001). If F > 1.00 supercritical flow is found, this is relatively shallow and fast flowing. If F = 1.00 critical flow is said to be in evidence which is a transitional flow between the two. When F < 1.00 subcritical flow is present and consists of a relatively deep and slow flow of liquid (Hamill, 2001). Most streams will have Froude numbers of less than 1.00 and the experiments taking place in the flume were all at F number less than 1.00 in order to have subcritical flow and simulate natural rivers, typical F values for rivers are F = 0.36, 0.38 and 0.56 for a gravel bed creek in Quebec, Canada (MacVicar and Roy, 2007), F = 0.34 for Girnock Burn in Scotland (Moir et al., 1998), and F = 0.333 - 0.757 in south eastern Spain (Conesa-Garcia and Garcia-Lorenzo, 2009).

The Froude number is important as supercritical and subcritical flows are very different in character, as flow conditions and depths in subcritical flow can be controlled by downstream

factors such as blockages whilst on super critical flow control of these factors is dependent upon upstream parameters (Hamill 2006). As such calculating the Froude number is an important first step of any investigation;

$$F = \frac{U}{\sqrt{gD_M}} \tag{5.6}$$

U is the mean velocity of flow obtained from the equation $U = Q/A$, and g is the acceleration due to gravity.

With this in mind the nature of flow within the flume is an important factor. Two main types of flow exist; laminar flow is associated with slow moving viscous fluids and is rare in nature, although the slow moving groundwater of an aquifer is one example, (Hamill, 2001). The other is turbulent flow which is much faster and chaotic and is the type usually encountered in mountain streams, (Hamill, 2001), transitional flow, a third type, exists between the two. The type of flow can be determined by the Reynolds number:

$$Re = U\,L\,/\,v \tag{5.7}$$

U is the mean velocity, L is a characteristic length, which here is the hydraulic radius R, (Chaudry, 2007), and v is kinematic viscosity of the liquid, 1.004×10^{-6} m^2 s^{-1} for water, (Best et al., 1997). In open channels a Reynolds number of less than 500 would typically indicate laminar flow, a value of 500-2000 would suggest transitional flow whilst a number greater than 2000 indicates turbulent flow, (Hamill, 2001). Table 5.2 provides details of the hydraulic parameters of the channel used in the experiments that took place.

H (m)	F	Re	Q (l/s)	V (m/s)	B (m)	A (m2)	R	P (m)
0.08	0.23	9053	3.56	0.20	0.24	0.02	0.05	0.39
0.06	0.23	6506	2.31	0.17	0.24	0.01	0.04	0.35
0.04	0.37	6513	2.07	0.23	0.24	0.01	0.03	0.32
0.02	0.71	5031	1.40	0.31	0.24	0.00	0.02	0.28

Table 5.2 Hydraulic parameters for the four different depths that were trialled for the NP experiments conducted using the benchtop flume.

After these parameters had been determined it was decided that experiments involving the NPs inside the benchtop flume would be conducted at a depth of three plastic sphere diameters (57 mm). As discussed earlier in this chapter this choice represented the best possible comparison with collaborative work on pore flow and allowed disruption free sampling.

5.3.3 Velocity profiles

Figure 5.10 shows velocity profiles for four different depths of flow above the bed in the benchtop flume. These profiles show small boundary layer effects as there is an increase in *V/(Q/A)* as measurement depth (d_m) / stream depth (d) increases for most of the velocity profiles plotted before *V/(Q/A)* again decreases slightly at the surface (most evident at 3D positions 2 and 3). This generally does not appear to be the case for measuremtns taken at position 1 due to the fact that this is at the entrance of the flume and the flow may not have had time to stabilise by this point. This is an idealised situation that works due to the small scale of the flume and though not totally representative of a real stream it is suitable in this situation due to the problems with water volume discussed above. The measurement positions 1 – 4 are located as described in Figure 5.7b.

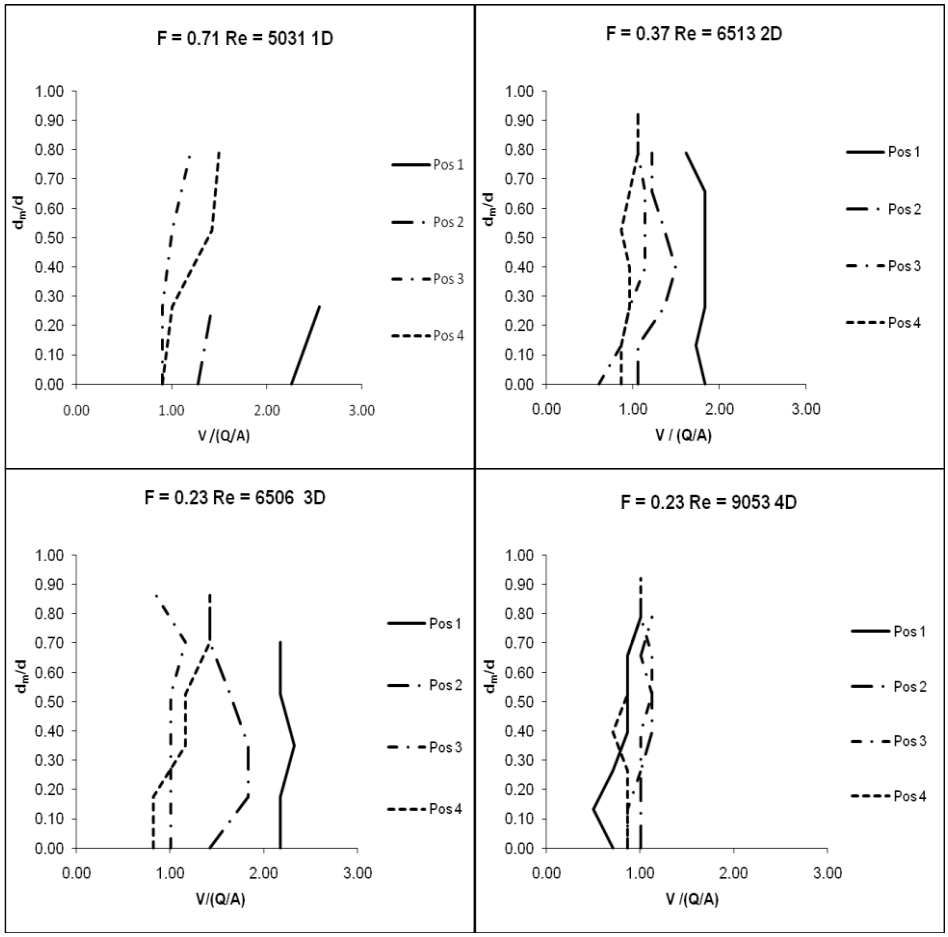

Figure 5.10 Velocity profiles plotting measurement depth (d_m) against the Velocity/(Discharge/A) at four different depths of flow and associated Froude number for the benchtop flume.

As can be seen from the velocity profiles for the experiments at 1, 2 and 3 D in Figure 5.10 the local point velocities taken at position 1 are in each case clearly faster than is found for the other positions. This is a result of the water accelerating as it passes over the weir and enters the test section, it is this acceleration that results in a shallower depth at this upstream section, explaining why limited data is available for positions 1 and 2 at a depth of 1D and the uneven water profiles at the shallower depths (see Table 5.3).

	Test position			
Experiment	1	2	3	4
1 D	5	5	19	19
2 D	30	35	38	38
3 D	55	57	57	57
4 D	73	76	76	76

Table 5.3 Local depths at the four velocity measuring positions for the four velocity profile experiments. (Depths are in mm).

For the experiments at 4 D this increased velocity at position 1 is not apparent and this is due to the fact that at this depth the effect is not seen as the local depth at position 1 of the water surface is now significantly above the height of the small weir used to regulate flow and the actual streamwise velocity for this depth is also considerably slower. These two factors coupled together result in less acceleration at this depth.

For the sake of comparison Figure 5.11 shows the velocity profile for flow within the large flume which was to be used originally at a depth of 3D, as can be seen the profiles are much more established and the boundary layer effects more clearly evident, i.e. the velocity increases in a systematic manner away from the bed. It can also be noted from the Froude and Reynolds numbers (See section 5.3.2) that the flow in the original flume had a much higher overlying velocity and thus would give more pronounced exchange between the bed and free flow (Arnon et al., 2010).

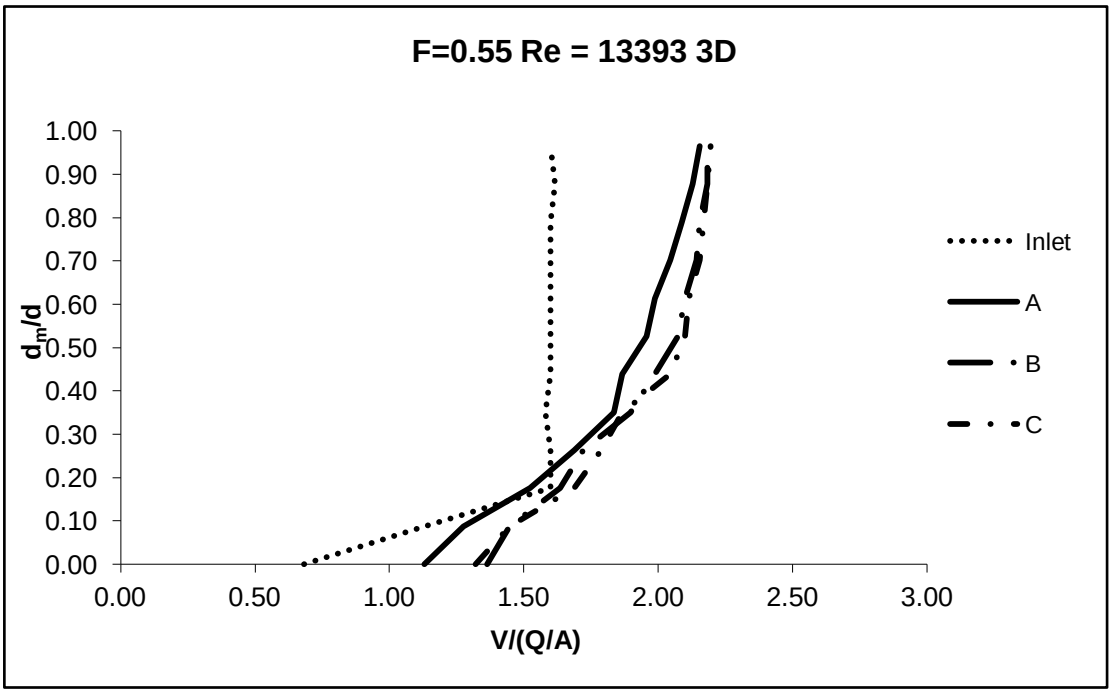

Figure 5.11 Velocity profile from initial larger flume at a depth of three plastic sphere diameters, 57mm. Inlet indicates the channel opening, whilst A, B and C are arbitrary measuring points moving downstream respectively.

In order to reflect the presence of the many natural variations in riverbed topography, such as, sand dunes, pools and riffles, experiments in the bench top flume were conducted using two distinct bed configurations. The first was with a bedform present, in the form of a metal block (19 mm in height and 57 mm long), and the second without this bedform present. This also allows the effects of pressure variations (with bedform) and purely turbulence (plane bed) to be considered. Figure 5.12 shows the velocity profile for the addition of the bedform at a depth of 3D and includes readings that were made to the left (designated a–c 1) and right (designated a-c 2) of the centre line at the three measuring points. This was in an attempt to analyse the boundary layer effect upon the flow caused by the walls of the flume.

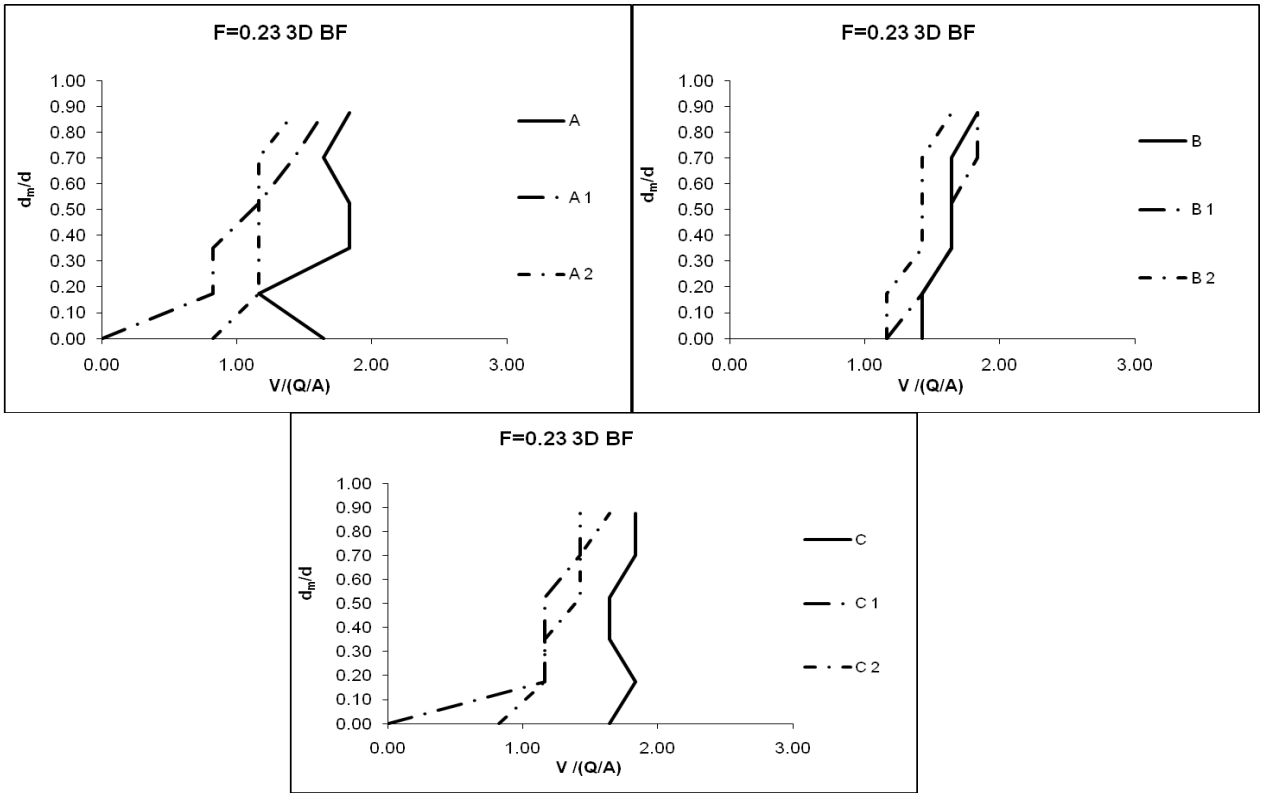

Figure 5.12 Velocity profile s in the benchtop flume at depth 3D with the bedform present a) shows the velocity across the channel at the position furthest upstream b) Shows the velocity profile across the channel at position B c) The velocity profile across the channel at the position furthest downstream.

From these velocity profiles it is apparent that as would be expected at the lower depths there is a reduced velocity along the sides of the channel due to friction and this results in boundary layer effects that are clearly shown in Figures 5.12 a and c. Hence the magnitude of the velocity in the centre is greater than at any other lateral position. This is not however the case for position B as acceleration due to the presence of the bedform has a more pronounced effect than these boundary layer effects and so the velocity is of a more equal magnitude at all three position across the channel. These velocity profiles give an indication that though

there is some effect on flow caused by drag along the side of the channel, uniform flow existed within the centre of the channel and this is where all samples were taken allowing the effects of exchange upon NPs to be analysed.

5.4 Nanoparticles in flume

5.4.1 Nanoparticle introduction

NPs were added to the holding tank at the reservoir located at the upstream end of the recirculating flume to create as even a dispersion as possible by the time they reached the test section (Boncagni et al., 2009). Samples were taken at 2, 25, 50 and 75 minutes after the nanoparticle solution had been added. These times were chosen after two pilot studies showed that it took around 4 minutes in order to collect the samples from the various points and this gap allows the inaccuracy in sampling at those specific times to be much smaller ~16% rather than 20% or 26% for the twenty and fifteen minute gaps respectively that were initially planned. The samples were taken at the points illustrated in Figures 3.11 and 5.7b using a syringe from above. For the samples taken in the freeflow this was done at a point upstream of the bedform (or where the bedform would be in the case of the experiments conducted in the absence of the bedform) and a point downstream. This process was undertaken for all experiments and at several points, upstream and downstream, within the stream free flow as well. These locations were chosen as they provided full coverage both upstream and downstream of the midpoint location where the bedform was to be situated and at different depths within the stream bed. This gave a comprehensive view of what happened within the bed (results from the pilot studies confirmed that these locations would result in differing concentrations, i.e., they were far enough apart from each other for there to be variations in the concentration).

There was one slight variation to this as for the first experiment conducted with a bedform (labelled experiment F3, see Table 5.5) as in addition to the full scale sampling at the times used in the other experiments there were two extra samples taken every five minutes. One of which was within the bed just upstream of the bedform and one taken in the free flow. This was found to be not repeatable for the rest of the experiments due to the large volume of samples awaiting ICP-MS analysis. After sampling and filtration all of the samples were then analysed using ICP-MS to give absolute concentrations and then these concentrations were normalised against the concentration reading taken in the free flow at $t = 0$, immediately after the nanoparticles had been added to the flume. This was in order to compare different data sets so that comparability could be ensured between different experiments and nanoparticle batches by the use of the value C/C_0. When analysing gold the associated error with the concentration as determined from the ICP-MS is ~ ± 10% which was the maximum RSD accepted when analysing the samples using the ICP-MS and this value is taken as the error in the concentration of the samples throughout.

5.4.2 Attachment of nanoparticles

One factor that could be important in the tendency of the NPs to remain within the bed or release back into the stream free flow is the likelihood that they will attach onto the bed material, in this case the nylon 66 plastic spheres. As such a small study was conducted using the same spheres that were used in the bed construction. In this study a 250 ml beaker was half filled with the plastic spheres and filled with a ~ 300 mg L^{-1} solution of gold NPs. This solution was shaken for 1 hr in order to facilitate the binding of the nanoparticles to the surface of the plastic spheres and help to simulate the forces that would bring them into

contact with the plastic spheres during the flume experiments. Following this, another sample of the water was taken. The balls were then placed in a fresh beaker which was filled with the same volume of UHP water and shaken for a further hour upon which another sample was taken in order to assess whether any binding to the plastic spheres and subsequent release had occurred. Afterward the beakers were also refilled with 100 ml of UHP water and shaken to analyse the amount of gold that may be binding to the glassware. These experiments were repeated 3 times and the following results obtained.

Sample	Concentration (ppb)	RSD ±
Initial	3171.0	349.5
1hr Shaking	3246.7	515.8
Spheres re-Shaking	52.1	51.0
Beakers re-Shaking	26.8	1.5

Table 5.4 ICP-MS determined gold concentrations showing the initial and final concentrations of NPs within the beaker indicating that no significant deposition of the particles occurred.

It can be seen that after being shaken for one hour there was no reduction in the concentration of the gold NP solution, in fact there was a slight increase which is acceptable due to the margin of error. When the spheres had been shaken again it can be seen from Table 5.4 that a very insignificant amount of NPs were re-suspended, this was ~ 1.5 % of the total and well within the experimental error. From these results it becomes clear that no significant deposition occurred either onto the spheres or the glass beaker.

5.4.3 Flume experiment overview

As mentioned in section 5.2.1, based on the velocity profiles and in order to achieve conditions that would allow exchange to proceed readily (i.e. enough depth of flow yet still allowing sampling to occur without significant loss of water due to channel overflow) all experiments conducted were undertaken at a depth of 3 sphere diameters (57 mm). Two experiments were conducted using a plane bed i.e. flat uniform face centred cubic bed structure, with sampling undertaken as described in section 5.2.3. Two experiments only were conducted for the plane bed and the bedform bed configurations due to the fact that (as mentioned in the previous section) ICP-MS analysis of this many samples resulted in a backlog in the system and meant a turnaround of somewhere in the region of 4-6 weeks, it was felt that given the fact AuNPs used were known to be stable for a period of several months (Hoppet et al., 2006) then the NPs would not aggregate out of the samples in this time period. As such due to time constraints it was felt that one repetition of each experiment was the best that could be done on a realistic timescale, these experiments have been labelled F1-4 within the text and Table 5.5 indicates the bed configuration used for each.

Experiment	Bed	Average difference between bed and stream flow concentration
F1	Plane	0.10
F2	Plane	0.27
F3	Bedform	0.17
F4	Bedform	0.16

Table 5.5 Experimental labels and bed configurations. Also shown is the average difference found in AuNPs concentration found in the stream bed and stream flow, these values are non directional and simply show the magnitude of difference and not whether the bed or stream flow has a higher concentration.

5.4.4 Plane bed (no bedform present)

5.4.4.1 Results and discussion

To fully analyse the behaviour, and to provide a further point of comparison to when the bedform is present, concentration distributions in the form of contour maps were examined. These contour maps provide a qualitative image of the NP distribution within the bed as time progresses and the visualisation of the movement within the bed due to flow and exchange: the maps use 24 different levels of colour on a 0 – 2 scale with a gap of 0.08 between each. It should be noted at this point that these images are providing a snap shot of what is happening within the flume at this time and it is impossible to distinguish from these contour plots between whether any movements of NPs is slow and evolves over time or is rapidly changing with short lived distributions. At two minutes (Figure 5.13) there is a qualitatively similar area of higher NP concentrations in both the upstream and downstream portions of the bed test section centred upon two hotspots of similar magnitude, whilst the NP concentration within the free flow is similar at the two measuring points but less than that seen in the bed. This is more apparent using this view of the data than when using the average values which are used later in Figure 5.16b as in the upstream bed section the far left (sampling points (SP) 1 and 2 – See Figures 3.11 and 5.7b) area of the bed has a relative concentration almost 3 times the size of that taken at Sampling point 3, the section immediately downstream of it.

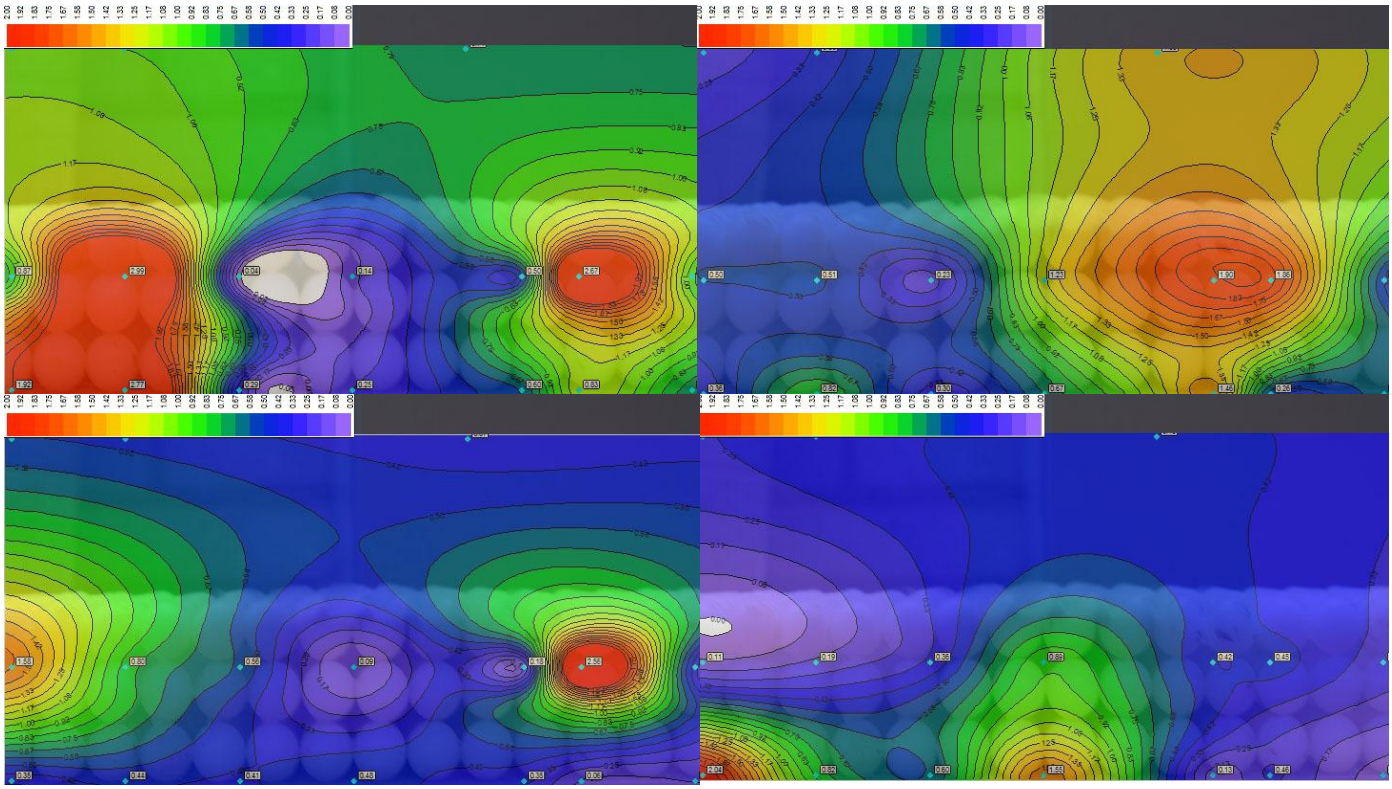

Figure 5.13 Contour maps showing concentration distribution throughout the bed and free flow. F1 Top left) 2 minutes. Top Right) 25 minutes. Bottom Left) 50 minutes. Bottom right) 75 minutes.

This higher value in the bed initially could be put down to the NPs being washed through very quickly from the stream free flow. At twenty five minutes the hot spot within the bed upstream has disappeared whilst a larger area of NP concentration remains downstream, centred on SP 7 and 8 within the bed and into the free flow. The concentration in the bed is higher toward the surface at this point as it was in the previous image.

Again after fifty minutes the higher concentrations are positioned closest to the surface (SP 9), but here there is also a concentration hotspot has appeared again upstream (SP 1), elsewhere though the concentrations are much lower relative to the these peaks. It is important to note that these are instantaneous snapshots of the movement of what appears to

be clumps of NPs as they appear to be centred on hotspot areas. This is important at this stage as the contour maps of 2, 25 and 50 minutes show hotspots of clumps of NPs higher in the bed whilst after seventy five minutes (Figure 5.13) the higher concentrations have moved further into the bed which could be representative of the slower velocities deep within the bed and the time taken for the nanoparticles to get to these points or it may be that, due to the instantaneous snapshot nature of the sampling and the time in between, these could have been simply missed prior to this. This latter case is somewhat supported by the time 2 contour map showing the broad upstream hotspot extending deep into the bed. It becomes clear that there is no uniformly even distribution and diffusion of the nanoparticles and that there is ready exchange of clumps of NPs taking place between the pore and surface waters, even with the absence of the bedform, as was to be expected.

Experiment F2 was conducted using the same conditions as F1 and in this case the distributions of the particles is more clear as there are more high concentration areas, throughout the bed and the free flow, though overall there seems to be less areas of high relative concentrations.

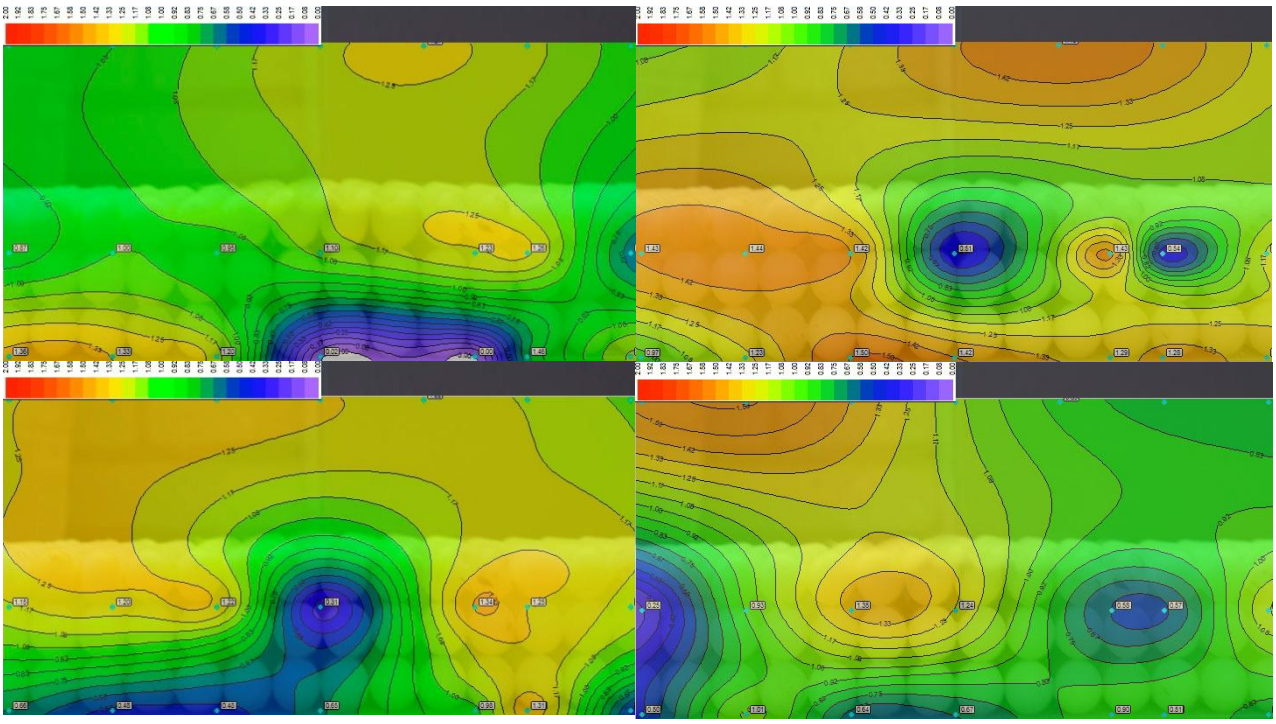

Figure 5.14 Contour maps showing concentration distribution throughout the bed and free flow. F2 Top left) 2 minutes. Top Right) 25 minutes. Bottom Left) 50 minutes. Bottom right) 75 minutes.

At two minutes (Figure 5.14) there are more evenly dispersed than in experiment F1 and this is reflected mostly in the lower relative concentrations and a lack of as intense hotpots, this notwithstanding there are still two main centres of NP concentration peaks, one deep in the upstream portion of the bed (SP 4) and a second at a point within the bed downstream (SP 7) and above within the free flow of the stream. This coupled with the low concentration patch midstream deep within the bed again seems to indicate that even with some dispersion, the NPs are moving in clumps of high concentrations both within the bed and within the stream free flow. After twenty five minutes a number of low concentration points within the bed have developed but other high concentration positions have emerged both deeper in the bed around the midstream section (SP 11) and higher in the bed upstream (SP 1 and 2) - this may suggest that the flow within the bed and exchange between the bed and the free flow is occurring throughout and that there is no one area of build up as flow and exchange is

occurring at many points due to turbulence and that the clumps of NPs move readily with the flow of the water.

Fifty minutes fits with this pattern as high and low concentration areas within the bed continue to develop and shift positions. The stream free flow concentrations match up with the bed concentrations fairly well as was discussed earlier in this section and remain fairly constant throughout. After seventy five minutes there are less higher concentration points throughout the system and within the bed higher concentration areas have moved toward the surface. This seems to indicate that any sinking of the NPs within the bed seen in F1 over time could be a product, merely of the shifting flow patterns and not a steady build up over time and could be put down to coincidence and the sampling pattern.

With only two repetitions of each experiment (with bedform and without) it is not possible to calculate an error through the RSD. As such it is hard to understand the significance of the differences for the values obtained at the same sampling points for the experiments F1 and F2 and the fact that the results do not appear to be repeatable. This being said however some of the variation may be down to the error within the ICP-MS analysis which is ~ ± 10%. This would mean certainly that some values may fall a lot closer than at first it appears. As said however without further study this cannot be definitively answered.

5.4.5 Bedform present

5.4.5.1 Results and discussion

At times of 2, 25, 50 and 75 minutes after the addition of the nanoparticles a full profile of samples were taken within the bed. This hopefully would allow a more detailed view of the fate and transport of the nanoparticles within the bed and show any differences that are apparent with the bedform present. Figure 5.20 shows the distribution of NPs within the bed and free flow at times of 2, 25, 50 and 75 minutes after the addition of the NPs for experiment F3 (Figure 5.15).

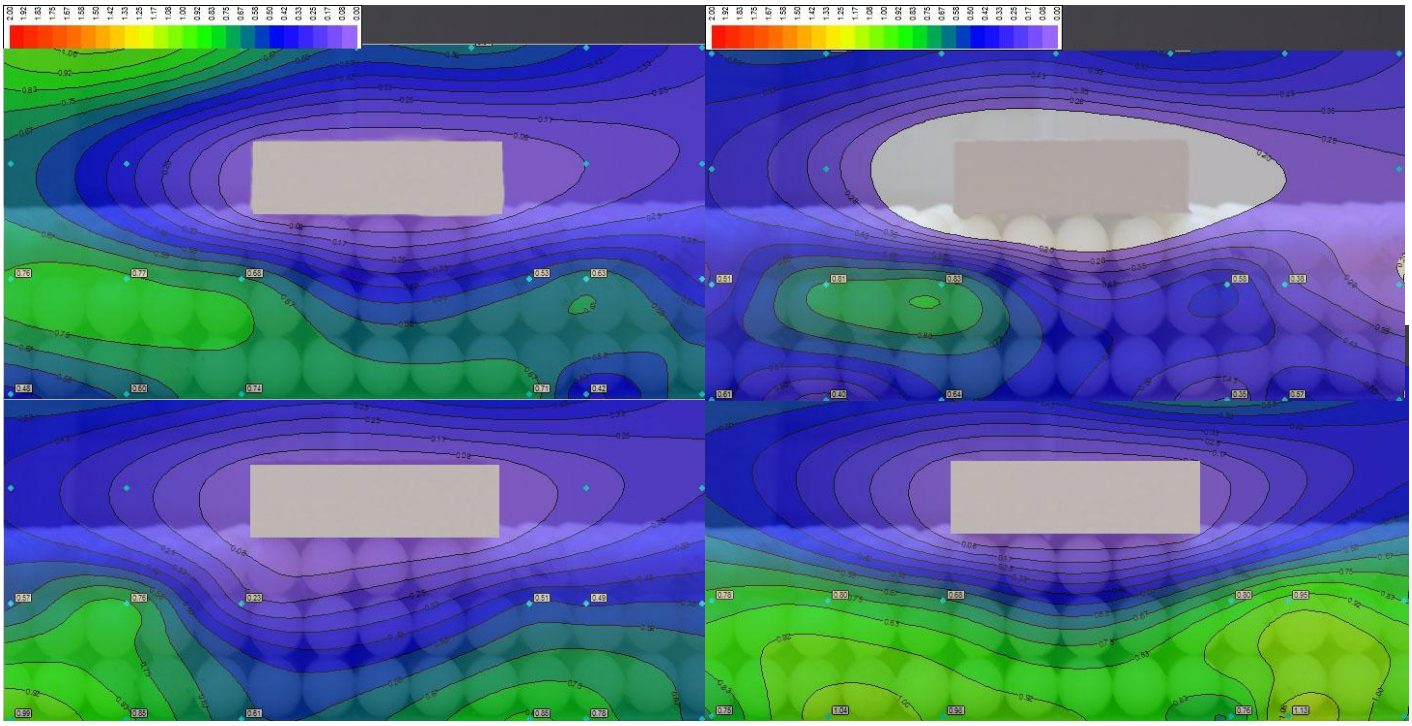

Figure 5.15 Contour maps showing concentration distribution throughout the bed and free flow. F3 Top left) 2 minutes. Top Right) 25 minutes. Bottom Left) 50 minutes. Bottom right) 75 minutes. The white spot in the model reflects the fact that since the bedform is solid the concentration at this point must be zero.

One thing of immediate note when looking at these contour maps in comparison to the two sets for the plane bed is that the relative concentrations are much lower. This could be put down to a very high initial concentration which would cause any following lower results to be relatively small but this is not the case as the actual concentration for the first sampling point used to normalise the data was only the second highest of the group. In fact it most likely stems from a significantly lower concentration initially for one of the experiments (F1, 2 or 3) and throughout that data set that resulted in a larger variation between concentrations for that experiment percentage wise and subsequently in a larger scale being required throughout for all of the contour maps as they all retain the same scale for comparability.

Notwithstanding this, the results are considered sufficient for the current purposes since it is still possible to view areas of different concentrations with ease. At two minutes a hotspot of higher concentration NPs is evident in the upstream free flow and just creeping into the bed (SP 1), indicating that on this occasion they have been detected prior to being washed through the stream free flow. After twenty five minutes the highest concentration of nanoparticles has moved into the bed, upstream of the bedform (SP 2 and 3). This location corresponds with the high pressure area created in the surface flow by the presence of the bedform.

At fifty minutes and seventy five minutes the higher NP concentrations have moved to the downstream side within the bed, whilst concentration within the free flow has remained fairly consistent. Again it can be seen from these maps that the NPs seem to be moving as clumps of particles within the flow, though of course this could be a product of the snapshot nature of these contour maps and this sampling technique. These initial results from experiment F3 seem to show an interesting qualitative correlation with the expected advective flow into and within the bed as the NPs seem to be following the projected flow paths by entering the bed

upstream of the bedform and then flowing within the bed downstream of the bedform location (Figures 2.9 and 2.10). This pattern is not as readily identifiable with the contour maps produced from repeat experiment F4.

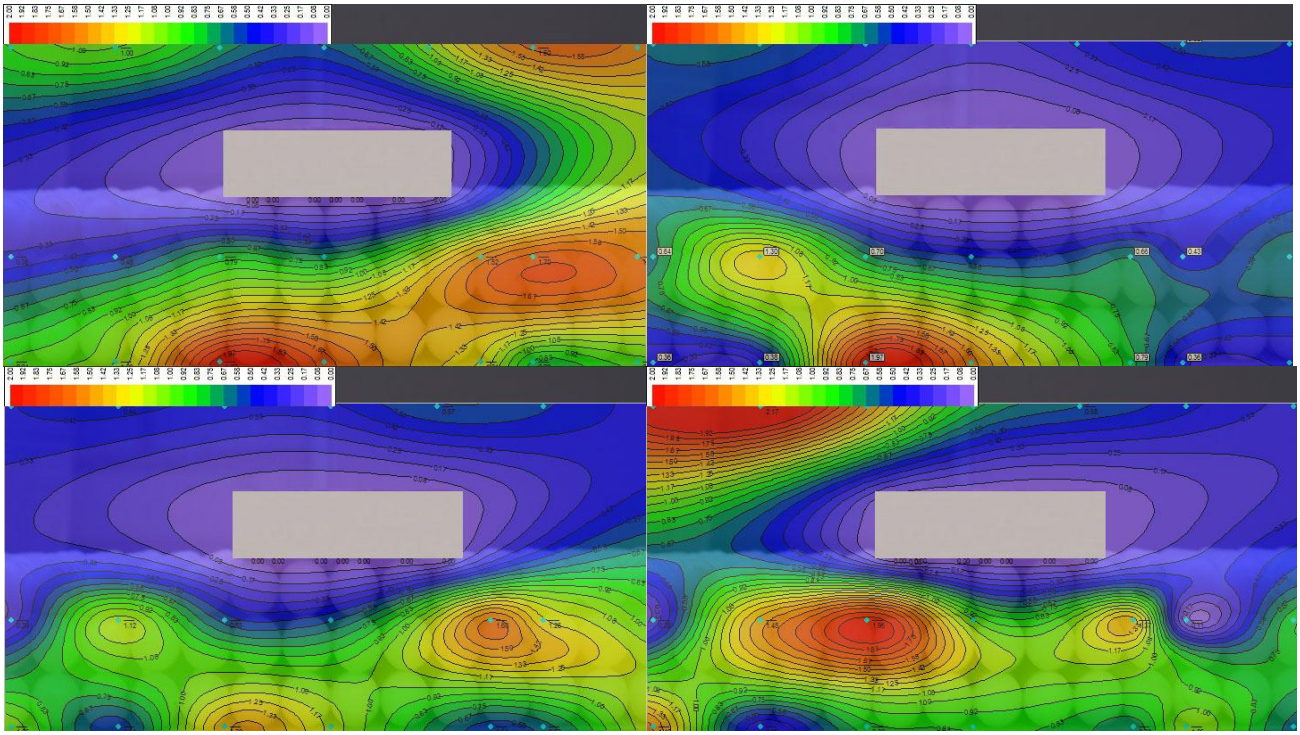

Figure 5.16 Contour maps showing concentration distribution throughout the bed and free flow. F4 Top left) 2 minutes. Top Right) 25 minutes. Bottom Left) 50 minutes. Bottom right) 75 minutes.

For experiment F4 the initial concentrations sampled at time 2 (figure 5.16), show high concentration areas of NPs within the bed, both upstream of the bedform deep within the bed (SP 6) and downstream of the bedform higher up within the bed (SP 7, 8 and 9). More in keeping with the results obtained in F3 after seventy five minutes, though this could be a sign of the fast moving nature of the NP clumps and be an indication that they have already advanced this far in the flow due to a possibly slightly longer delay in the sampling after the

NP insertion into the tank. After twenty five minutes the distribution pattern shows a high concentration area upstream of the bedform and much lower concentrations throughout the rest of the test area, both in the stream free flow and the bed. This pattern is more consistent with that seen in F3 after twenty five minutes. After fifty minutes higher concentration hotspots within the bed, upstream and downstream of the bedform are shown and again there is a lower concentration within the stream than the bed in this instance. One of these points within the bed shows a very low concentration, this was the point used to produce the C/C_0 vs. *t* plots (Figure 5.21, the sampling point in the upper bed immediately upstream of the bed, this low value is raised during the averaging of the upstream bed values and this is reflected in the averaged values plot (Figure 5.21b).

The final map in the bedform experiments (Figure 5.16) shows a very high concentration within the free flow and upstream of the bed form with a more even dispersion throughout the rest of the bed, with the exception of a very low point downstream of the bed. What appears important from these images is that the concentration gradients within different portions the bed, are very distinct and there appears to be no overall diffusion or sink point at any stage. This seems to indicate that the NPs travel freely anywhere in the bed and free flow and that there seem to be high concentration areas in the likely flow paths of water within the bed beneath a bedform (Figure 5.19), as is the case for F3 25, 75 and F4 2, 50, 75. This could then be due to the clumps of NPs following flow paths brought on by the advective pumping caused by the bed form, this idea of NP clumps is certainly of interest based on the results seen in the TEM images shown in Chapter 4 which showed that though not aggregating the NPs certainly were grouped together. F4 75 minutes seems to confirm that the NPs are not building up within the bed but are following the flow paths of the water and are being recirculated. This further helps to illustrate the point that the results are snapshots of what

happens and that NP movement is dynamic and occurring much faster than the 25 minute sampling divide is allowing us to view.

In addition to the contour maps, Figures 5.18 and 5.19 show the concentration of nanoparticles within the bed and in the stream free flow with respect to time. In each figure, plot A shows the concentration at specific point (SP 3) within the bed and one point in the free flow 10 cm upstream of where the bedform is to be placed in the later experiment and one location 10 cm downstream (SP 7) of where it is to be placed (Figure 5.16).

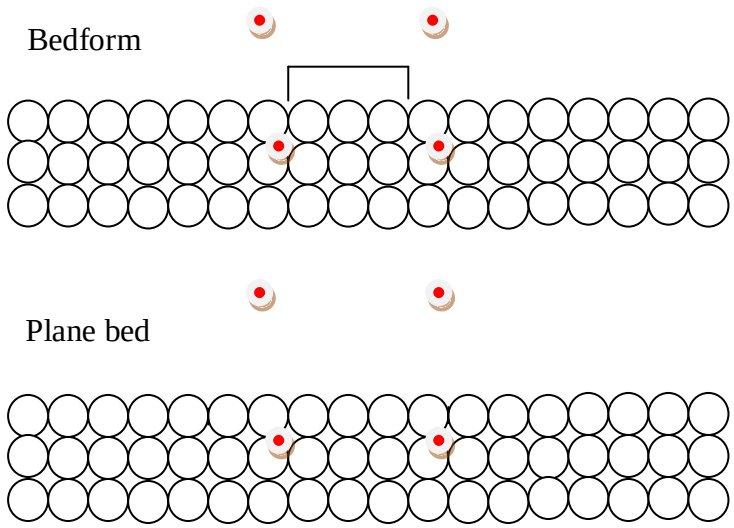

Figure 5.17 The red dots show the upstream (left) and downstream (right) sampling points referred to in Figures 5.16 and 5.17

Plot B (Figure 5.18) shows the average of concentrations of all the sampling points within the bed upstream (Sampling points 1-6) and downstream (7-12) of this location in order to give a greater feel for what is happening for these bed sections. The plots show the discrete sampling points whilst the lines give an indication of the general trend. The values for the free flow and bed, upstream and downstream of the where the bedform will be placed in the

later experiments, show high levels of variation in concentration at each time period while toward 75 minutes this has been reduced. Pointing toward a flux of nanoparticles from the free flow and into the bed, though this may in fact indicate a rather more consistent and even distribution between the two flow profiles as time progresses. Upstream in the experiment F1 there does appear to be a decrease in the concentration in the free flow over time with the bed concentration increasing correspondingly. This trend however is not evident in the data for experiment F2 (Figure 5.18) and indeed the opposite may be true when based upon the average values.

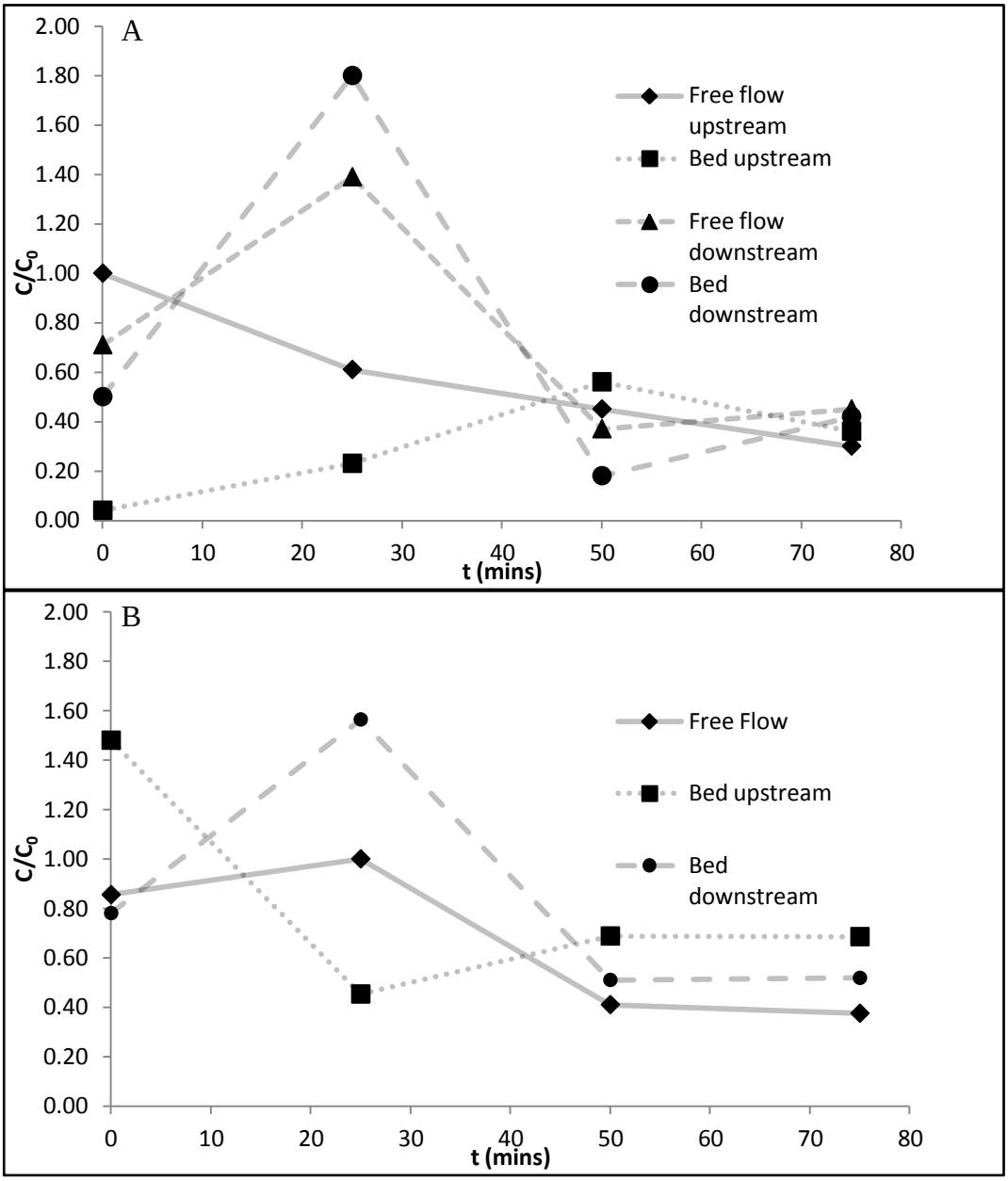

Figure 5.18 Normalised concentrations of AuNPs in the a) free flow and two points within the bed and b) average values in the free flow and upstream and downstream sections of the bed for the experiment F1.

This possible flux of NPs toward the bed over time however is not seen in the data for F2, where the opposite, in fact, is seen as the free flow concentration seems to build over time. From this it might seem likely that the concentrations of NPs is rapidly moving between the

bed and the stream flow and these snapshots have picked up different stages of that dynamic behaviour.

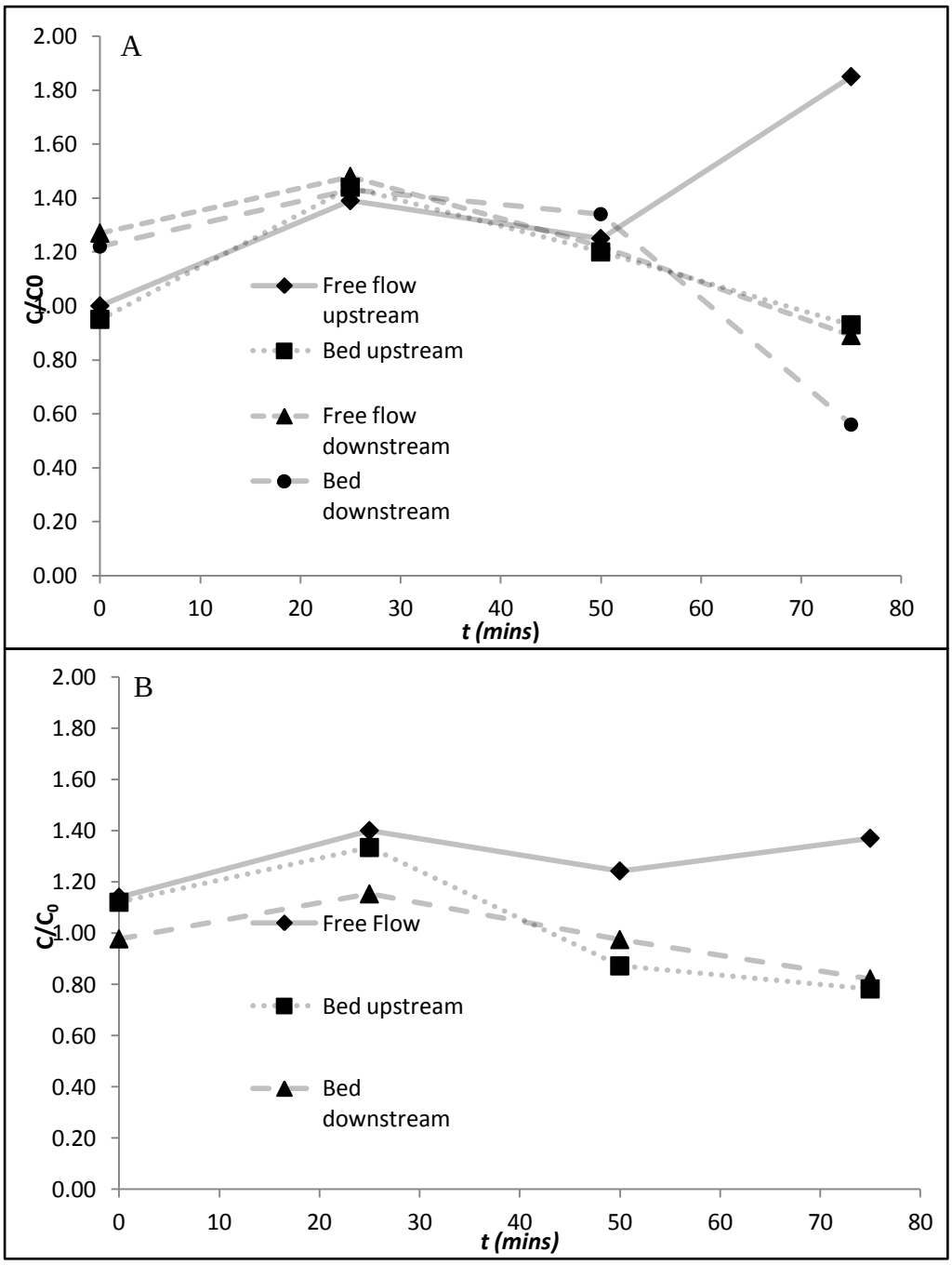

Figure 5.19 Normalised concentrations of AuNPs in the A) free flow and two points within the bed and B) average values in the free flow and upstream and downstream sections of the bed for the experiment F2.

Figure 5.20 shows the concentration of the NPs in the free flow and the bed for the initial experiment F3. As mentioned in the introduction to this chapter the first bedform experiment consisted of additional samples taken between the full sets at 0, 25, 50 and 75 minutes, which were taken at two points, at five minute intervals between the main sets. It is for this reason that in Figure 5.20a that a trend is indicated rather than discrete points as on the other plots. The averaged data shown (Figure 5.20b) uses the data from only the full sampling sets. Though far from conclusive the overall trend seems to indicate a very fast mixing of the NPs throughout the system as spikes and dips in concentration seem to correspond for both sampling sites at equivalent times, indicative of the NPs being washed through the channel and recirculated repeatedly. Toward the end the concentration within the bed is of greater magnitude than that of the flow and appears to be increasing more rapidly. This is illustrated in the averaged samples as the concentration within the bed is increasingly steadily over time. However, there is also a corresponding increase in the free flow concentration at this time and is most likely indicative of a clump of NPs coming through this part of the system as this sample is being taken.

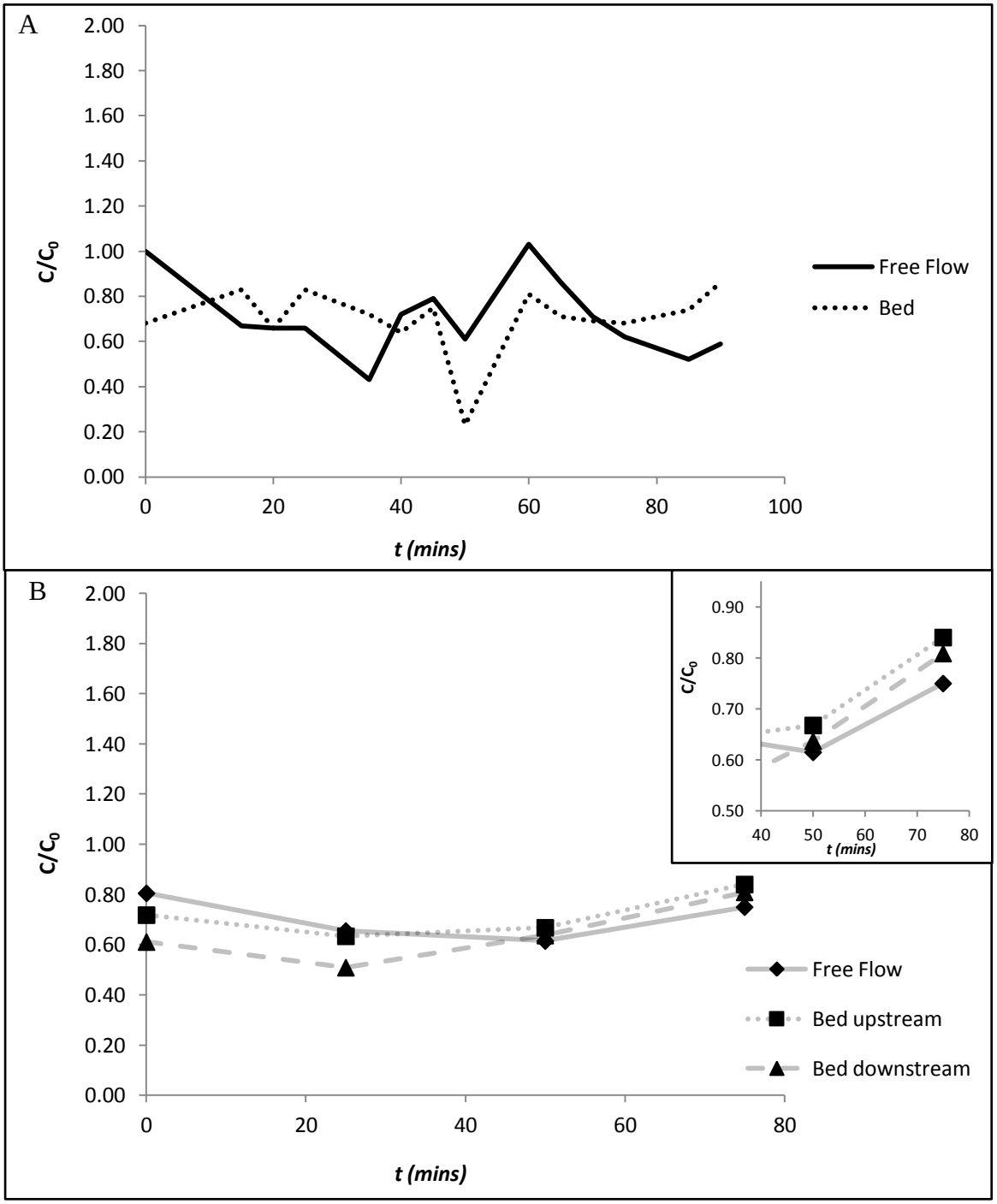

Figure 5.20 Normalised concentrations of AuNPs in the a) free flow and two points within the bed and b) average values in the free flow and upstream and downstream sections of the bed for the experiment F3 (inset shows zoomed section on the values after 50 and 75 minutes).

A similar pattern of fast mixing as seen in the other experiments seems to emerge for the upstream sample sites in experiment F4, (Figure 5.21) whilst the downstream sample site shows the concentration within the bed to be much greater than the downstream fast flow as time goes on.

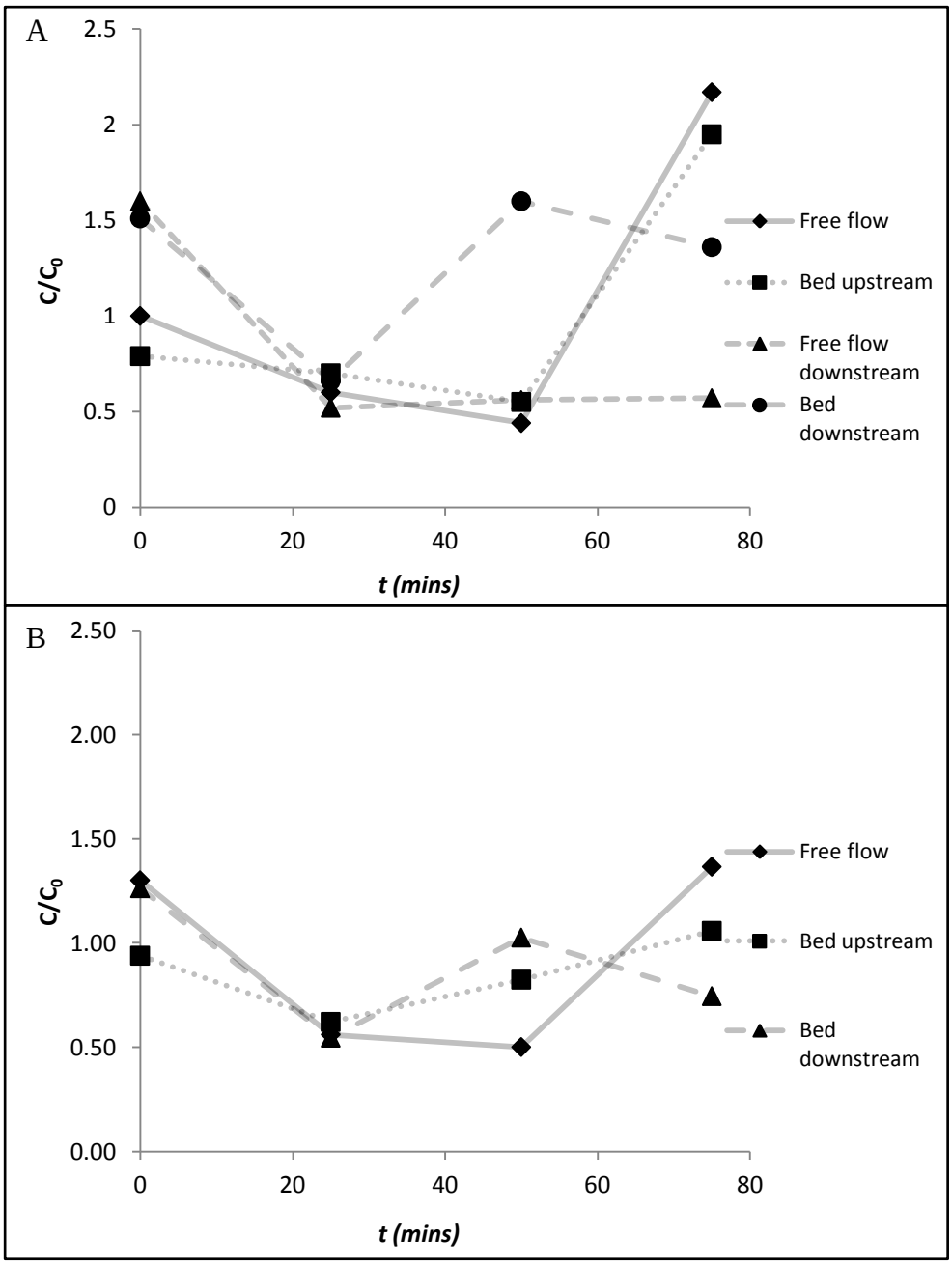

Figure 5.21 Normalised concentrations of AuNPs in the a) free flow and two points within the bed and b) average values in the free flow and upstream and downstream sections of the bed for the experiment F4.

One thing of interest from Figure 21a and b is that the concentration of NPs within upstream portion of the bed is well correlated with the free flow while downstream there is a decoupling of this relationship. Another possible indication of recirculation and that the NPs are collecting within the bed along the length of the flow path before being recirculated once again. What can be seen from these plots is the fact that there is a ready mixing of the NPs between the free flow and sub surface and as well as a build up of nanoparticles within the bed over time. This could be due to the presence of the bedform and the enhanced exchange that results from the surface pressure changes it causes.

One way in which to analyse how the NPs are moving through the channel and to try understand the amount that is moving into the bed is to look at values for the average difference, at the same point in time, between the concentration in the free flow and the concentration in bed as this will give some relativity to the concentration numbers as the NPs are being recirculated.

For the experiments F1, F2, F3 and F4 the average difference at the same points were 0.10, 0.27, 0.17 and 0.16 respectively, there is no significant difference in the average difference between the stream flow and bed flow for plane bed configuration and the bedform based configuration (Table 5.4) ($p = 0.67$).

However from a more subjective point of view this value for F2 becomes 0.04 if the spike seen in experiment F2 after 75 minutes is excluded (Figure 5.17a), which does appear to be more significant. This is confirmed when looking at the average values for the concentration within the upstream and downstream sections of the bed rather than at the two sampling points (Figure 5.19b), with the spike present the difference between the two is 0.16 ± 0.01 for

the bedform and 0.18 ± 0.09 for the plane bed (p = 0.84), but again when the outlier value is excluded this dramatically changes the plane bed value to 0.07 ± 0.001 and the difference between the bedform and plane bed configurations does become significant, p = 0.04. This could point toward a less dramatic exchange between the bed and free flow, or a more universal exchange between the two due to the reduced pressure change effects for the plane bed when compared with the bedform configuration. Though, obviously this is not a rigorous assessment due to the fact that the spike seen at 75 minutes F4 does occur.

When looking at the results for the experiments together (Figure 5.22 and Figure 5.23) it seems to indicate for the plane bed experiments the NPs become increasingly mixed between the bed and the free flow as time has increased while for the bedform experiments the level of variation between the free flow and bed stays relatively similar throughout the period with the difference between the downstream area and the free flow increasingly slightly, as noted above.

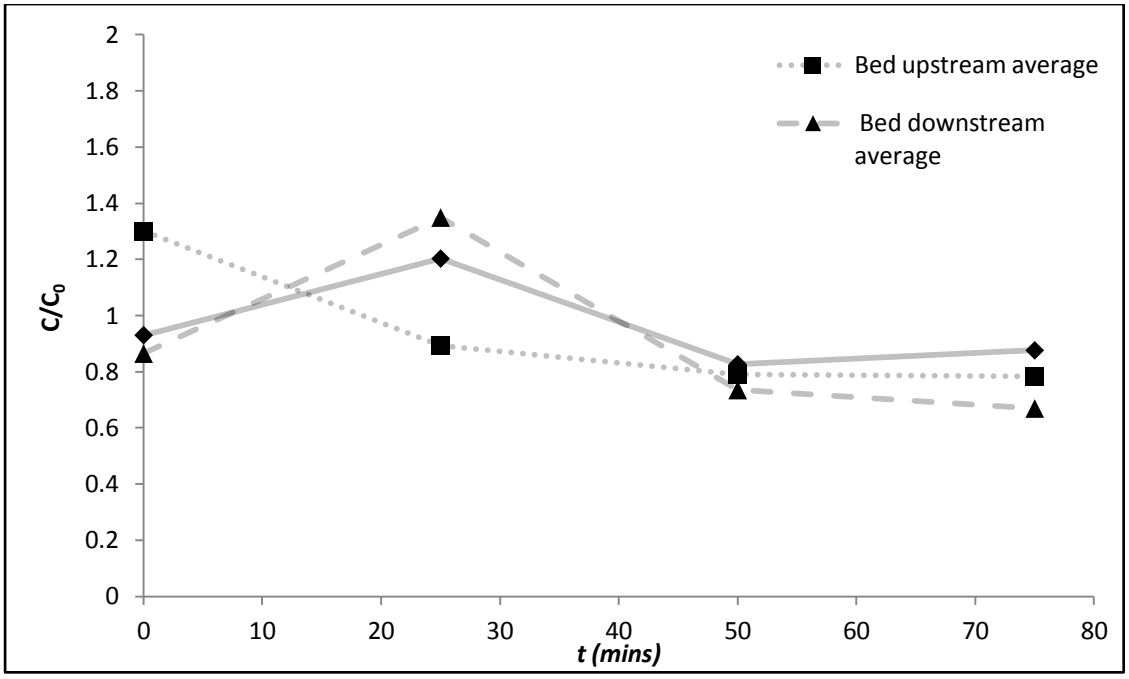

Figure 5.22 Average concentrations in the free flow, and upstream and downstream sections of the bed for plane bed experiments.

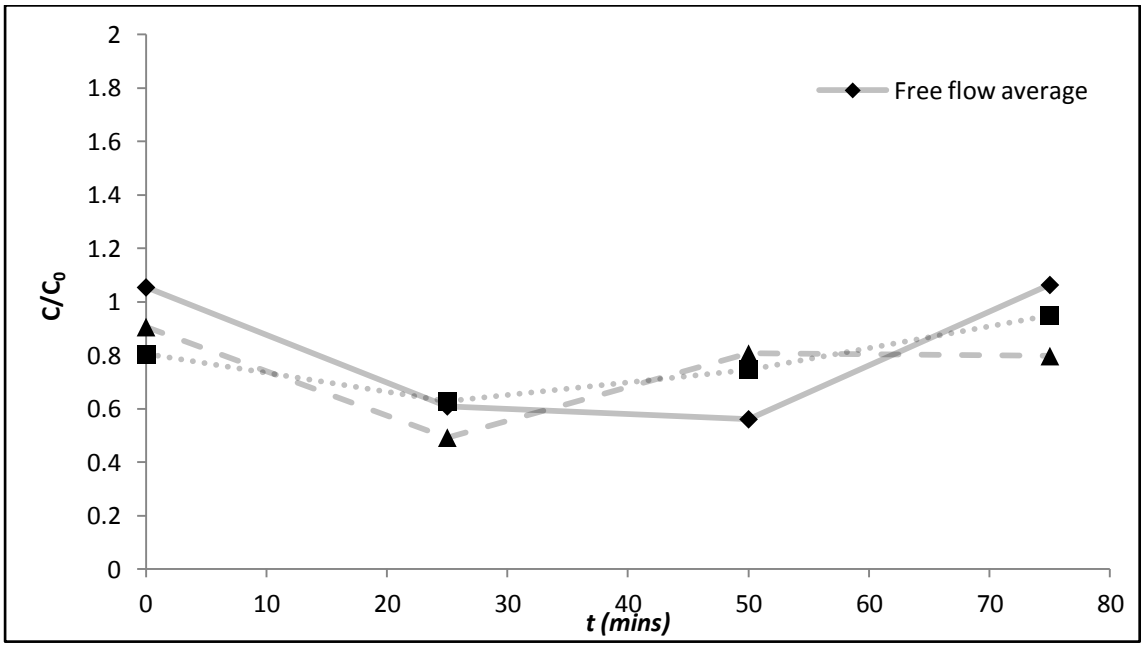

Figure 5.23 Average concentrations in the free flow, and upstream and downstream sections of the bed for bedform experiments.

When looking at both the bedform and plane bed experiments together (Figure 5.24) it appears that after the effects of a higher starting concentration have been taken into account the mixing of NPs between bed and free flow is fairly ubiquitous throughout for both.

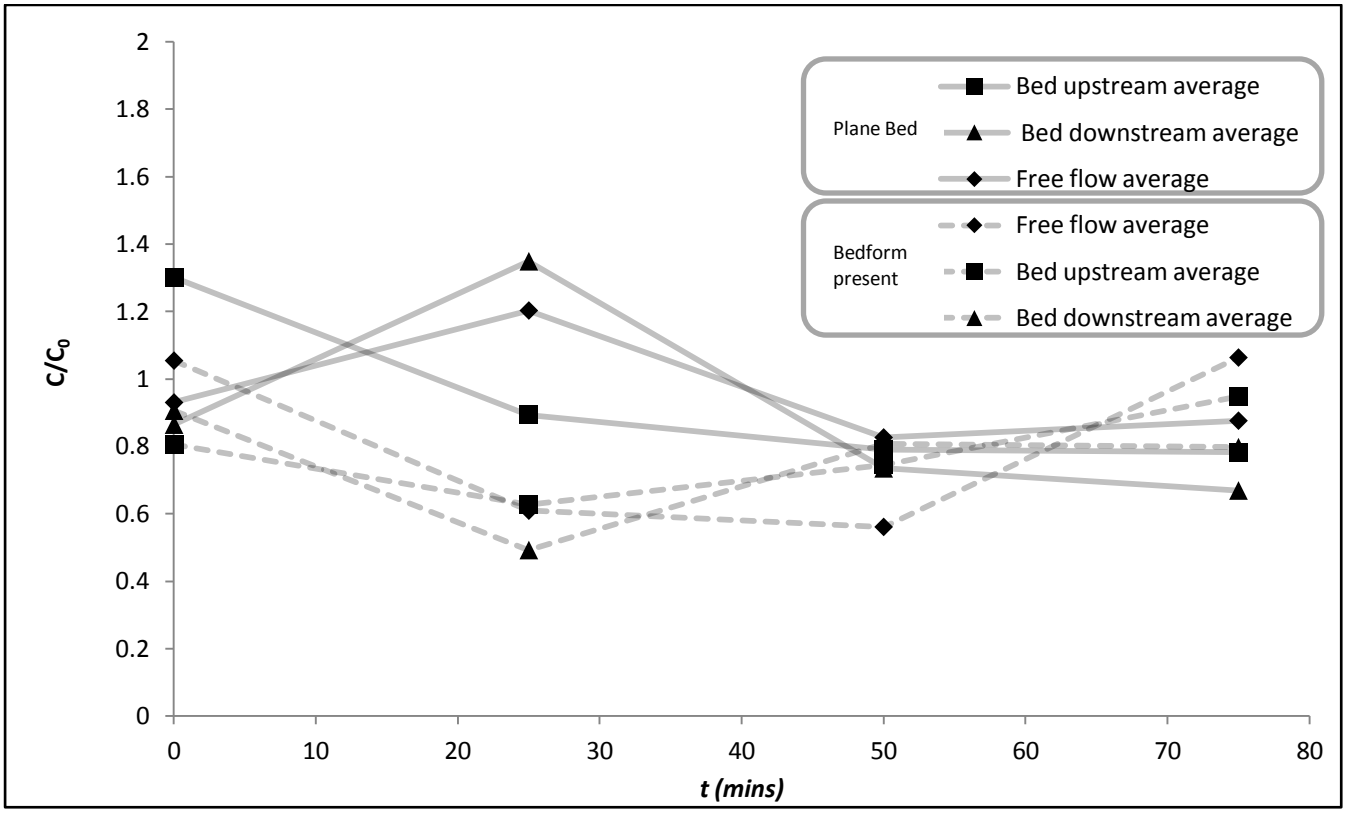

Figure 5.24 Average concentrations in the free flow, and upstream and downstream sections of the bed for plane bed and bedform experiments.

5.6 Conclusions

Though no conclusive pattern for flow of these NPs within the bed of a gravel river seems to be present here, there does appear to be more of a trend with the bedform present of NP flow into the bed. What can be taken from these results in this case is that the nanoparticles seem to freely exchange between the bed and the free flow and appear to follow flow paths within the bed after entry before being recirculated. This is of particular note as river beds are known to be potential sinks for many contaminants (Wiesner et al., 2006), this reduced deposition within the bed could result in long range transportation of these nanoparticles

under similar conditions, though part of this could be explained by the nanoparticle surface properties (previous chapter) and that once driven into the bed they are easily released back into the free flow as they do not deposit onto the bed spheres and may simply follow the flow. It also seems from this study at least that the NPs move in clumps of higher concentration areas throughout both the stream free flow and the gravel river bed. As noted in the discussion of the plane bed results there is also an increased separation of bed and free flow concentrations at the same time in comparison to the bedform experiments, suggesting that the pressure changes produce a more uneven mixing of the nanoparticles than is the case with the bedform present.

6.0 Conclusions

6.1 Summary

NP proliferation appears to be set to continue for the foreseeable future (Biswas and Wu, 2005) and their release into the environment from both point and non point sources is probable (Wiesner et al., 2006) and in fact it is likely that, with production levels of NP based products increasing in recent years, that this is already occurring (Moore, 2006). As such the fate and behaviour of these NPs when they have entered environmental systems and the risk that they may subsequently play is an important factor. These NPs come in many different shapes and sizes with greatly varying properties that can be manipulated for use in medicine, cosmetics, catalysis and environmental remediation, amongst many other applications (Ju-Nam and Lead, 2008). Due to this wide variety of usage, the actual physical properties of these NPs and subsequently their behaviour when exposed to various environmental conditions differ widely. As such it becomes impossible to issue a coverall declaration of how all NPs will behave within the environment. Instead the varying different types of NPs must be studied in various environmentally relevant conditions and where appropriate these results extrapolated to other NPs for which the original NP studied may be analogous.

For this work one particular NP was chosen as it was felt the stability that the sterically stabilised PVP supported gold NPs exhibited would allow the recirculating flume experiments to be conducted with a NP that would not aggregate immediately and allow the effects of the exchange processes that are caused by the stream bed and the bedform to impact the NPs and their distribution. The NPs used were monodisperse and sterically stabilised which was determined by robust characterisation using a variety of analytical techniques.

This NP also allowed a full examination of the effects of different ionic strengths, pH and the presence of NOM upon sterically stabilised NPs which is an area where little work had been undertaken compared with the large amount of data available for the effect of different water chemistries on charge stabilised NPs. This proved interesting as the gold NPs used here showed almost no signs of aggregation at significant levels which contrasts with previously reported work by (Baalousha et al., 2008; Diegoli et al., 2008).

The effect that changes in pH, ionic strength and the presence of NOM had upon the gold NPs used was found to be almost nonexistent. No significant changes in size were noted using a variety of analytical methods, nor did surface properties such as surface plasmon resonance and zeta potential undergo any change. This lack of aggregation indicates that the NPs used here are likely to prove very stable in the aquatic environment and due to this there is the potential that they will not settle out of this environ via sedimentation, which is one route that provides a sink for some pollutants and can prevent long range transportation. This coupled with evidence that there was no deposition of the NPs to the bed structure indicates that based on these factors alone long term transport of these gold NPs could be deemed likely.

These results played an important role in guiding the interpretation of the results for the next section as the surface properties of the NPs and the extent of any aggregation will affect how the NPs behave when influenced by flow between the stream flow and stream bed, and then within the bed itself. The previous chapter illustrated how the particles show a slight build up within the bed over time which was consistent with the work undertaken by Boncagni et al. (2009), however, in general the split between bed concentrations and stream free flow concentrations was very narrow, probably due to the rerelease of NPs back into the stream

free flow as they follow the water flow paths. This seems to be an important point of difference when compared to the work of Boncagni which was undertaken on much larger, charge stabilised NPs which, likely more susceptible to aggregation and sedimentation when released into the flume and showed a definitive build up within the bed over time. The flow of NPs into the bed seems to be slightly increased by the presence of a bedform here. This is attributed to the high pressure area forming upstream of the bedform coupled with the low pressure area downstream driving the flow (and NPs) into the bed and around. This is in line with expectations based on the work undertaken by Packman and colleagues (2009). Perhaps even shedding some light on which is the more dominant factor, bedform induced advective pumping, or turbulent mixing of bed and stream waters. From the contour maps it is visible that at certain points in time NPs entered the vast majority of the bed and that the areas of higher concentrations have moved throughout it readily. Illustrating visually the extent of flow within the bed and the degree to which the NPs are transported within the bed and stream as a whole by the water. It also appeared clear from these contour maps that the NPs moved in large clumps and were not diffused evenly. This is most likely a reflection of the NPs themselves, which, although not aggregated were clearly grouped together loosely in the TEM images.

With respect to the objectives and in addition to the above, the project produced well characterised, stable NPs that have been exposed to different and relevant environmental conditions and the extent of any affects determined. The fate and behaviour of these NPs has then been analysed with a recirculating flume, which although not on the scale that was desired at the outset, has allowed an initial understanding of what may happen to such NPs if in future they become released to the natural environment. Also, unfortunately, the outputs from the associated modelling are unavailable at this time which will provide a further

opportunity for development of this work and a more complete understanding of the fate and behaviour of AuNPs in the environment.

6.2 Future work

Now that this work is complete the next steps would be to consider how changes in the size of these same PVP stabilised NPs may influence their behaviour in the flume and to see if larger particles may behave any differently. Given that these larger particles are slightly less stable (Hoppe et al., 2006) than the ones used here it would also be of interest to see whether the environmentally relevant conditions used herein may accelerate the aggregation process in any way. In a similar vein it would also be of value to see how charge stabilised NPs behaved under the flume conditions and whether these different particles may deposit more readily and how contour maps of concentrations created based on a particle such as this may compare to the ones generated for these gold NPs. The next step in this study of environmentally relevant conditions and exchange processes would be to then use either real river water or water with controlled ionic strength and pH as well as using SRFA within the flume in order to create a complete overview of behaviour within the benchtop flume used here.

After this the obvious next step would be to use a larger flume with multiple bedforms and hopefully use multiple depths of flow as was initially trialled in these experiments. Though it may provide a sampling challenge such a study would provide an as complete laboratory based analysis of NP fate and behaviour within the hyporheic zone of gravel bed rivers as would be possible. Once these steps had been taken the use of real gravel beds should be considered to see how a more irregular bed may influence movement, also sand based bed configurations would give a comprehensive picture. After this a final experimental step

would be to use a test channel in a real river and conduct experiments using the natural water and bed configuration, though this would not be recommended immediately as it would involve the introduction of the NPs directly to the environment.

List of References

Adams, L.K., Lyon, D.Y. and Alvarez, P.J.J., 2006. Comparative eco-toxicity of nanoscale tio2, sio2, and zno water suspensions. Water Research, 40(19): 3527-3532.

Ah, C.S. et al., 2005. Size-controlled synthesis of machinable single crystalline gold nanoplates. Chemistry of Materials, 17(22): 5558-5561.

Aitken, R.J., Chaudry, M.Q., Boxall, A.B.A. and Hull, M., 2006. Manufacture and use of nanomaterials: Current status in the uk and global trends. Occupational Medicine, 56: 300-306.

Alessandrini, A. and Facci, P., 2005. Afm: A versatile tool in biophysics. Measurement Science & Technology, 16(6): R65-R92.

Arami, H., Mazloumi, M., Khalifehzadeh, R. and Sadmezhaad, S.K., 2007. Sonochemical preparation of tio2 nanoparticles. Materials Letters, 61(23-24): 4559-4561.

Arnon, S., Marx, L.P., Searcy, K.E. and Packman, A.I., 2010. Effects of overlying velocity, particle size, and biofilm growth on stream-subsurface exchange of particles. Hydrological Processes, 24(1): 108-114.

Baalousha, M., Manciulea, A.L., Cumberland, S., Kendall, K. and Lead, J.R., 2008. Aggregation and surface properties of iron oxide nanoparticles: Influence of ph and natural organic matter. Environmental Toxicology and Chemistry, 27(9): 1875-1882.

Baalousha, M., Motelica-Heino, M., Galaup, S. and Le Coustumer, P., 2005. Supramolecular structure of humic acids by tem with improved sample preparation and staining. Microscopy Research and Technique, 66(6): 299-306.

Baalousha, M., Motelica-Heino, M. and Le Coustumer, P., 2006. Conformation and size of humic substances: Effects of major cation concentration and type, ph, salinity, and residence time. Colloids and Surfaces a-Physicochemical and Engineering Aspects, 272(1-2): 48-55.

Bajpai, S.K., Mohan, Y.M., Bajpai, M., Tankhiwale, R. and Thomas, V., 2007. Synthesis of polymer stabilized silver and gold nanostructures. Journal of Nanoscience and Nanotechnology, 7(9): 2994-3010.

Bencala, K.E. and Walters, R.A., 1983. Simulation of solute transport in a mountain pool-and-riffle stream - a transient storage model. Water Resources Research, 19(3): 718-724.

Berne, B.J. and Pecora, R., 2003. Dynamic light scattering, 384 pp.

Best, J., Bennett, S., Bridge, J. and Leeder, M., 1997. Turbulence modulation and particle velocities over flat sand beds at low transport rates. Journal of Hydraulic Engineering-Asce, 123(12): 1118-1129.

Bidell, W. et al., 1998. Synthesis and characterisation of c_{60} derivatives containing functionalised anthraquinone groups and an unusual fullerene-stabilised cation. Journal of Organometallic Chemistry, 562: 115-122.

Binnig, G., Quate, C.F. and Gerber, C., 1986. Atomic force microscope. Physical Review Letters, 56(9): 930-933.

Binnig, G. and Rohrer, H., 1982. Scanning tunneling microscopy. Helvetica Physica Acta, 55(6): 726-735.

Biswas, P. and Wu, C.Y., 2005. 2005 critical review: Nanoparticles and the environment. Journal of the Air & Waste Management Association, 55(6): 708-746.

Blaser, S.A., Scheringer, M., MacLeod, M. and Hungerbühler, K., 2008. Estimation of cumulative aquatic exposure and risk due to silver: Contribution of nano-

functionalized plastics and textiles. Science of The Total Environment, 390(2-3): 396-409.
Blois, G., Sambrook Smith, G.H., Best, J.L., Hardy, R.J. and Lead, J.R., 2010. Investigation of topographically-induced flow in a pore space using endoscopic piv, 15th International Symposium on Applications of Laser Techniques to Fluid Mechanics, Lisbon, Portugal.
Boncagni, N.T. et al., 2009. Exchange of tio2 nanoparticles between streams and streambeds. Environmental Science & Technology, 43(20): 7699-7705.
Borm, P.J.A. et al., 2006. The potential risks of nanomaterials: A review carried out for ecetoc. Part Fibre Toxicol, 3: 11.
Bosetti, M., Masse, A., Tobin, E. and Cannas, M., 2002. Silver coated materials for external fixation devices: In vitro biocompatibility and genotoxicity. Biomaterials, 23(3): 887-892.
Boulton, A.J., Marmonier, P. and Sarriquet, P.E.X., 2007. Hyporheic invertebrate community composition in streams of varying salinity in southwestern australia: Diversity peaks at intermediate thresholds. River Research and Applications, 23(6): 579-594.
Bradford, S.A., Yates, S.R., Bettahar, M. and Simunek, J., 2002. Physical factors affecting the transport and fate of colloids in saturated porous media. Water Resources Research, 38(12).
Brant, J., Lecoanet, H. and Wiesner, M.R., 2005a. Aggregation and deposition characteristics of fullerene nanoparticles in aqueous systems. Journal of Nanoparticle Research, 7(4-5): 545-553.
Brant, J.A., Labille, J., Bottero, J.-Y. and Wiesner, M., 2006. Characterizing the impact of preparation method on fullerene cluster structure and chemistry. Langmuir, 22: 3878-3885.
Brant, J.A., Lecoanet, H., Hotze, M. and Wiesner, M., 2005b. Comparison of electrokinetic properties of colloidal fullerenes (*n*-c_{60}) formed using two procedures Environmental Science and Technology, 39(17): 6343-6351.
Brausch, K.A., Anderson, T.A., Smith, P.N. and Maul, J.D., 2011. The effects of fullerenes and functionalised fullerenes on *daphnia magna* photoaxis and swimming behaviour. Environmental Toxicology and Chemistry, 30(4): 878-884.
Bronsted, J.N., 1922. On the theory of the chemical reaction rate. Zeitschrift Fur Physikalische Chemie--Stochiometrie Und Verwandtschaftslehre, 102(2): 169-207.
Buffle, J., Wilkinson, K.J., Stoll, S., Filella, M. and Zhang, J.W., 1998. A generalized description of aquatic colloidal interactions: The three-colloidal component approach. Environmental Science & Technology, 32(19): 2887-2899.
Burns, C., Spendel, W.U., Puckett, S. and Pacey, G.E., 2006. Solution ionic strength effect on gold nanoparticle solution color transition. Talanta, 69(4): 873-876.
Busch, H., 1926. Calculation of the channel of the cathode rays in axial symmetric electromagnetic fields. Annalen Der Physik, 81(25): 974-993.
Cardenas, M.B. and Wilson, J.L., 2006. The influence of ambient groundwater discharge on exchange zones induced by current-bedform interactions. Journal of Hydrology, 331(1-2): 103-109.
Chaudry, M.H., 2007. Open-channel flow. Springer, 523 pp.
Chen, K.L. and Elimelech, M., 2006. Aggregation and deposition kinetics of fullerene (c_{60}) nanoparticles. Langmuir, 22: 10994-11001.
Chen, K.L. and Elimelech, M., 2007. Influence of humic acid on the aggregation kinetics of fullerene (c-60) nanoparticles in monovalent and divalent electrolyte solutions. Journal of Colloid and Interface Science, 309(1): 126-134.

Chen, W., 2008. Nanoparticle fluorescence based technology for biological applications. Journal of Nanoscience and Nanotechnology, 8(3): 1019-1051.
Chen, X. and Mao, S.S., 2007. Titanium dioxide nanomaterials: Synthesis, properties, modifications, and applications. Chemical Reviews, 107(7): 2891-2959.
Chen, X.W. and Chiew, Y.M., 2004. Velocity distribution of turbulent open-channel flow with bed suction. Journal of Hydraulic Engineering-Asce, 130(2): 140-148.
Chen, Y.S., Hung, Y.C., Liau, I. and Huang, G.S., 2009. Assessment of the in vivo toxicity of gold nanoparticles. Nanoscale Research Letters, 4(8): 858-864.
Choi, O. et al., 2008. The inhibitory effects of silver nanoparticles, silver ions, and silver chloride colloids on microbial growth. Water Research, 42(12): 3066-3074.
Chou, K.S. and Lai, Y.S., 2004. Effect of polyvinyl pyrrolidone molecular weights on the formation of nanosized silver colloids. Materials Chemistry and Physics, 83(1): 82-88.
Christian, P., Von der Kammer, F., Baalousha, M. and Hofmann, T., 2008. Nanoparticles: Structure, properties, preparation and behaviour in environmental media. Ecotoxicology, 17(5): 326-343.
Conesa-Garcia, C. and Garcia-Lorenzo, R., 2009. Local scour estimation at check dams in torrential streams in south east spain. Geografiska Annaler Series a-Physical Geography, 91A(3): 159-177.
Connor, E.E., Mwamuka, J., Gole, A., Murphy, C.J. and Wyatt, M.D., 2005. Gold nanoparticles are taken up by human cells but do not cause acute cytotoxicity. Small, 1(3): 325-327.
Corbierre, M.K., Cameron, N.S. and Lennox, R.B., 2004. Polymer-stabilized gold nanoparticles with high grafting densities. Langmuir, 20(7): 2867-2873.
Costerton, J.W., 1995. Overview of microbial biofilms. Journal of Industrial Microbiology, 15(3): 137-140.
Csempesz, F. and Csaki, K.F., 2000. Mixed adsorption layers of uncharged polymers at particle/solution interfaces. Langmuir, 16(14): 5917-5920.
Dabbousi, B.O. et al., 1997. (cdse)zns core-shell quantum dots: Synthesis and characterization of a size series of highly luminescent nanocrystallites. Journal of Physical Chemistry B, 101(46): 9463-9475.
Daughton, C.G., 2004. Non-regulated water contaminants: Emerging research. Environmental Impact Assessment Review, 24(7-8): 711-732.
Davies, M. et al., 2005. Characterization of drug particle surface energetics and young's modulus by atomic force microscopy and inverse gas chromatography. Pharmaceutical Research, 22(7): 1158-1166.
de Broglie, L., 1936. The photon theory and the system relativistic wave mechanics. Comptes Rendus Hebdomadaires Des Seances De L Academie Des Sciences, 203: 473-477.
De Smedt, F., 2007. Analytical solution and analysis of solute transport in rivers affected by diffusive transfer in the hyporheic zone. Journal of Hydrology, 339(1-2): 29-38.
Degueldre, C., Favarger, P.Y. and Wold, S., 2006. Gold colloid analysis by inductively coupled plasma-mass spectrometry in a single particle mode. Analytica Chimica Acta, 555(2): 263-268.
Deivaraj, T.C., Lala, N.L. and Lee, J.Y., 2005. Solvent-induced shape evolution of pvp protected spherical silver nanoparticles into triangular nanoplates and nanorods. Journal of Colloid and Interface Science, 289(2): 402-409.
Delgado, A.V., Gonzalez-Caballero, E., Hunter, R.J., Koopal, L.K. and Lyklema, J., 2005. Measurement and interpretation of electrokinetic phenomena - (iupac technical report). Pure and Applied Chemistry, 77(10): 1753-1805.

Derjaguin, B. and Landau, L., 1945. Theory of stability of highly charged liophobic sols and adhesion of highly charged particles in solutions of electrolytes. Zhurnal Eksperimentalnoi I Teoreticheskoi Fiziki, 15(11): 663-682.
Dhawan, A. et al., 2006. Stable colloidal dispersions of c_{60} fullerenes in water: Evidence for genotoxicity. Environmental Science and Technology, 40(23): 7394-7401.
Diegoli, S. et al., 2008. Interaction between manufactured gold nanoparticles and naturally occurring organic macromolecules. Science of the Total Environment, 402(1): 51-61.
Domingos, R.F. et al., 2009. Characterizing manufactured nanoparticles in the environment: Multimethod determination of particle sizes. Environmental Science & Technology, 43(19): 7277-7284.
Dong, H., Fey, E., Gandelman, A. and Jones, W.E., 2006. Synthesis and assembly of metal nanoparticles on electrospun poly(4-vinylpyridine) fibers and poly(4-vinylpyridine) composite fibers. Chemistry of Materials, 18(8): 2008-2011.
El Badawy, A.M. et al., 2010. Impact of environmental conditions (ph, ionic strength, and electrolyte type) on the surface charge and aggregation of silver nanoparticles suspensions. Environmental Science & Technology, 44(4): 1260-1266.
Elimelech, M., Nagai, M., Ko, C.H. and Ryan, J.N., 2000. Relative insignificance of mineral grain zeta potential to colloid transport in geochemically heterogeneous porous media. Environmental Science & Technology, 34(11): 2143-2148.
Elliott, A.H. and Brooks, N.H., 1997. Transfer of nonsorbing solutes to a streambed with bed forms: Theory. Water Resources Research, 33(1): 123-136.
Fabrega, J., Fawcett, S.R., Renshaw, J.C. and Lead, J.R., 2009a. Silver nanoparticle impact on bacterial growth: Effect of ph, concentration, and organic matter. Environmental Science & Technology, 43(19): 7285-7290.
Fabrega, J., Renshaw, J.C. and Lead, J.R., 2009b. Interactions of silver nanoparticles with pseudomonas putida biofilms. Environmental Science & Technology, 43(23): 9004-9009.
Federici, G., Shaw, B.J. and Handy, R.D., 2007. Toxicity of titanium dioxide nanoparticles to rainbow trout (oncorhynchus mykiss): Gill injury, oxidative stress, and other physiological effects. Aquatic Toxicology, 84: 415-430.
Franklin, N.M. et al., 2007. Comparative toxicity of nanoparticulate zno, bulk zno, and zncl2 to a freshwater microalga (pseudokirchneriella subcapitata): The importance of particle solubility. Environmental Science & Technology, 41(24): 8484-8490.
Gao, J. et al., 2009. Dispersion and toxicity of selected manufactured nanomaterials in natural river water samples: Effects of water chemical composition. Environmental Science & Technology, 43(9): 3322-3328.
Garzon, F.H., Mukundan, R. and Brosha, E.L., 2000. Solid-stale mixed potential gas sensors: Theory. Experiments and challenges. Solid State Ionics, 136: 633-638.
Gebhardt, R., Doster, W., Friedrich, J. and Kulozik, U., 2006. Size distribution of pressure-decomposed casein micelles studied by dynamic light scattering and afm. European Biophysics Journal with Biophysics Letters, 35(6): 503-509.
Germain, V., Li, J., Ingert, D., Wang, Z.L. and Pileni, M.P., 2003. Stacking faults in formation of silver nanodisks. Journal of Physical Chemistry B, 107(34): 8717-8720.
Giddings, J.C., 1993. Field-flow fractionation - analysis of macromolecular, colloidal, and particulate materials. Science, 260(5113): 1456-1465.
Giersig, M. and Mulvaney, P., 1993. Preparation of ordered colloid monolayers by electrophoretic deposition. Langmuir, 9(12): 3408-3413.

Gimbert, L.J., Hamon, R.E., Casey, P.S. and Worsfold, P.J., 2007. Partitioning and stability of engineered zno nanoparticles in soil suspensions using flow field-flow fractionation. Environmental Chemistry, 4(1): 8-10.
Gimbert, L.J., Haygarth, P.M., Beckett, R. and Worsfold, P.J., 2006. The influence of sample preparation on observed particle size distributions for contrasting soil suspensions using flow field-flow fractionation. Environmental Chemistry, 3(3): 184-191.
Gimenez-Lopez, M.D.C. et al., 2010. Endohedral metallofullerenes in self-assembled monolayers. Physical Chemistry Chemical Physics, 12(1): 123-131.
Goettmann, F., Moores, A., Boissiere, C., Le Floch, P. and Sanchez, C., 2005. A selective chemical sensor based on the plasmonic response of phosphinine-stabilized gold nanoparticles hosted on periodically organized mesoporous silica thin layers. Small, 1(6): 636-639.
Goodman, C.M., McCusker, C.D., Yilmaz, T. and Rotello, V.M., 2004. Toxicity of gold nanoparticles functionalized with cationic and anionic side chains. Bioconjugate Chemistry, 15(4): 897-900.
Griffitt, R.J., Hyndman, K., Denslow, N.D. and Barber, D.S., 2009. Comparison of molecular and histological changes in zebrafish gills exposed to metallic nanoparticles. Toxicological Sciences, 107(2): 404-415.
Griffitt, R.J. et al., 2007. Exposure to copper nanoparticles causes gill injury and acute lethality in zebrafish (danio rerio). Environmental Science & Technology, 41(23): 8178-8186.
Gu, H. and Soucek, M.D., 2007. Preparation and characterization of monodisperse cerium oxide nanoparticles in hydrocarbon solvents. Chemistry of Materials, 19(5): 1103-1110.
Gulson, B. and Wong, H., 2006. Stable isotopic tracing - a way forward for nanotechnology. Environmental Health Perspectives, 114(10): 1486-1488.
Gustafsson, A., Lindstedt, E., Elfsmark, L.S. and Bucht, A., 2011. Lung exposure of titanium dioxide nanoparticles induces innate immune activation and long-lasting lymphocyte response in the dark agouti rat. Journal of Immunotoxicology, 8(2): 111-121.
Ha, Y., Tsay, O.G. and Churchill, D.G., 2011. A tutorial and mini-review of the icp-ms technique for determinations of transition metal ion and main group element concentration in the neurodegenerative and brain sciences. Monatshefte fur Chemie / Chemical Monthly, 142: 385-398.
Haaf, F., Sanner, A. and Straub, F., 1985. Polymers of *n*-vinylpyrrolidone: Synthesis, characterization and uses. Polymer Journal, 17(1): 143-152.
Hall, S., Bradley, T., Moore, J.T., Kuykindall, T. and Minella, L., 2009. Acute and chronic toxicity of nano-scale tio2 particles to freshwater fish, cladocerans, and green algae, and effects of organic and inorganic substrate on tio2 toxicity. Nanotoxicology, 3(2): 91-97.
Hamill, L., 2001. Understanding hydraulics. Palgrave Macmillan.
Handy, R.D. et al., 2008. The ecotoxicology and chemistry of manufactured nanoparticles. Ecotoxicology, 17(4): 287-314.
Hannah, D.M., Malcolm, I.A. and Bradley, C., 2009. Seasonal hyporheic temperature dynamics over riffle bedforms. Hydrological Processes, 23(15): 2178-2194.
Hardy, R.J., Bates, P.D. and Anderson, M.G., 1999. The importance of spatial resolution in hydraulic models for floodplain environments. Journal of Hydrology, 216(1-2): 124-136.
Hasan, M., Bethell, D. and Brust, M., 2002. The fate of sulfur-bound hydrogen on formation of self-assembled thiol monolayers on gold: H-1 nmr spectroscopic evidence from

solutions of gold clusters. Journal of the American Chemical Society, 124(7): 1132-1133.
Heinlaan, M., Ivask, A., Blinova, I., Dubourguier, H.C. and Kahru, A., 2008. Toxicity of nanosized and bulk zno, cuo and tio2 to bacteria vibrio fischeri and crustaceans daphnia magna and thamnocephalus platyurus. Chemosphere, 71(7): 1308-1316.
Hirai, H. and Yakura, N., 2001. Protecting polymers in suspension of metal nanoparticles. Polymers for Advanced Technologies, 12(11-12): 724-733.
Hirano, K., Nitta, H. and Sawada, K., 2005. Effect of sonication on the photo-catalytic mineralization of some chlorinated organic compounds. Ultrasonics Sonochemistry, 12(4): 271-276.
Hirano, M. and Inagaki, M., 2000. Preparation of monodispersed cerium(iv) oxide particles by thermal hydrolysis: Influence of the presence of urea and gd doping on their morphology and growth. Journal of Materials Chemistry, 10(2): 473-477.
Hoppe, C.E., Lazzari, M., Pardinas-Blanco, I. and Lopez-Quintela, M.A., 2006. One-step synthesis of gold and silver hydrosols using poly(*n*-vinyl-2-pyrrolidone) as a reducing agent. Langmuir, 22: 7027-7034.
Huff, T.B., Hansen, M.N., Zhao, Y., Cheng, J.X. and Wei, A., 2007. Controlling the cellular uptake of gold nanorods. Langmuir, 23(4): 1596-1599.
Hund-Rinke, K. and Simon, M., 2006. Ecotoxic effect of photocatalytic active nanoparticles tio2 on algae and daphnids. Environmental Science and Pollution Research, 13(4): 225-232.
Hung, C.H. and Whang, W.T., 2003. A novel low-temperature growth and characterization of single crystal zno nanorods. Materials Chemistry and Physics, 82(3): 705-710.
Hussain, I. et al., 2005. Size-controlled synthesis of near-monodisperse gold nanoparticles in the 1-4 nm range using polymeric stabilizers. Journal of the American Chemical Society, 127(47): 16398-16399.
Hyung, H., Fortner, J.D., Hughes, J.B. and Kim, J.H., 2007. Natural organic matter stabilizes carbon nanotubes in the aqueous phase. Environmental Science & Technology, 41(1): 179-184.
Iijima, S., 1991. Helical microtubules of graphitic carbon. Nature, 354(6348): 56-58.
Ishii, T., Otsuka, H., Kataoka, K. and Nagasaki, Y., 2004. Preparation of functionally pegylated gold nanoparticles with narrow distribution through autoreduction of auric cation by alpha-biotinyl-peg-block-[poly(2-(n,n-dimethylamino)ethyl methacrylate)]. Langmuir, 20(3): 561-564.
Jiang, J.K., Oberdorster, G. and Biswas, P., 2009. Characterization of size, surface charge, and agglomeration state of nanoparticle dispersions for toxicological studies. Journal of Nanoparticle Research, 11(1): 77-89.
Ju-Nam, Y. and Lead, J.R., 2008. Manufactured nanoparticles: An overview of their chemistry, interactions and potential environmental implications. Science of the Total Environment, 400(1-3): 396-414.
Kallay, N. and Zalac, S., 2002. Stability of nanodispersions: A model for kinetics of aggregation of nanoparticles. Journal of Colloid and Interface Science, 253(1): 70-76.
Kamat, P.V., 2002. Photophysical, photochemical and photocatalytic aspects of metal nanoparticles. Journal of Physical Chemistry B, 106(32): 7729-7744.
Kan, C.X., Zhu, X.G. and Wang, G.H., 2006. Single-crystalline gold microplates: Synthesis, characterization, and thermal stability. Journal of Physical Chemistry B, 110(10): 4651-4656.

Kanade, K.G., Kale, B.B., Aiyer, R.C. and Das, B.K., 2006. Effect of solvents on the synthesis of nano-size zinc oxide and its properties. Materials Research Bulletin, 41(3): 590-600.
Kanzer, J. et al., 2010. In situ formation of nanoparticles upon dispersion of melt extrudate formulations in aqueous medium assessed by asymmetrical flow field-flow fractionation. J Pharm Biomed Anal, 53(3): 359-65.
Karlsson, M.N.A., Deppert, K., Wacaser, B.A., Karlsson, L.S. and Malm, J.O., 2005. Size-controlled nanoparticles by thermal cracking of iron pentacarbonyl. Applied Physics a-Materials Science & Processing, 80(7): 1579-1583.
Kasas, S. et al., 1997. Biological applications of the afm: From single molecules to organs. International Journal of Imaging Systems and Technology, 8(2): 151-161.
Kasuga, T., Hiramatsu, M., Hoson, A., Sekino, T. and Niihara, K., 1999. Titania nanotubes prepared by chemical processing. Advanced Materials, 11(15): 1307-+.
Kazezyilmaz-Alhan, C.M., 2008. Analytical solutions for contaminant transport in streams. Journal of Hydrology, 348(3-4): 524-534.
Keck, P.E., McElroy, S.L., Strakowski, S.M. and Soutullo, C.A., 1999. Antipsychotics in the treatment of mood disorders and risk of tardive dyskinesia, Symposium on Update on Tardive Dyskinesia. Physicians Postgraduate Press, Dallas, Texas, pp. 33-38.
Kemal, L., Jiang, X.C., Wong, K. and Yu, A.B., 2008. Experiment and theoretical study of poly(vinyl pyrrolidone)-controlled gold nanoparticles. Journal of Physical Chemistry C, 112(40): 15656-15664.
Khan, J.A., Pillai, B., Das, T.K., Singh, Y. and Maiti, S., 2007. Molecular effects of uptake of gold nanoparticles in hela cells. Chembiochem, 8(11): 1237-1240.
Khanna, P.K. et al., 2005. Pva stabilized gold nanoparticles by use of unexplored albeit conventional reducing agent. Materials Chemistry and Physics, 92(1): 229-233.
Khlobystov, A.N., Britz, D.A. and Briggs, G.A.D., 2005. Molecules in carbon nanotubes. Accounts of Chemical Research, 38(12): 901-909.
Kim, D.J. and Koo, K.K., 2009. Synthesis of colloidal znse nanospheres by ultrasonic-assisted aerosol spray pyrolysis. Crystal Growth & Design, 9(2): 1153-1157.
Kim, K., Ryoo, H., Lee, Y.M. and Shin, K.S., 2010. Adsorption characteristics of au nanoparticles onto poly(4-vinylpyridine) surface revealed by qcm, afm, uv/vis, and raman scattering spectroscopy. Journal of Colloid and Interface Science, 342(2): 479-484.
Kim, Y.J., Johnson, R.C. and Hupp, J.T., 2001. Gold nanoparticle-based sensing of "Spectroscopically silent" Heavy metal ions. Nano Letters, 1(4): 165-167.
Klaine, S.J., 2009. Considerations for research on the environmental fate and effects of nanoparticles. Environmental Toxicology and Chemistry, 28(9): 1787-1788.
Klaine, S.J. et al., 2008. Nanomaterials in the environment: Behavior, fate, bioavailability, and effects. Environmental Toxicology and Chemistry, 27(9): 1825-1851.
Knoll, M. and Ruska, E., 1932. Article on the geometric electron optics pi. Annalen Der Physik, 12(6): 641-661.
Krause, S., Hannah, D.M. and Fleckenstein, J.H., 2009. Hyporheic hydrology: Interactions at the groundwater-surface water interface preface. Hydrological Processes, 23(15): 2103-2107.
Kreibig, U. and Vollmer, M., 1996. Optical properties of metal clusters. Springer series in materials science. Springer, Berlin.
Kretzschmar, R. and Schafer, T., 2005. Metal retention and transport on colloidal particles in the environment. Elements, 1(4): 205-210.

Kroto, H.W., Heath, J.R., Obrien, S.C., Curl, R.F. and Smalley, R.E., 1985. C-60 - buckminsterfullerene. Nature, 318(6042): 162-163.
Kuhn, L.T., Bojesen, A., Timmermann, L., Nielsen, M.M. and Morup, S., 2002. Structural and magnetic properties of core-shell iron-iron oxide nanoparticles. Journal of Physics-Condensed Matter, 14(49): 13551-13567.
Kumar, R., Howdle, S. and Munstedt, H., 2005. Polyamide/silver antimicrobials: Effect of filler types on the silver ion release. Journal of Biomedical Materials Research Part B-Applied Biomaterials, 75B(2): 311-319.
Labande, A. and Astruc, D., 2000. Colloids as redox sensors: Recognition of h2po4- and hso4- by amidoferrocenylalkylthiol-gold nanoparticles. Chemical Communications(12): 1007-1008.
Lasagna-Reeves, C. et al., 2010. Bioaccumulation and toxicity of gold nanoparticles after repeated administration in mice. Biochemical and Biophysical Research Communications, 393(4): 649-655.
Lead, J.R., Balnois, E., Hosse, M., Menghetti, R. and Wilkinson, K.J., 1999. Characterization of norwegian natural organic matter: Size, diffusion coefficients, and electrophoretic mobilities. Environment International, 25(2-3): 245-258.
Lead, J.R. and Wilkinson, K.J., 2006. Aquatic colloids and nanoparticles: Current knowledge and future trends. Environmental Chemistry, 3(3): 159-171.
Li, D., Lyon, D.Y., Li, Q. and Alvarez, P., 2008. Effect of soil sorption and aquatic natural organic matter on the antibacterial activity of a fullerene water suspension. Environmental Toxicology and Chemistry 27(9): 1888-1894.
Li, D.X., He, Q., Cui, Y. and Li, J.B., 2007. Fabrication of ph-responsive nanocomposites of gold nanoparticles/poly(4-vinylpyridine). Chemistry of Materials, 19(3): 412-417.
Li, X.Q., Elliott, D.W. and Zhang, W.X., 2006. Zero-valent iron nanoparticles for abatement of environmental pollutants: Materials and engineering aspects. Critical Reviews in Solid State and Materials Sciences, 31(4): 111-122.
Lim, B. et al., 2009. Shape-controlled synthesis of pd nanocrystals in aqueous solutions. Advanced Functional Materials, 19(2): 189-200.
Link, S. and Ei-Sayed, M.A., 2003. Optical properties and ultrafast dynamics of metallic nanocrystals. Annual Review of Physical Chemistry, 54: 331-366.
Liu, C. et al., 2004. Polyol process synthesis of monodispersed fept nanoparticles. Journal of Physical Chemistry B, 108(20): 6121-6123.
Liu, R., Lead, J.R. and Baker, A., 2007a. Fluorescence charcterisation of cross flow filtration derived dissolved and colloidal organic matter. Chemosphere, 68: 1304-1311.
Liu, W.T., 2006. Nanoparticles and their biological and environmental applications. Journal of Bioscience and Bioengineering, 102(1): 1-7.
Liu, Y.Q. et al., 2007b. Debundling of single-walled carbon nanotubes by using natural polyelectrolytes. Nanotechnology, 18(36): 6.
Liz-Marzán, L.M., 2004. Nanometals: Formation and color. Materials Today, 7(2): 26-31.
LizMarzan, L.M., Giersig, M. and Mulvaney, P., 1996. Synthesis of nanosized gold-silica core-shell particles. Langmuir, 12(18): 4329-4335.
Lovern, S.B. and Klaper, R., 2006. Daphnia magna mortality when exposed to titanium dioxide and fullerene (c-60) nanoparticles. Environmental Toxicology and Chemistry, 25(4): 1132-1137.
Lovern, S.B., Strickler, J.R. and Klaper, R., 2007. Behavioral and physiological changes in daphnia magna when exposed to nanoparticle suspensions (titanium dioxide, nano-c-60, and c(60)hxc(70)hx). Environmental Science & Technology, 41(12): 4465-4470.

Lu, C.Y. and Su, F.S., 2007. Adsorption of natural organic matter by carbon nanotubes. Separation and Purification Technology, 58(1): 113-121.
MacVicar, B.J. and Roy, A.G., 2007. Hydrodynamics of a forced riffle pool in a gravel bed river: 1. Mean velocity and turbulence intensity. Water Resources Research, 43(12).
Makishima, A., Kubo, H., Wada, K., Kitami, Y. and Shimohira, T., 1986. Yellow coatings produced on glasses and aluminum by the sol-gel process. Journal of the American Ceramic Society, 69(6): C127-C129.
Mallick, K., Witcomb, M.J. and Scurrell, M.S., 2005. Redox catalytic property of gold nanoclusters: Evidence of an electron-relay effect. Applied Physics a-Materials Science & Processing, 80(4): 797-801.
Malvern, 2001. Zeta potential - an introduction in 30 minutes, Malvern Instruments Worcester.
Malvern, 2009. Zetasizer nano series customer training.
Manzo, S. et al., 2011. Investigation of zno nanoparticles' ecotoxicological effects towards different soil organisms. Environmental Science and Pollution Research, 18(5): 756-763.
Mao, Z.W., Wang, B., Ma, L., Gao, C. and Shen, J.C., 2007. The influence of polycaprolactone coating on the internalization and cytotoxicity of gold nanoparticles. Nanomedicine-Nanotechnology Biology and Medicine, 3(3): 215-223.
Marini, M. et al., 2007. Antibacterial activity of plastics coated with silver-doped organic-inorganic hybrid coatings prepared by sol-gel processes. Biomacromolecules, 8(4): 1246-1254.
Maynard, A.D. et al., 2004. Exposure to carbon nanotube material: Aerosol release during the handling of unrefined single-walled carbon nanotube material. Journal of Toxicology and Environmental Health-Part A, 67(1): 87-107.
Medina-Ramirez, I., Gonzalez-Garcia, M. and Liu, J.L., 2009. Nanostructure characterization of polymer-stabilized gold nanoparticles and nanofilms derived from green synthesis. Journal of Materials Science, 44(23): 6325-6332.
Meyer, E., 1992. Atomic force microscopy. Progress in Surface Science, 41: 3-49.
Meyer, W.H., 1998. Polymer electrolytes for lithium-ion batteries. Advanced Materials, 10(6): 439-+.
Mie, G., 1908. Articles on the optical characteristics of turbid tubes, especially colloidal metal solutions. Annalen Der Physik, 25(3): 377-445.
Mogensen, M., Sammes, N.M. and Tompsett, G.A., 2000. Physical, chemical and electrochemical properties of pure and doped ceria. Solid State Ionics, 129(1-4): 63-94.
Moir, H.J., Soulsby, C. and Youngson, A., 1998. Hydraulic and sedimentary characteristics of habitat utilized by atlantic salmon for spawning in the girnock burn, scotland. Fisheries Management and Ecology, 5(3): 241-254.
Montes-Burgos, I. et al., 2010. Characterisation of nanoparticle size and state prior to nanotoxicological studies. Journal of Nanoparticle Research, 12(1): 47-53.
Moore, M.N., 2006. Do nanoparticles present ecotoxicological risks for the health of the aquatic environment? Environment International, 32(8): 967-976.
Moores, A. and Goettmann, F., 2006. The plasmon band in noble metal nanoparticles: An introduction to theory and applications. New Journal of Chemistry, 30(8): 1121-1132.
Moores, A., Goettmann, F., Sanchez, C. and Le Floch, P., 2004. Phosphinine stabilised gold nanoparticles; synthesis and immobilisation on mesoporous materials. Chemical Communications(24): 2842-2843.

Mueller, N.C. and Nowack, B., 2008. Exposure modeling of engineered nanoparticles in the environment. Environmental Science & Technology, 42(12): 4447-4453.
Murdock, R.C., Braydich-Stolle, L., Schrand, A.M., Schlager, J.J. and Hussain, S.M., 2008. Characterization of nanomaterial dispersion in solution prior to in vitro exposure using dynamic light scattering technique. Toxicological Sciences, 101(2): 239-253.
Murphy, C.J. et al., 2009. Gold nanoparticles in biology: Beyond toxicity to cellular imaging. Accounts of Chemical Research, 41(12): 1721-1730.
Music, S., Dragcevia, D., Popovic, S. and Ivanda, M., 2005. Precipitation of zno particles and their properties. Materials Letters, 59(19-20): 2388-2393.
Naiman, R.J. et al., 2002. Legitimizing fluvial ecosystems as users of water: An overview. Environmental Management, 30(4): 455-467.
Nel, A., Xia, T., Madler, L. and Li, N., 2006. Toxic potential of materials at the nanolevel. Science, 311(5761): 622-627.
Niidome, T. et al., 2006. Peg-modified gold nanorods with a stealth character for in vivo applications. Journal of Controlled Release, 114(3): 343-347.
Nikolaev, P. et al., 1999. Gas-phase catalytic growth of single-walled carbon nanotubes from carbon monoxide. Chemical Physics Letters, 313(1-2): 91-97.
Nikora, V. and Goring, D., 2000. Flow turbulence over fixed and weakly mobile gravel beds. Journal of Hydraulic Engineering-Asce, 126(9): 679-690.
Nikora, V., Goring, D., McEwan, I. and Griffiths, G., 2001. Spatially averaged open-channel flow over rough bed. Journal of Hydraulic Engineering-Asce, 127(2): 123-133.
Noguez, C., 2007. Surface plasmons on metal nanoparticles: The influence of shpae and physical environment. Journal of Physical Chemistry C, 111(10): 3806-3819.
Obare, S.O., Hollowell, R.E. and Murphy, C.J., 2002. Sensing strategy for lithium ion based on gold nanoparticles. Langmuir, 18(26): 10407-10410.
Oberdorster, E., 2004. Manufactured nanomaterials (fullerenes, c-60) induce oxidative stress in the brain of juvenile largemouth bass. Environmental Health Perspectives, 112(10): 1058-1062.
Oberdorster, E., Zhu, S., Blickley, T.M., McClellan-Green, P. and Haasch, M.L., 2006a. Ecotoxicology of carbon-based engineered nanoparticles: Effects of fullerene (c_{60}) on aquatic organisms. Carbon, 44(6): 1112-1120.
Oberdorster, E., Zhu, S.Q., Blickley, T.M., McClellan-Green, P. and Haasch, M.L., 2006b. Ecotoxicology of carbon-based engineered nanoparticles: Effects of fullerene (c-60) on aquatic organisms. Carbon, 44(6): 1112-1120.
Pachon, L.D. and Rothenberg, G., 2008. Transition-metal nanoparticles: Synthesis, stability and the leaching issue. Applied Organometallic Chemistry, 22(6): 288-299.
Packman, A., Salehin, M. and Zaramella, M., 2004. Hyporheic exchange with gravel beds: Basic hydrodynamic interactions and bedform-induced advective flows. Journal of Hydraulic Engineering-ASCE, 130(7): 647-656.
Packman, A.I., Brooks, N.H. and Morgan, J.J., 2000a. Kaolinite exchange between a stream and streambed: Laboratory experiments and validation of a colloid transport model. Water Resources Research, 36(8): 2363-2372.
Packman, A.I., Brooks, N.H. and Morgan, J.J., 2000b. A physicochemical model for colloid exchange between a stream and a sand streambed with bed forms. Water Resources Research, 36(8): 2351-2361.
Packman, A.I. and Salehin, M., 2003. Relative roles of stream flow and sedimentary conditions in controlling hyporheic exchange. Hydrobiologia, 494: 291-297.

Patra, H.K., Banerjee, S., Chaudhuri, U., Lahiri, P. and Dasgupta, A.K., 2007. Cell selective response to gold nanoparticles. Nanomedicine-Nanotechnology Biology and Medicine, 3(2): 111-119.

Petosa, A.R., Jaisi, D.P., Quevedo, I.R., Elimelech, M. and Tufenkji, N., 2010. Aggregation and deposition of engineered nanomaterials in aquatic environments: Role of physicochemical interactions. Environmental Science & Technology, 44(17): 6532-6549.

Phenrat, T., Saleh, N., Sirk, K., Tilton, R.D. and Lowry, G.V., 2007. Aggregation and sedimentation of aqueous nanoscale zerovalent iron dispersions. Environmental Science & Technology, 41(1): 284-290.

Pitcairn, I.K., Warwick, P.E., Milton, J.A. and Teagle, D.A.H., 2006. Method for ultra-low-level analysis of gold in rocks. Analytical Chemistry, 78(4): 1290-1295.

Porter, A.E. et al., 2007. Visualising the uptake of c_{60} to the cytoplasm and nucleus of human monocyte-derived macrophage cells using energy-filtered transmission electron microscopy and electron tomography. Environmental Science and Technology, 41(8): 3012-3017.

Ratanathanawongs, S.K., Giddings, J.C, 1993. Particle size analysis using flow-field flow fractionation. American Chemical Society Symposium Series, 521(13).

Ratte, H.T., 1999. Bioaccumulation and toxicity of silver compounds: A review. Environmental Toxicology and Chemistry, 18(1): 89-108.

Raveendran, P., Fu, J. and Wallen, S.L., 2003. Completely "Green" Synthesis and stabilization of metal nanoparticles. Journal of the American Chemical Society, 125(46): 13940-13941.

Ren, J. and Packman, A.I., 2004a. Modeling of simultaneous exchange of colloids and sorbing contaminants between streams and streambeds. Environmental Science and Technology, 38(10): 2901-2911.

Ren, J.H. and Packman, A.I., 2002. Effects of background water composition on stream-subsurface exchange of submicron colloids. Journal of Environmental Engineering-ASCE, 128(7): 624-634.

Ren, J.H. and Packman, A.I., 2004b. Stream-subsurface exchange of zinc in the presence of silica and kaolinite colloids. Environmental Science & Technology, 38(24): 6571-6581.

Ren, J.H. and Packman, A.I., 2005. Coupled stream-subsurface exchange of colloidal hematite and dissolved zinc, copper, and phosphate. Environmental Science & Technology, 39(17): 6387-6394.

Roberts, A.P. et al., 2007. In vivo biomodification of lipid-coated carbon nanotubes by daphnia magna. Environmental Science & Technology, 41(8): 3025-3029.

Rosgen, D.L., 1994. A classification of natural rivers. Catena, 22(3): 169-199.

Rosi, N.L. et al., 2006. Oligonucleotide-modified gold nanoparticles for intracellular gene regulation. Science, 312(5776): 1027-1030.

Ross, S. and Morrison, I.D., 1988. Colloidal systems and interfaces. John Wiley and Sons.

Sakamoto, M., Tachikawa, T., Fujitsuka, M. and Majima, T., 2006. Acceleration of laser-induced formation of gold nanoparticles in a poly(vinyl alcohol) film. Langmuir, 22(14): 6361-6366.

Scheffer, A., Engelhard, C., Sperling, M. and Buscher, W., 2008. Icp-ms as a new tool for the determination of gold nanoparticles in bioanalytical applications. Analytical and Bioanalytical Chemistry, 390(1): 249-252.

Schierz, A. and Zanker, H., 2009. Aqueous suspensions of carbon nanotubes: Surface oxidation, colloidal stability and uranium sorption. Environmental Pollution, 157(4): 1088-1094.
Schimpf, M., Caldwell, K., Giddings, J.C., 2000. Field-flow fractionation handbook. John Wiley and Sons, New York.
Scown, T.M., van Aerle, R. and Tyler, C.R., 2010. Review: Do engineered nanoparticles pose a significant threat to the aquatic environment? Critical Reviews in Toxicology, 40(7): 653-670.
Service, R.F., 1998. Superstrong nanotubes show they are smart, too. Science, 281(5379): 940-942.
Shan, J. and Tenhu, H., 2007. Recent advances in polymer protected gold nanoparticles: Synthesis, properties and applications. Chemical Communications(44): 4580-4598.
Shaw, D.J., 1992. Introduction to colloid and surface chemistry. Butterworth Heinemann.
Shimizu, Y., Tsujimoto, T. and Nakagawa, H., 1990. Experiment and macroscopic modelling of flow in highly permeable porous medium under free-surface flow. Journal of Hydroscience and Hydraulic Engineering, 8(1): 69-78.
Shipway, A.N., Katz, E. and Willner, I., 2000. Nanoparticle arrays on surfaces for electronic, optical, and sensor applications. Chemphyschem, 1(1): 18-52.
Shukla, R. et al., 2005. Biocompatibility of gold nanoparticles and their endocytotic fate inside the cellular compartment: A microscopic overview. Langmuir, 21(23): 10644-10654.
Sitterberg, J., Ozcetin, A., Ehrhardt, C. and Bakowsky, U., 2010. Utilising atomic force microscopy for the characterisation of nanoscale drug delivery systems. European Journal of Pharmaceutics and Biopharmaceutics, 74(1): 2-13.
Smith, C.J., Shaw, B.J. and Handy, R.D., 2007. Toxcicity of single walled carbon nanotubes to rainbow trout, *(oncorhynchus mykiss)*: Respiratory toxicity, organ pathologies, and other physiological effects. Aquatic Toxicology, 82: 94-109.
Smith, J.W.N., 2005. Groundwater-surface water interactions in the hyporheic zone. In: E. Agency (Editor).
Srivastava, R.K. et al., 2011. Multi-walled carbon nanotubes induce oxidative stress and apoptosis in human lung cancer cell line-a549. Nanotoxicology, 5(2): 195-207.
Starowicz, M. and Stypula, B., 2008. Electrochemical synthesis of zno nanoparticles. European Journal of Inorganic Chemistry(6): 869-872.
Suekane, T., Yokouchi, Y. and Hirai, S., 2003. Inertial flow structures in a simple-packed bed of spheres. Aiche Journal, 49(1): 10-17.
Sun, Y.G. and Xia, Y.N., 2002. Shape-controlled synthesis of gold and silver nanoparticles. Science, 298(5601): 2176-2179.
Sun, Y.G. and Xia, Y.N., 2003. Gold and silver nanoparticles: A class of chromophores with colors tunable in the range from 400 to 750 nm. Analyst, 128(6): 686-691.
Sun, Y.P., Li, X.Q., Cao, J.S., Zhang, W.X. and Wang, H.P., 2006. Characterization of zero-valent iron nanoparticles. Advances in Colloid and Interface Science, 120(1-3): 47-56.
Sze, A., Erickson, D., Ren, L.Q. and Li, D.Q., 2003. Zeta-potential measurement using the smoluchowski equation and the slope of the current-time relationship in electroosmotic flow. Journal of Colloid and Interface Science, 261(2): 402-410.
Takahashi, H. et al., 2006. Modification of gold nanorods using phospatidylcholine to reduce cytotoxicity. Langmuir, 22(1): 2-5.
Tanguchi, J., Murata, H. and Okamura, Y., 2009. Analysis of aggregation and dispersion states of small particles in concentrated suspension by using diffused photon density wave spectroscopy. Colloids Surf B Biointerfaces, 76(1): 137-44.

Tashiro, J. et al., 2002. Room-temperature epitaxial growth of indium tin oxide thin films on si substrates with an epitaxial ceo2 ultrathin buffer. Thin Solid Films, 415(1-2): 272-275.
The Royal Society, 2009. Geoengineering the climate: Science, governance and uncertainty, The Royal Society.
Thibodeaux, L.J. and Boyle, J.D., 1987. Bedform-generated convective-transport in bottom sediment. Nature, 325(6102): 341-343.
Thomas, R., 2007. Practical guide to icp-ms: A tutorial for beginners. CRC, Boca Raton.
Tiraferri, A. and Sethi, R., 2009. Enhanced transport of zerovalent iron nanoparticles in saturated porous media by guar gum. Journal of Nanoparticle Research, 11(3): 635-645.
Tsunekawa, S., Fukuda, T. and Kasuya, A., 2000. Blue shift in ultraviolet absorption spectra of monodisperse ceo2-x nanoparticles. Journal of Applied Physics, 87(3): 1318-1321.
Turner, Y.T.A., Roberts, C.J. and Davies, M.C., 2007. Scanning probe microscopy in the field of drug delivery. Adv Drug Deliv Rev, 59(14): 1453-73.
United States Geological Survey, 2007. River science at the u.S. Geological survey. In: C.o.R.S.a.U.S.G. Survey (Editor). The National Academy of Sciences.
University Corporation for Atmospheric Research, 2011. The comet project, Boulder.
van der Ploeg, M.J.C. et al., 2011. Effecst of c_{60} nanoparticle exposure on earthworms (*lumbricus rubellus*) and implications for population dynamics. Environmental Pollution, 159: 193-203.
Wang, C.B. and Zhang, W.X., 1997. Synthesizing nanoscale iron particles for rapid and complete dechlorination of tce and pcbs. Environmental Science & Technology, 31(7): 2154-2156.
Wang, Y., Wong, J.F., Teng, X.W., Lin, X.Z. and Yang, H., 2003. "Pulling" Nanoparticles into water: Phase transfer of oleic acid stabilized monodisperse nanoparticles into aqueous solutions of alpha-cyclodextrin. Nano Letters, 3(11): 1555-1559.
Washington, U.o., 2011. Van der waals attractive potential.
Wick, P. et al., 2007. The degree and kind of agglomeration affect carbon nanotube cytotoxicity. Toxicology Letters, 168: 121-131.
Wiesner, M., Lowry, G.V., Alvarez, P., Dionysiou, D. and Biswas, P., 2006. Assessing the risks of manufactured nanomaterials. Environmental Science and Technology: 4337-4345.
Wiley, B., Sun, Y.G., Mayers, B. and Xia, Y.N., 2005. Shape-controlled synthesis of metal nanostructures: The case of silver. Chemistry-a European Journal, 11(2): 454-463.
Williams, D.B. and Carter, C.B., 1996. Transition electron microscopy - a textbook for materials science - basics. Plenum Press, New York.
Winter, T.C., Harvey, J.W., Franke, O.H. and Alley, W.M., 1998. Ground water and surface water: A single resource. In: USGS (Editor). The National Academy of Sciences.
Worman, A., 2002. Effect of flow-induced exchange in hyporheic zones on longitudinal transport of solutes in streams and rivers (vol 38, pg 1001, 2002). Water Resources Research, 38(6).
Wu, R., Xie, C.S., Xia, H., Hu, J.H. and Wang, A.H., 2000. The thermal physical formation of zno nanoparticles and their morphology. Journal of Crystal Growth, 217(3): 274-280.
Xia, X.H. et al., 2007. Ultrasonic synthesis and photocatalytic activity investigation of tio2 nanoarrays. Materials Letters, 61(11-12): 2571-2574.
Xia, Y.N. and Halas, N.J., 2005. Shape-controlled synthesis and surface plasmonic properties of metallic nanostructures. MRS Bulletin, 30(5): 338-344.

Xie, B., Xu, Z.H., Guo, W.H. and Li, Q.L., 2008. Impact of natural organic matter on the physicochemical properties of aqueous c-60 nanoparticles. Environmental Science & Technology, 42(8): 2853-2859.

Xu, H.X., Aizpurua, J., Kall, M. and Apell, P., 2000. Electromagnetic contributions to single-molecule sensitivity in surface-enhanced raman scattering. Physical Review E, 62(3): 4318-4324.

Xu, Q. et al., 2010. Surface structural transformation and the phase transition kinetics of brookite tio_2. Chemistry - An Asian Journal, 5(10): 2158-2161.

Yang, K., Lin, D.H. and Xing, B.S., 2009. Interactions of humic acid with nanosized inorganic oxides. Langmuir, 25(6): 3571-3576.

Yu, X.J., Xie, P.B. and Su, Q.D., 2001. Size-dependent optical properties of nanocrystalline ceo2 : Er obtained by combustion synthesis. Physical Chemistry Chemical Physics, 3(23): 5266-5269.

Yuan, H.G. et al., 2011. Single walled carbon nanotubes exhibit dual-phase regulation to exposed arabidopsis mesophyll cells. Nanoscale Research Letters, 6.

Yun, Y.J. et al., 2005. Fabrication of versatile nanocomponents using single-crystalline au nanoplates. Applied Physics Letters, 87(23): 3.

Zhang, F. et al., 2002a. Cerium oxide nanoparticles: Size-selective formation and structure analysis. Applied Physics Letters, 80(1): 127-129.

Zhang, F.X. et al., 2002b. Colorimetric detection of thiol-containing amino acids using gold nanoparticles. Analyst, 127(4): 462-465.

Zhang, W.X., 2003. Nanoscale iron particles for environmental remediation: An overview. Journal of Nanoparticle Research, 5(3-4): 323-332.

Zhao, H.Y., Kang, X.L. and Liu, L., 2005. Comb-coil polymer brushes on the surface of silica nanoparticles. Macromolecules, 38(26): 10619-10622.

Zharov, V.P., Mercer, K.E., Galitovskaya, E.N. and Smeltzer, M.S., 2006. Photothermal nanotherapeutics and nanodiagnostics for selective killing of bacteria targeted with gold nanoparticles. Biophysical Journal, 90(2): 619-627.

Zhou, J., Xu, N.S. and Wang, Z.L., 2006a. Dissolving behavior and stability of zno wires iin biofluids: A study on biodegradability and biocompatibility of zno nanostructures. Advanced Materials, 18(18): 2432-+.

Zhou, M., Chen, S.H. and Zhao, S.Y., 2006b. Synthesis of icosahedral gold nanocrystals: A thermal process strategy. Journal of Physical Chemistry B, 110(10): 4510-4513.

Zhu, Y., Zhao, Q.F., Li, Y.G., Cai, X.Q. and Li, W., 2006. The interaction and toxicity of multi-walled carbon nanotubes with stylonychia mytilus. Journal of Nanoscience and Nanotechnology, 6(5): 1357-1364.

UNIVERSITY OF BIRMINGHAM

University of Birmingham Research Archive

e-theses repository

This unpublished thesis/dissertation is copyright of the author and/or third parties. The intellectual property rights of the author or third parties in respect of this work are as defined by The Copyright Designs and Patents Act 1988 or as modified by any successor legislation.

Any use made of information contained in this thesis/dissertation must be in accordance with that legislation and must be properly acknowledged. Further distribution or reproduction in any format is prohibited without the permission of the copyright holder.